Spring 1-1-2016

Seismic Performance of Shallow-Founded Structures on Liquefiable Ground: an Experimental and Numerical Study

Zana Karimi
University of Colorado at Boulder, zana.karimi@colorado.edu

SEISMIC PERFORMANCE OF SHALLOW-FOUNDED STRUCTURES ON LIQUEFIABLE GROUND: AN EXPERIMENTAL AND NUMERICAL STUDY

by

Zana Karimi

B.Sc., University of Kurdistan, Sanandaj, Iran, 2008

M.Sc. Sharif University of Technology, Tehran, Iran, 2010

A thesis submitted to the

Faculty of the Graduate School of the

University of Colorado in partial fulfillment

of the requirements for the degree of

Doctor of Philosophy

Department of Civil, Environmental and Architectural Engineering

2016

This thesis entitled:
Seismic Performance of Shallow-Founded Structures on Liquefiable Ground:
An Experimental and Numerical Study
written by Zana Karmi
has been approved for the Department of Civil, Environmental and Architectural Engineering

_____

Prof. Shideh Dashti

_____

Prof. Abbie Liel

_____

Prof. Ahmed Elgamal

_____

Prof. Richard Regueiro

_____

Prof. Kevin Franke

Date _____

The final copy of this thesis has been examined by the signatories, and we find that both the content and the form meet acceptable presentation standards of scholarly work in the above mentioned discipline.

Zana Karimi (Ph.D. Civil Engineering)

Seismic Performance of Shallow-Founded Structures on Liquefiable Ground: An Experimental and Numerical Study

Thesis directed by Professor Shideh Dashti

Recent earthquakes have shown that even buildings designed according to local seismic regulations may suffer damage due to liquefaction. This is because the mechanisms that lead to a loss of building serviceability due to liquefaction are not well understood and considered in the design of structures. The current state-of-practice for estimating liquefaction-induced building settlement is primarily based on procedures that assume free-field conditions and are known to be unreliable, because they do not account for changes in stress distribution, flow patterns, and soil-foundation-structure interaction.

In this research, results from centrifuge experiments are used to: 1) gain insight into the underlying mechanisms of deformation near structures on softened ground; and 2) validate and evaluate the capabilities and shortcoming of an advanced numerical tool, which are then employed in a parametric study.

Solid-fluid, fully-coupled, nonlinear, effective stress, 3D, finite element analyses are performed in the OpenSees platform. The key Engineering Demand Parameters (EDPs) of interest that quantify the performance of the soil-foundation-structure system (e.g., excess pore pressures, accelerations, and settlements, foundation tilt, and transient inter-story drift) were compared numerically and experimentally. For the cases considered, numerical predictions compared fairly well with experimental results, with the exception of free-field settlement and permanent foundation tilt.

A numerical parametric study, validated against experiments was then performed, in which different soil, structural, and ground motion Input Parameters (IPs) were systematically

varied to investigate the influence and relative importance of different IPs, and to search for and identify optimum Intensity Measures (IMs) that minimized the variability and uncertainty in estimating different EDPs. The extent of excess pore pressure generation (EDP = $r_{u,peak}$) in the free-field and near the structure was significantly influenced by relative density and thickness of the liquefiable layer. These factors along with the foundation contact pressure and area were shown to significantly influence building settlements. Spectral acceleration at the initial period of the site as well as Arias Intensity were identified as optimum IMs for predicting $r_{u,peak}$ and foundation settlement, respectively. Additional simulations validated against case histories will be necessary to develop a probabilistic method for predicting the performance of structures on softened ground.

DEDICATION

To Monireh, Nasrin and Karim …

ACKNOWLEDGEMENTS

I would like to humbly thank my advisor, Professor Shideh Dashti, for her support, advice, and guidance that constantly helped me to stay on the right track throughout this PhD research. She taught me how to aim high and be effective, as an engineer and a researcher, by setting high standards and helped me to reach those standards; by believing in my capabilities, being accessible to my numerous questions even during weekends, listening to my research ideas, and guiding me through the right path. Her advice helped me in all the time of research and writing of this dissertation. The guidance she provided was crucial to my technical work at the University of Colorado Boulder, as well as preparing professionally for my career. She has been a tremendous mentor.

I would also like to thank Professors Ahmed Elgamal, Abbie Liel, Kevin Franke, and Richard Regueiro for serving as my committee members. Their feedback and recommendations throughout this research were essential to deliver this work.

Although words are short to express how much I am grateful to have such a strong support and encouragement from my family and friends, I want to thank all of them for always being there for me in happiness and hardship, even though, some of them were thousands of miles away.

This work was partly supported by the National Science Foundation (NSF) under Grant no. 1454431 and partly by the department of Civil, Environmental, and Architectural

Engineering at the University of Colorado Boulder through Teaching Assistant and Instructor positions during my study at CU Boulder. Any opinions, findings, and conclusions or recommendations expressed in this material are those of the author and do not necessarily reflect the views of the NSF. This work utilized the Janus supercomputer, which is supported by the NSF (award number CNS-0821794) and the University of Colorado Boulder.

CONTENTS

CHAPTER

List of Tables

List of Figures

CHAPTER 1

INTRODUCTION

1.1. Research Motivation

Observations of previous earthquakes have revealed that even buildings designed according to local seismic regulations may experience extensive damage due to liquefaction, including bearing capacity failure, excessive settlement, and tilting, which mostly affect buildings on shallow foundations and their surrounding lifelines.

The current state-of-practice for estimating liquefaction-induced building settlement still relies heavily on simplified empirical procedures that assume free-field conditions and are known to be unreliable for predicting building settlement. These procedures do not take into account the change in static and dynamic stress distribution, water flow patterns, and more importantly, dynamic soil-foundation-structure interaction (SFSI) by ignoring the presence of the superstructure. They assume that the mechanism of volumetric strain due to post-shaking consolidation and dissipation of excess pore water pressures is the main contributor to the total permanent settlements in a liquefied layer. However, this is neither the only active nor the dominant mechanism of the seismically-induced settlement under shallow-founded structures that are founded on liquefiable ground. Moreover, estimation of the seismic demand imposed on the structural components and the performance of the structure under combined shaking and

permanent ground deformations is impossible when no structure is considered in the available procedures.

Previous case histories and physical model studies have shown that the presence and properties of a structure affect the static and dynamic stresses and flow patterns in the underlying soil in a three-dimensional (3D) manner, which strongly influence liquefaction triggering and the resulting accelerations and deformations. The available methods ignore the presence of the structure, its interaction with the underlying liquefiable soil, and the key displacement mechanisms that are active under a structure. Hence, they cannot reliably evaluate the consequences of liquefaction, the need for ground improvement, and the subsequent evaluation of the proposed mitigation scheme in terms of improved building performance.

Physical modeling in parallel with well-calibrated fully coupled, nonlinear numerical simulations of the SFS systems will help evaluate dynamic soil-foundation-structure interaction effects on softened ground and the underlying mechanisms of damage. Once validated against experimental data with a range of conditions, numerical simulations may be employed in design or in developing improved simplified procedures for evaluating building performance on softened ground. They can also be used to identify the most optimum ground motion Intensity Measures (IM) for predicting soil liquefaction triggering and consequences in terms of building performance, which is currently lacking. Knowledge of optimum IMs will reduce the uncertainty in our predictions, regardless of the complexity of the procedure employed.

1.2. Research Objectives and Methodology

In the first phase (Phase 1) of this study, centrifuge experimental results are used to test and validate an existing state-of-the-art, nonlinear numerical tool. Solid-fluid, fully-coupled,

effective stress, nonlinear, dynamic, finite element analyses are performed. The Pressure-Dependent Multi-Yield plasticity surface (PDMY02) constitutive soil model, previously implemented in the OpenSees[1] platform are used. Of particular interest is the reproducibility of: 1) ground motions and excess pore pressures in the free-field and near-field; 2) soil settlement patterns; 3) the building's flexible-base response and inter-story drift (proxies for SFSI and damage). The direct comparisons of the structure-only (fixed-base), soil-only (free-field), and SFS models are essential for quantifying the discrepancies between the modeling approach and experimental data, identifying the capabilities and shortcomings of the numerical tool, and their relative importance.

In the second phase of this study, the numerical model, calibrated and validated in Phase 1, is employed in a parametric study to develop an improved understanding of the effects of liquefaction on accelerations, excess pore pressures, displacements, and damage near buildings. One of the main goals is to identify the key predictors of damage to the soil-structure system in a more comprehensive manner than possible in centrifuge. In a parametric study, the key properties of the ground motion, soil, and building (Input Parameters or IPs) are systematically varied, and their effects and relative importance are evaluated on the key Engineering Demand Parameters, EDPs, that describe building performance (e.g., settlement, tilt, inter-story drift). The other main objective of this program is to search for and identify an optimum Intensity Measure (IM) for predicting the main EDPs. Knowledge and use of an optimum IM in selecting and scaling ground motions will reduce variability and uncertainty in predicting the liquefaction hazard and its consequences in terms of building performance. Results from this parametric study will set the groundwork for the future development of

[1] OpenSees is a software framework for developing applications to simulate the performance of structural and geotechnical systems subjected to earthquakes.

probabilistic performance-based procedures for predicting the effects of liquefaction on shallow-founded structures.

1.3. Organization of this Dissertation

This thesis is based on the compilation of manuscripts of four published or submitted journal articles and one conference proceeding on the work conducted in this study. These articles are co-authored, but the authors and the journal to which the manuscript was submitted appear in the first part of each chapter. The organization of this dissertation is as follows:

Chapter 2 reviews the incidents of seismic soil liquefaction during previous earthquakes, followed by observations of its consequences, mainly focusing on the performance of shallow-founded structures. Next, the previously conducted physical model tests that included shallow-founded structures on liquefiable ground are reviewed, and their key findings affecting the performance of the SFS system are discussed. Then, a review of previously performed numerical studies to simulate the response of the SFS system on liquefiable ground are presented, and their distinct contributions, capabilities, and limitations are discussed. Lastly, the available procedures to evaluate the response of shallow foundations on liquefiable ground, the existing gaps in the state of knowledge, and the research approach undertaken to address these gaps are discussed.

Chapter 3 focuses on the numerical simulations of earthquake-induced soil liquefaction validated with two centrifuge experiments (free-field and the SFS system) with a homogeneous liquefiable deposit but a range of earthquake motions. These experiments were conducted using the centrifuge facility at the University of Colorado Boulder by the author, which set the stage for other centrifuge experiments with saturated sand and more complicated configurations performed by other graduate students. The centrifuge experiment with no structure (free-field) was particularly valuable in calibrating and validating the numerical tool, due to its simplicity and limited use of instruments and

structures. The overview of the centrifuge experiments followed by the numerical methodology, and calibration procedure is presented. A direct comparison between numerical and experimental measurements of the excess pore pressure and accelerations in the free-filed and near-field is provided in this chapter, and the quality of comparisons is quantified.

Chapter 4 provides a comprehensive discussion on numerical modeling of seismic SFSI on layered liquefiable ground validated against a series of previously conducted centrifuge experiments by Dashti et al. (2010a,b). The calibration procedure is presented in detail, followed by the comparison of numerical results with experimental measurements. The strain-compatible fundamental frequency of the free-field soil undergoing softening, changes in foundation accelerations compared to the free-field due to both inertial and kinematic interaction, period lengthening of the structure due to a flexible base, and the total inter-story drift ratio of the building are evaluated, in addition to building settlement and tilt. Numerical predictions are directly compared with experimental recordings in great detail for one single-degree-of-freedom (SDOF) structure only, but different ground motions. Only one type of soil profile is investigated, with one variation in the relative density of the liquefiable ground. The capabilities and limitations of an advanced, state-of-the-art numerical tool in predicting site response (accelerations, excess pore pressures, and settlements) in the free-field and SFSI (accelerations, excess pore pressures, settlement, tilt, and total drift) for one structure using centrifuge test results are identified and quantified.

Chapter 5 provides a detailed comparison between numerical simulations and experimental recordings on the performance of structures with different dynamic properties on different soil profiles, including a liquefiable layer. The influence of foundation bearing pressure, size, building's height/width aspect ratio, and fixed-base natural frequency of

the building, as well as the presence of a low permeability silt layer above liquefiable sand are investigated on different EDPs for different structures in detail, both experimentally and numerically. Lastly, this chapter includes a discussion on the importance of performing 3D analyses by comparing the experimental results with both 2D and 3D predictions for one representative case. This chapter aims to provide a detailed evaluation of the capabilities of an advanced, state-of-the-art numerical tool in capturing the key EDPs describing the performance and damage potential of buildings on softened ground: foundation acceleration, settlement, transient and permanent tilt, total inter-story drift and its two components (flexural and rocking drift).

Chapter 6 presents the results of a numerical parametric study, validated against centrifuge results, to evaluate the influence of different soil, structural and ground motion IPs on the liquefaction hazard in the free-field and in the vicinity of shallow-founded structures. The generation, dissipation, and redistribution of pore pressure redistribution and soil-structure interaction are directly considered in estimating the liquefaction hazard in terms of peak excess pore pressure ratio ($r_{u,peak}$). The IMs with the best combination of efficiency, sufficiency, and predictability are identified for predicting $r_{u,peak}$ in the free-field and under the edge and center of the foundation.

Chapter 7 focuses on the structural response of the parametric study of shallow-founded structures on layered, liquefiable soils. The influence of different soil and structural IPs are evaluated on EDPs that specifically relate to structural performance and damage potential, such as permanent foundation settlement and peak, transient, inter-story drift ratio. The IMs with the best combination of efficiency, sufficiency, and predictability in predicting the structural EDPs of interest are identified.

Chapter 8 summarizes the conclusions of this research and discusses the need for future research.

CHAPTER 2

LITERATURE REVIEW AND BACKGROUND

2.1. Case Histories of Liquefaction

The importance of liquefaction studies primarily emerged with observations of significant damage to structures during two major earthquakes of Niigata and Alaska in 1964. Going further back, liquefaction occurrences were reported in the 1811-1812 New Madrid Missouri; 1872 Hamada, Japan; 1906 San Francisco, California; 1946 Vancouver Island, British Colombia, Canada earthquakes, and many others around the world (Kuribayashi and Tatsuoka 1977; Keefer and Tannaci 1981; Broadhead 1902; Coffman and von Hake 1973).

In the 1906 San Francisco earthquake, seismic-induced soil liquefaction caused extensive damage to different structures. Ground subsidence and settlements were major damages observed in soil filled areas, such as the Market Street and Mission Creek. The severe ground subsidence broke off major lifelines and temporarily barricaded the capability to extinguish massive fire, which led to more than 85% damage to the city (Derleth 1907).

In 1989, the Loma Prieta earthquake again hit the San Francisco Bay Area. Evidence of liquefaction such as sand boils and damage to several buildings due to excessive settlement and tilt was reported primarily in the soil filled areas, similar to the 1906 San Francisco earthquake (Taylor et al. 1994).

During the 1971 San Fernando event, post-earthquake liquefaction damage on the Lower San Fernando Dam resulted in sliding of the upstream slope and reduced freeboard of the dam to 1.5 m. The failure occurred one minute after the end of ground shaking and led to mandatory evacuation of the downstream residential areas (Seed et al. 1975a). The Lower San Fernando Dam failure is a good example of liquefaction-induced flow failure, which is relatively well studied and investigated with a good deal of information available for researchers (Gastro et al. 1992; Lee et al. 1975; Seed et al. 1975b).

On March 27, 1964, the Prince William Sound in Alaska was shaken by an 8.3 M_L earthquake, and seismic-induced soil liquefaction was the main reason for significant damage and economic loss. Several major earthquake-induced landslides also occurred and caused a serious halt in lifelines from functioning (Coulter and Migliaccio 1966; Eckel 1967; Wison 1967).

On June 16, 1964 in the same year of the Alaska earthquake, a 7.25-7.5 M_L earthquake hit Niigata, Japan. The Niigata earthquake is well known amongst geotechnical engineers and researchers, because it is now a frequent example of earthquake-induced liquefaction damage, and also along with the knowledge from 1964 Alaska event, it raised a widespread awareness of liquefaction disastrous consequences. Consequently, the need for more serious investigations to better understand the liquefaction mechanism and its consequences was recognized by researchers. Regions with loose sand deposits were the main victim of the event. Upward floating of underground structures, sand flows for 20 min after the ground shaking, and 80 degree tilting of an apartment building due to bearing capacity failure were reported. (Kuribayashi and Tatsuoka 1977; Wakamatsu 1992; Seed and Idriss 1967).

In August 1999, the 7.4 M_w Kocaeli (Izmit) earthquake occurred in Turkey. Substantial geotechnical effects, especially earthquake-induced liquefaction and consequent settlements and subsidence were reported in Adapazari. Lateral displacements of approximately 0.1–2.5 m

were observed along the coast of Izmit Bay (Scawthorn and Johnson 2000; Cetin, et al. 2004). The Sapanca Hotel was located on a site with a soft alluvial stratum that experienced extensive liquefaction-induced damage, including damage to the access roads and structural components of the main building, which prevented hotel from operation. The main structure of the hotel settled about 0.2-0.5 m. Employees of the hotel observed sand boiling while evacuating the building (Cetin, et al. 2002; Bardet, et al. 2000). The site of the hotel previously experienced liquefaction-induced ground deformations during the 7.1 M_w Mudurnu Valley earthquake in 1967 (Ambraseys and Zatopek 1969).

On 12 January 2010, the 7.0 M_w Haiti earthquake shook the physiographically diverse area of Port-au-Prince. Although the amount of damage varied among different sites, it was reported that sever earthquake liquefaction failures are responsible for the disastrous damage along the Gulf of Gonave coastline, along rivers north of Port-au-Prince. Liquefaction-induced total bearing capacity failure of a three-story concrete building along the southern coast of the Gulf was observed. Reports after reconnaissance stated that the most severely affected areas are located in downtown Port-au-Prince underlain by Holocene alluvium with average shear wave velocities about 350 m/s in the top 30 m (Rathje et al. 2011; Olson et al. 2011).

The 22 February 2011, 6.2-6.3 M_w Christchurch earthquake is one in a series of earthquakes that hit Christchurch in New Zealand from September 2010 to June 2011. Leaving behind 181 fatalities, extreme damage to different structures including residential and commercial buildings, superstructures, and lifelines made this event one of the most catastrophic ones in the area. Review of geotechnical evidences revealed the role of soil liquefaction as the major reason for the severity of the loss. Spatial extend of liquefaction and lateral spreading in the natural soil affected commercial structures in the Central Business District in different forms, such as excessive punching settlement of shallow-founded structures, total and differential permanent settlements, and tilting of buildings. Soil-structure

interaction and the interaction among adjacent buildings in dense urban areas were reported to influence the overall behavior of the system (Cubrinovski et al. 2011a,b). In many cases, shallow-founded structures that suffered excessive rotation or settlement had to be demolished and rebuilt. The city of Christchurch is still undergoing the rebuilding process in 2016.

In March 11, 2011, the 9.0 M_w Tohoku earthquake shook the extended area from Tokyo to Hachnohe in Japan. Although the Tsunami followed by earthquake washed away the majority of liquefaction manifestations, liquefaction-induced ground failure was recognized to be the dominant cause of damage in the Tokyo Bay and Tone River areas. Even though these sites were at a great distance from the epicenter and experienced a weak level of shaking, liquefaction was observed due to a long duration of shaking. Larger permanent tilt and settlements were observed in this event for light commercial and residential buildings that mostly had mat-type foundations with deep grade beams. Hence damage on superstructures was often related to excessive settlement and tilt of the foundation rather than structural failure (Ashford et al. 2011).

2.1.1. Observation of building performance during past earthquakes

Observations of building performance on liquefied sites during previous seismic events showed significant damage to the structures and surrounding lifelines. Excessive displacement of softened ground resulted in punching settlement, bearing failure, tilt, and lateral shifting of primarily buildings with shallow foundations.

In the 1964 Niigata (Japan) and the 1990 Luzon, Philippines earthquakes, most of the damaged buildings were two to four stories, founded on shallow foundations and relatively thick and uniform deposits of clean sand. The confining pressure and shear stresses imposed by the building were observed to affect its settlement (Tokimatsu et al. 1994). In the 1999 Kocaeli, Turkey earthquake, many of the damaged structures were influenced by the liquefaction of thin deposits of silt and silty sand (Sancio et al. 2004; Bray et al. 2000; Bird and

Bommer 2004). Building settlement was directly proportional to its contact pressure, and the building's height/width (H/B) aspect ratio greatly affected the degree of tilt (Sancio et al. 2004), showing the significance of building's dynamic properties influence on the total resulting settlement of its foundation. This led to guide geotechnical engineers' attention towards the importance of soil-foundation-structure interaction (SFSI) and its contribution to the seismic performance of shallow-founded structures on liquefiable ground.

More recently during the 2011, 6.1 M_w Christchurch, New Zealand earthquake, liquefaction-induced settlements of 1 to 2 m and tilts exceeding 2 degrees were observed in low- to mid-rise structures primarily on shallow foundations (Cubrinovski and McCahon 2012). Ground motions recorded on liquefiable sites showed amplified spectral content for frequencies less than about 0.5 Hz. The uplift forces from groundwater pressures caused floors to bulge upward and the foundations to damage and tilt due to lateral spreading. Similarly, during the 2011, 9.0 M_w Tohoku-Kanto, Japan earthquake, building damage in the Kanto region was dominated by liquefaction, not ground shaking alone (Ashford et al. 2011).

In summary, previous case histories showed damage to structures founded on liquefiable ground due to excessive settlement, tilt, and lateral shifting, which were affected by the properties of soil, structure, and ground motion. Although, these observations have helped improve our understanding of liquefaction and its effect on structure, they do not provide sufficient information to thoroughly understand the consequences of soil liquefaction, mitigation strategies, and dynamic SFSI, because of the inherent uncertainty associated with case histories. Physical model studies under more controlled conditions can help evaluate these effects and mechanisms more systematically, which can be used to calibrate and validate advanced numerical tools that are used in design.

2.2. Experimental Studies

Despite well-documented case histories, the relation between key ground motion characteristics and the response of building, in terms of settlement, tilt, lateral displacement, and subsequently building performance, associated with soil liquefaction are not well understood. Because of the uncertainties involved in interpreting case histories and limited instrumental recordings at key locations, physical modeling under controlled conditions provides valuable insights to improve understanding of liquefaction mechanism.

Several researchers have used reduced-scale shaking table and centrifuge tests in the past to study the response of rigid, shallow model foundations situated atop uniform deposits of saturated, loose to medium dense, clean sand (e.g., Yoshimi and Tokimatsu 1977; Liu and Dobry 1997; Hausler 2002). Yoshimi and Tokimatsu (1977) were first to identify the influence of shallow foundation contact area on the average settlement of buildings located on a liquefied sand deposit through the observations of Niigata Earthquake. This finding was later confirmed when they conducted a series of 1-g shaking table tests. Observations by Adachi et al. (1992) after the Luzon Earthquake also confirmed the relation between foundation contact area and its total permanent settlement; Buildings with larger foundation area settled less (although, the simultaneous influence of contact area and contact pressure was not mentioned).

Hausler (2002) used physical model tests and showed that most of the building settlement occurs during strong shaking (i.e., cyclic loading) and the contribution of volumetric settlement during post-shaking consolidation due to dissipation of excess pore water pressure is minor. The foundation settlement was observed to be larger compared to the free-field, and foundations settled in an approximately linear manner with time during cyclic loading. It was also recognized that building dynamic properties and soil-structure interaction influence the resulting settlement of buildings. Yet, the role of different soil, structure, and ground shaking properties on the performance of shallow-founded structures has not been well characterized.

A series of four centrifuge experiments were later performed by Dashti et al. (2010a,b) to identify the dominant mechanisms of building settlement on layered soil deposits, including a liquefiable layer of clean sand. These tests employed elastic, single-degree-of-freedom (SDOF) structural models with realistic fundamental frequencies (as opposed to a rigid mass) on liquefiable ground. The relative influence of various testing parameters and structural properties were investigated by Dashti et al (2010a,b). Conceptually, the study classified the primary settlement mechanisms as: (a) volumetric types: rapid drainage ($\varepsilon_{p\text{-}DR}$), sedimentation ($\varepsilon_{p\text{-}SED}$), and consolidation ($\varepsilon_{p\text{-}CON}$); and (b) deviatoric types: partial bearing capacity loss ($\varepsilon_{q\text{-}BC}$) and soil-structure-interaction (SSI) induced building ratcheting ($\varepsilon_{q\text{-}SSI}$). The relative importance of these mechanisms was found to depend strongly on several parameters: the liquefiable soil's initial relative density (D_r) and thickness, the presence of a low-permeability layer cap, ground shaking intensity, and the building's fundamental frequency, geometry, and foundation pressure. Further, these tests revealed that the settlement-time history of buildings during each earthquake followed the shape of the Arias Intensity-time history of the motion. Dashti et al. (2010b) showed that the slope of the Arias Intensity with respect to time (Shaking Intensity Rate, SIR) captures roughly the rate and timing of soil particle disturbance and the seismic demand on structures.

Previous studies have shown the important influence of SFSI on the deformation and inertial response of the underlying soil and the demand imposed on the structure (e.g., Stewart et al. 1999a,b; Pecker and Pender 2000; Martin and Lam 2000; Pitilakis et al. 2008; Dashti et al. 2010a; Chen et al. 2010; Kausel 2010). SFSI is generally described in terms of two mechanisms: 1) kinematic interaction, which is responsible for the difference between the motion far from the structure (i.e., free-field – FF) and the motion on a stiff foundation (i.e., foundation motion – FM); and 2) inertial interaction, which is controlled by the vibration and inertial response of the structural mass (Kramer and Stewart 2004). These two mechanisms are

active simultaneously, one often being more dominant depending on the properties of the soil-foundation-structure system.

When the building is treated as a rigid foundation load only, its dynamic properties and the influence of inertial interaction on its settlement and tilt potential are ignored. Inertial interaction is often ignored on softened ground, because the liquefying soil is assumed to act as a seismic isolator to the foundation (Karamitros et al. 2013). However, building's dynamic properties that control inertial interaction (e.g., mass, stiffness, height/width) have been shown to significantly influence the pore pressure generation and settlement trends near a structure (e.g., Dashti et al. 2010a,b), as well as its tilt potential (Sancio et al. 2004), which, in turn, influence building's overall performance and damage potential. Therefore, it is critical to consider the dynamic properties of the oscillator when evaluating its performance on liquefiable ground.

2.3. Numerical Studies

Following the recent advances in constitutive modeling and numerical method, researchers have conducted numerical simulations to investigate the response of foundations of structures in liquefiable ground. Popescu and Prevost (1993), Elgamal et al. (2005), Naesgaard et al. (1998), Cascone and Bouckovalas (1998), Bouckovalas et al. (2005), Popescu et al. (2006), Andrianopoulos et al. (2006, 2010), Lopez-Caballero and Farahmand-Razavi (2008, 2013), Shahir and Pak (2010), Dashti and Bray (2013), and Karamitros et al. (2013) conducted 2D (plane strain) and 3D, fully-coupled, nonlinear, finite element and finite difference analyses to numerically study the dynamic interaction between homogeneous and layered liquefiable sand and a structure. In these analyses, the structure was simulated either as a surface load, rigid structure, or an elastic SDOF or MDOF model on stiff, mat foundations. The foundation was mostly fixed to the soil mesh, assuming no relative movement at the interface. Most of these numerical simulations did not include a detailed verification process

to evaluate their ability in predicting SFSI and structural response on softened ground for a range of soil, structural, and ground motion properties.

Popescu and Prevost (1993) performed class A, 2D finite element numerical simulations with “plain strain” assumptions to validate a numerical tool against several centrifuge tests conducted at Princeton University and Cambridge University as a part of the VELACS (verification of liquefaction analysis by centrifuge studies) project (Arulmoli et al. 1992). A Class A prediction is one in which the numerical simulation is performed prior to the actual experiment being conducted (Lambe 1973). The saturated medium was modeled as a two-phase porous material using a multi-yield plasticity constitutive model with a simple J2 theory to model soil nonlinearity and cyclic shear-induced anisotropy. A rigid structure was used to model the building. Several important prescribed boundary conditions were implemented into the numerical simulations. They assumed nodes with the same elevation at the circumference of the finite element mesh had the same motion to simulate the movement of infinitely long horizontal soil layers (i.e., deep beam shear-type deformation). Acceleration was applied to the fixed nodes at the base of the model. Perfect friction at the soil-structure interface (not at the sides of the structure) was assumed. In other word, they directly connected soil and foundation nodes together without any interface element. Lastly, nodes at the boundary and at the soil-structure surface were set as impervious. In general, the numerically computed excess pore water pressure and acceleration responses were in the ranges of experiments, noting that numerical simulation results showed a more dilative response under the structure.

Elgamal et al. (2005) conducted 3D finite element numerical simulation using a more advance constitutive model to explore the performance of shallow founded structure. They conducted a series of solid-fluid, fully-coupled, nonlinear, dynamic, effective stress analyses with the previously calibrated Pressure-Dependent Multi-Yield (PDMY) plasticity surface constitutive model. The effect of superstructure was numerically modeled by only applying a

vertical distributed load to the soil surface. Their goal was to evaluate the effect of soil compaction and/or increased permeability on the settlement of the shallow foundation on liquefiable ground. No direct comparisons of numerical simulation results were made with experimental measurements, as their main goal was to demonstrate the promising capability of the numerical simulations in capturing the key response features of a liquefiable soil during cyclic loading. They showed that more advanced numerical tools are capable of capturing the overall behavior of soils due to liquefaction.

Shahir and Pak (2010) numerically simulated the previously conducted centrifuge experiments by Hausler (2002) to investigate the settlement of shallow-founded rigid box structures mounted on a 20 m-thick layer of liquefiable Nevada sand. They performed a series of 3D finite element numerical simulations followed by a parametric study, in which, they varied the relative density of the liquefiable layer (D_r≈30-50%), foundation pressure (q≈40-120 kPa), footing width (B≈3-60 m), and peak ground acceleration of the input base motion (PGA≈0.15-0.3 g). The prescribed boundary conditions were consistent with those used by Popescu and Prevost (1993). In these simulations, the value of hydraulic conductivity of the liquefiable sand was varied during different stages of cyclic loading as a function of peak excess pore pressure ratio, r_u, as presented by Shahir et al. (2012), in order to match the experimental values of excess pore pressure and settlement in the free-field. The critical state two-surface plasticity constitutive model (Dafalias and Manzari 2004) was employed in these simulations to model the monotonic and cyclic response of liquefiable sand. This model is based on the bounding surface plasticity theory (Dafalias 1986) within the framework of critical state soil mechanics (Schofield and Wroth 1986). It is worth mentioning that different versions of this model have been recently developed by several researchers to improve its capabilities in capturing plastic strain under constant stress ratio and hence, the prediction of post-liquefaction volumetric strains in liquefiable soils (e.g., Taiebat and Dafalias 2008; Boulanger

and Ziotopoulou 2013). In their numerical simulations, Shahir and Pak (2010) captured foundation settlement on softened ground (after soil hydraulic conductivity was varied as a function of r_u), and proposed an equation to estimate the settlement of rigid shallow-founded structures on homogeneous liquefiable deposits. However, this study did not comprehensively investigate the influence of the dynamic properties of structure (e.g., structures with realistic fundamental frequencies and inertial response), soil layering, and ground motions with different intensities, frequency contents, and durations on the integrated response of SFS system when founded on liquefiable ground. In addition, representing the building with a rigid box structure did not make it possible to quantify the seismic demand imposed onto the superstructure (e.g., maximum lateral drift). Considering these limitations, results of this study showed the ability of a well-calibrated numerical tool in capturing the key response parameters of soil and structure on softened ground. Further investigation and validation against experiments and case histories (with a wide range of conditions) is needed prior to the development of practical guidelines.

Dashti and Bray (2013) numerically simulated centrifuge experiments of layered soil profiles including a liquefiable layer with different linear-elastic, single-degree-of-freedom (SDOF) structures with rigid shallow foundations (Dashti et al. 2010a). They conducted class C, 2D, finite difference, fully-coupled nonlinear numerical simulations using the UBCSAND constitutive model (Puebla et al. 1997) and plain strain conditions. Class C predictions are those conducted after the experiment, while the experimental results are known to the predictor (Lambe 1973). Their main assumptions of the prescribed boundary conditions were similar to those of Popescu and Prevost (1993). The foundation and structure system were modeled by linear-elastic beam elements. Direct comparisons between numerical simulations and experiments were made to evaluate the capability of the numerical tool in capturing seismically-induced excess pore pressures and foundation settlements. Soil hydraulic

conductivity was decreased to capture the measured excess pore pressure response during strong shaking. A general agreement was observed between numerically computed and experimentally measured seismically-induced permanent foundation settlements, mostly within factors of 0.7 and 1.8 of the measured values. Although plain strain conditions cannot properly represent the 3D drainage conditions and the induced static and dynamic stress distributions in the underlying soil due to the presence of the superstructure, the numerical model could capture the primary mechanisms of settlement underneath the foundation relatively well (i.e., deviatoric strains and volumetric strains due to partial drainage).

2.4. Summary of Observations

Previous earthquakes have revealed that even buildings designed according to local seismic regulations may experience extensive damage due to soil liquefaction, including bearing capacity failure, excessive settlement, and tilting of shallow-founded structures. Observations from case histories, experimental studies, and numerical simulations point to the significant importance of SFSI effects in the integrated performance of the soil-structure system. The potential of liquefaction triggering and its adverse consequences on structures are controlled by the properties of soil (e.g., layering, relative density, thickness and depth of the liquefiable layer), structure (e.g., foundation contact pressure, footprint area, height over width ratio, and fundamental frequency), and importantly, ground motion (e.g., intensity, frequency content, and duration). A reliable evaluation of the liquefaction hazard and its consequences requires a good understanding of the influence and relative importance of these parameters.

The current state-of-practice for estimating building settlement on liquefiable deposits is still based on simplified empirical procedures developed for post-liquefaction consolidation settlements in the free-field, which are known to be unreliable for predicting the settlement of buildings. By ignoring the presence of the superstructure, these procedures ignore the static and dynamic stress distribution, drainage paths, and more importantly, dynamic SFSI effects

near structures. They also assume fully undrained conditions during earthquake loading, which may not be accurate (Dashti et al. 2010a). Hence, they are not able to capture the active and dominant mechanisms of displacement (e.g., deviatoric strain as well as volumetric strains due to partial drainage) underneath the foundation. Hence, they should not be used to estimate foundation settlement or tilt.

In addition to the estimation of foundation settlement and tilt, the seismic demand imposed on the superstructure itself is an important consideration for structural design. Knowledge of the characteristics of the ground motion experienced by the structure at the foundation level (FM), flexible-based modal frequencies of the structure (e.g., period lengthening), and inter-story drift ratio will provide structural engineers with more information to effectively design the structural elements on liquefiable ground (with or without mitigation).

Most of the previously conducted numerical simulations did not include a detailed verification process to evaluate their ability in predicting SFSI and structural response on softened ground for a range of soil, structural, and ground motions properties. A well-calibrated and validated numerical tool that is able to capture the key mechanisms of deformation near shallow-founded structures is expected provide important insights into the influence of SFSI and properties of soil, structure, and ground motion on the performance of the soil-structure system.

CHAPTER 3

NUMERICAL SIMULATIONS OF EARTHQUAKE INDUCED SOIL LIQUEFACTION: VALIDATION AGAINST CENTRIFUGE EXPERIMENTAL RESULTS

This chapter is based on the following reference:

Karimi, Z., and Dashti, S. (2015a). Numerical Simulation of Earthquake Induced Soil Liquefaction: Validation against Centrifuge Experimental Results. IFCEE 2015, Geo-institute, ASCE, USA, 11-20. doi: 10.1061/9780784479087.002.

3.1. Introduction

In numerical studies, soil-foundation-structure interaction (SFSI) effects are commonly evaluated employing equivalent-linear, visco-elastic soil models. In reality, soil response is nonlinear, particularly when it undergoes significant strength loss and softening, as in liquefaction. Previous case histories and experiments point to the need for fully-coupled, effective stress, nonlinear, dynamic analyses of the soil-structure system that capture the influence of key factors on the soil and building response and their interaction (e.g., Dashti et al. 2010; Dashti and Bray 2013). These analysis tools consider liquefaction triggering, post-liquefaction strength loss, and the resulting deformations simultaneously. Due to their

complexity, however, these tools need to be validated against physical model studies or case histories for a range of conditions before used in practice.

Two centrifuge experiments were performed at the University of Colorado Boulder to fundamentally study the response of soil and structure under a range of earthquake motions with different characteristics. These tests also enabled an evaluation of the capability of a state-of-the-art numerical tool in capturing the key response parameters and SFSI on softened ground. This chapter, presents a summary of the centrifuge testing program, numerical model calibration, and a brief comparison between class-C numerical predictions with centrifuge experimental results.

3.2. Centrifuge Testing Overview

3.2.1. Experiment layouts

Two centrifuge experiments were performed at the University of Colorado Boulder to evaluate the seismic response of a uniform layer of saturated, medium-dense, Nevada Sand in the free-field (1-D conditions) and in the vicinity of a shallow-founded structure (3-D). Soil response was monitored during a series of 1-D (horizontal) earthquake motions in terms of acceleration, excess pore pressure, and settlement at key locations with respect to the structure. 3-D motions could significantly influence soil and structural response, but are beyond the scope of this study. In this chapter we focus on acceleration and excess pore pressure patterns during two different earthquake base motions in the free-field and under the center of the structure.

The soil specimen was first spun to the target centrifugal acceleration level of 77 g. Then a series of ground motions were applied to the base of the model in flight. A series of six earthquake motions were selected as the base motion, to cover a wide range of characteristics as summarized in Table 3.1.

A transparent, Flexible-Shear-Beam (FSB) container (Ghayoomi et al. 2013) was used to construct the model specimen. The first experiment, Test FF, included a uniform layer of saturated Nevada Sand with prototype thickness (H_L) of 21.2 m and a nominal relative density (D_r) of approximately 60%, with no structure present (1-D free-field conditions). The second experiment, Test SFS, had the same soil properties as Test FF but with an added structure placed at the center of the container. The setup and instrumentation layout of both tests are shown in Figure 3.1. The models were spun at a centrifugal acceleration off 77 g. All dimensions presented are in prototype scale.

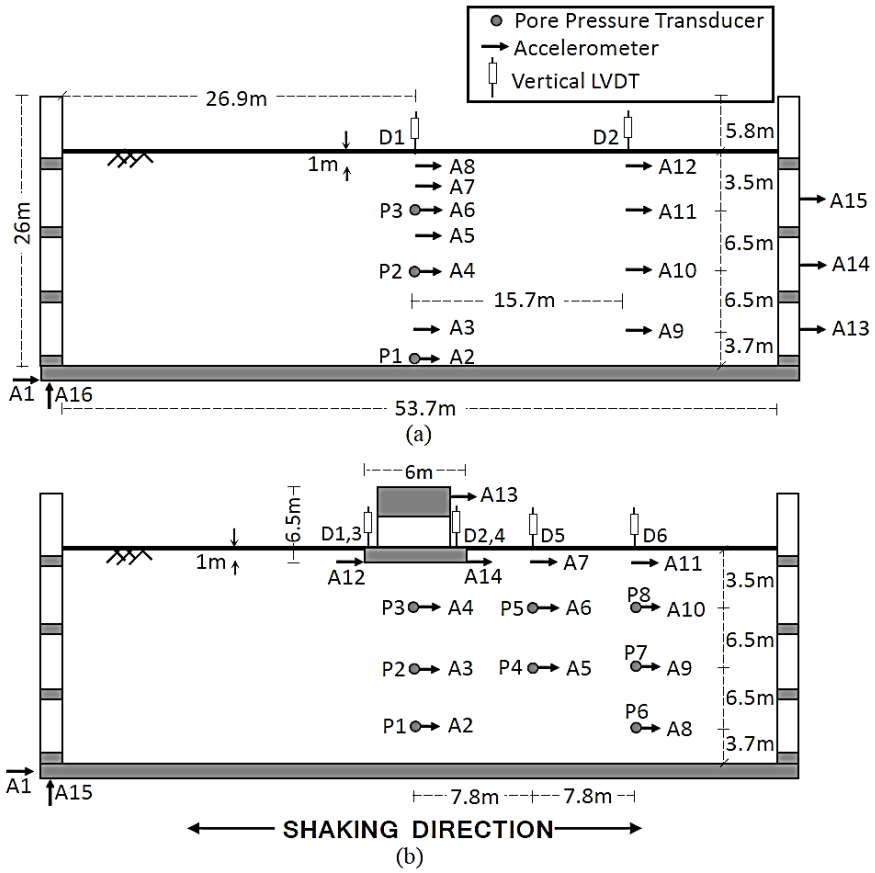

Figure 3. 1. Centrifuge experiment instrumentation layout: (a) Test FF, (b) Test SFS. All dimensions are provided in prototype scale units.

3.2.2. Soil properties

The deposit of uniform, fine Nevada Sand (No. 120) with e_{min}≈0.55 and e_{max}≈0.843 was dry-pluviated using a barrel hopper at a constant drop height to attain D_r≈60% in both tests. The models were saturated with a solution of hydroxypropyl methylcellulose in water (Stewart et al. 1998) to achieve a viscosity of approximately 33 times that of water to speed up the saturation process.

Table 3. 1. Base Ground Motion Characteristics (as Measured)

Event	**Year**	**M_w**	**Station**	**PGA (g)**	**Tp (s)**	**AI (m/s)**	**$D_{5\text{-}95}$ (s)**
Landers	1992	7.3	Joshua Tree	0.33	0.64	2.78	27
Loma Prieta	1989	7.0	Santa Cruz Lick Observ.	0.33	0.16	2.12	11.34
Northridge	1994	6.7	Newhall W Pico Canyon	0.6	0.4	1.98	13.88
Chi-Chi	1999	7.6	TCU078	0.47	0.34	6.03	28.76
Landers	1992	7.3	Lucerne	0.55	0.28	7.06	14.12
Kobe	1995	6.9	Takatori	0.76	0.4	9.16	25.78

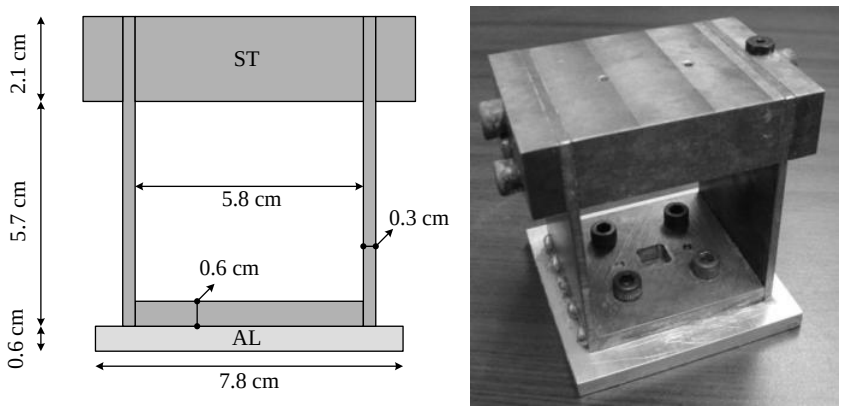

Figure 3. 2. The structural model used in centrifuge testing: (a) schematic drawing (dimensions shown in model-scale); and (b) photograph of the assembled model.

3.2.3. Structural properties

A single-degree-of-freedom (SDOF) structural model made of steel and aluminum was placed on a 1 m-thick, stiff mat foundation with height over width ratio of H/B≈2 and a bearing pressure of q≈80 kPa in Test SFS. Approximately 73% of the total mass was attributed to the oscillator and the remaining to the foundation. A schematic drawing and a photograph of the assembled structural model are shown in Figure 3.2. Once assembled, thin, light-weight plastic pieces were glued to the edges of the foundation to prevent sand from falling in from all sides, as the foundation was embedded in the soil. Model structure was secured on a 1-g shaking table and a white noise acceleration time history was applied to the base of the model structure. This test and a hammer test was used to measure fixed-based natural frequency and damping ratio of the structure.

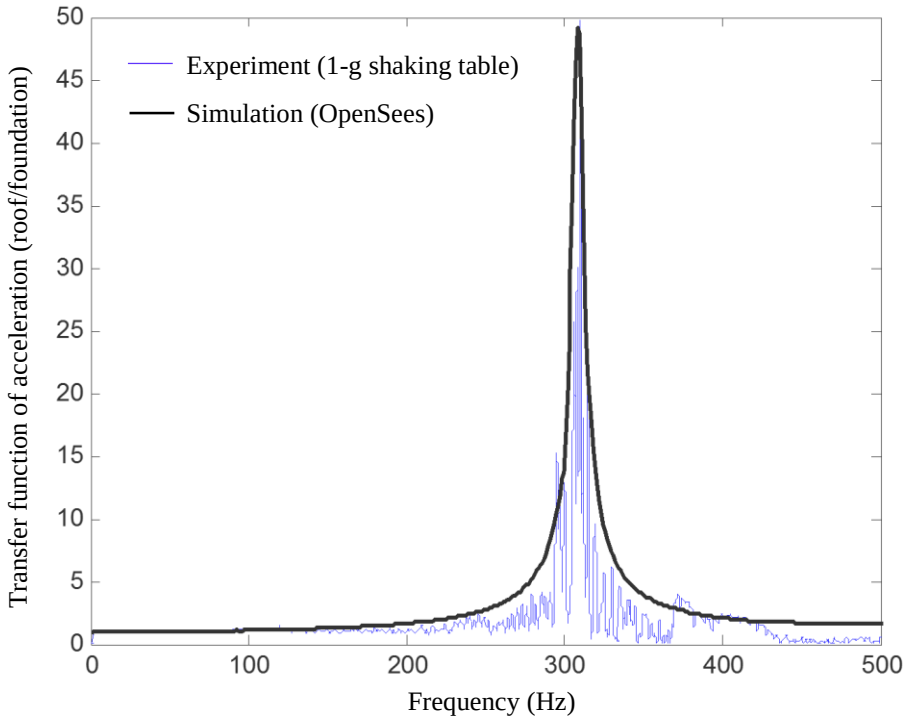

Figure 3. 3. Transfer function of acceleration (roof/foundation) for model structure based on 1-g shake table excitation experiment and numerical simulation in OpenSees.

The fixed-based natural frequency of the structure was measured as 315 Hz at 1 g, corresponding to 4 Hz in prototype scale at 77 g. Figure 3.3 shows the numerically simulated and experimentally measured (i.e., using 1-g shaking table test) transfer function of accelerations on top of the mass to the fixed base of the structure.

3.3. Numerical Simulations

Three-dimensional (3-D), fully-coupled, nonlinear finite element simulations were performed in the OpenSees v.2.4.3 platform (Mazzoni et al. 2006) to evaluate the capability of a state-of-the-art constitutive model to capture soil response in the free-field and near a building. The saturated soil was modeled as a two-phase material based on the Biot theory (Biot 1962) for porous media, in which displacement of the soil skeleton (u) and pore pressure (p) are the primary unknowns (u-p formulation).

The soil elements were modeled using 8-node brick u-p elements. The pressure-dependent multiple-yield-surface (PDMY02) constitutive model (Elgamal et al. 2002; Yang et al. 2003; Yang et al. 2008) was used for soil. The yield criteria are defined by the number of open conical shaped yield surfaces with their apex at the origin. This model uses a non-associative flow rule that develops volumetric dilation and contraction under shear deformation. The plastic flow in this model is purely deviatoric. Hence, no plastic change of volume takes place under a constant stress ratio.

The model structure was initially simulated under fixed-based conditions and the results compared with 1-g tests to confirm its natural frequency and damping, before connecting the structure to soil elements. The mat foundation was modeled using brick elements and linear elastic material properties. Linear elastic column elements and a rigid diaphragm was used to model the SDOF structure. Figure 3.4 shows the finite element discretization of the soil-foundation-structure system.

The foundation was connected to the soil using equal degrees of freedom. All surrounding nodes of the soil medium were impervious except those at the surface. In order to model 1-D wave propagation in a 3-D space, all circumferential soil nodes at the same elevation were assumed to have the same displacement using the master/slave node technique in OpenSees. The motions recorded in centrifuge at the base of the container were applied to the base nodes. The value of hydraulic conductivity was calculated according to the scaling laws and the viscosity of the pore fluid used in centrifuge, which was assumed to remain constant throughout the time of shaking. The fluid bulk modulus was estimated assuming a soil degree of saturation of approximately $S_r \approx 98\text{-}100\%$, which was judged appropriate based on previous studies (Byrne et al. 2004; Dashti and Bray 2013). The maximum allowable element size was calculated at each depth based on the soil's shear wave velocity profile and the maximum frequency content of the ground motions (e.g., 15 Hz after filtering). Due to the large size of the simulation, the parallel version of OpenSees (OpenSees SP) was used in this study on a High Performance Computer (HPC).

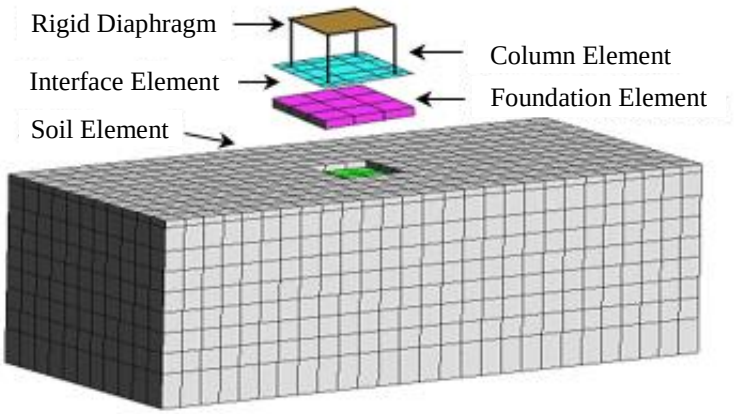

Figure 3. 4. Finite element model of the structure-foundation-soil system.

In both Test FF and SFS, the same motion sequence (Table 3.1) was applied to the container base. The soil densified substantially after each shake (e.g., volumetric strain due to the first motion ≈3.1%), significantly changing the soil relative density prior to the next motion.

Based on the settlement measurements at the surface, an average relative density of 80% was estimated in the free-field after the first motion.

The soil model parameters were calibrated to capture the response of saturated Nevada Sand as observed during previous cyclic simple shear (CSS) tests with different overburden stresses and relative densities (Arulmoli et al. 1992; Kammerer et al. 2000). The calibrated soil model parameters are summarized in Table 3.2. A comparison of experimentally measured and numerically predicted soil response during a representative cyclic simple shear test (D_r=63%, σ'_{vo}=80 kPa, and CSR=0.3) is presented in Figure 3.5. The relation between the corrected SPT blow count ($N_{1,60}$) and cyclic stress ratio (CSR= τ/σ'_{vo}) to cause liquefaction (3% single-amplitude shear strain) in 15 cycles obtained from the numerical simulations is compared with NCEER's relation (NCEER 1997) in Figure 3.6.

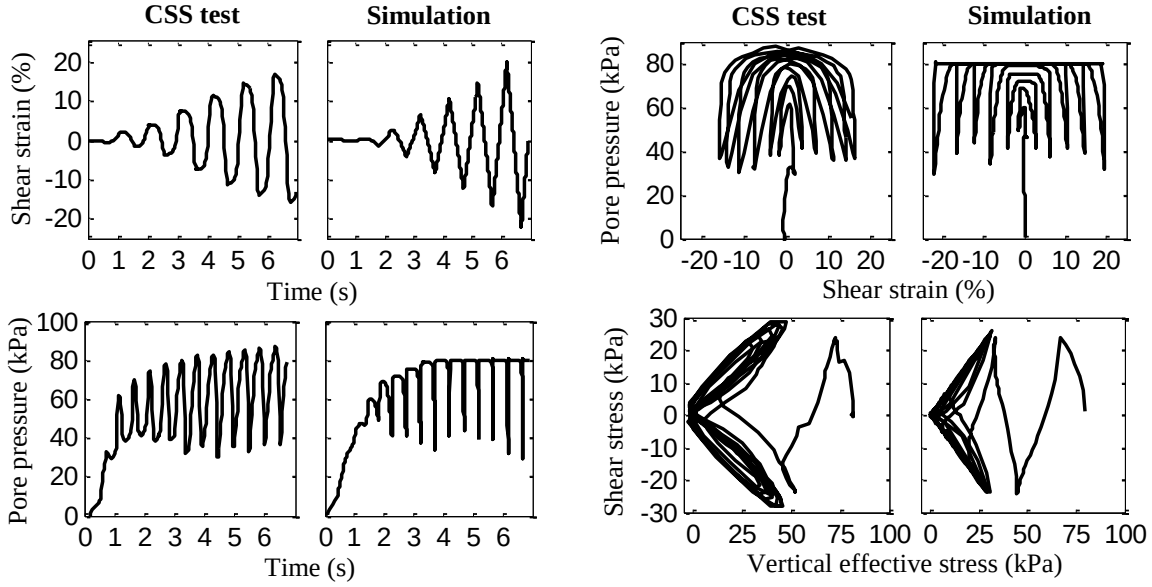

Figure 3. 5. Comparison of the simulated and measured response during a Cyclic Simple Shear (CSS) test performed on (Dr=63%, σ'_{vo}=80 kPa, and CSR=0.3).

3.4. Comparison Between Numerical and Centrifuge Results

This section provides a comparison of numerical simulations with centrifuge experimental results in terms of excess pore pressures and accelerations at key locations with

respect to the structure during the first two motions (Landers JT and Loma Prieta). To better quantify the capability of the numerical simulations in capturing the dynamic response of soil and structure, residuals were calculated between numerical and experimental results as:

$$\text{Residual } X = \log\left(X_{\text{experimental}} / X_{\text{numerical}}\right) \tag{3.1}$$

where X refers to a given quantity in time or frequency domain, which was measured in the experiment or numerically computed. A positive residual indicates that the numerical predication underestimated experimental observations, and vice versa.

Table 3. 2. Calibrated PDMY02 model parameters for Nevada Sand (No. 120) at different relative densities.

Dr (%)	**63%**	**68%**	**90%**	**Description**
$P_r^{'}$ (kPa)	101	101	101	Reference effective confining pressure at which other model parameters are calibrated
$G_{max,1,oct}$ (MPa)	72.5	77.1	101.9	Octahedral low-strain shear modulus at $P_r^{'}$ (1 atm)
$\gamma_{max,r}$	0.1	0.1	0.1	Maximum octahedral shear strain
B_r (MPa)	193.6	205.9	272.1	Bulk modulus
d	0.5	0.5	0.5	Pressure dependency coefficient
φ_{TXC}	34.5 ^{o}	36^o	40.0 ^{o}	Triaxial friction angle used in the model.
φ_{PT}	26.5 ^{o}	26 ^{o}	26.5 ^{o}	Phase transformation angle
c_1	0.04	0.02	0.016	Non-negative parameter that controls the shear-induced volumetric change
c_2	2.5	1.5	1.45	Non-negative constant that reflects contraction tendency based on the dilation history or fabric damage
c_3	0.2	0.15	0.14	Accounts for the overburden stress effect
d_1	0.07	0.15	0.25	Reflects the dilation tendency (along with friction angle and phase transformation angle) above PT angle
d_2	3.0	3.0	3.0	This value reflects fabric damage (stress history)
d_3	0.0	0.0	0.0	This parameter with c_3 accounts for overburden stress (K_σ effect); this effect can be accounted for by c_3 solely

3.4.1. Excess pore pressure response

Figures. 3.7 and 3.8 compare experimentally measured and numerically computed excess pore pressure time histories at different depths in Test FF (free-field) and in Test SFS (under the center of the foundation) during the first motion respectively. The comparisons show

reasonable agreement. The higher resistance of soil to liquefaction triggering under the higher overburden stress of the foundation is evident experimentally (e.g., lower excess pore pressure ratios $r_u = p_{excess}/\sigma_v^{'}$ at shallow depths under the footing), which was captured successfully numerically.

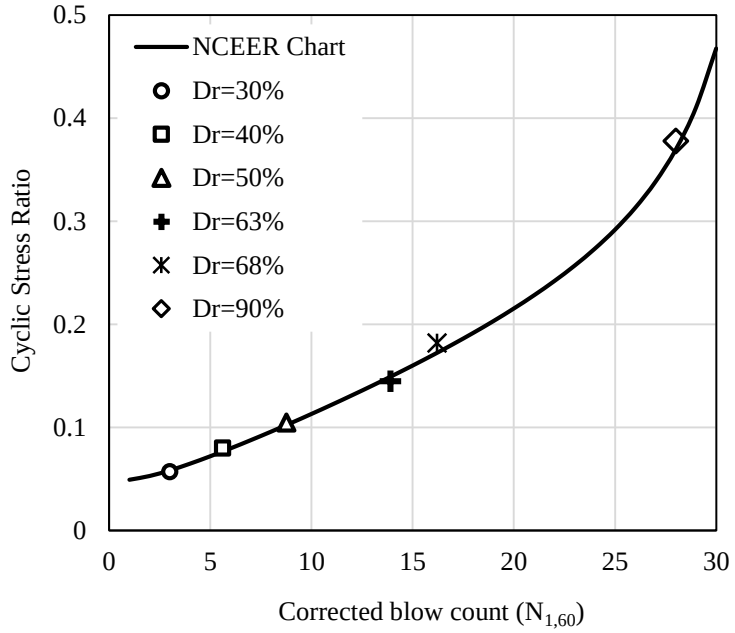

Figure 3. 6. Relationship between $N_{1,60}$ and Cyclic Stress Ratio (CSR) for liquefaction in 15 cycles in simulations compared with NCEER (1997).

3.4.2. Acceleration Response

Figure 3.9 shows representative acceleration time histories at different depths in Test FF during the first shake obtained experimentally and numerically. De-amplification of accelerations due to liquefaction-induced soil softening was observed both in numerical simulations and experiments. In Test SFS, liquefaction (with a definition of r_u = 1.0) was not observed at shallow depths under the footing during these ground motions, due to a higher foundation overburden stress. Hence, the softening behavior or acceleration de-amplifications was not observed experimentally compared to the equivalent free-field case. As the influence of foundation overburden stress reduced with depth, the results of Tests FF and SFS started to converge.

Residuals between the numerical and experimental Arias Intensities (I_a) and 5%-damped Spectral Accelerations (S_a) at different depths in Test FF during the first two motions are shown in Figure 3.10. Numerical simulations show a reasonable match with experiments in terms of S_a in both events (residuals ranging from -1 to 1 in frequencies 0.1 to 10 Hz). The numerical simulations tended to under-predict or over-predict Arias Intensities depending on the event, with residuals ranging from -1.5 to 1.

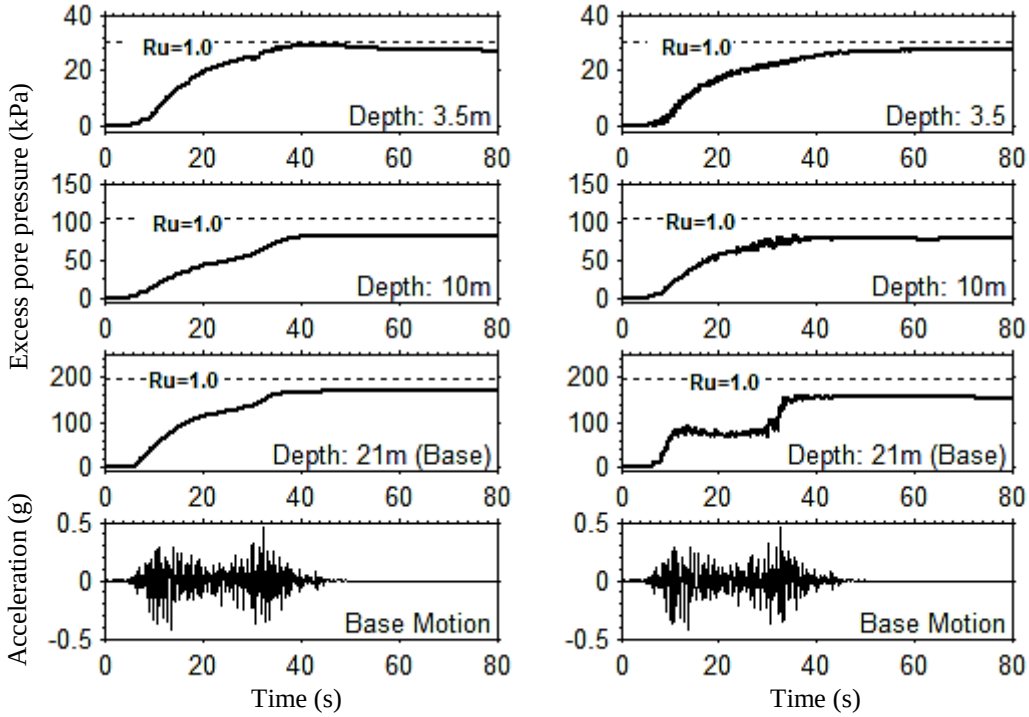

Figure 3. 7. Numerically computed (left column) and experimentally measured (right column) excess pore pressure time histories at different depths of the free-field model during the Landers JT event.

The transmissibility function between the acceleration recorded on the foundation and in the free-field soil (both at a depth of 1m) may be used to evaluate the impact of kinematic and inertial interaction on the translational component of foundation motion. The transmissibility function, TF(f), was calculated as:

$$TF(f)=\sqrt{S_{yy}(\omega)/S_{xx}(\omega)} \tag{3.2}$$

where S_{xx} and S_{yy} are power spectral density functions of input (free-field soil surface) and output (foundation) accelerations respectively (Kim and Stewart 2003). Numerical and experimental transmissibility functions during the first motion are compared in Figure 3.11, which shows reasonable agreement. Importantly, contrary to previous observations of SFSI on dry sand, foundation accelerations did not reduce in amplitude compared to the free-field (Mason 2011), likely due to larger excess pore pressures generated in the free-field.

3.5. Conclusion

Two centrifuge experiments were performed to evaluate the dynamic response of soil, structure, and their interaction on saturated, medium-dense sand under a range of broadband earthquake motions with different characteristics. These tests also enable a comprehensive evaluation of the ability of a state-of-the-art numerical tool in capturing the key response factors under general loading conditions. Experimentally measured and numerically computed excess pore pressures and accelerations at key locations with respect to the structure were in reasonable agreement. The higher resistance of soil to liquefaction triggering under the higher overburden stress of the foundation that was observed experimentally was also captured numerically. Neither experimental nor numerical simulations showed a decrease in foundation accelerations (which include kinematic and inertial interaction effects) compared to the free-field soil. Instead, the results indicated large peaks at certain frequencies that may be detrimental to the structure if not taken into account in design.

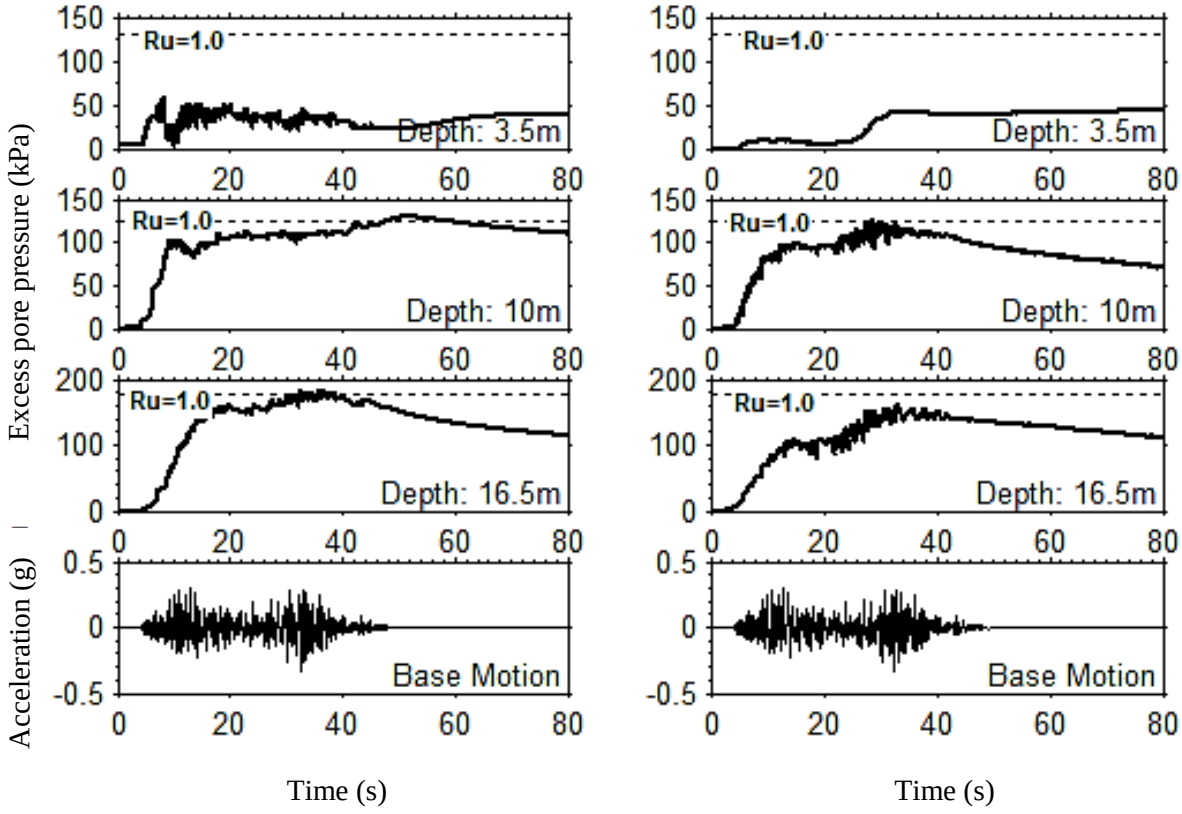

Figure 3. 8. Numerically computed (left column) and experimentally measured (right column) excess pore pressure time histories at different depths under the center of the foundation during the Landers JT event.

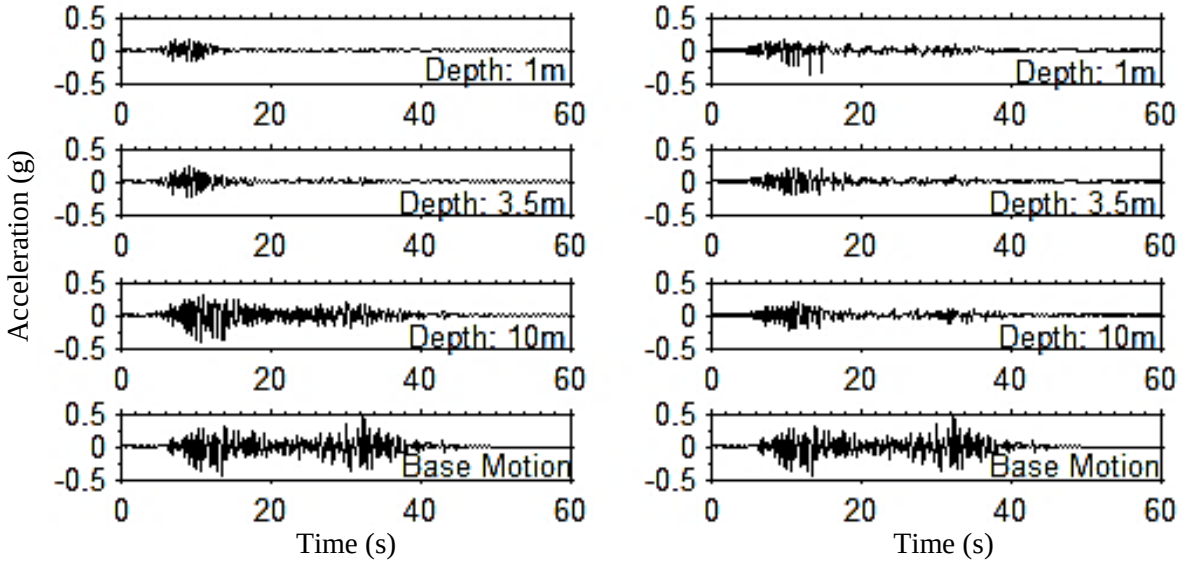

Figure 3. 9. Numerically computed (left column) and experimentally measured (right column) acceleration time histories at different depths of the free-field model during the Landers JT event.

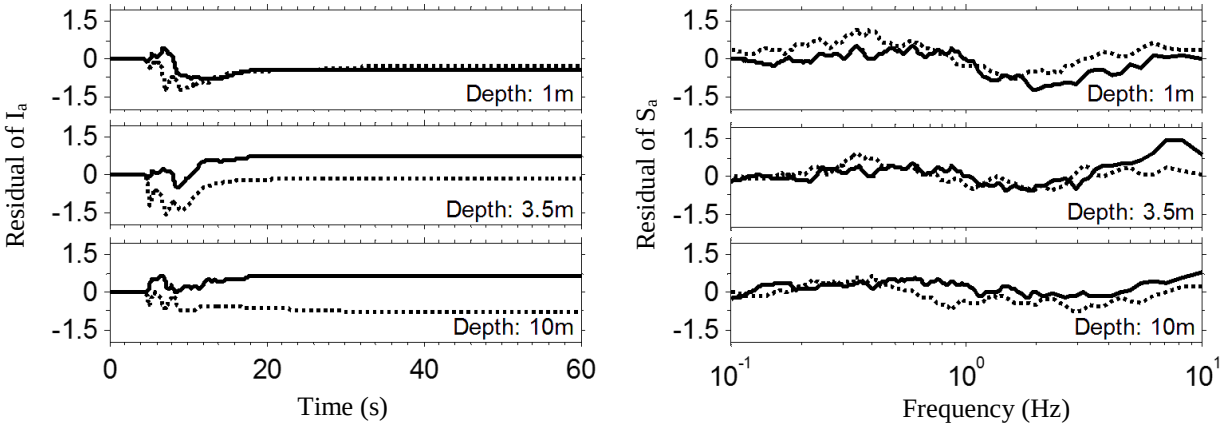

Figure 3. 10. Residuals between the numerical and experimental Arias Intensities (left column) and 5%-damped spectral accelerations (right column) at different depths of the free-field model during the Landers JT (dotted lines) and Loma Prieta (solid lines) events.

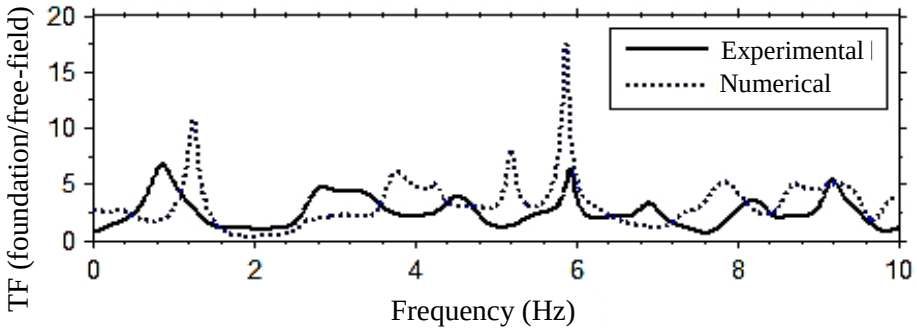

Figure 3. 11. Numerical and experimental transmissibility functions of foundation to free-field acceleration during the Landers JT motion.

CHAPTER 4

NUMERICAL AND CENTRIFUGE MODELING OF SEISMIC SOIL-FOUNDATION-STRUCTURE INTERACTION ON LIQUEFIABLE GROUND

This chapter is based on the following reference:

Karimi, Z., and Dashti, S. (2015b). Numerical and Centrifuge Modeling of Seismic Soil–Foundation–Structure Interaction on Liquefiable Ground. J. Geotech. Geoenviron. Eng., 10.1061/(ASCE)GT.1943-5606.0001346 , 04015061.

4.1. Introduction

Liquefaction continues to pose a significant risk of damage to the built environment. Liquefaction-induced settlement, tilt, and lateral sliding, which mostly affected buildings on shallow foundations and their surrounding lifelines, caused severe damage and economic losses in Christchurch following the 2010-2011 sequence of earthquakes (Green et al. 2011; Cubrinovski and McCahon 2012). In many cases, the structures were uneconomical to repair and were demolished. Future earthquakes in major cities around the world are expected to continue causing liquefaction-related damage.

Effective mitigation of the liquefaction hazard requires a thorough understanding of the potential consequences of liquefaction. The consequences of liquefaction in terms of ground shaking, permanent displacements, and building performance, in turn, depend on site

conditions, earthquake loading characteristics, and building properties. The presence of a structure affects the static and dynamic stresses and flow patterns in the underlying soil in a three-dimensional (3D) manner, which strongly influence liquefaction triggering and the resulting accelerations and deformations. Yet, the current state of practice for evaluating liquefaction-induced building settlement still relies on empirical procedures that assume free-field conditions (e.g., Tokimatsu and Seed 1987; Ishihara and Yoshimine 1992). These methods ignore the presence of the structure, its interaction with the underlying liquefiable soil, and the key displacement mechanisms that are active under a structure. Hence, they cannot reliably evaluate the consequences of liquefaction, the need for ground improvement, and the subsequent evaluation of the proposed mitigation scheme in terms of improved building response.

A solid-fluid, fully-coupled, 3D, dynamic, nonlinear, effective stress analysis is expected to provide valuable insight into the soil's nonlinear response, soil-foundation-structure-interaction (SFSI), and building performance. Triggering of liquefaction, post-liquefaction instability, and the resulting displacements can be considered in a single time-domain analysis. These models are, however, complex, have many parameters, and are often developed based on a limited set of laboratory test data that do not cover a variety of loading paths. Hence, they need to be validated rigorously against physical model studies for a range of structures, soils, and ground motion characteristics before used in practice or employed in a parametric study.

A series of centrifuge experiments were performed by Dashti et al. (2010a,b) to investigate the response of single-degree-of-freedom (SDOF) structures on stiff, mat foundations founded on a layered soil deposit including a liquefiable layer under a range of earthquake motions. These experiments enabled a comprehensive study of the underlying mechanisms of settlement under structures and the role and relative importance of various

testing parameters. Subsequently, Class C, solid-fluid, fully-coupled, nonlinear numerical simulations of the centrifuge tests were performed using the pressure-dependent, multi-yield-surface, nonlinear, plasticity-based soil constitutive model (PDMY02) implemented in OpenSees (Elgamal et al. 2002; Yang et al. 2003 and 2008). The prediction classification used in this study is that described by Lambe (1973). A Class C prediction is one made after the event being predicted has occurred and the results are known to the predictor. In this study, the author evaluates the capabilities and limitations of this numerical tool in capturing the response of soil, structure, and their interaction during a range of earthquake motions as observed in centrifuge. Numerically predicted accelerations, excess pore water pressures, and settlements in the free-field and near-field are compared against experimental measurements in both time and frequency domains, in addition to the building's tilting tendency and maximum roof drift. A comprehensive understanding of the capabilities and limitations of this numerical model is a necessary step before it may be employed reliably in predicting structural response under more general conditions.

4.2. Background

Observations of building performance on liquefied sites during previous earthquakes showed punching settlement, bearing failure, tilt, and lateral shifting of buildings. In the 1964 Niigata (Japan) and the 1990 Luzon (Philippines) Earthquakes, most of the damaged buildings were two to four stories, founded on shallow foundations and relatively thick and uniform deposits of clean sand. The confining pressure and shear stresses imposed by the building were observed to affect its settlement (e.g., Tokimatsu et al. 1994). In the 1999 Kocaeli (Turkey) Earthquake, many of the damaged structures were influenced by the liquefaction of thin deposits of silt and silty sand (Sancio et al. 2004; Bray et al. 2000; Bird and Bommer 2004). Building settlement was directly proportional to its contact pressure, and the building's

height/width (H/B) aspect ratio greatly affected the degree of tilt (Sancio et al. 2004), showing the importance of building's dynamic properties.

More recently during the M_w 6.1, 2011 Christchurch (New Zealand) Earthquake, liquefaction-induced settlements of 1 to 2 m and tilts exceeding 2 degrees were observed in low- to mid-rise structures primarily on shallow foundations (Cubrinovski and McCahon 2012). Ground motions recorded on liquefiable sites showed amplified spectral content for frequencies less than about 0.5 Hz. The uplift forces from groundwater pressures caused floors to bulge upward and the foundations to damage and tilt due to lateral spreading. Similarly, during the M_w 9, 2011 Tohoku-Kanto (Japan) Earthquake, building damage in the Kanto region was dominated by liquefaction, not ground shaking alone (Ashford et al. 2011).

Despite these well-documented case histories, the relation between key ground motion characteristics and the response of building (in terms of settlement, tilt, lateral displacement, and subsequently building performance) associated with soil liquefaction are not well understood. Because of the uncertainties involved in interpreting case histories and limited instrumental recordings at key locations, physical modeling under controlled conditions provides valuable insights to improve understanding of liquefaction. Several researchers have used reduced-scale shaking table and centrifuge tests in the past to study the response of rigid, shallow model foundations situated atop uniform deposits of saturated, loose to medium dense, clean sand (e.g., Yoshimi and Tokimatsu 1977; Liu and Dobry 1997; Hausler 2002). A series of four centrifuge experiments were later performed by Dashti et al. (2010a,b) to identify the dominant mechanisms of building settlement on layered soil deposits, including a liquefiable layer of clean sand. These tests employed elastic, single-degree-of-freedom (SDOF) structural models with realistic fundamental frequencies (as opposed to a rigid mass) on liquefiable ground (as shown in Figure 4.1). The relative influence of various testing parameters and structural properties was investigated. Conceptually, the study classified the primary settlement

mechanisms as: (a) volumetric types: rapid drainage ($\varepsilon_{p\text{-}DR}$), sedimentation ($\varepsilon_{p\text{-}SED}$), and consolidation ($\varepsilon_{p\text{-}CON}$); and (b) deviatoric types: partial bearing capacity loss ($\varepsilon_{q\text{-}BC}$) and soil-structure-interaction (SSI) induced building ratcheting ($\varepsilon_{q\text{-}SSI}$).

The relative importance of these mechanisms was found to depend strongly on several parameters: the liquefiable soil's initial relative density (D_r) and thickness, the presence of a low-permeability layer cap, ground shaking intensity, and the building's fundamental frequency, geometry, and weight. Further, these tests revealed that the settlement-time history of buildings during each earthquake followed the shape of the Arias Intensity-time history of the motion. Dashti et al. (2010b) showed that the slope of the Arias Intensity with respect to time (Shaking Intensity Rate, SIR) captures roughly the rate and timing of soil particle disturbance and the seismic demand on structures.

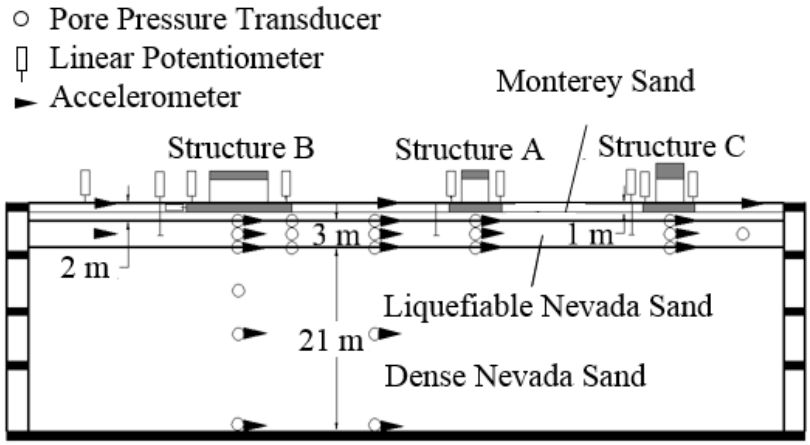

Figure 4. 1. Centrifuge model layout in experiment T3-30 (all dimensions are given in prototype scale meters).

Previous studies have shown the important influence of SFSI on the deformation and inertial response of the underlying soil and the demand imposed on the structure (e.g., Stewart et al. 1999a,b; Pecker and Pender 2000; Martin and Lam 2000; Pitilakis et al. 2008; Dashti et al. 2010a; Chen et al. 2010; Kausel 2010). SFSI is generally described in terms of two mechanisms: 1) kinematic interaction, which is responsible for the difference between the

motion far from the structure (i.e., free-field – FF) and the motion on a stiff foundation (i.e., foundation motion – FM); and 2) inertial interaction, which is controlled by the vibration and inertial response of the structural mass (Kramer and Stewart 2004). These two mechanisms are active simultaneously, one often being more dominant depending on the properties of the soil-foundation-structure system.

When the building is treated as a rigid foundation load only, its dynamic properties and the influence of inertial interaction on its settlement and tilt potential are ignored. Inertial interaction is often ignored on softened ground, because the liquefying soil is assumed to act as a seismic isolator to the foundation (Karamitros et al. 2013). However, building's dynamic properties that control inertial interaction (e.g., mass, stiffness, height/width) have been shown to significantly influence the pore pressure generation and settlement trends near a structure (e.g., Dashti et al. 2010a,b), as well as its tilt potential (Sancio et al. 2004), which, in turn, influence building's overall performance and damage potential. Therefore, it is critical to consider the dynamic properties of the oscillator when evaluating its performance on liquefiable ground.

Popescu and Prevost (1993), Naesgaard et al. (1998), Cascone and Bouckovalas (1998), Elgamal et al. (2005), Bouckovalas et al. (2005), Popescu et al. (2006), Andrianopoulos et al. (2006, 2010), Lopez-Caballero and Farahmand-Razavi (2008, 2013), Shahir and Pak (2010), Dashti and Bray (2013), and Karamitros et al. (2013) conducted 2D (plane strain) and 3D, fully-coupled, nonlinear, finite element and finite difference analyses to numerically study the dynamic interaction between homogeneous and layered liquefiable sand and a structure. In these analyses, the structure was simulated either as a surface load, rigid structure, or an elastic SDOF or MDOF model on stiff, mat foundations. The foundation was mostly fixed to the soil mesh, assuming no relative movement at the interface. Most of these numerical simulations did not include a detailed verification process to evaluate their ability in predicting SFSI and

structural response on softened ground for a range of soil, structural, and ground motions properties.

This chapter presents an integrated modeling approach in which triggering of liquefaction, post-liquefaction instability, the resulting displacements and ground shaking, and the response of a SDOF structure are considered simultaneously. This approach brings in the complexities of soil and structure, validated to results of centrifuge tests, in order to more accurately evaluate SFSI and the performance of structures on softened ground in terms of foundation acceleration, settlement, tilt, and maximum roof drift.

4.3. Centrifuge Testing Overview

4.3.1. experimental layout

A series of four dynamic centrifuge experiments were performed by Dashti et al. (2010a,b) to investigate the seismic response of SDOF structures on stiff, mat foundations founded on a layered soil deposit including a liquefiable layer. This chapter focuses on the response of one structure (Structure A) in two centrifuge tests, T3-30 and T3-50, which had a liquefiable layer thickness (H_L) = 3 m (in prototype scale) and relative densities (D_r) ≈ 30 and 50%, respectively. The instrumentation layout of centrifuge experiment T3-30 is shown in Figure 4.1 The models were spun to a nominal centrifugal acceleration of 55g prior to the application of base motions. All units presented in this chapter are in prototype scale, unless stated otherwise.

4.3.2. Soil properties

The lower deposit of uniform, fine Nevada sand (D_{50} = 0.14 mm, C_u =2.0, e_{min} = 0.55, e_{max} = 0.84) was dry pluviated to attain D_r ≈ 85% and thickness of 21 m. The same Nevada sand with D_r ≈ 30 or 50% and H_L =3 m was then dry pluviated as the liquefiable material. Monterey 0/30 sand (D_{50} = 0.40 mm, C_u = 1.3, e_{min} = 0.54, e_{max} = 0.84) was placed at D_r ≈ 85%

with a thickness of 2 m as the surficial layer to minimize capillary rise and liquefaction directly below the foundation. The models were saturated below a depth of 1 m with a solution of hydroxypropyl methylcellulose in water (Stewart et al. 1998) to achieve a viscosity of approximately 22 times that of water.

4.3.3. Structural properties

In this chapter, only the performance of Structure A located at the center of the container in both tests is evaluated. Structure A was a model SDOF structure made of steel and aluminum placed on a 1 m-thick, stiff mat foundation with a bearing pressure of approximately 80 kPa. The fixed-base natural frequency (f_n) of the structure was designed to be ≈ 2.5 Hz. Figure 4.2 shows a photograph of Structure A and the foundation along with dimensions in model scale. The embedment depth of the foundation was 1 m.

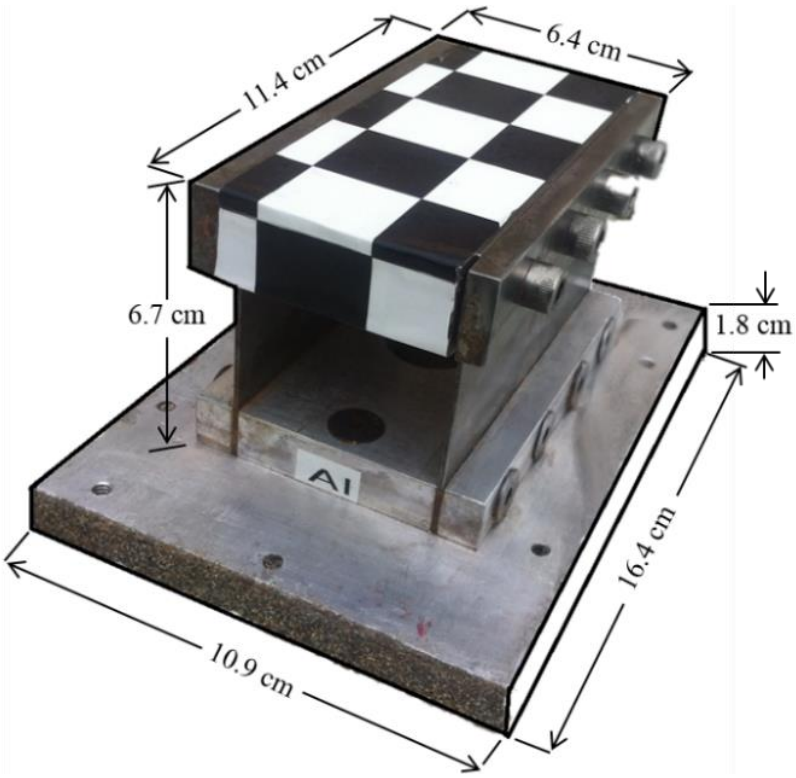

Figure 4. 2. Photo of Structure A used in the centrifuge experiments T3-30 and T3-50 with dimensions shown in model scale.

4.3.4. Ground motion properties

In each experiment, a series of earthquake motions were applied to the base of the container consecutively. A list of the base motions (as recorded) and their properties are presented in Table 4.1 in order of their application in each experiment. The earthquake motions were selected to cover a range of intensities, durations, and frequency contents, in order to enable a comprehensive evaluation of SFSI on softened ground. The PGA, PGV, and PGD values in Table 4.1 are the maximum absolute values of acceleration, velocity, and displacement for each base motion. Arias Intensity (I_a) is a more holistic ground motion intensity measure (Arias 1970) and is defined as:

$$I_a = \frac{\pi}{2g}\int_0^D a^2(t)\,dt \tag{4.1}$$

where a(t) is the acceleration time history, g is the gravitational acceleration, D is the duration of the motion, and t is time. Shaking Intensity Rate (SIR) was introduced by Dashti et al. (2010b) as:

$$SIR = I_{a(5\text{-}75)}/D_{5\text{-}75} \tag{4.2}$$

where $I_{a(5\text{-}75)}$ is the change in Arias Intensity from 5 to 75% of its total value, and $D_{5\text{-}75}$ is its corresponding time duration. And lastly, $D_{5\text{-}95}$ is the significant duration of the base motion, the time corresponding to a change in Arias Intensity from 5 to 95% of its total value (Husid 1969).

4.4. Numerical Simulations

Class C, 3D, nonlinear, solid-fluid, fully-coupled, effective stress, dynamic finite element (FE) analyses were performed in the OpenSees platform (Mazzoni et al. 2006) to numerically simulate SFSI on liquefiable ground. The goal was to evaluate the capability of a state of the art numerical model in capturing the response of soil, structure, and their interaction on liquefiable ground as observed in centrifuge. 3D simulations were conducted to better represent

a boundary value problem with a 3D stress field and flow pattern (Elgamal 2007, Fenves 2003). OpenSees is an object oriented software framework to model the response of structural and geotechnical systems.

Table 4. 1. Base motion properties in centrifuge experiments T3-30 and T3-50 (as Measured).

#	Test ID		Record	PGA (g)	PGV (cm/s)	PGD (cm)	I_a (m/s)	SIR (m/s/s)	$D_{5\text{-}95}$ (s)
1	T3-30	SM PI	Small Port Island 1995 Kobe	0.04	6.97	2.06	0.02	0.003	7.9
2		MD PI	Moderate Port Island 1995 Kobe	0.17	25.61	7.19	0.50	0.08	8
3		LG PI	Large Port Island 1995 Kobe	0.58	62.41	20.78	4.88	0.92	9.2
4	T3-50	MD PI	Moderate Port Island 1995 Kobe	0.13	21.66	6.20	0.29	0.04	8.5
5		TCU	TCU078 1999 Chi-Chi	0.12	14.94	4.69	0.61	0.02	28
6		LG PI	Large Port Island 1995 Kobe	0.38	48.36	17.13	2.66	0.29	11

The pressure-dependent, multiple-yield-surface (PDMY02) constitutive model implemented in OpenSees (Elgamal et al. 2002; Yang et al. 2008) was used to simulate the nonlinear response of Nevada and Monterey sands used in centrifuge. The soil elements were modeled using 20-8 node brick u-p elements (Lu et al. 2004; Yang et al. 2008). The saturated soil was modeled as a two-phase material based on the Biot theory (Biot 1962) for porous media, in which displacement of the soil skeleton, u, and the pore water pressure, p, are the primary unknowns (u-p formulation). A total number of 11,066 nodes and 9,471 elements resulting in 44,004 DOFs were used in the presented numerical simulations. To speed up the simulations, the parallel version of OpenSees (OpenSeesSP version 2.4.3) was used on a High Performance Computer (HPC) at the NEEShub HPC facility (Hacker et al. 2013).

Figure 4.3 shows the finite element discretization of the soil-foundation-structure system simulated in prototype scale. The minimum wavelength was initially estimated based on the soil's small strain shear wave velocity profile (V_s) and the maximum frequency content of the ground motions (e.g., f_{max} = 6 Hz after filtering, based on the shake table's capacity).

The maximum element size at different depths required to allow this wave propagation was subsequently calculated by dividing the minimum wavelength by 4. This element size was further divided by a factor of 6 to allow for soil softening (reduction in V_s). A series of preliminary 1-D free-field simulations of the liquefiable soil with different element sizes confirmed that this choice was adequate. Finer elements were used near the soil surface and building foundation to better capture the larger deformation gradients. The mat foundation and structure were modeled using 8-node brick elements (SSPbrick) with a single integration point (McGann 2013) and linear elastic material properties.

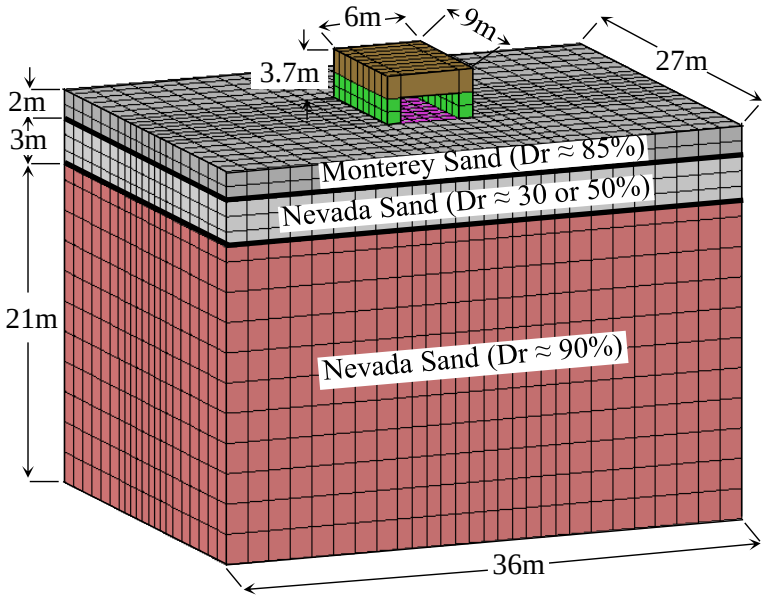

Figure 4. 3. Finite element model of the soil-foundation-structure system.

The foundation elements were connected to the soil elements using equal degrees of freedom (e.g., the master/slave technique in OpenSees, with soil DOFs set as master). All surrounding nodes of the soil medium were impervious except those at the surface. The ground water level was set at 1 m below the surface during the initial static analyses, similar to the centrifuge experiments. In order to simulate 1D wave propagation in 3D space, elements on the boundary at the same elevation were assumed to have the same motion using the

master/slave node technique. The acceleration time histories recorded in centrifuge at the base of the container were applied to the base nodes in numerical simulations.

The values of soil hydraulic conductivity (k) were calculated according to the scaling laws and the viscosity of the pore fluid used in centrifuge (k estimated for a given soil with water at 1g × 55/22), which were kept constant throughout the entire time of shaking in these simulations. The fluid bulk modulus was estimated assuming a soil degree of saturation (S_r) ranging from 99.5% to 100%, corresponding to a fluid bulk modulus ranging from $B_f = 2\times10^4$ to 2×10^6 kPa at atmospheric pressure. This level of saturation was observed to slightly improve excess pore pressure predictions compared to the centrifuge, as also observed by Byrne et al. (2004) and Dashti and Bray (2013).

In centrifuge experiments T3-30 and T3-50, a sequence of 1D, horizontal earthquake motions was applied to the container base (summarized in Table 4.1). The soil densified substantially after each shake (e.g., total volumetric strain (ε_p) in the free-field due to the first motion in T3-50 ≈ 0.4%), changing the soil relative density and properties prior to the next motion. Based on the settlements measured in the free-field, the average soil relative densities were estimated in each layer after each motion and used in the corresponding numerical simulation.

4.4.1. The Pressure-Dependent-Multi-Yield (PDMY02) constitutive model

The Pressure-Dependent-Multi-Yield (PDMY02) soil constitutive model developed by Yang et al. (2000, 2003, 2008) and previously by Parra (1996), is based on the multi-yield surface plasticity model initially introduced by Iwan (1967) and Mroz (1967) and later implemented for soils by Prevost (1985). The yield criteria are defined by a number of open conical shaped yield surfaces. This model uses a non-associative flow rule that develops volumetric dilation and contraction under shear deformation. The plastic flow in this model is

purely deviatoric. Hence, no plastic change of volume takes place under a constant stress ratio, since yield surfaces are open ended.

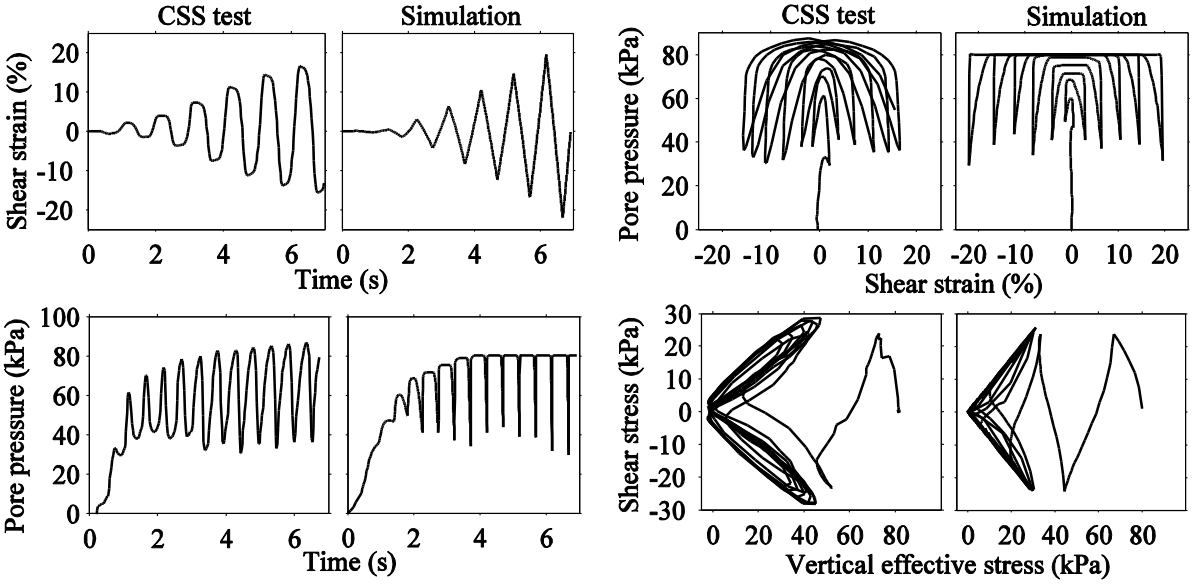

Figure 4. 4. Comparison of the numerically simulated and experimentally measured soil response during a representative Cyclic Simple Shear (CSS) test performed on Nevada sand by Arulmoli et al. (1992). Test conditions: Dr=63%, σ'_{vo}=80 kPa, and CSR=0.3.

4.4.2. Model parameter calibration

The soil model parameters were calibrated for this study by the author, in order to capture the response of saturated Nevada and Monterey sands as observed during previous undrained cyclic simple shear (CSS) tests with different overburden stresses (σ'_{vo}), relative densities (D_r), and cyclic stress ratios (CSR= τ/σ'_{vo}) (Arulmoli et al. 1992; Kammerer et al. 2000, 2004). The calibrated soil model parameters are summarized in Table 4.2. A comparison of experimentally measured and numerically predicted soil response during a representative cyclic simple shear test on Nevada sand (D_r=63%, σ'_{vo}=80 kPa, and CSR=0.3) is presented in Figure 4.4. Additionally, Figures 4.5 and 4.6 compare the relation between the number of cycles required to cause liquefaction (single amplitude shear strain of 3%) and CSR in numerical simulations with the available CSS experiments on Nevada and Monterey sands,

respectively. It must be noted that the available CSS tests were performed under undrained conditions, meaning that no drainages and volume change was allowed during cyclic loading, and hence no cyclic densification.

Table 4. 2. PDMY02 Calibrated Parameters for #120 Nevada and Monterey 0/30 sand models at different relative densities.

Parameter	**Nevada sand**						**Monterey sand**	**Description**
D_r (%)	30	40	50	63	68	90	85	Relative density
e	0.76	0.73	0.70	0.66	0.65	0.58	0.56	Void ratio
ρ (ton/m^3)	1.95	1.96	1.97	2.00	2.01	2.06	2.01	Saturated unit weight
$P_r^{'}$ (kPa)	101	101	101	101	101	101	101	Reference effective confining pressure
$G_{max,1,oct}$(MPa)	34.5	46.2	57.1	72.5	77.1	101.9	133.3	Octahedral low-strain shear modulus
$\gamma_{max,r}$	0.1	0.1	0.1	0.1	0.1	0.1	0.1	Maximum octahedral shear strain
B_r (MPa)	92.0	123.3	152.4	193.6	205.9	272.1	264.0	Bulk modulus
d	0.5	0.5	0.5	0.5	0.5	0.5	0.5	Pressure dependency coefficient
$\varphi_{TXC\ (PDMY)}$	31 ^{o}	32 ^{o}	33.5^o	34.5^o	36^o	40.0 ^{o}	42.0 ^{o}	Triaxial friction angle used by model
φ_{PT}	31 ^{o}	30 ^{o}	25.5 ^{o}	26.5 ^{o}	26 ^{o}	26.5 ^{o}	32 ^{o}	Phase transformation angle
c_1	0.087	0.067	0.05	0.04	0.02	0.016	0.014	Control the shear-induced volumetric change, contraction tendency based on the dilation history, and overburden stress effect, respectively.
c_2	5.0	4.5	4.0	2.5	1.5	1.45	2.0	
c_3	0.3	0.27	0.25	0.2	0.15	0.14	0.15	
d_1	0.01	0.02	0.06	0.07	0.15	0.25	0.36	Reflect dilation tendency, stress history, and overburden stress, respectively.
d_2	3.0	3.0	3.0	3.0	3.0	3.0	3.0	
d_3	0.0	0.0	0.0	0.0	0.0	0.0	0.005	
NYS	20	20	20	20	20	20	20	Number of yield surfaces generated by model
liq_1	1.0	1.0	1.0	1.0	1.0	1.0	1.0	Account for permanent shear strain (slip strain or cyclic mobility) in sloping ground.
liq_2	0.0	0.0	0.0	0.0	0.0	0.0	0.0	

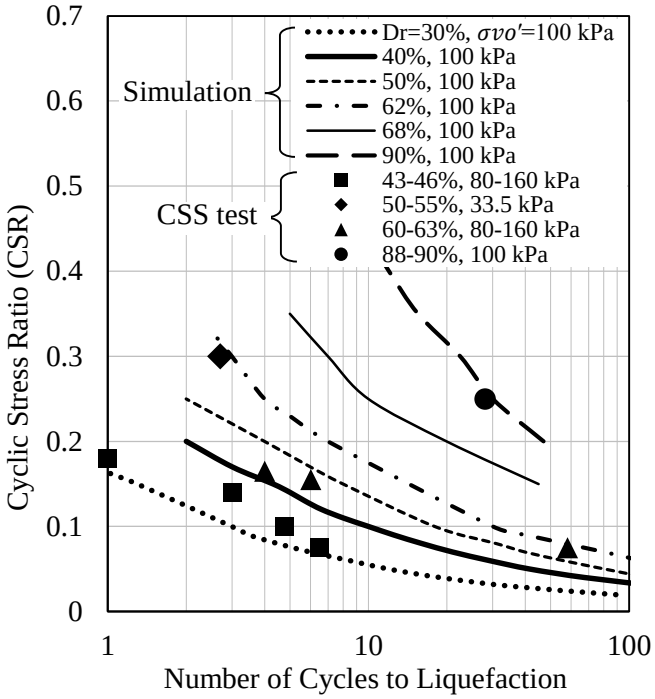

Figure 4. 5. Relation between number of cycles required to cause liquefaction (single amplitude shear strain of 3%) and Cyclic Stress Ratio (CSR) in numerical simulations and CSS experiments performed by Arulmoli (1992) and Kammerer et al. (2000) on Nevada sand.

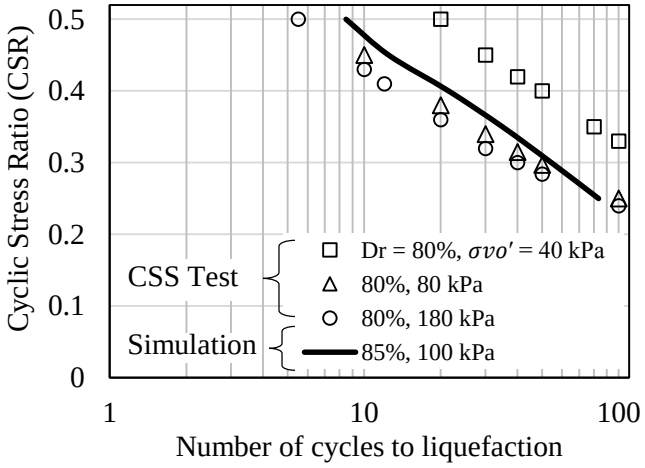

Figure 4. 6. Relation between number of cycles required to cause liquefaction (single amplitude shear strain of 3%) and Cyclic Stress Ratio (CSR) in numerical simulations and CSS experiments performed by Kammerer et al. (2004) on Monterey sand.

4.5. Numerical and Experimental Results

The response of the soil-foundation-structure system was numerically simulated in OpenSees and analyzed in terms of excess pore pressures, accelerations, and settlements in the

free-field (FF) and near-field (NF) soil, horizontal acceleration of the foundation and structural mass, settlement and tilt of the foundation, and transient roof drift.

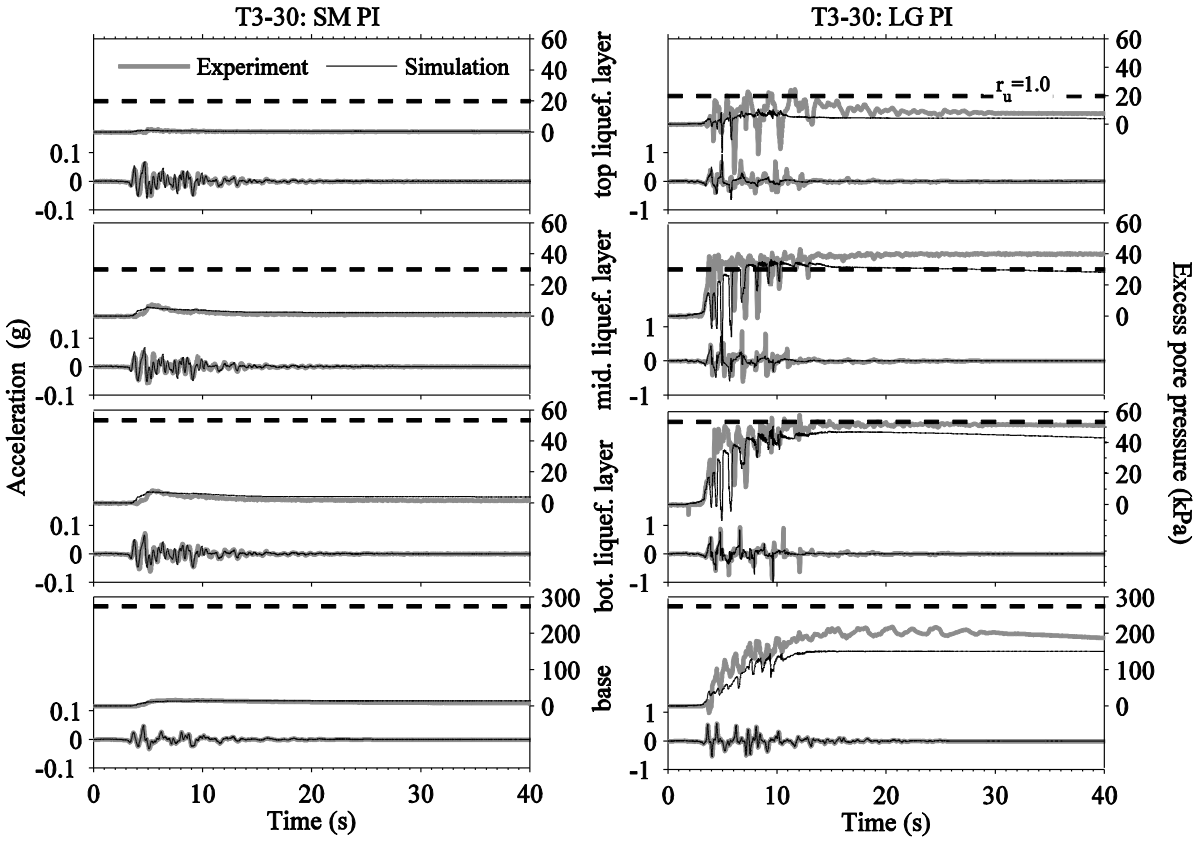

Figure 4. 7. Numerically computed and experimentally measured excess pore pressure and acceleration time histories at different depths of the liquefiable layer and the base of the model in the free-field in T3-30 during the Small and Large Port Island (PI) events.

The numerical results were then compared with centrifuge experimental measurements during different ground motions, and the difference in a given response was quantified in terms of residuals as:

$$\text{Residual } X = \log\left(\frac{X_{\text{experimental}}}{X_{\text{numerical}}}\right) \tag{4.3}$$

where X refers to a given quantity obtained numerically or experimentally. A positive residual indicates that the numerically predicted value underestimates the experimental measurement, and vice versa.

4.5.1. Soil response in the Free-Field (FF)

One-dimensional (1D), nonlinear site response in the free-field (without the influence of the structure) was first numerically simulated using a single soil column subject to the base accelerations recorded in the centrifuge for each test. The results were compared with centrifuge recordings at locations away from the buildings and the container boundaries (e.g., halfway between Building A and B in Figure 4.1), where structure and boundary effects were assumed to be minimum. Figures 4.7 and 4.8 show numerically computed and experimentally measured excess pore water pressure and acceleration time histories at different depths within the liquefiable layer and the base of the soil model in the free-field in experiment T3-30 during the Small and Large Port Island (PI) motions and in T3-50 during the Moderate PI and TCU motions (as representative cases).

The nonlinear simulations captured free-field site response well in terms of excess pore pressures and accelerations, particularly during the Small PI motion, which induced small strains, little tendency for excess pore pressure buildup, and little soil densification due to shaking. During the stronger events, the contractive and dilative soil response was captured well during the first few cycles of loading (as shown in the acceleration comparisons).

The model was able to capture the recovery of shear strength and stiffness in each cycle at larger shear strains due to soil's dilative response (Elgamal et al. 2005). However, the relative density and dynamic response of soil changes during shaking upon large settlements and densification. This numerical model does not update soil properties due to shaking-induced densification in a single time domain analysis. Hence, capturing the dilation cycles that lead to sharp acceleration spikes and drops in excess pore pressures became difficult after the initial cycles that caused substantial settlement and densification. Moreover, with generation of excess pore pressure ($r_u \approx 1.0$), the hydraulic conductivity significantly increases, the soil stiffness reduces, and consequently soil undergoes relatively large deformations, which makes

it more difficult for the numerical tool to capture the level of complexity and nonlinearity of responses. These are couple of many possible explanations for the observed differences between numerical predictions and experimental results.

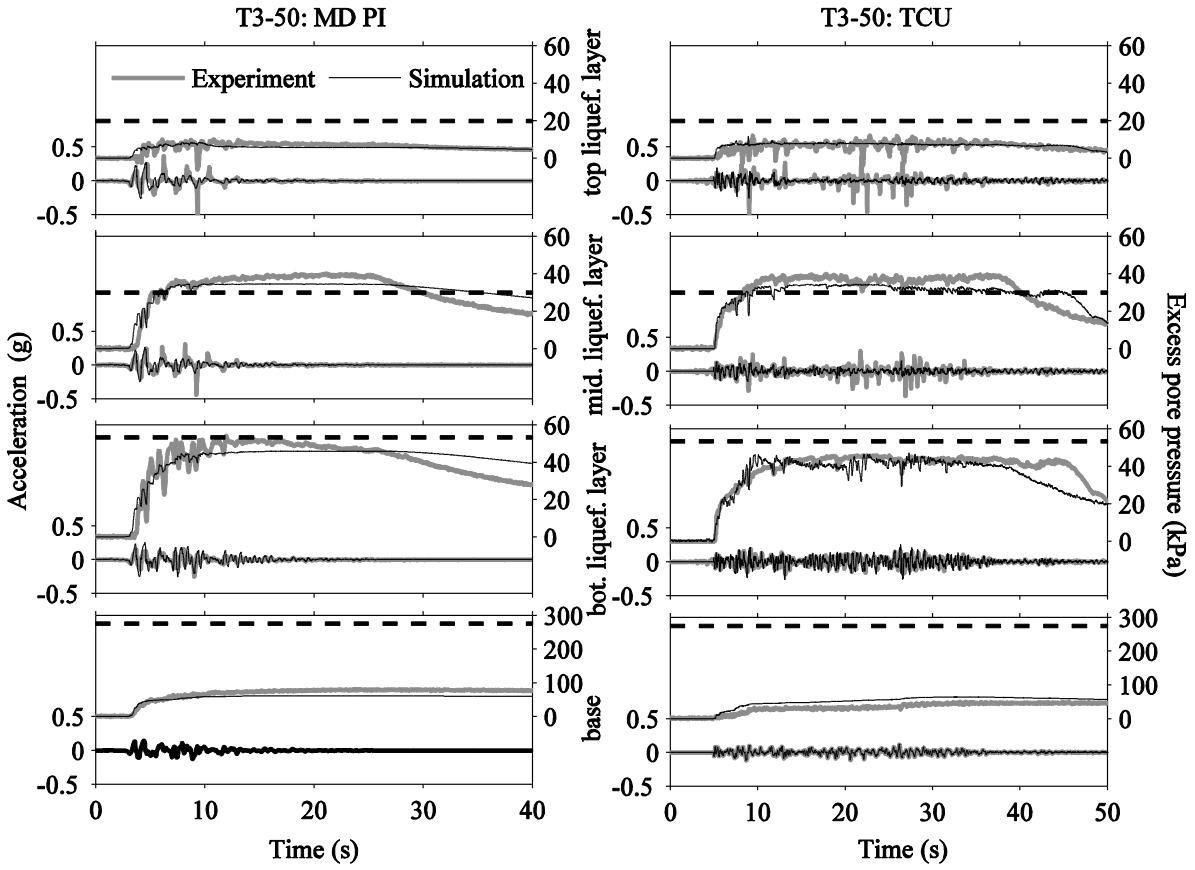

Figure 4. 8. Numerically computed and experimentally measured excess pore pressure and acceleration time histories at different depths of the liquefiable layer in the free-field in T3-50 during the Moderate PI and the TCU motions.

The PDMY02 constitutive model parameters were calibrated for the corresponding relative density of each soil layer in the experiments prior to a given motion, based on undrained CSS test results that allow no change in volume during cyclic loading. These calibrated parameters were then assumed to remain constant throughout the entire time history in a given simulation. The approximate change in soil relative density after each shake was, however, taken into account in estimating soil parameters for the subsequent ground motion. The calibrated soil relative densities presented in Table 4.2 reflect these changes.

The residuals between the numerical and experimental Arias Intensity (I_a) time histories and 5%-damped spectral accelerations (S_a) at the top of the liquefiable layer in the free-field are presented in Figure 4.9. This figure shows general agreement between experimental and numerical Arias Intensities during the Small and Moderate PI motions.

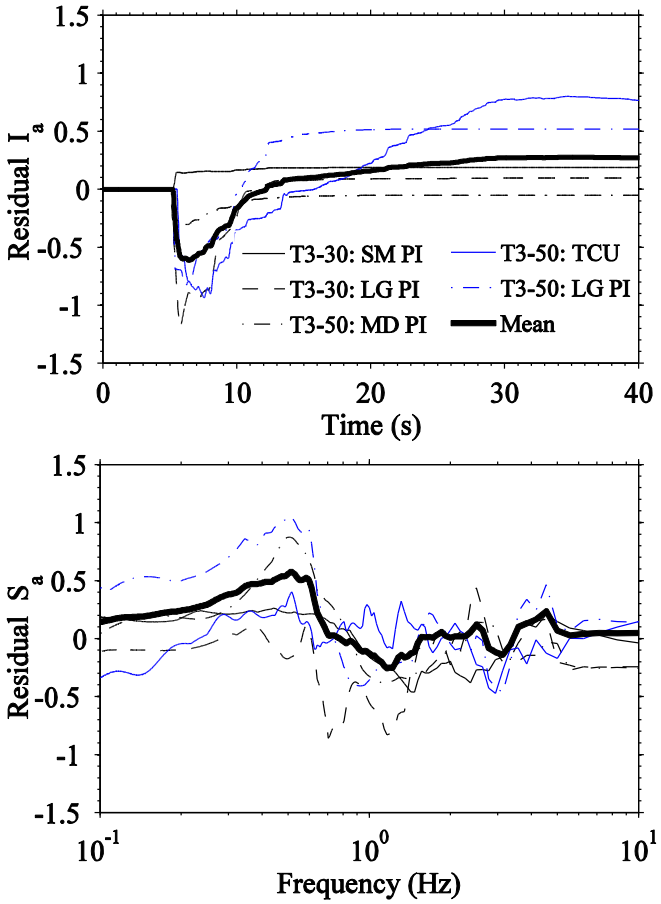

Figure 4. 9. Residuals between the numerical and experimental Arias Intensity (I_a) time histories and 5%-damped spectral accelerations (S_a) at the top of the liquefiable layer in the free-field.

During the stronger motions, however, the numerical simulations initially overestimated the Arias Intensity followed by its decrease and eventually underestimation (e.g., positive residuals as high as 0.5 to 0.8 were observed during the Large PI and TCU motions). One possible explanation for this observation may be the inability of the numerical model to capture shaking-induced densification with time, the subsequent change in soil properties, and

the larger dilation cycles in acceleration caused by densification and stiffening, which are particularly important during stronger or longer motions that induce larger settlements. The numerical spectral accelerations were generally underestimated in frequencies between about 0.3 to 0.6 Hz and slightly overestimated in frequencies between 0.6 and 2 Hz. But overall, the mean residual of spectral acceleration was close to zero, showing reasonable agreement between the numerical and experimental results.

To identify the site fundamental frequency in the free-field during each test and ground motion, frequency-dependent Transfer Functions (TF) were obtained experimentally and numerically, to relate the Fourier amplitude of acceleration at the surface (output) to the base of the soil column (input), as shown in Figure 4.10.

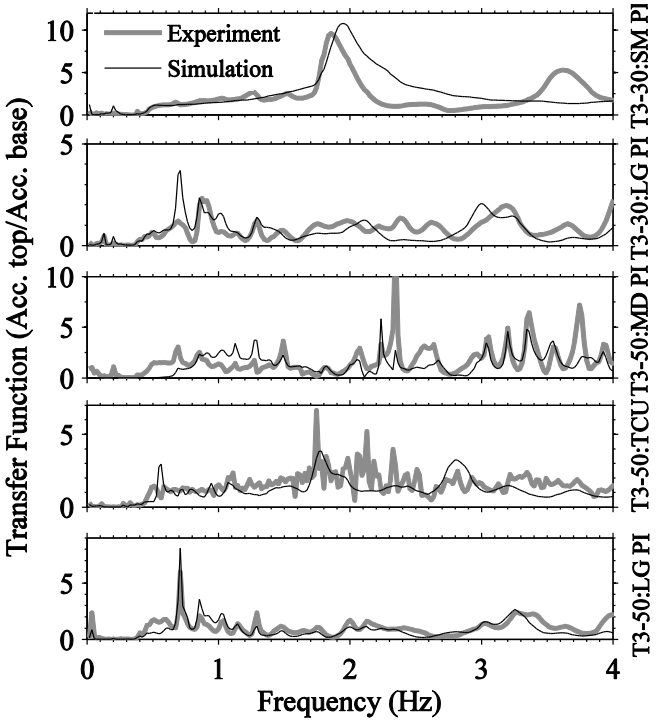

Figure 4. 10. Numerical and experimental Transfer Functions (TF) of free-field acceleration (surface/base).

The small-strain, initial fundamental frequency (f_{so}) of the soil column in the free-field was first estimated analytically as $f_{so} \approx \overline{V}_s / 4H \approx 1.6\text{-}2.2$ Hz, where $\overline{V}_s$ is the average shear wave

velocity of the soil column obtained from empirical procedures (e.g., Seed and Idriss 1970; Kramer 1996; Bardet et al. 1993; Menq et al. 2010); and H is the total height of the soil specimen. It must be noted that soil response and properties are not stationary, particularly during stronger motions, as they change with time. This leads to a change in soil fundamental frequency over time. Despite this effect, a comparison of transfer functions during different motions was found useful in obtaining the fundamental frequency of the site in an average sense. The fundamental frequency estimated numerically and experimentally (the frequency corresponding to the peak of TF) during the Small PI motion was consistent with the estimated small-strain frequency of approximately 2 Hz. During stronger motions, the fundamental frequency of the site was expected to decrease in a given test due to softening and excess pore pressure generation, which was captured both numerically and experimentally.

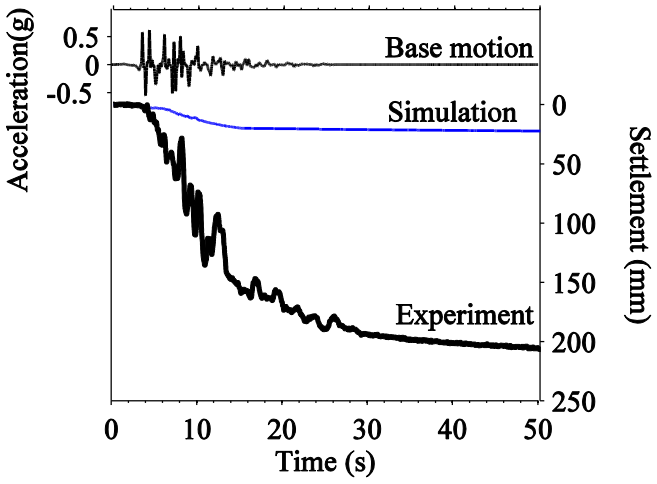

Figure 4. 11. Numerically computed and experimentally measured surface settlement time histories in the free-field in T3-30 during Large PI event.

Numerical and experimental free-field soil surface settlements are compared in Figure 4.11 during T3-30, Large PI event, as a representative example. Numerical simulations significantly underestimated settlements in the free-field during all ground motions. Dashti et al. (2010a,b) identified volumetric strains due to sedimentation and drainage during cyclic loading as primarily responsible for free-field settlement. Flow and loss of water that cause

volumetric strains in soil may be significant during shaking because: 1) the hydraulic conductivity of soil may increase drastically (Shahir et al. 2012) when approaching a liquefied state ($r_u \approx$ 0.8-1.0); 2) hydraulic gradients are kept at their peak during the time of strong shaking while large excess pore pressures are continuously being generated.

The PDMY02 constitutive model is pressure-dependent, meaning that it can capture the loss of shear or volumetric stiffness (softening) as the effective stress decreases due to excess pore pressure generation. The model was also calibrated to properly capture the stress-strain and pore pressure generation response observed during undrained CSS tests for each soil layer. Hence, the excess pore water pressures, hydraulic gradients, accelerations, and softening were captured relatively well in the free-field. Yet, the volumetric strains were largely underestimated, partly because a constant value of hydraulic conductivity was used in the simulations throughout the entire time history, and also because the PDMY02 model is known to underestimate the coefficient of volumetric compressibility (e.g., Howell et al. 2015). The value of hydraulic conductivity assumed during shaking is expected to significantly influence the total value of volumetric strain not just its rate, because during this time excess pore pressures are continuously generated as they dissipate, and hydraulic gradients are kept at their peak. As a result, the model largely underestimated the flow velocity and the resulting volumetric strains during the time of shaking.

4.5.2. Soil response in the Near-Field (NF)

Numerically computed and experimentally measured excess pore pressure and acceleration time histories within the liquefiable layer under the center of the foundation in T3-50 are presented in Figure 4.12 during the Moderate PI and TCU events, as a representative case. Both experimental and numerical results showed a reduction in excess pore pressure ratios ($r_u = \Delta u / \sigma'_{vo}$) under the center of the foundation compared to the free-field during this test. Sand with a higher relative density (e.g., T3-50 compared to T3-30) is more resistant to

seismically induced excess pore pressure generation and strength loss. But the impact of soil relative density on pore pressure generation and liquefaction potential is notably stronger under the higher confinement of the building and during less intense motions (Dashti et al. 2010b).

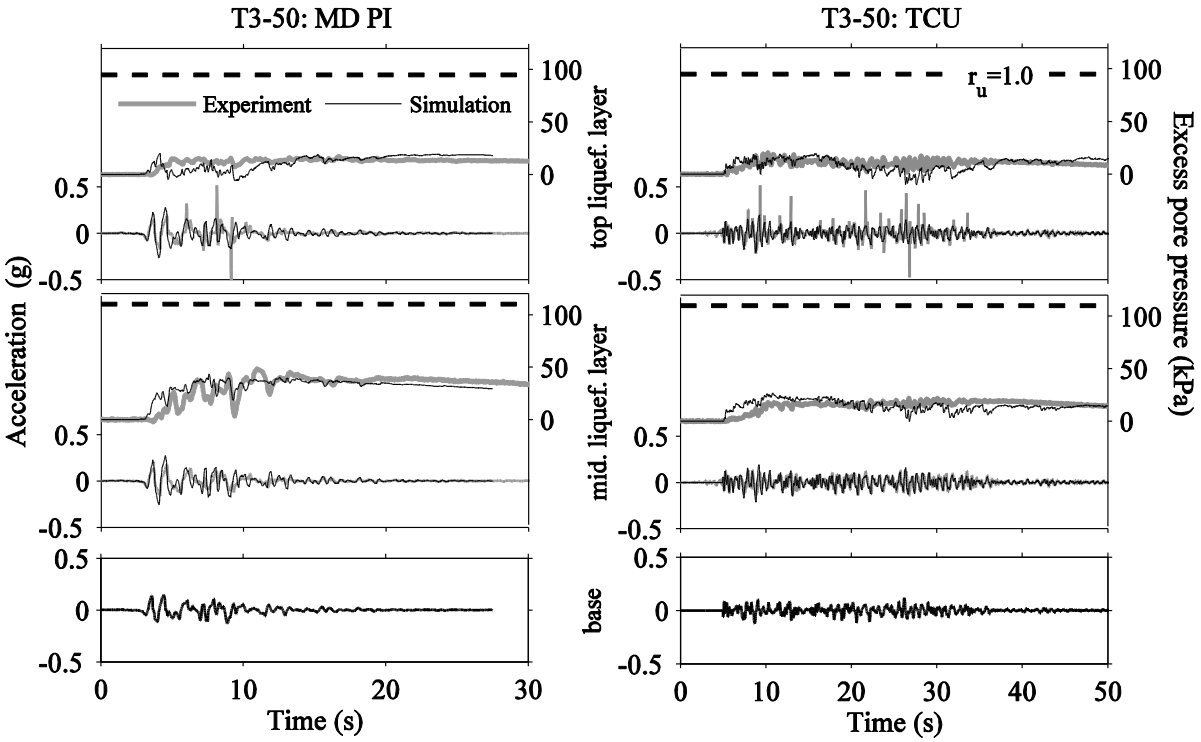

Figure 4. 12. Numerically computed and experimentally measured excess pore pressure and acceleration time histories at different depths of the liquefiable layer under the foundation center in T3-50 during the Moderate PI and TCU events.

Sand's cyclic strength and resistance to excess pore pressure generation increases under the higher confining pressure of a structure. Hence, liquefaction ($r_u \approx 1$) was observed in the free-field in T3-50 during the Moderate PI and TCU motions, but not under the foundation. However, if shaking is strong enough to overcome this higher resistance under higher confinement (e.g., T3-30, Large PI motion), larger excess pore pressures may generate under the foundation compared to the free-field for the same r_u (Dashti et al. 2010a), causing an outward flow potential that further amplifies building settlements. The numerical simulations were able to capture the influence of relative density and confining pressure on the resulting pore pressures, as observed experimentally.

The residuals between numerical and experimental Arias Intensities and spectral accelerations at the top of the liquefiable layer under the center of the foundation are presented in Figure 4.13. The residuals in Arias Intensity mostly followed a similar pattern under the building as in the free-field, with the exception of T3-30 (Large PI motion) and T3-50 (TCU motion). In order to understand the changes in acceleration predictions, it is important to evaluate the settlement patterns under the foundation compared to the free-field during both experiments, as shown in Figure 4.14.

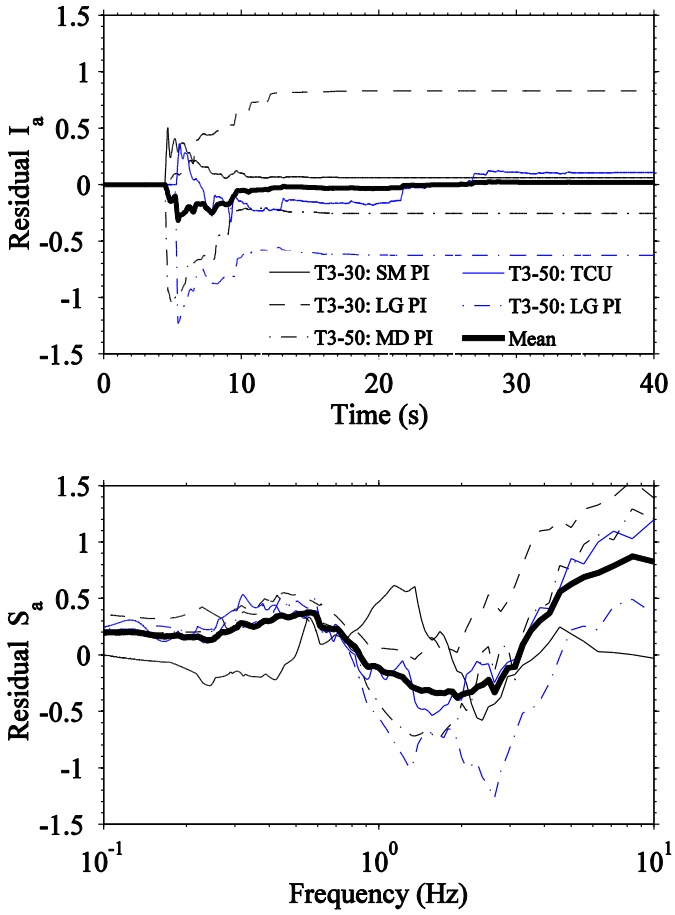

Figure 4. 13. Residuals between numerical and experimental Arias Intensity (I_a) time histories and 5%-damped spectral accelerations at the top of the liquefiable layer under the center of the foundation.

This figure also shows the Arias Intensity time histories of the corresponding base motions. Significantly larger settlements and excess pore water pressures were experimentally measured

under the foundation in T3-30 (Large PI) compared to the free-field. Larger excess pore pressures generated under the foundation created a strong tendency for outward flow and volumetric strains during cyclic loading due to drainage, increasing soil's relative density and stiffness during the shake, which is not taken into account numerically. This led to an underestimation of dilation spikes in acceleration and hence, Arias Intensity that grew with time to a residual of approximately 0.8 in Arias Intensity (compared to 0.5 in the free-field). In T3-50 (TCU), smaller total settlements and excess pore pressures were observed under the foundation compared to the free-field experimentally (Dashti et al. 2010b). Hence, larger volumetric strains were observed in the free-field with larger excess pore pressures that were sustained over a long duration compared to the soil under the foundation. As a result, there was less densification under the foundation compared to the free-field in T3-50 during the TCU motion. This led to improved (smaller) residuals in Arias Intensity under the building compared to free-field.

Trends in spectral acceleration residuals were mostly similar to those in the free-field, with the exception of higher frequencies. In frequencies greater than about 3 Hz, spectral accelerations were largely underestimated numerically, a trend not observed in the free-field. In other words, the numerical model over-damped accelerations at higher frequencies under the foundation but not in the free-field. However, higher frequency accelerations are not expected to strongly influence building settlement and tilt predictions, nor structural drift, with the exception of very stiff structures.

Numerical and experimental total foundation settlements in T3-30 and T3-50 are compared in Figure 4.15 during different motions. Total foundation settlements were obtained by averaging the settlement at the four corners of the foundation during each motion. The shape of foundation settlement time histories was experimentally observed to follow the shape of the

Arias Intensity of the ground motion (Figure 4.14). The numerical model captured the shape and magnitude of foundation settlements well.

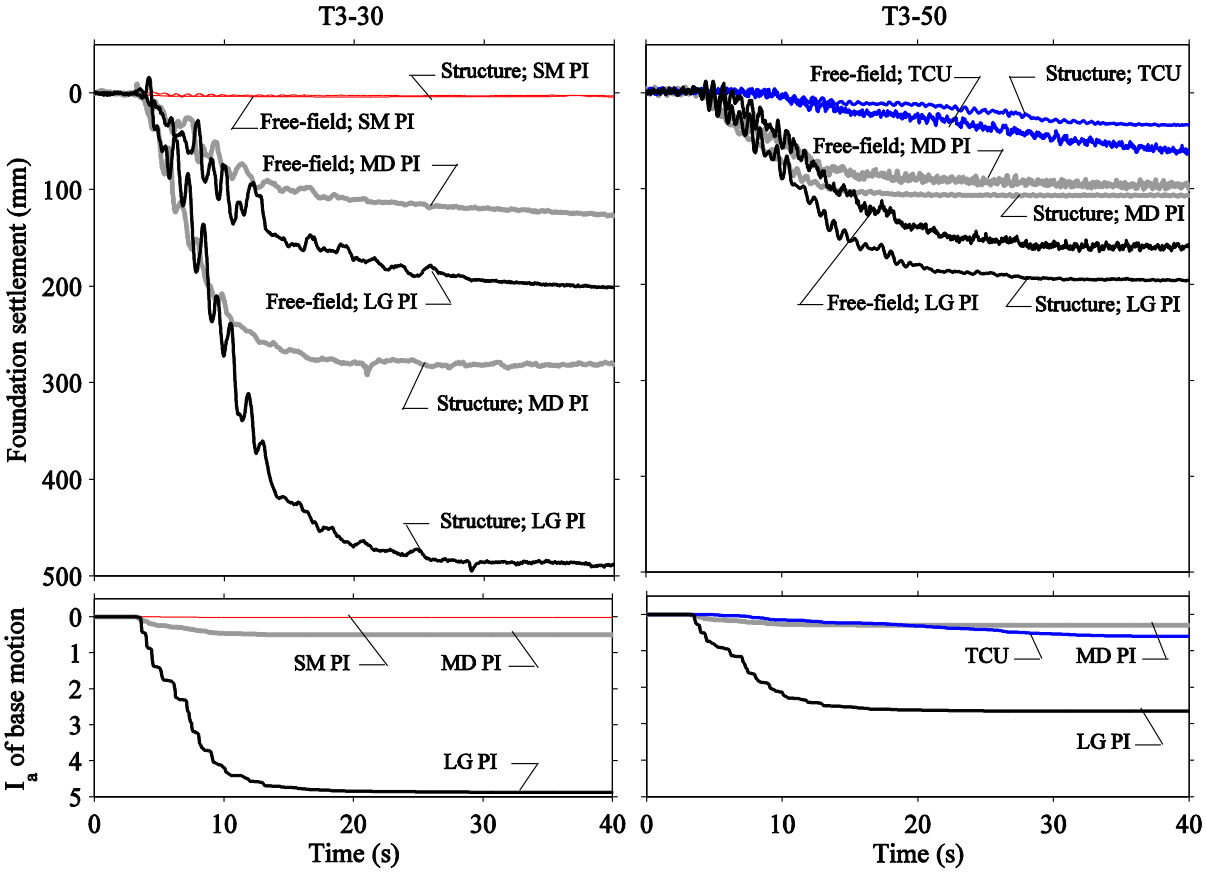

Figure 4. 14. Experimentally measured average foundation and free-field soil settlement in tests T3-30 and T3-50.

By capturing the excess pore pressure and acceleration patterns in the near-field, the numerical model could reasonably predict the most important mechanisms of settlement that are active under a shallow-founded structure: deviatoric strains under static and dynamic shear stresses imposed by the structure ($\varepsilon_{q\text{-}BC}$ and $\varepsilon_{q\text{-}SSI}$). The model does not capture volumetric strains well when assuming a constant hydraulic conductivity, as discussed previously. However, the contribution of volumetric strains to total building settlement is often less significant compared to the free-field, particularly when smaller excess pore pressures are generated under the foundation (e.g., T3-50 during all motions). As a result, despite a few

shortcomings in the model, total building settlements were captured well for the cases evaluated in this study.

4.5.3. Response of the foundation and structure

This section presents the response of foundation and structure in terms of acceleration, tilt, and lateral roof drift, as observed experimentally and numerically. The term "foundation motion" (FM) in this study refers to the horizontal motion recorded on the stiff mat foundation experimentally or numerically, which includes the influence of both kinematic and inertial interactions (i.e. the seismic demand felt by the structure at the foundation level). Frequency-dependent Transfer Functions (TF) of horizontal acceleration were computed, this time relating the Foundation Motion (FM) to the surface motion in the free-field (FF), shown in Figure 4.16 to evaluate the impact of the structure on accelerations at the foundation level.

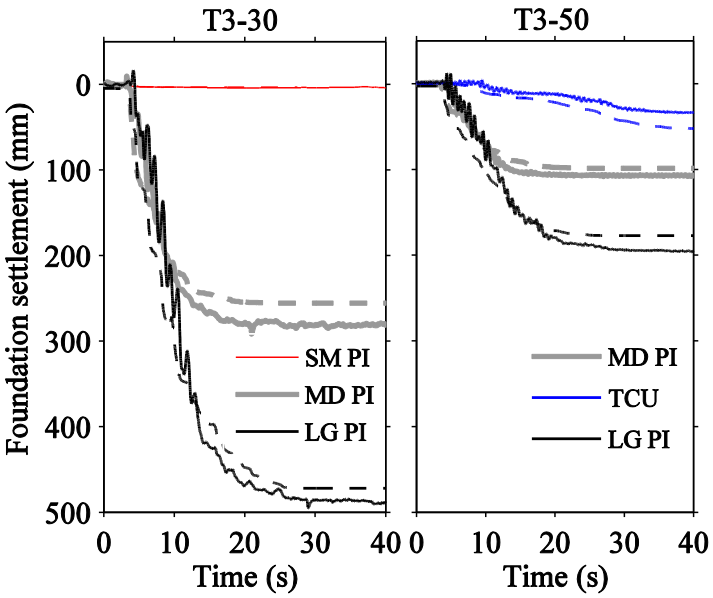

Figure 4. 15. Experimentally measured (solid lines) and numerically computed (dashed lines) total, average foundation settlement in tests T3-30 and T3-50.

Previous studies on non-liquefiable ground have revealed that the translational (horizontal) component of the foundation motion reduces in amplitude at higher frequencies compared to the free-field due to base-slab averaging (kinematic interaction), while the

rotational (rocking) component is amplified due to inertial interaction (e.g., Kim and Stewart 2003). Records from real earthquakes with more complex waveforms are expected to result in more base-slab averaging compared to a simple centrifuge experiment under 1-D horizontal shaking. However, previous centrifuge tests on dry sand have also shown this effect to some extent (Mason 2011; Ghayoomi and Dashti 2014). In this study with a saturated soil model susceptible to liquefaction, a similar de-amplification of the translational component of FM compared to FF was not evident at higher frequencies experimentally or numerically.

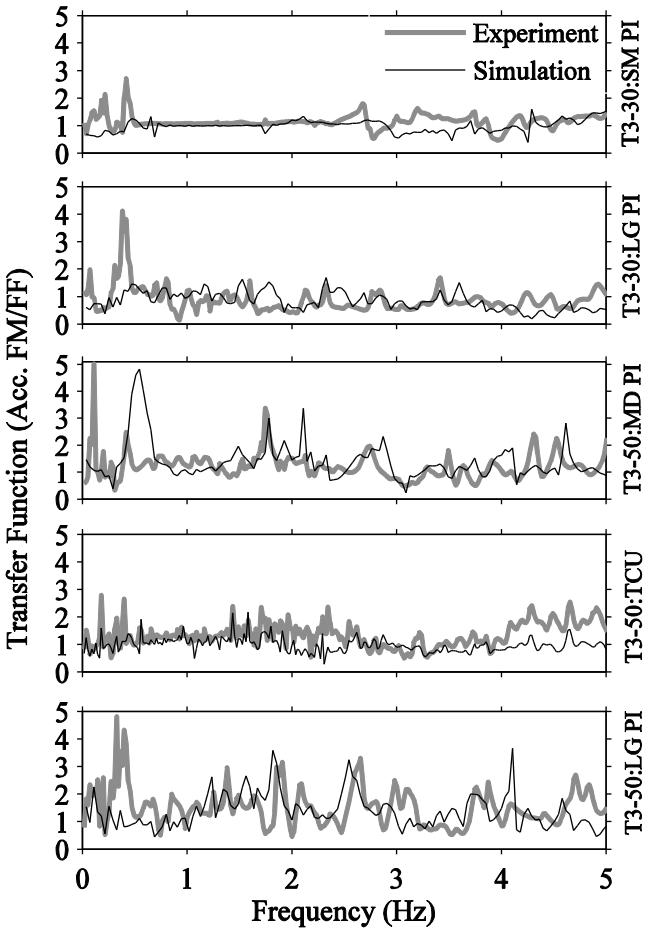

Figure 4. 16. Numerically computed and experimentally measured Transfer Functions of acceleration (FM/FF).

The flexible-based response of the SDOF oscillator was evaluated during different motions through Transfer Functions (TF) that relate the horizontal acceleration of the mass to

foundation. Figure 4.17 compares the TF of Mass/Foundation accelerations obtained experimentally and numerically, with the estimated fixed-based TF. The fixed-based fundamental frequency of the SDOF structure was estimated to be $f_n \approx 2.5$ Hz. The flexible-based response was similar to fixed-base during the Small PI event in T3-30, while they started to diverge during stronger events, as expected, caused by amplified inertial interaction. The reduction in the flexible-based natural frequency of the structure (i.e., period lengthening) during more intense events was captured both numerically and experimentally.

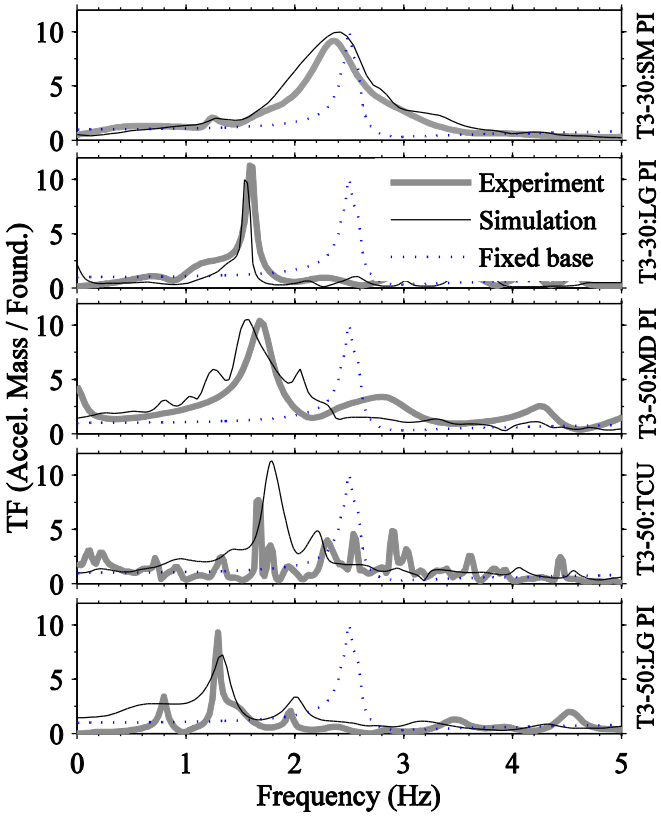

Figure 4. 17. Numerically computed and experimentally measured Transfer Functions of acceleration (Mass/Foundation).

The rotational or tilting response of the SDOF structure (rocking) was first computed in the time domain as the difference between vertical displacement time histories on the two sides of the foundation normalized by the width of the foundation. The Fourier Amplitude Spectrum of the foundation tilt was then obtained, to evaluate the rotational fundamental

frequency of the oscillator both numerically and experimentally, which are compared in Figure 4.18. The numerical model captured the rocking response of the SDOF oscillator well, both in terms of amplitude and fundamental frequency, during all experiments and motions.

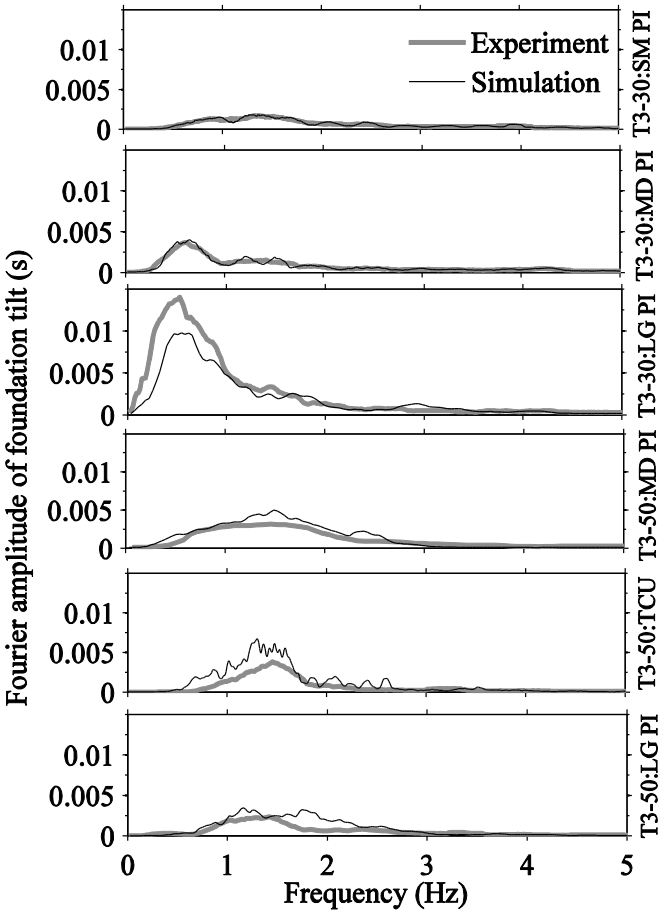

Figure 4. 18. Numerically computed and experimentally measured Fourier amplitude spectra of foundation tilt.

The peak roof drift ratio was computed as the peak value of relative horizontal displacement between the mass and foundation normalized by the height of the center of gravity above the foundation. The peak drift ratio is often used as a proxy for building damage. The residuals between numerical and experimental peak drift ratios were computed during different tests and ground motions. These residuals were then compared with the corresponding residuals in different acceleration intensity measures at the foundation level (FM), as shown in Figure 4.19. The results indicate a good correlation between the residuals in the building's peak

drift ratio and the residuals in PGA, I_a, and SIR of the FM. This shows the importance of capturing ground motion intensity measures at the foundation level (particularly PGA), in order to reliably evaluate building performance.

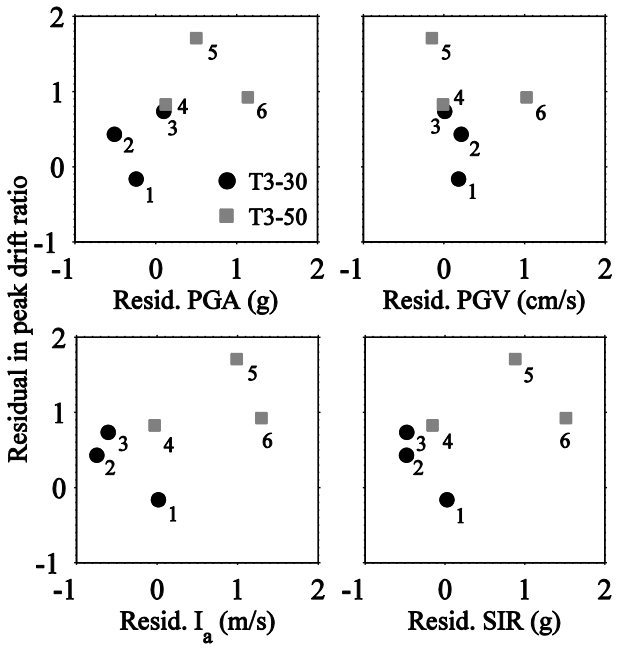

Figure 4. 19. Residual of maximum drift against residuals of different foundation motion (FM) characteristics (the numbers next to data refer to the ground motion number in Table 4.1).

4.6. Concluding Remarks

A series of centrifuge experiments were performed to investigate the response of single-degree-of-freedom (SDOF) structures on stiff, mat foundations founded on a layered soil deposit including a liquefiable layer under a range of earthquake motions. These experiments enabled a study of seismic soil-foundation-structure-interaction on softened ground and the impact of various testing parameters on structural response. Class C, solid-fluid, fully-coupled, nonlinear numerical simulations of the centrifuge experiments were performed using the pressure-dependent, multi-yield-surface, nonlinear soil constitutive model (PDMY02) implemented in OpenSees. In this chapter, the author evaluates the capabilities and limitations of this numerical tool in capturing the key responses of soil, structure, and their interaction

during a range of ground motions as observed experimentally. This validation is a necessary step before the model may be employed reliably in predicting structural response under more general conditions.

The nonlinear simulations captured 1-D, free-field, site response well in terms of excess pore pressures and accelerations, particularly during less intense motions that induced smaller strains, excess pore pressures, and soil densification. During the stronger events, the contractive and dilative soil response was predicted well during the first few cycles of loading. However, because this model did not update soil properties with time, it could not take into account shaking-induced densification and stiffening during a single time domain analysis. Hence, capturing the amplified dilation cycles due to soil stiffening that produce sharp acceleration spikes and drops in excess pore pressures became difficult in later cycles. This led to a numerical underestimation of Arias Intensities in the free-field during the stronger or longer duration motions.

With reasonable estimation of accelerations and excess pore pressures in the free-field in most cases, the numerical model captured the site's effective fundamental frequency well. Soil settlements, however, were largely underestimated in the free-field numerically during all motions. This is because the numerical simulations did not consider the drastic increase in soil hydraulic conductivity and flow velocity during shaking, and also because soil's volumetric compressibility was largely underestimated.

Experimental results often showed a reduction in excess pore pressure ratios (r_u) under the center of the foundation compared to the free-field, due to the increase in confining pressure. However, this increased resistance to excess pore pressure generation and liquefaction under the foundation was experimentally shown to depend on building's confining pressure, soil's relative density, and ground motion intensity. The observed trends were captured well by the numerical model. By capturing excess pore pressures and accelerations

under the foundation fairly well, the numerical model could capture static and dynamic shear type deformations under the building. Hence, numerically computed building settlements and tilts compared well with experimental measurements, both in terms of time rate and magnitude.

The numerical model generally captured kinematic and inertial interaction by reasonably capturing the change in foundation motion compared to the free-field, the reduction in building's flexible-based fundamental frequency compared to fixed-based, and the building's rocking amplitude and fundamental frequency. This study showed both experimentally and numerically that no significant de-amplification of the foundation motion may be observed at higher frequencies compared to the free-field when significantly lower excess pore pressures are generated under the foundation. Hence, in saturated sand, smaller excess pore pressures and larger accelerations may develop under the foundation compared to free-field. In such cases, ignoring SFSI will not be conservative.

Lastly, the residuals between numerical and experimental peak roof drift ratios were shown to correlate with the corresponding residuals in the properties of the foundation motion, particularly its PGA, Arias Intensity, and Shaking Intensity Rate. This proves the importance of properly evaluating SFSI and the intensity measures at the foundation level, in order to reliably evaluate building's response and potential for nonlinearity and damage.

CHAPTER 5

SEISMIC PERFORMANCE OF SHALLOW FOUNDED STRUCTURES ON LIQUEFIABLE GROUND: VALIDATION OF NUMERICAL SIMULATIONS USING CENTRIFUGE EXPERIMENTS

This chapter is based on the following reference:

Karimi, Z., and Dashti, S. (2016). Seismic Performance of Shallow Founded Structures on Liquefiable Ground: Validation of Numerical Simulations using Centrifuge Experiments, J. Geotech. Geoenviron. Eng., 10.1061/(ASCE)GT.1943-5606.0001479.

5.1. Introduction

Soil liquefaction has led to excessive settlement, tilt, and lateral displacement of many buildings on shallow foundations during previous earthquakes, causing damage to the structures and their nearby lifelines (e.g., 1964 Niigata, Japan; 1990 Luzon, Philippines; 1999 Kocaeli, Turkey; 2011 Christchurch, New Zealand). The existing procedures in practice for assessing liquefaction-induced settlements (e.g., Tokimatsu and Seed 1987; Ishihara and Yoshimine 1992) assume free-field conditions, which either completely neglect the existence of the building or bring in the foundation load as an added overburden stress alone. These procedures ignore the influence of structures on static and dynamic stresses induced in the foundation soil, and the impact of soil liquefaction on building performance. These

shortcomings hamper the development of mitigation strategies that enhance building performance in terms of foundation settlement and tilt as well as flexural inter-story drift of the structure that is a proxy for building damage.

In order to simulate more realistically the seismic response of shallow-founded structures on liquefiable soil, the stress field around the foundation, and the drainage conditions, fully-coupled, 3D, dynamic, nonlinear numerical analyses are often warranted. These simulations can provide insight into soil nonlinearity, its interaction with the superstructure, and building's settlement, tilt, period lengthening, and drift. A single time-domain analysis can evaluate the timing and location of liquefaction triggering, post-liquefaction softening followed by stiffening, and the resulting accelerations and displacements imposed on structures. Nonlinear soil constitutive models developed for soil liquefaction are, however, complex with many parameters, and they are often validated against a limited set of laboratory test data that do not cover a variety of loading paths and drainage conditions. Further, interpretation of data from case histories are often associated with uncertainties due to lack of sufficient high quality recordings of structural response as well as soil response at key locations. Physical modeling under controlled conditions can provide valuable insights into the extent and timing of soil liquefaction and its resulting consequences on the soil-foundation-structure system (e.g., Yoshimi and Tokimatsu 1977; Liu and Dobry 1997; Hausler 2002; Dashti et al. 2010a,b). Further, physical model studies that cover a range of structures, soils, and ground motions enable a comprehensive evaluation and validation of advanced numerical tools, before they are used in a systematic parametric study.

Centrifuge experiments performed by Dashti et al. (2010a,b) investigated the seismic response of different single-degree-of-freedom (SDOF) structures with stiff, mat foundations on a layered deposit, including a liquefiable layer. Solid-fluid, fully-coupled, 3D, nonlinear finite element numerical simulations of the centrifuge tests were performed using the pressure-

dependent, multi-yield-surface, plasticity-based soil constitutive model (PDMY02) implemented in OpenSees by Elgamal et al. (2002); Yang et al. (2003 and 2008). These analyses are classified as Class C predictions, in which the results are known to the predictor prior to running the numerical simulation (Lambe 1973).

Most of the previous numerical studies on soil liquefaction and its effects on structures (e.g., Elgamal et al. 2005a,b; Popescu et al. 2006; Andrianopoulos et al. 2006, 2010; Lopez-Caballero and Farahmand-Razavi 2008, 2013; and Karamitros et al. 2013) did not include a detailed verification process covering a range of soil, structural, and ground motion properties. Karimi and Dashti (2015b) evaluated the capabilities and limitations of this numerical tool in capturing the response of one SDOF structure founded on one type of layered liquefiable soil profile as observed in centrifuge, focusing primarily on the foundation motion compared to the free-field as well as structure's period lengthening, settlement, tilt, and total drift. In this chapter, a more comprehensive comparison of numerical simulation results with experimental recordings are provided for a range of structures, soil layering, and ground motions. The fundamental period, foundation contact pressure, building height/width (H/B) aspect ratio, and foundation contact area are varied among the three SDOF structures studied experimentally and numerically. The relative density and drainage capacity of the liquefiable layer are also varied, allowing an evaluation of their effects on the response of different structures. Numerical and experimental results are compared in terms of acceleration, settlement, tilt, flexible-base fundamental period, and importantly, the different components of transient inter-story drift (total, rocking, and flexural) in both time and frequency domains. The goal of this chapter is to provide insights into the model's capabilities and limitations in predicting the key engineering demand parameters that control building performance and damage potential for a range of conditions. The experimental and numerical results presented in this study also aim to guide future analyses and mitigation decisions.

5.2. Overview of Centrifuge Experiment

Dynamic centrifuge tests were performed by Dashti et al. (2010a,b) to assess the response of three different SDOF structures with stiff, shallow mat foundations placed on layered, liquefiable soil deposits. Experiment T3-30 had a soil profile consisting of a 2 m-thick (prototype scale) Monterey Sand (D_{50} = 0.40 mm, C_u = 1.3, e_{min} = 0.54, e_{max} = 0.84) with relative density (D_r) ≈ 85% overlying a 3 m-thick liquefiable layer of Nevada Sand (D_{50} = 0.14 mm, C_u =2.0, e_{min} = 0.55, e_{max} = 0.84) with D_r ≈ 30%, both overlying a 21 m-thick layer of dense Nevada Sand with D_r ≈ 85%. Experiment T3-50 had the same profile as T3-30, but the initial relative density of the liquefiable layer was increased from 30% to 50%. Lastly, in experiment T3-50-Silt, the 2 m-thick Monterey Sand was replaced by a 0.8 m-thick layer of Silica Silt (D_{50} = 0.02 mm) underlying a 1.2 m-thick layer of Monterey Sand. The models were saturated below a depth of 1 m with a solution of hydroxypropyl methylcellulose in water (Stewart et al. 1998) to obtain a viscosity of approximately 22 times that of water (Dashti et al. 2010a,b). The instrumentation layout of the centrifuge experiments is presented in Figure 5.1. The models were spun to a nominal centrifugal acceleration of 55g and then, ground motions were applied to the base of the models. All units presented in this chapter are in prototype scale.

Three elastic SDOF model Structures A, B, and C were made of steel and aluminum mounted on 1 m-thick, stiff mat foundations placed on soil with an embedment depth of 1 m. Bearing pressure and fixed-base natural frequencies (f_n) of structures ranged from 80 to 130 kPa and 2.5 to 3.5 Hz, respectively. Structure A represented a 2-story building on a mat foundation. Structure B had the same contact pressure as A, but increased weight and foundation area. Structure C had the same foundation area as A, but increased pressure and H/B. Structural properties are summarized in Table 5.1 and their configurations are shown in Figure 5.1. A series of earthquake motions was applied to the base of the container in the same

sequence during each experiment. Base motions (as recorded) along with their properties are presented in Table 5.1 in order of their application during each experiment.

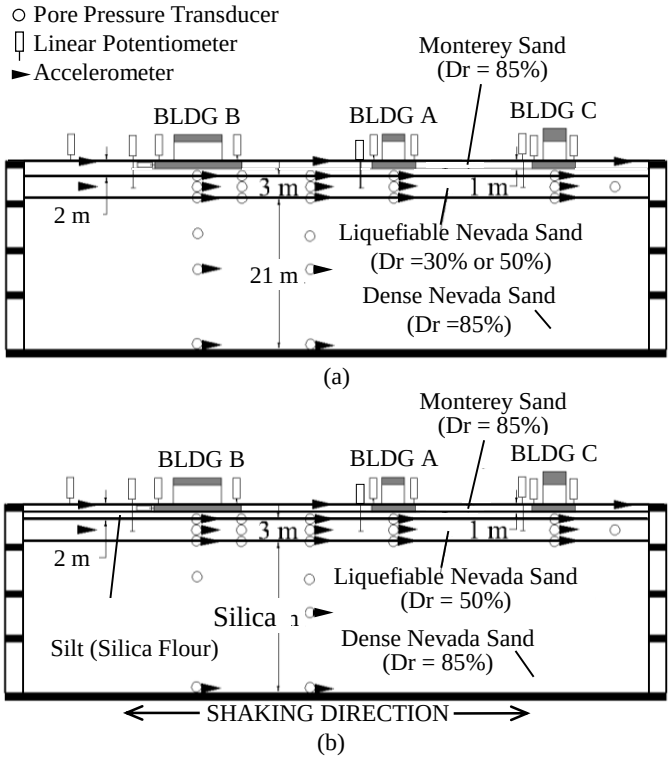

Figure 5. 1. Centrifuge model layout in experiments: (a) T3-30 and T3-50, and (b) T3-50-Silt (all dimensions are provided in prototype scale meters).

5.3. Overview of Numerical Simulations

Three-dimensional (3D), nonlinear, solid-fluid, fully-coupled, effective stress, dynamic finite element (FE) analyses of the centrifuge tests were performed in OpenSees platform (Mazzoni et al. 2006). Nonlinear response of the soil was simulated using the pressure-dependent, multiple-yield-surface (PDMY02) constitutive model implemented in OpenSees (Elgamal et al. 2002; Yang et al. 2008). In this model, the yield criteria are defined by a number of open conical-shaped yield surfaces with the common apex at the origin of principal stress space. PDMY02 follows a non-associative flow rule to simulate volumetric dilation and contraction under shear deformation. Because of open-ended yield surfaces, no plastic change of volume is predicted by this model under a constant stress ratio. The dynamic response of

soil-foundation-structure systems was numerically simulated in a 3D space to account for 3D stress fields and fluid flow patterns (as also discussed by Karimi and Dashti 2015a,b). A two-phase material behavior based on the Biot theory (Biot 1962) was used to model the response of saturated porous media. Soil was modeled using 8-node or 20-8-node brickUP elements (Lu et al. 2004; Yang et al. 2008) and the *u-p* formulation. In this formulation, the density gradient of the fluid and the relative fluid acceleration are neglected during a relatively slow excitation as in the case of earthquake loading (Chan 1988; Zienkiewicz et al. 1990). This reduces the primary unknown to the soil skeleton displacement (u) and the pore fluid pressure (p).

Table 5. 1. Base motion (as measured) and structural model properties in centrifuge experiments (prototype scale).

Test ID	**Record**	**PGA (g)**	**PGV (cm/s)**	**PGD (cm)**	**I_a (m/s)**	**SIR (m/s/s)**	**$D_{5\text{-}95}$ (s)**	**Structural Model**
T3-30	SM PI (Small Port Island 1995 Kobe)	0.04	6.97	2.06	0.02	0.003	7.9	Buildings on 1m-thick mat foundations: **A**: W×L×H=6×9×5 m (q=80 KPa, f_o=2.5 Hz) **B**: W×L×H=12×18×5 m (q=80 KPa, f_o=3.5 Hz) **C**: W×L×H=6×9×9.2 m (q=130 KPa, f_o=2.5 Hz)
	MD PI (Moderate Port Island 1995 Kobe)	0.17	25.61	7.19	0.50	0.08	8.0	
	LG PI (Large Port Island 1995 Kobe)	0.58	62.41	20.78	4.88	0.92	9.2	
T3-50-Silt	SM PI	0.05	7.10	2.39	0.02	0.003	7.9	
	MD PI	0.19	26.04	8.32	0.47	0.07	8.0	
	LG PI	0.55	53.18	24.71	4.38	0.64	9.1	
T3-50	MD PI	0.13	21.66	6.20	0.29	0.04	8.5	Building **A**
	TCU (TCU078 1999 Chi-Chi)	0.12	14.94	4.69	0.61	0.02	28	
	LG PI	0.38	48.36	17.13	2.66	0.29	11	

A linear elastic material was adopted to simulate the response of the mat foundation and structure. A total number of 83,887 DOFs was used, for instance, when modeling the response of Structure B. Analyses were performed on high performance computing facility of Network for Earthquake Engineering Simulation, NEEShub (Hacker et al. 2013) in the parallel

version of OpenSees (OpenSeesSP 2.4.3, McKenna et al. 2000; McKenna and Fenves 2008) in order to reduce the running time of each numerical simulation. This was particularly important for the parametric studies that followed.

Figure 5.2 shows the finite element discretization of the soil-foundation-structure system for a representative case (Structure C in T3-30), similar to those presented by Karimi and Dashti (2015b). To choose the element size in these analyses, the minimum wavelength was estimated based on the soil's shear wave velocity (V_s) and the maximum frequency content of the base motions (e.g., f_{max} = 6 Hz after filtering). The maximum allowable element size at different depths was subsequently calculated by dividing the minimum wavelength by 24 to account for soil softening (reduction in small strain V_s). Finer elements were used near the soil surface and building foundation to better capture larger strain.

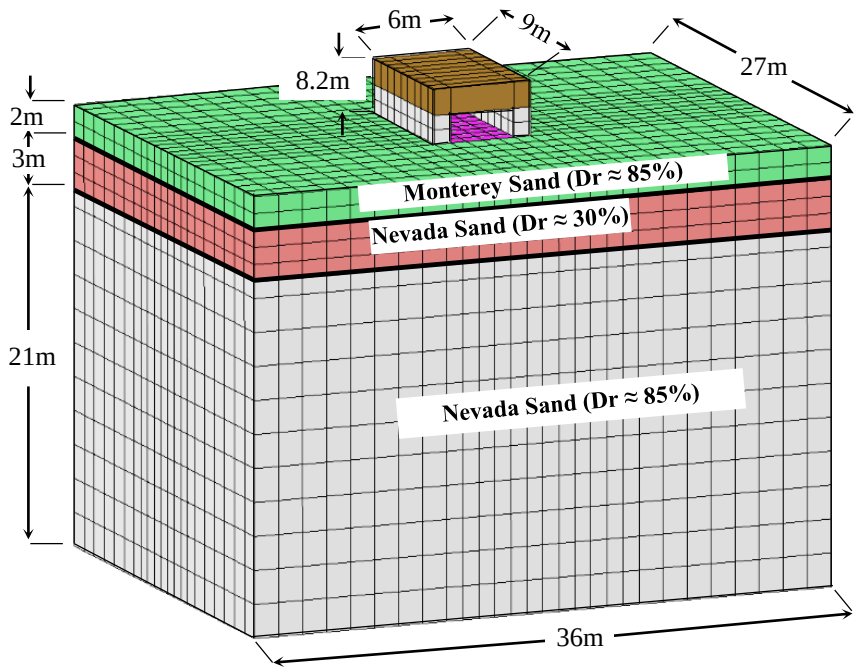

Figure 5. 2. Finite element model of the soil-foundation-structure system with the presence of Structure C in T3-30.

Similar to Karimi and Dashti (2015b), the foundation elements were connected to the soil elements directly with no interface elements. All surrounding nodes of the soil medium

were set as impervious except those at the surface, to allow vertical flow. The ground water level was set at 1 m below the surface. The nodes on the boundary at the same elevation were tied together to have the same motion. The acceleration time histories recorded in centrifuge at the base of the container were applied to the base nodes in all numerical simulations.

Soil hydraulic conductivity (k) was calculated based on the scaling laws (Schofield 1981) and the viscosity of the pore fluid used in centrifuge (k with water at 1g × 55/22). The fluid bulk modulus was estimated assuming a soil degree of saturation (S_r) ranging from 99.5% to 100%, corresponding to a fluid bulk modulus ranging from $B_f \approx 2\times10^4$ to 2×10^6 kPa at atmospheric pressure (Karimi and Dashti 2015b).

In the centrifuge experiments, the liquefiable soil layer densified after the application of each base motion (e.g., volumetric strain (ε_v) within the liquefiable layer in the free-field during the MD PI motion in T3-50 ≈ 1.4%). This led to a change in soil relative density and properties prior to the next shake. Based on the vertical displacements measured in the free-field (at the surface and within liquefiable layer) in centrifuge after each motion, the average soil relative densities were approximated in each layer prior to the following motion and used in the corresponding numerical simulation.

5.3.1. Calibration of Soil Model Parameters

Undrained cyclic simple shear (CSS) tests available on Nevada and Monterey Sands with different overburden stresses (σ'_{vo}), relative densities (D_r), and cyclic stress ratios (CSR= τ/σ'_{vo}) (Arulmoli et al. 1992; Kammerer et al. 2000, 2004) were used to calibrate the soil model parameters. The parameters used to model soil behavior in this study are summarized in Table 5.2, and the calibration process and the response of the constitutive model were discussed in more detail by Karimi and Dashti (2015b).

Table 5. 2. PDMY02 calibrated parameters for #120 Nevada Sand, Silica Silt, and Monterey 0/30 Sand at different relative densities.

Parameter	**Nevada Sand**						**Silica Silt**	**Monterey Sand**	**Description**
D_r (%)	30	40	50	63	68	90	85	85	Relative density
e	0.76	0.73	0.70	0.66	0.65	0.58	0.88	0.56	Void ratio
ρ (ton/m^3)	1.95	1.96	1.97	2.00	2.01	2.06	1.86	2.01	Saturated unit weight
$P_r^{'}$ (kPa)	101	101	101	101	101	101	101	101	Reference effective confining pressure
$G_{max,1,oct}$(MPa)	34.5	46.2	57.1	72.5	77.1	101.9	87.6	133.3	Octahedral low-strain shear modulus
$\gamma_{max,r}$	0.1	0.1	0.1	0.1	0.1	0.1	0.1	0.1	Maximum octahedral shear strain
B_r (MPa)	92.0	123.3	152.4	193.6	205.9	272.1	233.8	264.0	Bulk modulus
d	0.5	0.5	0.5	0.5	0.5	0.5	0.5	0.5	Pressure dependency coefficient
$\varphi_{TXC\ (PDMY)}$	31 ^{o}	32 ^{o}	33.5^o	34.5^o	36^o	40.0 ^{o}	41.0	42.0 ^{o}	Triaxial friction angle used by model
φ_{PT}	31 ^{o}	30 ^{o}	25.5 ^{o}	26.5 ^{o}	26 ^{o}	26.5 ^{o}	36.0	32 ^{o}	Phase transformation angle
c_1	0.087	0.067	0.05	0.04	0.02	0.016	0.3	0.014	Control the shear-induced volumetric change, contraction tendency based on the dilation history, and overburden stress effect, respectively.
c_2	5.0	4.5	4.0	2.5	1.5	1.45	5.0	2.0	
c_3	0.3	0.27	0.25	0.2	0.15	0.14	1.5	0.15	
d_1	0.01	0.02	0.06	0.07	0.15	0.25	0.02	0.36	Reflect dilation tendency, stress history, and overburden stress, respectively.
d_2	3.0	3.0	3.0	3.0	3.0	3.0	3.0	3.0	
d_3	0.0	0.0	0.0	0.0	0.0	0.0	0.0	0.005	
NYS	20	20	20	20	20	20	20	20	Number of yield surfaces generated by model
liq_1	1.0	1.0	1.0	1.0	1.0	1.0	1.0	1.0	Account for permanent shear strain (slip strain or cyclic mobility) in sloping ground.
liq_2	0.0	0.0	0.0	0.0	0.0	0.0	0.0	0.0	

Figure. 5.3 compares the relation between the number of cycles required to cause liquefaction (using single amplitude shear strain of 3% for Nevada and Monterey Sand and 3.75% for silt) and CSR in numerical simulations with the available CSS experiments on Nevada and Monterey Sands as well as Fraser River Silt. Because laboratory test results were not available for Silica Silt (used only in experiment T3-50-Silt), the PDMY02 model parameters for this thin layer were calibrated to capture the liquefaction triggering response of Fraser River Silt instead (ML, PI ≈ 4%, e ≈ 0.94, G_s = 2.69, w_c≈ 35%), as performed by

Wijewickreme (2010). The nonlinear properties of the thin layer of Silica Silt used in T3-50-Silt (approximately 0.8m thick in the prototype scale) was not expected to significantly influence the structural settlements because of its small thickness compared with that of sand. But its hydraulic conductivity was critical in these simulations.

5.4. Comparison of Numerical and Experimental

The response of the different soil-foundation-structure systems was numerically simulated in OpenSees and compared with centrifuge measurements in terms of excess pore pressures, accelerations, and settlements away from the structures (i.e., free-field or FF), near the structures (i.e., near-field or NF), and on the structure. The response of each structure was evaluated in terms of horizontal accelerations on the foundation and structural mass, settlement and tilt, and transient total, rocking, and flexural inter-story drift. The numerical results were then compared with experimental measurements for all structures and soil conditions during different ground motions to evaluate the capabilities of the numerical model.

5.4.1. Soil Response in the Free-Field (FF)

The value of hydraulic conductivity (k) for all soil layers (summarized in Table 5.3) was assumed to remain constant throughout the entire analysis time in all cases, except for the thin silt layer in T3-50-Silt. Settlements measured in the free-field and near the structures during strong shaking in centrifuge experiment T3-50-Silt showed that drainage may occur despite the presence of silt on top of the liquefiable deposit (Dashti et al. 2010a).

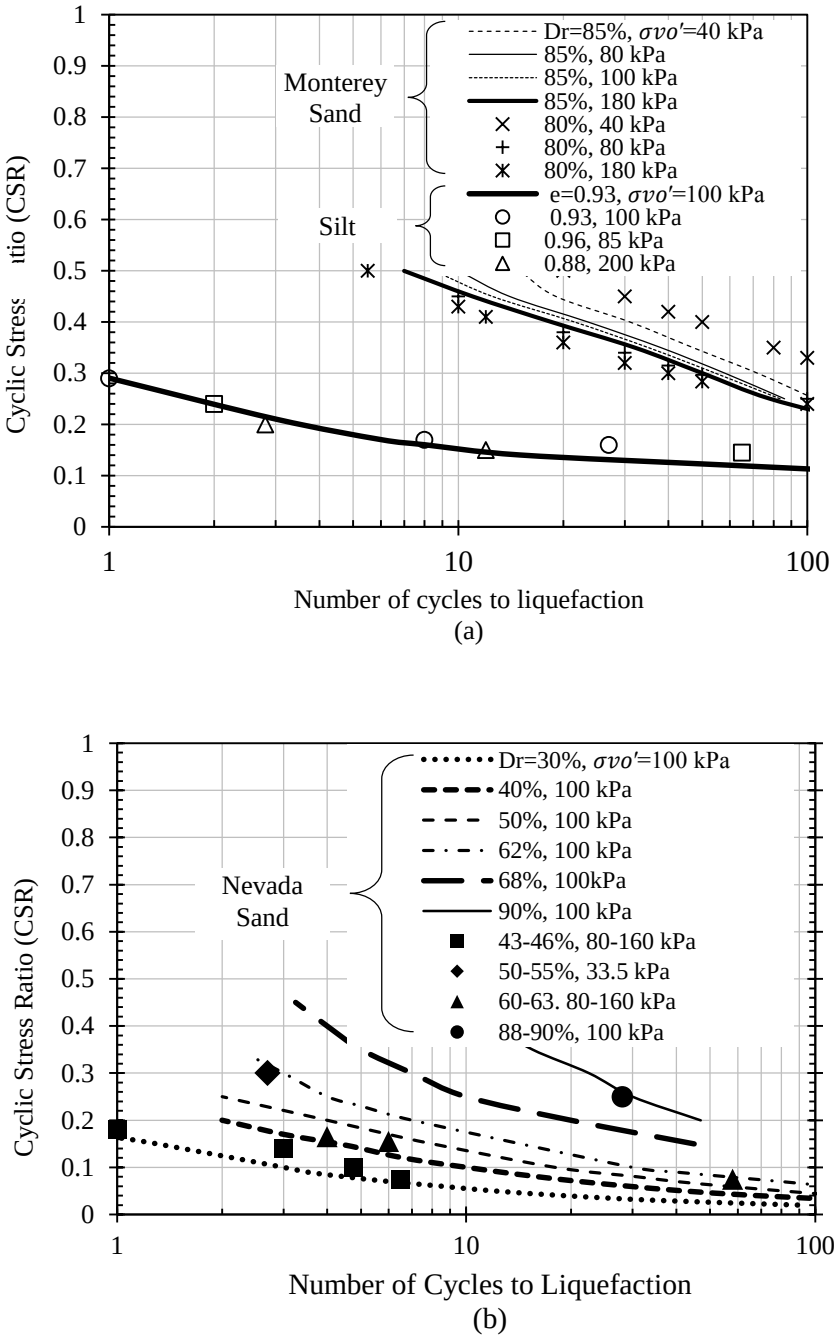

Figure 5. 3. Relation between number of cycles required to cause liquefaction (single amplitude shear strain of 3% for Monterey and Nevada Sand and 3.75% for silt) and Cyclic Stress Ratio (CSR) in numerical simulations (lines) and CSS experiments (markers) performed by: (a) Kammerer et al. (2004) on Monterey Sand and Wijewickreme (2010) on Fraser River Silt, and (b) Arulmoli (1992) and Kammerer et al. (2000) on Nevada Sand.

In this experiment, the effective k of silt likely approached that of the lower sand deposit during strong shaking. This is due to sedimentation and void redistribution in the lower layer of liquefiable sand as well as excessive upward seepage forces acting on silt. Similar to

experimental observations, the OpenSees simulations of free-field site response showed a better match between the measured and computed excess pore pressures when k of silt was increased at the start of shaking and then hyperbolically decreased back to its original value toward the end of shaking.

Table 5. 3. Values of soil hydraulic conductivity (k) used in numerical simulations

Soil Type	D_r (%)	Hydraulic conductivity k (m/s)		
		k at 1g with water	Source	k at 55 g with fluid 22 times more viscous than water
Nevada Sand	30-35	7.50×10^{-5}	Arulmoli et al. (1992)	1.88×10^{-4}
	40-45	6.50×10^{-5}		1.63×10^{-4}
	50-55	6.00×10^{-5}		1.50×10^{-4}
	60-65	5.00×10^{-5}		1.25×10^{-4}
	85-90	2.25×10^{-5}		5.63×10^{-5}
Monterey Sand	85	5.29×10^{-4}	McCartney et al. (2005)	1.32×10^{-3}
Silica Silt	—	3.00×10^{-8}	Malvick et al. (2006)	7.50×10^{-8}

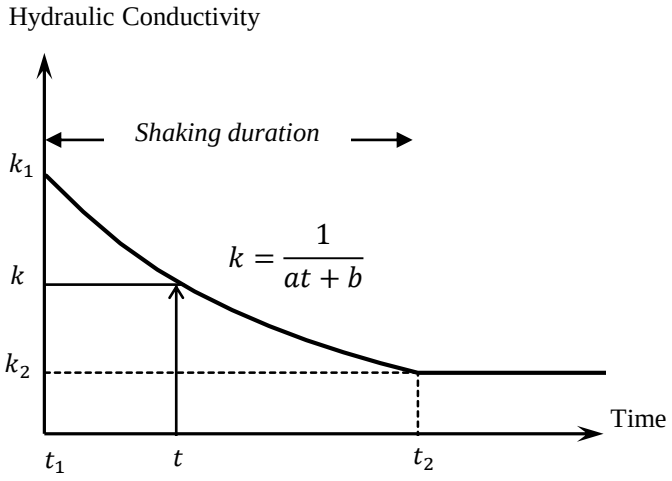

Figure 5. 4. The k function used in OpenSees simulations in relation to the duration of shaking for the thin silt layer in T3-50-Silt.

Figure 5.4 shows the approximate k function with time suggested to use in the OpenSees simulations of the thin silt layer above liquefiable Nevada Sand in T3-50-Silt to improve the fit between numerical and experimental excess pore pressure response. In this function t_1 and t_2 correspond to the beginning and end time of dynamic excitation, and k_1 and k_2 are the initial k values of liquefiable Nevada Sand and Silica Silt, respectively (listed in Table 5.3). This suggested function assumes that k of silt rises to that of the lower liquefied Nevada Sand at the start of shaking, and it hyperbolically reduces back to its original value toward the end of shaking as silt regains its strength. The values of *a* and *b* constants may be estimated based on a parabolic function of k and two known pairs of (t_1,k_1) and (t_2,k_2) for a given ground motion. Numerical and experimental excess pore pressure and acceleration time histories in the free-field in T3-50-Silt are compared during the MD PI motion in Figure 5.5, showing a reasonable match at all locations based on the proposed k function shown in Figure 5.4.

Figure 5.6 shows numerically computed and experimentally measured excess pore water pressure and acceleration time histories at different depths within the liquefiable layer and the base of the soil model in the free-field in experiments T3-30 and T3-50-Silt during the Large Port Island (LG PI) motion. In general, the nonlinear 1-D simulations in OpenSees captured free-field site response well in terms of excess pore pressures and accelerations during different motions. During the stronger events, such as LG PI shown in Figure 5.6, the contractive and dilative soil response was captured well particularly during the first few cycles of loading. The regaining of shear strength and stiffness at larger strains was captured by the model (Elgamal et al. 2005b). However, the relative density and dynamic response of soil are known to change during cyclic loading as large settlements and densification occur. This numerical model does not update soil properties in a single time domain analysis. Therefore, the increased dilation tendencies of soil that led to spikes of acceleration and simultaneous

drops in pore water pressure became more difficult to model numerically after the initial cycles. Further, the model parameters were calibrated based on a limited number of cyclic simple shear tests with a limited range of initial effective stresses and loading paths, which may not have always been applicable to the conditions in centrifuge. In general, settlements were largely under-estimated in the free-field, as discussed in detail by Karimi and Dashti (2015b). This is mainly because a constant value of hydraulic conductivity was used in the simulations, and also because the PDMY02 model is known to underestimate the coefficient of volumetric compressibility (e.g., Howell et al. 2015).

5.4.2. Soil Response in the Near-Field (NF)

Figures 5.7 and 5.8 compare the numerically computed and experimentally measured acceleration and excess pore pressure time histories within the liquefiable layer under the center of three different structures (A, B, and C) during the LG PI motion in T3-30 and T3-50-Silt, respectively. Generally, the numerical results showed good agreement with experimental recordings under and adjacent to the foundations.

The extent of excess pore pressure generation under the structure depends on factors that control the rate of excess pore pressure generation and dissipation during and after shaking: 1) intensity of shaking, 2) soil properties (e.g., thickness, relative density, and permeability of the liquefiable layer), 3) foundation contact pressure; 4) the area affected by building's overburden pressure, and 5) drainage path for the dissipation of excess pore pressures. Compared to the free-field, the cyclic stress ratio (CSR) is expected to decrease slightly in soil under the center of the building but increase near the edges of the shallow foundation due to the large stresses induced by rocking near the edges and less influence from building confinement compared to the center (Travasarou et al. 2006). The cyclic resistance ratio (CRR) of the soil is also expected to decrease under higher confinement, because soil's resistance to liquefaction triggering does not increase as fast as the confining pressure. The combination of

changes in CRR and CSR usually lead to a higher factor of safety against liquefaction triggering under the center but lower under the edges of the foundation compared to the free-field soil (Travasarou et al. 2006). But if shaking is strong enough (large enough CSR) and the foundation area is large enough to increase the drainage path adequately, large excess pore pressures and liquefaction (i.e., $r_u = u_e/\sigma'_{vo} \approx 1$, where u_e is the excess pore water pressure and σ'_{vo} is the initial overburden vertical effective stress) can still be observed even under the center of the foundation, as shown in Figure 5.7.

Typically, greater net excess pore pressures developed within the liquefiable soil under Structure B (with the largest foundation contact area) compared to Structures A and C, particularly in T3-30. The building pressure over a wider area led to a higher capacity for excess pore pressure generation in a larger volume of soil under and around the foundation. Smaller excess pore pressure ratios (r_u) were developed within liquefiable Nevada Sand under Structure C in all experiments, which had the largest foundation contact pressure and H/B ratio compared to the other two structures. Although sand under higher confinement has the capacity to generate higher excess pore pressures (for a given excess pore pressure ratio, r_u), it also demonstrates a higher resistance to liquefaction and hence, requires more energy to develop large excess pore pressures. The response of Nevada Sand under the large confining pressure of Structure C may be partially explained by its higher resistance to excess pore pressure generation under the selected input motions and partially by the relatively small contact area of the footing facilitating more efficient dissipation of excess pore pressures. These patterns were captured numerically.

The dilative response evident through drops in excess pore pressures and sharp spikes in accelerations was better captured numerically during the first few cycles of excitation compared to later cycles, because this numerical model does not update the soil properties (e.g., densification and increase in dilation tendencies) with time, as mentioned previously.

Although settlements under shallow-founded structures are often dominated by shear or deviatoric type displacements (Dashti et al. 2010a,b), volumetric strains can also be large under the footing. For example, significantly larger excess pore water pressures (u_e) were experimentally measured under the foundation compared to the free-field, particularly in T3-30 during strong events. This created a strong tendency for outward flow and volumetric strains

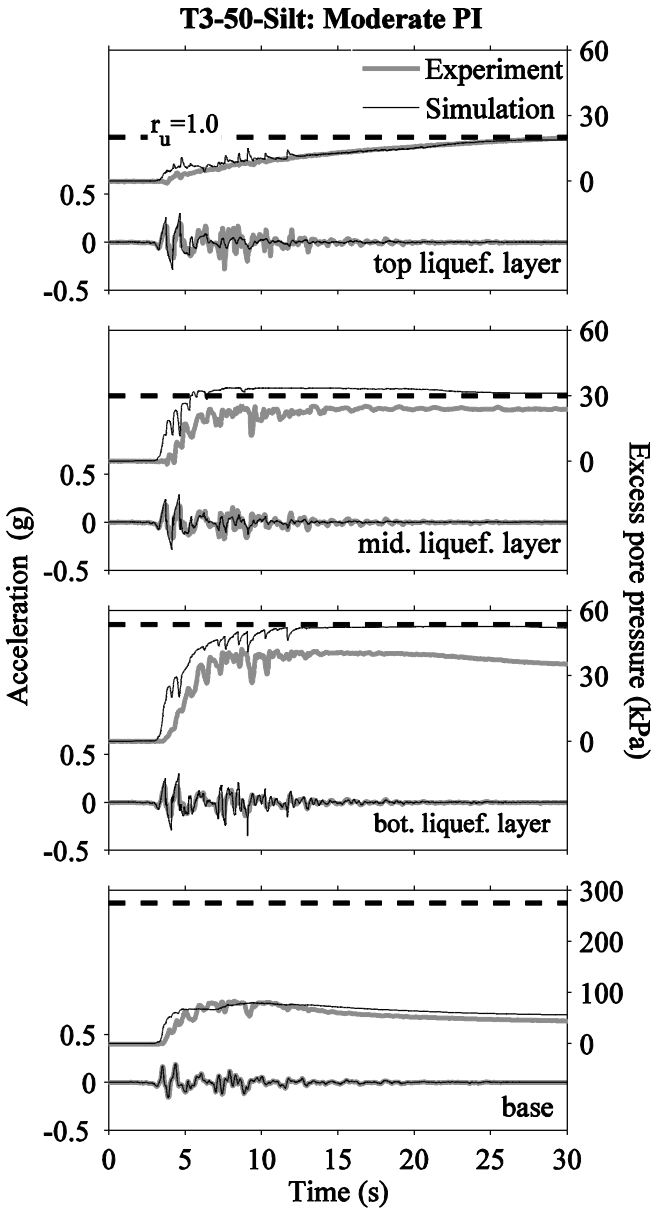

Figure 5. 5. Numerically computed and experimentally measured excess pore pressure and acceleration time histories at different depths of the liquefiable layer in the free-field in T3-50-Silt during the MD PI motion.

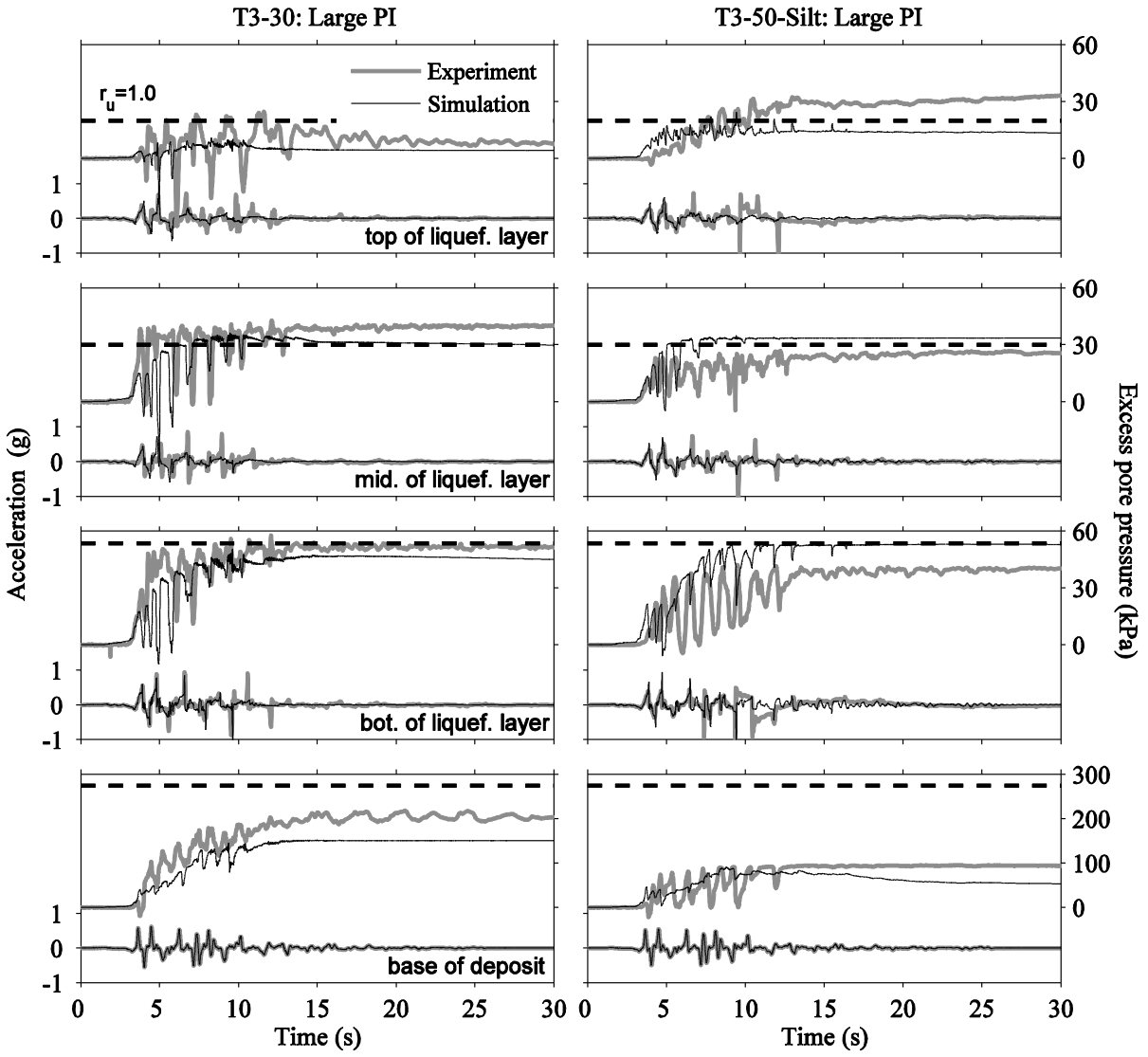

Figure 5. 6. Numerically computed and experimentally measured excess pore pressure and acceleration time histories in the free-field and at different depths of the liquefiable layer in T3-30 and T3-50-Silt during the LG PI event.

due to drainage during cyclic loading under the foundation, increasing soil's relative density and dilative tendencies over time, which are not taken into account numerically. This led to an underestimation of dilation spikes in acceleration that grew with time. In T3-50 and T3-50-Silt with a denser liquefiable soil layer (e.g., 50% instead of 30%), smaller excess pore pressures were observed under the foundation compared to T3-30. As a result, there was less volumetric strain and densification under the foundation caused by outward flow, leading to better acceleration and excess pore pressure predictions overall. Excess pore pressures and dilation

cycles were generally better captured under the edge of the foundation compared to the center, where large static and cyclic SFSI induced shear stresses and strains were present and simultaneously smaller volumetric strains were expected due to partial drainage because of smaller net excess pore pressures.

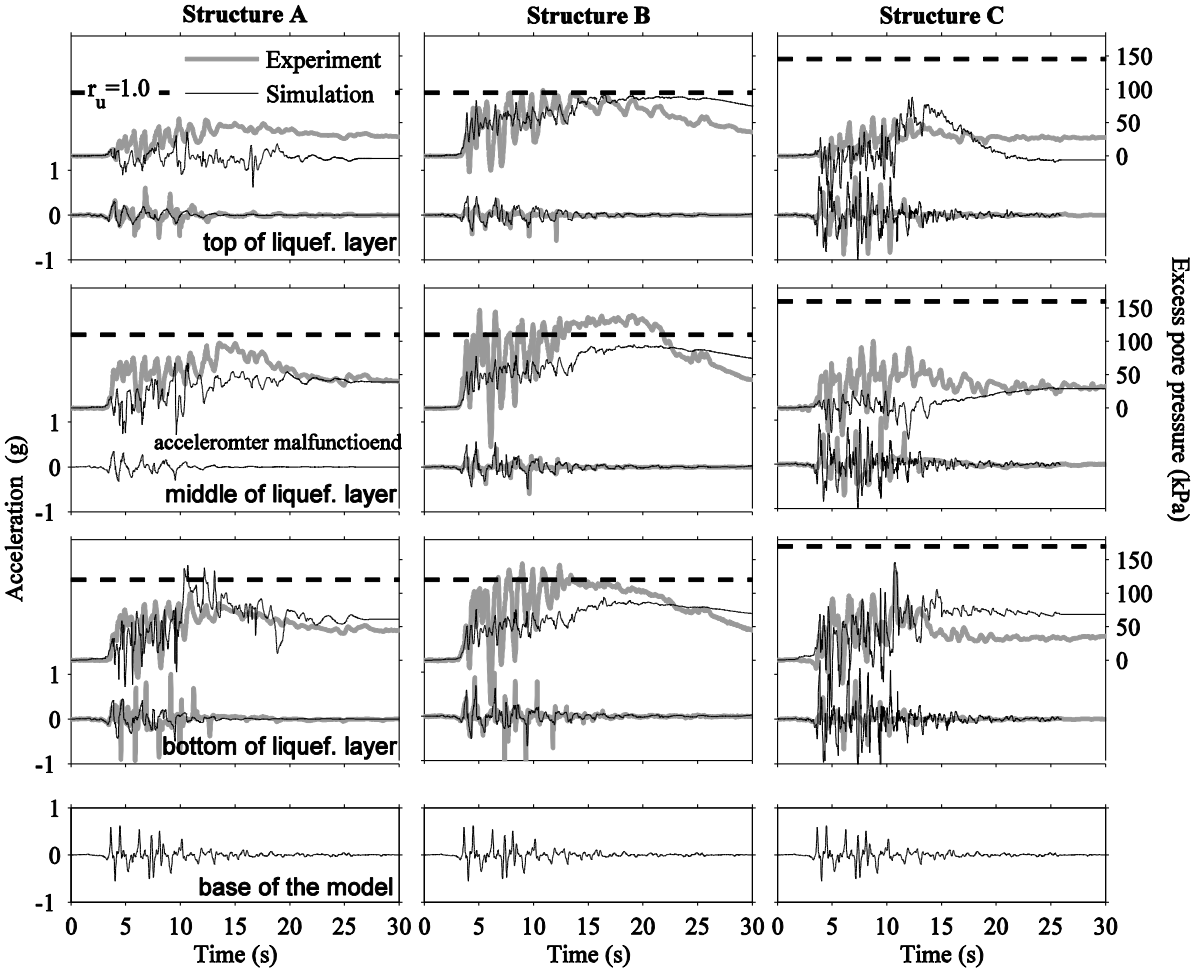

Figure 5. 7. Numerically computed and experimentally measured excess pore pressure and acceleration time histories at different depths of the liquefiable layer under the foundation center of different structures in T3-30 during the LG PI event.

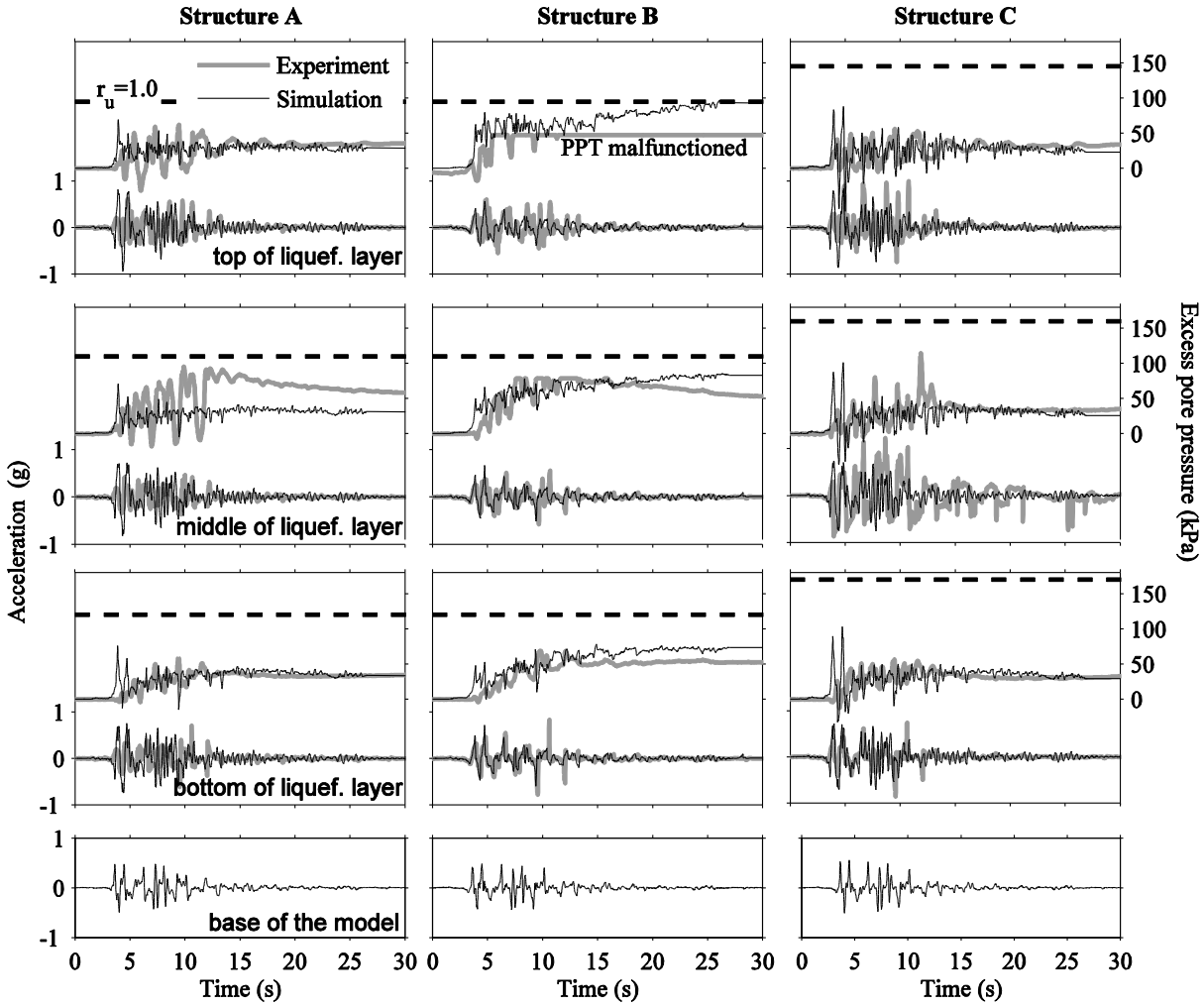

Figure 5. 8.Numerically computed and experimentally measured excess pore pressure and acceleration time histories at different depths of the liquefiable layer under the foundation center of different structures in T3-50-Silt during the LG PI event.

5.4.3. Response of the Foundation and Structure

5.4.3.1. Comparison between 2D and 3D Simulations

Since two-dimensional (2D) numerical simulations are computationally less expensive than 3D, they are advantageous if one can simplify the problem to “plain strain” conditions. The author performed 2D and 3D numerical simulations to compare the response of the foundation and structure. The structure properties were adjusted for plain strain conditions, assuming one unit length in the horizontal direction perpendicular to shaking. Because of the importance of SFSI-induced forces in this case, the same fundamental frequencies and

foundation contact pressures were adopted in the 2D and 3D analyses. The same constitutive soil model parameters were used in 2D and 3D simulations for this comparison. In addition to overall accelerations and excess pore pressure patterns in the underlying soil, the overturning moment and settlement versus rotation of the foundation was obtained from 2D and 3D analyses and compared with experimental recordings, as shown in Figure 5.9 for a representative case. P-δ effects were taken into account when calculating foundation overturning moments, considering the rocking and flexural lateral drift of the oscillatory mass relative to the foundation.

Although foundation overturning moments were predicted reasonably well in both simulations, overall, the plain strain assumption of 2D simulations led to a stiffer soil response with smaller net excess pore pressures, volumetric and shear strains, building total settlements, and foundation rotations compared to 3D simulations and experimental recordings. It is possible to compensate for a stiffer soil response in 2D by adjusting the calibrated PDMY02 model parameters for plain strain conditions and by increasing the hydraulic conductivity of soil to amplify volumetric strains under the footing due to partial drainage that in reality occurs in a 3D manner. But this approach was not taken in this study, since it may not be applicable to different boundary value problems and instead, 3D simulations were adopted with more confidence.

5.4.3.2. Fixed and Flexible-Base Structure Response

Fixed and flexible-base transfer functions of acceleration (mass/foundation) obtained numerically (from 3D analyses) and experimentally for all three structures in T3-30 during the LG PI event are compared in Figure 5.10. The flexible-base fundamental frequencies (corresponding to the peak value of transfer functions) were smaller than those under the numerically simulated fixed-base condition, as expected, particularly during stronger motions and for more slender structures (higher H/B ratios) with amplified rocking tendencies.

Numerical simulations captured the flexible-base fundamental frequency of the three structures well. Numerically computed and experimentally measured values of flexible-base fundamental period ($\tilde{T}$) of different structures during all experiments and motions are compared in Figure 5.11. The percentage difference ($d=\frac{X_{measured}-X_{computed}}{X_{measured}}\times 100$,where X is a quantity either measured experimentally, $X_{measured}$, or computed numerically, $X_{computed}$) for $\tilde{T}$ values obtained numerically and experimentally ranged from approximately -4 to 9% (with mean percentage difference, $d_{mean} \approx 3\%$) during these experiments. The numerical predictions of $\tilde{T}$ improved during less intense events and for Structure B (smaller H/B ratio compared to Structures A and C), where less period lengthening was expected.

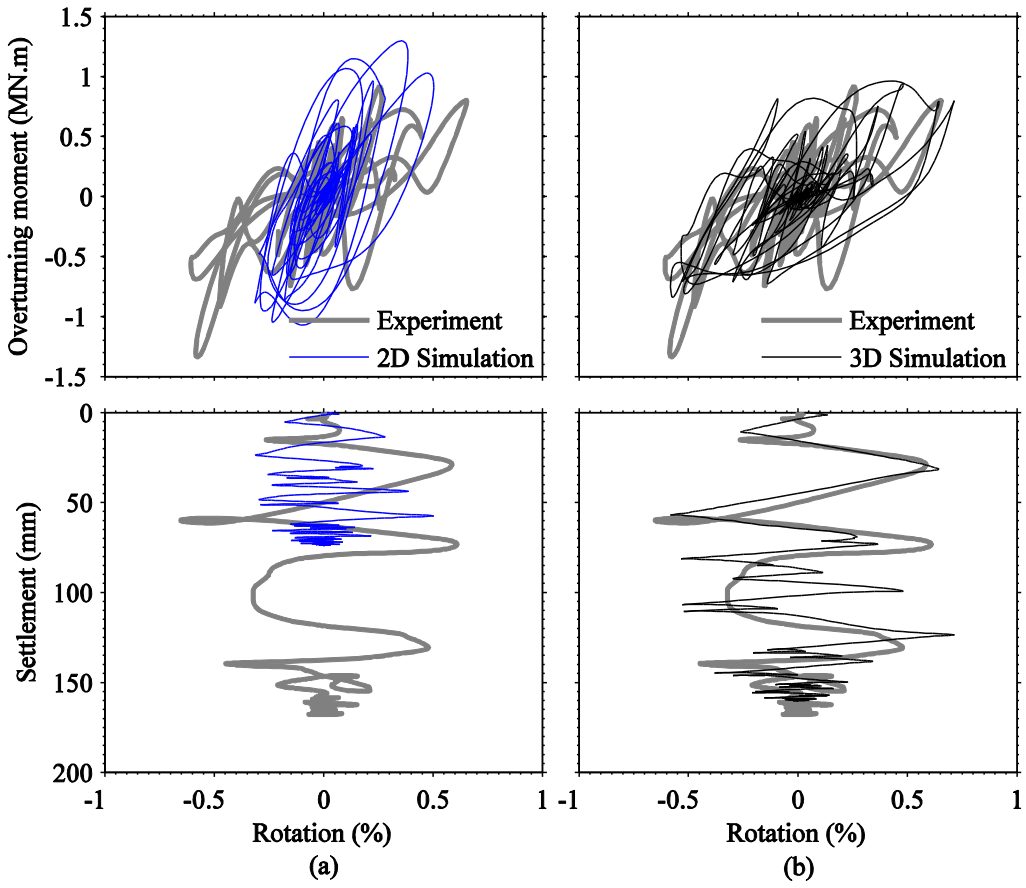

Figure 5. 9. Overturning moment and settlement versus the rotation of foundation for Structure C in T3-30 during the Moderate PI motion as measured experimentally and predicted through: (a) 2D and (b) 3D OpenSees simulations.

5.4.3.3. Foundation Settlement and Tilt

Experimentally measured and numerically computed settlements of the three structures in T3-30 and T3-50-Silt during LG PI event are compared in Figure 5.12. Settlement time histories of structures were obtained experimentally by averaging the recordings from four Linear Potentiometers (LPs) placed at the four corners of the foundation. Structures began settling after one significant loading cycle with a settlement rate that was roughly linear with time during this motion. Building settlements were shown to surpass quickly those measured in the free-field. Building settlement rates reduced dramatically after the end of strong shaking ($t \approx 12$ s) and became negligible at the end of shaking ($t \approx 25$ s). The observed trends suggest that the contribution of post-earthquake volumetric settlements to the total building settlement was relatively minor in both experiments and simulations.

The link between the initiation and intensity of shaking and the initiation and rate of building settlement point to the importance of a building's dynamic response and SFSI, which was captured well numerically in all tests. The presence of the low permeability silt layer on top of liquefiable Nevada Sand in experiment T3-50-Silt slightly increased the contribution of post-earthquake structural settlements.

Normalized foundation tilt was obtained by averaging the corner settlement recordings on each of the two sides of the foundation across its width (in the direction of shaking), subtracting the difference to obtain differential settlement, and normalizing it by the width of the foundation. Numerical and experimental values of normalized tilt are compared in Figure 5.13 for all structures in T3-30 during the LG PI motion both in terms of time histories and Fourier amplitude spectra. Although Structure C settled less than Structures A and B during this experiment and motion, it exhibited a stronger tendency for transient and permanent tilt. In most cases, an increase in building H/B amplified the tilting tendencies. However, the degree of excess pore pressure generation in the underlying soil also influences building tilt. For

example, in T3-50-Silt, Structure A (with a smaller H/B and contact pressure) tilted more than C during the LG PI motion, because of more extensive pore pressure generation in the soil below. Therefore, building's H/B and contact pressure in relation to the soil density and shaking intensity can all influence the extent of pore pressure generation and building's tilting potential. These trends were captured reasonably well numerically.

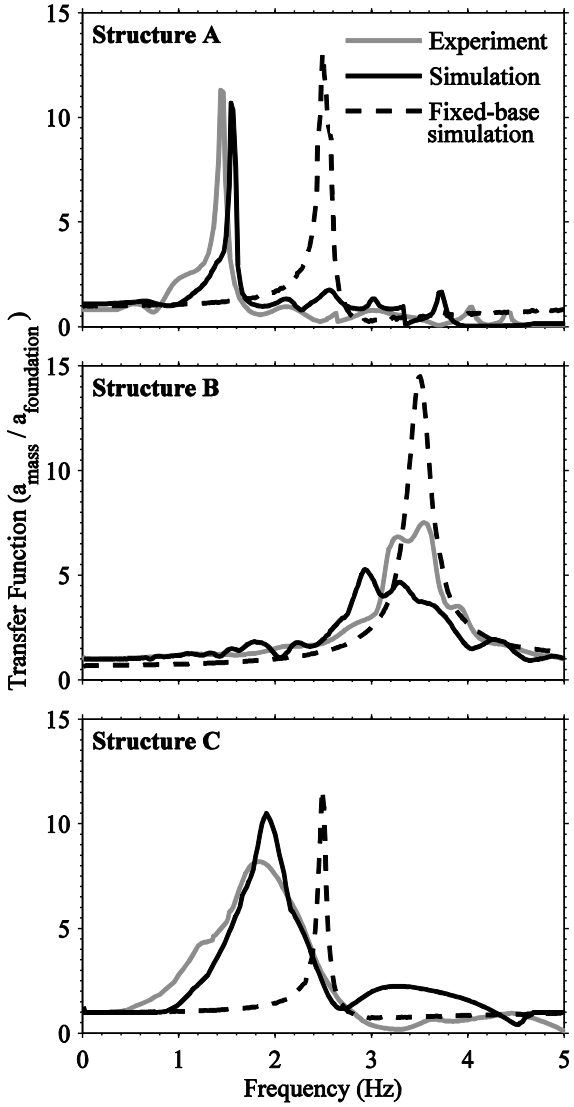

Figure 5. 10. Fixed and flexible-base transfer functions of acceleration (mass/foundation) for three structures in T3-30 during the LG PI event.

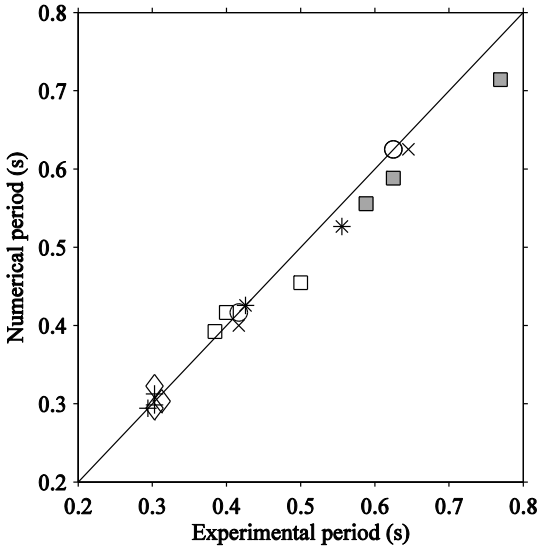

Figure 5. 11. Numerical and experimental flexible-base natural periods of three structures during different experiments and shaking events.

Although numerical simulations predicted the permanent tilt of structures relatively well, they often underestimated the amplitude of transient tilt. In the numerical simulations presented here, foundation elements were directly attached to soil. Adding zero length elements at the soil-foundation interface with a suitable choice of stiffness and damping is expected to improve the predicted transient tilt amplitudes by modeling the relative movement of the foundation and soil at their interface in a more realistic manner. The tilt or rocking fundamental frequency of structure was, however, predicted well (Figure 5.13b). The rocking fundamental frequency of all structures ranged from about 1.5 to 2.5 Hz during the SM PI motion, which decreased to about 0.4 to 0.6 Hz during the MD and LG PI motions with more extensive softening in the foundation soil both numerically and experimentally.

The performance of foundation in terms of permanent settlement and tilt are critical for design and selection of a mitigation technique. Numerical and experimental values of permanent settlement and tilt are compared for all structures and experiments in Figure 5.14. Building settlement trends were consistent in T3-30 and T3-50-Silt for structures that did not have a high tilting tendency (i.e., Structures A and B with lower H/B). Structure A settled

slightly more than B in all cases, and they both settled less during T3-50-Silt compared to T3-30. Therefore, increasing the foundation contact area or the relative density of the liquefiable material decreased total permanent building settlement in these experiments.

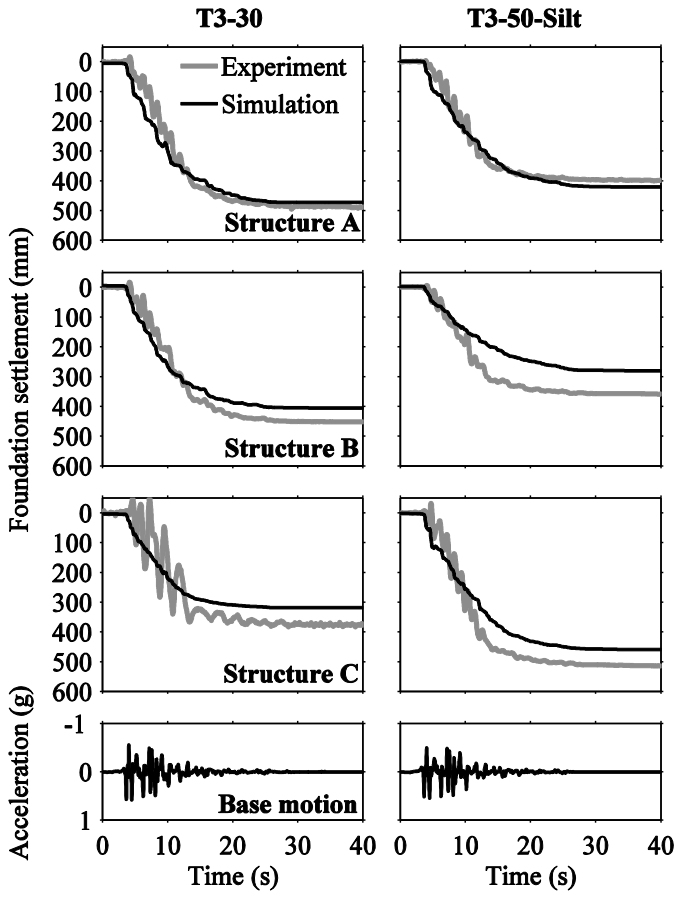

Figure 5. 12. Numerical and experimental settlement time histories of the three structures in T3-30 and T3-50-Silt during the LG PI event.

The response of Structure C was more difficult to predict, because SFSI effects were more important due to its larger contact pressure and higher center of gravity (larger H/B ratio). Structure C settled slightly less than Structure A during the LG PI motion in T3-30 but settled significantly more than the other structures in T3-50-Silt. A building's response to rocking is highly sensitive to the changes in building shaking and soil softening. Also, an increase in soil relative density in such cases might at times have an adverse effect on building settlements by reducing excess pore pressures and amplifying accelerations. In fact, Structure C settled more

in T3-50-Silt than in T3-30 during the LG PI motion (see Figure 5.12) due to its amplified base acceleration and SFSI-induced ratcheting into the softened foundation soil. This case, however, was unique to Structure C in the presented experiments, and in all other cases settlements decreased on a denser soil. Additional testing and simulations are needed before firm conclusions can be made.

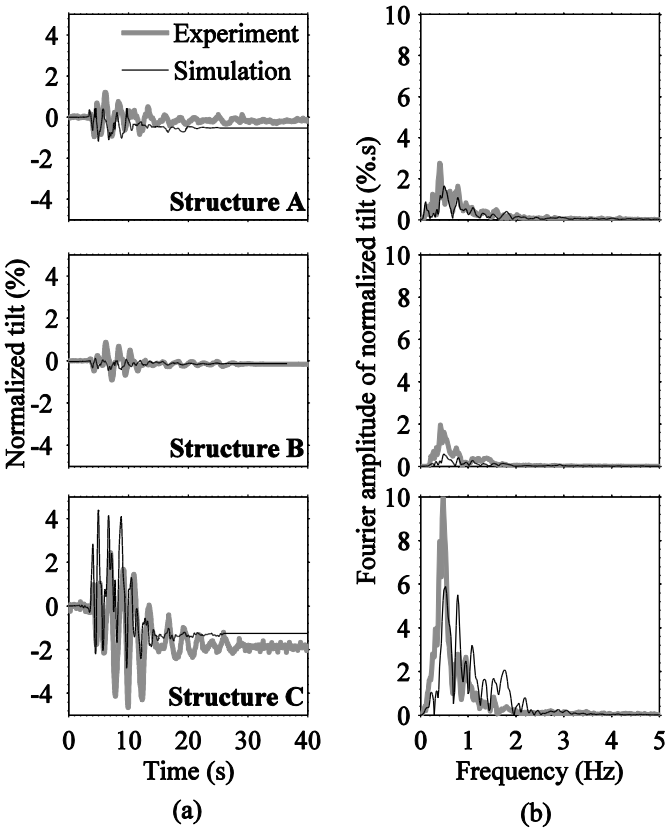

Figure 5. 13. Numerical and experimental permanent tilt (differential foundation settlement normalized by width) for three structures in T3-30 during the LG PI event: (a) time histories, and (b) Fourier amplitude spectra.

Numerical predictions of building permanent settlement captured the experimental trends well with a percent difference (d) ranging from -55 to 50% and $d_{mean} \approx 2\%$. The predictions mostly improved for larger values of settlement (greater than about 10 mm) corresponding to stronger motions. The percent difference between the numerical and experimental values of permanent foundation tilt ranged from $d \approx$ -700 to 90% (with $d_{mean} \approx$ -

83%), which was significantly larger than those of settlement, as demonstrated in Figure 5.14. This is due to the difficulty of capturing the building's cumulative tilt over time numerically.

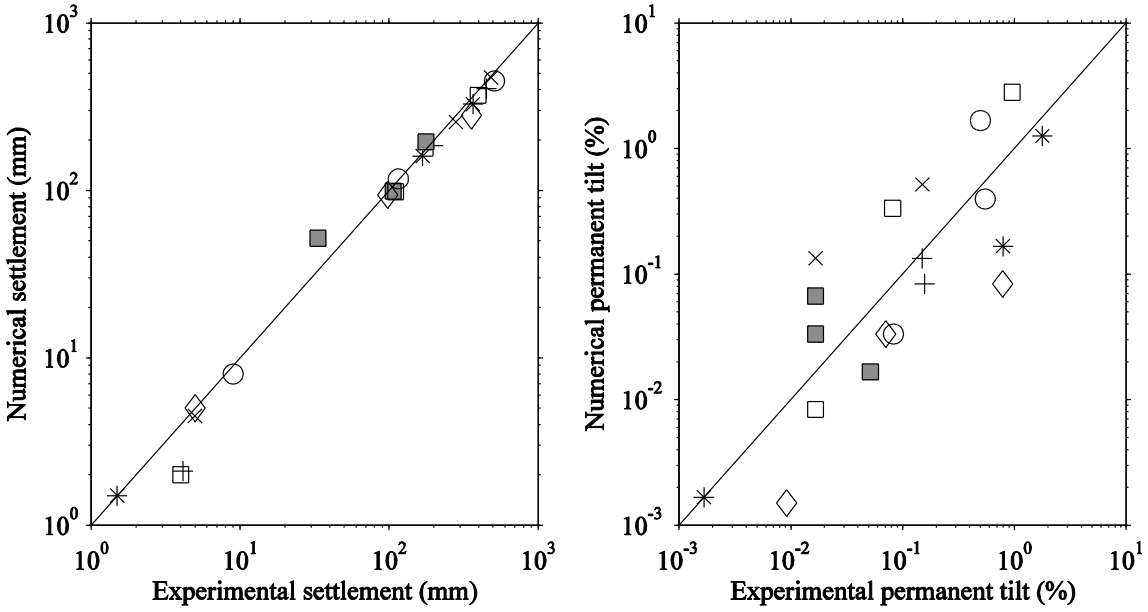

Figure 5. 14. Experimentally measured and numerically predicted values of: (a) permanent foundation settlement, and (b) permanent foundation tilt.

5.4.3.4. The Inter-Story Drift of Structures

The lateral transient displacement of the structure mass relative to its foundation is an important engineering demand parameter that affects building's performance and damage potential. This becomes important particularly when evaluating the effectiveness of mitigation techniques. Here, the total relative lateral displacement between the mass (roof) and foundation is referred to as 'total drift' (δ_T), which has two components (Gelagoti et al. 2012): 1) flexural drift (δ_F) due to the structure's flexural distortion, and 2) rocking drift (δ_R) due to foundation tilt (rigid body rotation) as depicted schematically in Figure 5.15. Foundation rocking (rotation) was experimentally measured using linear potentiometers (LPs) on the two sides of the foundation. The transient lateral displacement of the mass and foundation was, however, obtained indirectly through double integrating acceleration time histories from accelerometers.

No direct horizontal displacement measurements were obtained on structures, due to the concern that a spring-loaded LP would affect the building's response. Since no permanent flexural drift was expected on these structures, this approach was judged appropriate (i.e., structural deformations were kept in their elastic ranges). Numerical predictions of drift were obtained directly from the predicted lateral displacement of the mass and foundation and the vertical displacement of the two sides of foundation.

The values of δ_T, δ_F, and δ_R were divided by the height of center of gravity of a given structure to obtain its inter-story drift ratio. The numerical and experimental drift ratio time histories are compared for Structure A in T3-30 during the LG PI motion in Figure 5.16. The peak values of drift ratio are compared for all structures and experiments in Figure 5.17. The numerical predictions were generally acceptable, with d ≈ -303 to 88% (d_{mean} ≈ 10%) for total inter-story drift ratios, d ≈ -100 to 93% (d_{mean} ≈ -68%) for rocking inter-story drift ratios, and d ≈ -251 to 72% (d_{mean} ≈ 2%) for flexural inter-story drift ratios, which improved for larger drift values associated with stronger levels of shaking.

Flexural drift (δ_F) is expected to influence the structure's damage potential the most, because it is related to column bending as opposed to rigid body rotation. For the same δ_T, more rocking tends to reduce the building's δ_F and hence, its damage potential. Generally, the potential for total drift increased with the structure's H/B ratio, mass of the oscillator, and intensity of shaking. But rocking-induced drift (δ_R) also increased with these parameters in most cases. Therefore, δ_F ($=\delta_T-\delta_R$) did not always increase for a building with a greater H/B ratio. Importantly, increasing the D_r of the liquefiable soil (going from T3-30 to T3-50 or T3-50-Silt) amplified δ_F by amplifying the foundation motion (i.e., increase in demand that consequently increased δ_T) and de-amplifying rocking tendencies (δ_R), a trend observed both experimentally and numerically.

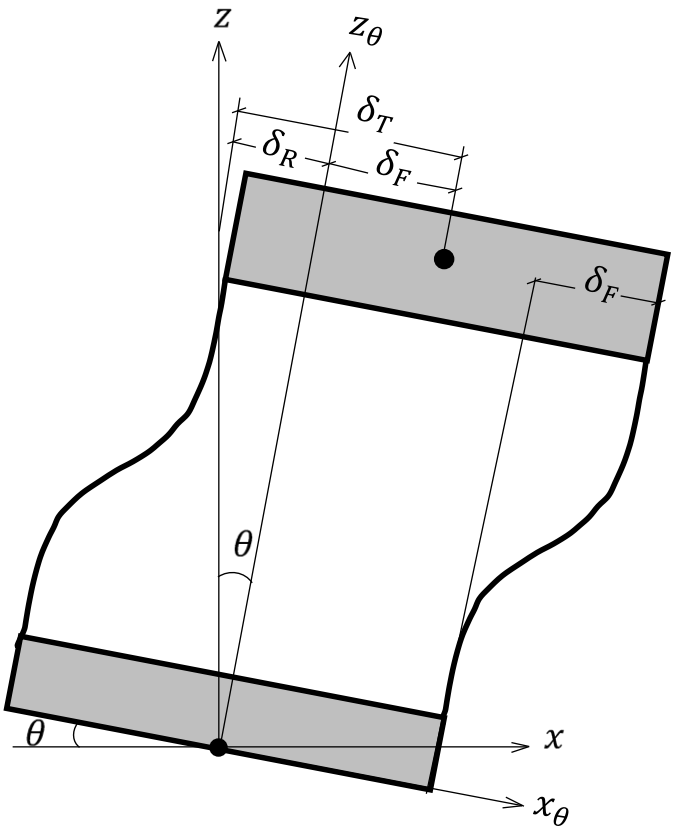

Figure 5. 15. Schematic drawing of total (δ_T), rocking (δ_R), and flexural (δ_F) inter-story drift for a rocking foundation-structure system.

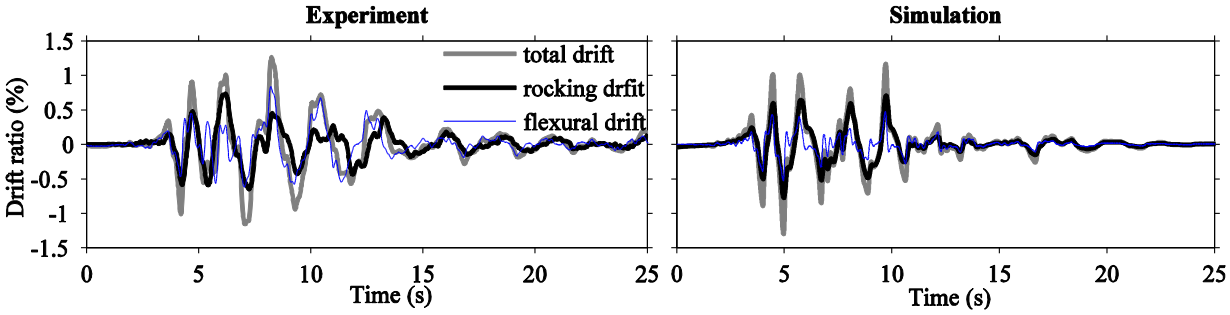

Figure 5. 16. Experimental and numerical total, rocking, and flexural inter-story drift ratio time histories of Structure A in T3-30 during the LG PI motion.

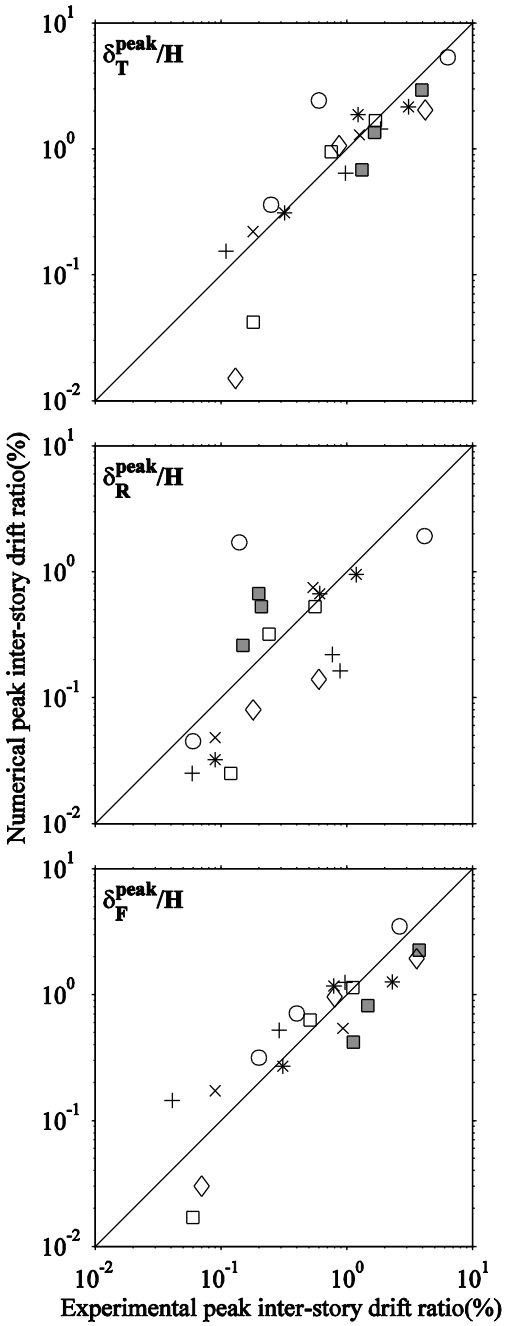

Figure 5. 17. Experimentally measured and numerically predicted peak total, rocking, and flexural inter-story drift ratios for all structures and experiments.

5.5. Concluding Remarks

A series of centrifuge experiments was performed to investigate the seismic response of single-degree-of-freedom (SDOF) structures founded on stiff, mat foundations and layered liquefiable deposits. Solid-fluid, fully-coupled, 3-D, nonlinear numerical simulations of the

centrifuge tests were performed using the PDMY02 model implemented in OpenSees to evaluate and compare computed and measured structural response on softened ground.

Nonlinear, 1-D, site response analyses captured free-field soil behavior well in terms of excess pore pressures and accelerations during different motions, particularly during the initial cycles, while settlements were largely under-estimated. This was mainly attributed to the use of a constant hydraulic conductivity in the simulations as well as the under-estimation of soil volumetric compressibility.

Smaller net excess pore pressures were generated within the liquefiable layer under the structure with the highest contact pressure and H/B ratio for the cases considered. This may be partially explained by a higher resistance to excess pore pressure generation under higher confinement and partially by the relatively small contact area of the footing facilitating more efficient dissipation of excess pore pressures in a 3D manner. The patterns in the degree of excess pore pressure generation observed experimentally were captured well numerically.

The observed settlement patterns in experiments suggest that the contribution of post-earthquake volumetric settlements to the total building settlement was relatively minor. Volumetric strains due to partially drained cyclic loading as well as deviatoric strains under the static and dynamic shear stresses imposed by the building were responsible for the majority of building settlements, all of which primarily occurred during shaking. The numerical model could predict deviatoric displacements and hence, foundation settlements reasonably well by capturing excess pore pressures and accelerations under and near the foundation. For the cases considered in this study, numerical predictions of building permanent settlement compared fairly well with experimental results (percent difference, d, ranging from -55 to 50%, with $d_{mean} \approx$ 2%), while the predictions of permanent foundation tilt did not compare as well with the experiments (d ranging from -700 to 90%, with $d_{mean} \approx$ -83%).

Numerical simulations captured the different components of building drift reasonably with d_{mean} = 10, -68, and 2% for total, rocking, and flexural inter-story drift ratios, respectively. Increasing the structure's contact pressure and H/B generally amplified its rocking and total drift, but not necessarily the flexural drift. Importantly, increasing the relative density of soil amplified flexural drift (an indicator of damage) by decreasing excess pore pressures in the foundation soil and building's rocking tendencies, while amplifying foundation accelerations and seismic demand. These observations are intended to help future numerical parametric studies of the response of shallow-founded structures on layered liquefiable soil deposits for more general conditions and guide mitigation decisions that focus on improved building performance.

The observations made in this study are limited to the soil, structural, and loading conditions investigated in this study. Additional element level tests on granular soils under sinusoidal and irregular loading as well as different confining pressures will improve numerical models and their calibration. The structures employed in centrifuge and numerical simulations were simplified, linear-elastic, SDOF structures. The response of inelastic, MDOF structures that are capable of damage needs to be investigated on liquefiable ground with and without mitigation in future experimental and numerical studies, in order to better evaluate the effectiveness of remediation strategies in the context of building performance. Further, the influence and importance of multi-dimensional cyclic loading (as opposed to 1-D shaking) on the seismic performance of structures on softened ground need to be investigated in future studies.

CHAPTER 6

GROUND MOTION INTENSITY MEASURES TO EVALUATE THE LIQUEFACTION HAZARD IN THE VICINITY OF SHALLOW-FOUNDED STRUCTURES

This chapter is based on the following reference:

Dashti, S., and Karimi, Z. (forthcoming). Ground Motion Intensity Measures to Evaluate I: the Liquefaction Hazard in the Vicinity of Shallow-Founded Structures. Earthquake Spectra, EERI (under review).

6.1. Introduction

Geotechnical engineers increasingly need to evaluate the liquefaction hazard and its consequences within a performance-based earthquake engineering (PBEE) framework. The approach adopted may vary widely, ranging from empirical, simplified procedures to nonlinear, fully-coupled, dynamic numerical simulations. With any approach, however, the potential for liquefaction triggering and its effects on the site and structure need to be evaluated over a range of ground motion intensity levels. Knowledge and use of an optimum Intensity Measure (IM) during the selection and scaling of input motions in any analysis will help reduce variability and improve the confidence level in the predicted Engineering Demand Parameter

(EDP) of interest, such as peak excess pore pressure ratio or settlement (Kramer and Mitchell 2006).

The existing empirical procedures for evaluating liquefaction triggering (e.g., Youd et al. 2001; Seed et al. 2003; Idriss and Boulanger 2008) rely on ground motion IMs that may not be optimum in terms of their ability to reduce variability in the predicted response or their independence from source characteristics. In these procedures, the peak ground acceleration at the surface in the free-field ($PGA_{FF\text{-}Surface}$) is often used in combination with earthquake magnitude (M_w) to characterize the intensity and duration of seismic loading, which are compared with a measure of soil resistance to obtain a factor of safety against liquefaction triggering (FS_{liq}) at the site. The same IMs or the resulting FS_{liq} are used to evaluate liquefaction-induced soil settlement in the free-field (e.g., Ishihara and Yoshimine 1992; Tokimatsu and Seed 1987). The estimation of PGA at the surface of a highly nonlinear soil profile (e.g., susceptible to liquefaction) introduces a great deal of uncertainty in evaluating the liquefaction hazard and the resulting settlements. Further, the influence of traditional IMs (e.g., $PGA_{FF\text{-}Surface}$) on the variability of the predicted response (e.g., excess pore pressure generation or settlement) is not well understood. Lastly, none of the previous empirical procedures consider the influence of a building and soil-structure interaction (SSI) on the extent of excess pore pressure generation, the liquefaction hazard, and the resulting settlements, which are important near our built facilities.

Nonlinear, fully-coupled, dynamic numerical simulations of the soil-structure system are more regularly used by engineers, particularly in sensitive projects, in order to evaluate liquefaction triggering, post-liquefaction instability, and the resulting displacements in an integrated manner. As the speed of computationally intensive simulations improves and more advanced numerical models are validated against physical model studies or case histories, this trend will likely continue. Kramer and Mitchell (2006) showed numerically how the

liquefaction hazard, quantified as the mean value of final excess pore pressure ratio, $r_{u,mean}$, averaged over the saturated portion of the liquefiable layer in the free-field, is influenced by different IMs. Accordingly, they recommended an efficient and sufficient IM appropriate for this EDP. However, the influence of pore pressure redistribution (i.e., pore pressure dissipation) during and after cyclic loading, which strongly affects the response of the liquefiable soil and the presence of a building on the generated excess pore pressures were not considered in this pioneering study.

As excess pore pressures are generated, they simultaneously dissipate according to 3-D hydraulic gradients and hydraulic conductivities in the soil profile. The rate of flow is particularly high during shaking, as hydraulic gradients are kept at their peak and soil approaches a state near liquefaction (Dashti et al. 2010a; Shahir et al. 2012; Karimi and Dashti 2015b). The redistribution of pore pressures is expected to influence the net value of excess pore pressure ratio achieved at a given location and hence, the liquefaction hazard. Further, the extent of excess pore pressure generation depends on the level of shear strains imposed on the soil (e.g., Dobry et al. 1982). The level of induced shear strains depends on soil properties (e.g., thickness and stiffness of the liquefiable soil), input motion characteristics (e.g., amplitude, frequency content, and duration), and importantly properties of the superstructure (e.g., geometry, modal frequencies, and contact pressure). Therefore, excess pore pressure generation and its consequences are expected to be affected by the presence and properties of structures. The influence of different ground motion IMs on site performance (accelerations, excess pore pressures, and settlements) near a building when founded on liquefiable ground has not yet been explored. This shortcoming prevents the selection and scaling of input ground motions that minimize variance in the predicted response (EDP|IM) in the vicinity of buildings. This gap also hampers the development of future probabilistic predictive models for evaluating

liquefaction triggering and consequences not just in the free-field – where no structure is present – but also near structures.

In this and the following chapters, the author presents the results of a three-dimensional (3D), nonlinear, solid-fluid, fully-coupled, dynamic, finite element parametric study that was previously validated using centrifuge experimental results for a range of soil, structure, and ground motion characteristics. The influence of different IMs from ordinary and near-source ground motion recordings are evaluated on the response of the soil-structure system. Different IMs are evaluated and compared for each soil and structure EDP in terms of their efficiency, sufficiency, and predictability. This chapter focuses primarily on the influence of the site and structure on ground motion characteristics, and the subsequent effects on the liquefaction hazard (EDP = peak excess pore pressure ratio = $r_{u,peak}$ = peak excess pore pressure / initial vertical effective stress = u_{excess}/σ'_{vo}) both in the free-field and near the structure. In the next chapter, the influence of different IMs is explored on EDPs related to structural performance, such as permanent settlement, tilt, and peak transient inter-story drift ratio. The insight from this study is intended to guide the future selection and scaling of input motions used in the evaluation and mitigation of the liquefaction hazard and its consequences.

6.2. Modeling the Soil-Structure System

6.2.1. Numerical Simulations and Validations with Centrifuge Experiments

Dynamic centrifuge tests were performed by Dashti et al. (2010a,b) to evaluate the response of different SDOF structures with stiff, shallow mat foundations on layered, liquefiable soil deposits. The primary goal of these experiments was to identify the dominant mechanisms of liquefaction-induced building settlement and the influence and relative importance of different testing parameters on building response. The experiments modeled a soil profile consisting of a 2 m-thick (prototype scale) Monterey Sand (D_{50} = 0.40 mm, C_u =

1.3, e_{min} = 0.54, e_{max} = 0.84) with relative density (D_r) ≈ 85% overlying a 3 to 6m-thick liquefiable layer of Nevada Sand (D_{50} = 0.14 mm, C_u =2.0, e_{min} = 0.55, e_{max} = 0.84) with D_r ≈ 30% and 50%, both overlying an 18 to 21 m-thick layer of dense Nevada Sand with D_r ≈ 85%. One of the experiments also used a 0.8 m-thick layer of Silica Silt (D_{50} = 0.02 mm) underlying a 1.2 m-thick layer of Monterey Sand above the liquefiable layer to evaluate the influence of change in drainage conditions. The models were saturated below a depth of 1 m with a solution of hydroxypropyl methylcellulose in water, as detailed by Dashti et al. (2010a,b). Figure 6.1 presents a schematic drawing of a representative centrifuge experiment with its instrumentation. The models were spun to a nominal centrifugal acceleration of 55g and then, ground motions were applied to the base of the models in each test in the same sequence.

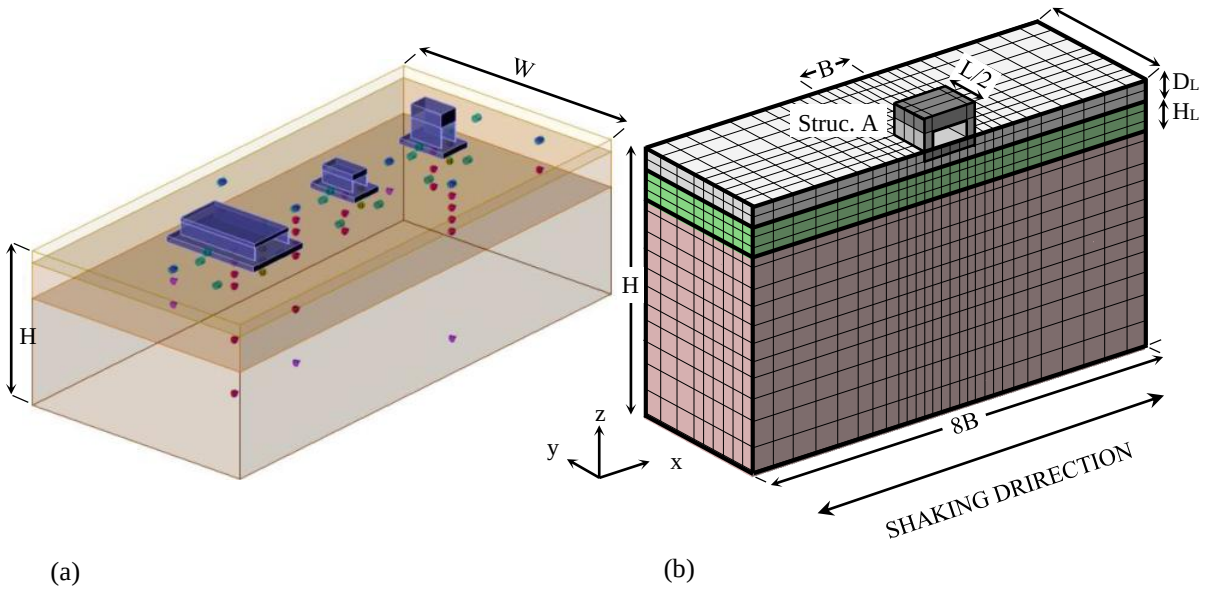

Figure 6. 1. Schematic drawing of: (a) centrifuge experiments performed by Dashti et al. (2010a,b) with three SDOF structures on a layered soil profile, including a liquefiable layer; (b) finite element discretization of the soil-structure system for one example structure (A).

Three elastic SDOF structures made of steel and aluminum were mounted on 1 m-thick, stiff mat foundations with varying modal frequencies, contact pressures, and height/width (H/B) ratios representative of 2 to 4 story structures. Bearing pressure and fixed-base natural

frequencies (f_n) of structures ranged from 80 to 130 kPa and 2.5 to 3.5 Hz, respectively. The properties of structures and base motions (as recorded) were presented by Dashti et al. (2010a,b) and Karimi and Dashti (2015b,2016), as discussed in the previous chapters.

Solid-fluid, fully-coupled, 3D, nonlinear finite element analyses of the centrifuge tests were subsequently performed using the pressure-dependent, multi-yield-surface, plasticity-based soil constitutive model (PDMY02) implemented in OpenSees by Elgamal et al. (2002) and Yang et al. (2003 and 2008). Analyses were performed in 3D to simulate the response of shallow-founded structures on liquefiable ground, the stress field around the foundation, soil nonlinearity, soil-structure interaction (SSI) effects, and the drainage conditions that are known to influence the seismic performance of the site and structure. The time and location of liquefaction triggering, softening followed by stiffening, and the resulting excess pore water pressures (i.e., the net result of excess pore pressure generation and redistribution), accelerations, and displacements in the free-field and near the structure were evaluated in a single time-domain analysis for each test.

The soil model parameters were first calibrated based on the undrained cyclic simple shear tests available on each test soil (detailed by Karimi and Dashti 2015b, 2016), in order to capture the generation of excess pore pressures and cyclic shear strains at an element level. The predicted soil response was also compared with field behavior (e.g., NCEER 1997) in terms of the number of cycles required to trigger liquefaction for a given cyclic stress ratio, CSR (Karimi and Dashti 2015a). Then, the calibrated soil parameters were used in modeling the centrifuge experiments in the free-field and near-field.

The nonlinear soil constitutive models developed to capture soil behavior during liquefaction are complex with many parameters. It is important to validate their response and evaluate their strengths and weaknesses for a particular boundary value problem with a range of soil, structural, and ground motion characteristics, before they are employed in a parametric

study. The accuracy of numerical predictions was evaluated by Karimi and Dashti (2015b) in terms of residuals:

$$\text{Residual X}=\left(\frac{X_{\text{experimental}}}{X_{\text{numerical}}}\right) \tag{6.1}$$

where X refers to a given quantity obtained numerically or experimentally.

Overall, accelerations and excess pore water pressures were captured reasonably well both in the free-field and near-field with mean residuals ranging from -0.2 to 0.6 for pseudo spectral accelerations (PSA) and from -0.5 to 0.2 for peak excess pore pressure ratios ($r_{u,peak}$) under and away from the building.

Figure 6.2 shows the residuals of PSAs (5% damped) in the middle of the liquefiable layer in the free-field and under the foundation. The numerically predicted $r_{u,peak}$ values in the middle of the liquefiable layer in the free-field and near-field are compared with the experimental measurements in Figure 6.3.

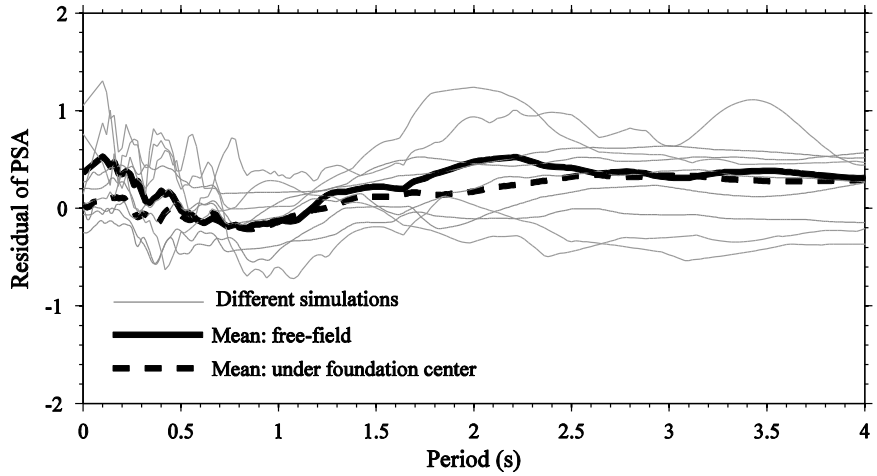

Figure 6. 2. Residual of 5%-damped pseudo spectral accelerations (PSA) predicted numerically compared to centrifuge measurements (Dashti 2009) obtained in the middle of the liquefiable layer in the free-field and under the foundation center.

Settlements in the free-field were highly underestimated in these simulations, which was attributed to a changing hydraulic conductivity in soil during shaking (not taken into

account numerically) and the underestimation of soil's volumetric compressibility under constant stress ratio by the constitutive model (Karimi and Dashti 2015b). As a result, in the parametric study that followed, free-field settlements were not investigated. The quality of estimated building settlement, tilt, and drift will be discussed in the next chapter that focuses primarily on building performance when founded on liquefiable ground.

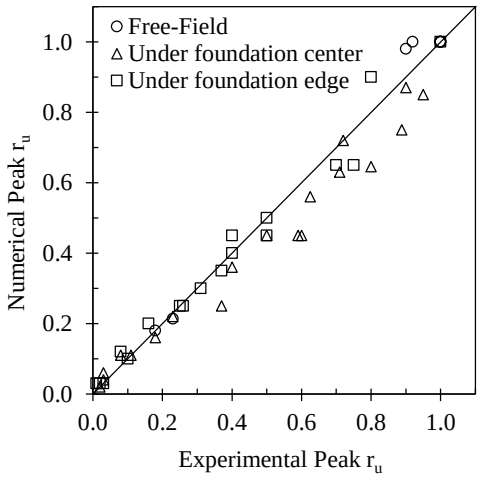

Figure 6. 3. Comparison of peak excess pore water pressure ratios (r_u) in the middle of the liquefiable layer in the: free-field, under the foundation center, and under the center of foundation edge obtained from centrifuge measurements and numerical simulations.

6.2.2. Numerical Parametric Study

Identification of optimal IMs for evaluating the liquefaction hazard and its effects on the site and structure was accomplished by performing similar 3D, solid-fluid, fully-coupled, nonlinear finite element analyses of layered liquefiable soil deposits and elastic SDOF structures on stiff mat foundations. Because the properties of soils and structures were calibrated and validated against centrifuge results, the parametric numerical study that followed was based on similar soil and structural conditions, now considering additional variables and earthquake motions that were not practical experimentally. It is recognized that centrifuge experiments and their subsequent numerical simulations are gross simplifications of soil conditions, structural complexities, and 3D earthquake motion characteristics encountered in

the field. Nevertheless, they provide valuable insights into the influence of ground motion characteristics and other variables on the liquefaction hazard and consequences, which will guide more complex simulations of real soil conditions in the future.

Several measures of the magnitude and timing of excess pore pressure generation were explored from the results of numerical simulations and plotted as a function of each candidate IM. The primary EDPs selected and presented in this chapter are the $r_{u,peak}$ values in the middle of the liquefiable layer in the free-field and near-field (center and middle-edge of the foundation).

Solid-fluid, fully-coupled, 3D, nonlinear finite element simulations of the soil-structure system are computationally intensive and often not practical. However, using the high performance computing facilities of Network for Earthquake Engineering Simulation, NEEShub (Hacker et al. 2013) and the Janus Supercomputer at the University of Colorado Boulder, as well as the parallel version of OpenSees (OpenSeesSP 2.4.3, McKenna et al. 2000; McKenna and Fenves 2008) reduced the running time of each simulation, making the presented parametric study possible.

Table 6.1 summarizes the properties of the soil-structure systems evaluated in the parametric study. Twenty-one cases were investigated with variations in the thickness (H_L) of, depth (D_L) to, and relative density (D_r) of the liquefiable layer, mass of structure (M), height over width ratio (H/B) of the structure, structure's contact pressure (q), fixed-base fundamental period (T_{STo}), the effective height of the structure which is the distance between the centers of mass of foundation and oscillatory mass (H_{eff}), as well as the contact area of foundation (B×L). Previous studies have shown the influence of a building's dynamic properties on its settlement and tilt response (Dashti et al. 2010a,b), which is why they were varied in this study. In several models, when changing a given structural property in the numerical simulations, other properties were kept the same. For example, when q was changed, only the foundation pressure

was varied without changing the mass of the structure, in order to keep the T_{STo} and inertial effects unchanged. When T_{STo} was changed, the stiffness was varied alone without changing the mass or center of gravity of the structure (H_{eff}). In this way, the impact of each parameter could be evaluated in isolation. In one case, the D_r of the liquefiable layer was increased to 85% (making it non-liquefiable), to evaluate the response of a densified site to the same motions.

Table 6. 1. Properties of the soil-structure models investigated in the numerical parametric study (all with a 1m thick mat foundation).

Model #	**H_L (m)**	**D_L (m)**	**$D_{r,Liquef.}$ (%)**	**q (KPa)**	**T_{STo} (s)**	**M (kg)**	**H_{eff} (m)**	**A= B×L**
1	3	2	50	76	0.39	m[2]	h_{eff}[3]	B[4]×L[5]
2	3	2	50	110	0.39	m	h_{eff}	B×L
3	3	2	50	76	0.65	m	h_{eff}	B×L
4	3	2	50	76	0.92	2m	h_{eff}	B×L
5	24	2	30	76	0.39	m	h_{eff}	B×L
6[1]	24	2	85	76	0.39	m	h_{eff}	B×L
7	2	2	50	76	0.39	m	h_{eff}	B×L
8	6	2	50	76	0.39	m	h_{eff}	B×L
9	3	3	50	76	0.39	m	h_{eff}	B×L
10	4	4	50	76	0.39	m	h_{eff}	B×L
11	3	2	50	76	0.24	m	h_{eff}	B×L
12	3	2	50	76	0.34	2m	h_{eff}	B×L
13	3	2	50	76	0.55	2m	h_{eff}	B×L
14	3	2	50	76	0.78	4m	h_{eff}	B×L
15	3	2	50	130	0.39	m	h_{eff}	B×L
16	3	2	50	76	0.39	m	$1.5h_{eff}$	B×L
17	3	2	50	130	0.39	m	$2.0h_{eff}$	B×L
18	3	2	50	76	0.39	m	$2.0h_{eff}$	B×L
19	3	2	50	76	0.58	2.25m	h_{eff}	1.5B×1.5L
20	3	2	50	76	0.26	2.25m	h_{eff}	1.5B×1.5L
21	3	2	50	76	0.39	m	$1.5h_{eff}$	1.5B×1.5L

[1] Same as model 5 but the relative density of Nevada sand is changed from 30 to 85%

[1], [2], [3], [4], [5] Values of m=412×10^3 kg, h_{eff}=342 cm, B=600 cm, and L=900 cm are based on the measured values of Structure A in the centrifuge experiment.

Table 6.2 summarizes the ground motion parameters that were evaluated in this study in terms of their influence on soil and structural response. A total of 52 ordinary ground motions

and 26 near-source ground motions was selected with a range of magnitude/distance combinations, and their effects were evaluated on different EDPs. The following criteria were used in selecting motions in this study:

- Earthquakes with moment magnitudes (M_w) between 5 and 7;
- Earthquakes with the closest distance to rupture surface (R) ranging from 16 to 40 km for ordinary motions and less than about 16 km for near-source motions;
- Sites classified either as rock or very dense soil/soft rock.

Table 6.3 details the list of earthquake motion recordings, the horizontal component of which was applied to the base of all the numerical models. All motions were obtained from the PEER Strong Motion Database (available at http://ngawest2.berkeley.edu/). The horizontal, strike-normal component of near-source motions was computed and used in simulations, in which the influence of forward-directivity could be better manifested. The fault parameters needed to compute the fault-normal component of motions were obtained from Somerville et al. (1997a).

In addition to traditional IMs (e.g., PGA, PGV, PGD, AI), parameters that characterize the frequency content or duration of the ground motion (e.g., T_p, T_m, or $D_{5\text{-}95}$) were also investigated in terms of their change due to site response or SSI effects. Each IM was then independently evaluated in terms of its efficiency and sufficiency in predicting a given EDP in a similar manner as Luco and Cornell (2001), Kramer and Mitchell (2008), and Hariri-Ardebili and Saouma (2016), while also considering their predictability with the available attenuation models. The degree of scatter in the computed EDPs (in this case $r_{u,peak}$) about the regression curve given a candidate IM was used to evaluate the efficiency of that IM. The degree to which the residual of EDP given an IM is statistically independent of source factors, such as magnitude and distance (M_w and R), was used to evaluate the sufficiency of that IM. This means that for a sufficient IM, having more information about source M_w and R does not help

reduce the variance in EDP. And lastly, the availability of attenuation models and the existing uncertainty in the estimation of a given IM was used to evaluate its overall predictability. A strong candidate IM, with optimum efficiency, sufficiency, and predictability, is aimed to reduce the dispersion of a given EDP and hence, improve its accuracy in future simulations.

6.3. Insight from Numerical Parametric Simulations

6.2.3. Effects of Site Response and SSI on Ground Motion Parameters

The response of soil was evaluated in the free-field and near-field under a range of different input ground motions. As detailed by Karimi and Dashti (2015b), Free-field (FF) soil acceleration response was numerically obtained at locations within the soil mesh sufficiently away from the building (e.g., at a horizontal distance larger than 3 times the foundation width). This response was compared to 3D single-column simulations of site response to ensure the simulated FF conditions was not affected by the presence of the structure. Near-field accelerations were obtained on the foundations directly.

Figure 6.4 compares the ground motion parameters computed at the free-field soil surface with those applied at the base (selected input rock motions) for all simulations, in order to evaluate the influence of site response in a saturated, layered soil profile on ground motion properties. This comparison is insightful, particularly when using empirical procedures that rely on IMs at the soil surface in the free-field (e.g., $PGA_{FF\text{-}Surface}$). Generally, most IMs were observed to amplify through the different sites simulated. For some IMs (e.g., PGV, PGD, and HI), no clear evidence of a plateau or a decrease in rate of amplification was observed at stronger levels of shaking for the models and motions considered. For a few other IMs, such as PGA, AI, CAV, SIR, PSA[T_{So}], and PSA[$1.5T_{So}$], an initial amplification was followed by de-amplification at stronger shaking for softer soil profiles, which was expected due to soil softening and increased damping.

Table 6. 2. Ground motion parameters, the influence of which was evaluated on the performance of the site and structures in the numerical parametric study.

#	Ground Motion Parameter	Index	Equation	Source
1	Peak ground acceleration	PGA	$\max\|a(t)\|$	-
2	Peak ground velocity	PGV	$\max\|v(t)\|$	
3	Peak ground displacement	PGD	$\max\|d(t)\|$	
4	Ratio of PGV over PGA	PGV/PGA	$\max\|v(t)\|/=\max\|a(t)\|$	
5	Root-mean-square of acceleration	a_{RMS}	$(\frac{1}{t_{tot}}\int_0^{t_{tot}}[a(t)]^2\ dt)^{1/2}$	McCaan and Shah (1979)
6	Root-mean-square of velocity	v_{RMS}	$(\frac{1}{t_{tot}}\int_0^{t_{tot}}[v(t)]^2\ dt)^{1/2}$	
7	Root-mean-square of displacement	d_{RMS}	$(\frac{1}{t_{tot}}\int_0^{t_{tot}}[d(t)]^2\ dt)^{1/2}$	
8	Arias intensity	AI	$\frac{\pi}{2g}\int_0^{t_{tot}}[a(t)]^2\ dt$	Arias (1970)
9	Characteristic intensity	CI	$(a_{RMS})^{3/2}(t_{tot})^{1/2}$	Park et al. (1985)
10	Cumulative absolute velocity	CAV	$\int_0^{t_{tot}}\|a(t)\|\ dt$	EPRI-NP-5930 (1988)
11	Cumulative absolute velocity with 5 cm/s^2 threshold acceleration	CAV_5	$\int_0^{t_{tot}}\langle\chi\rangle\|a(t)\|\ dt$, where $\langle\chi\rangle=\begin{cases}0 \text{ for } \|a(t)\|<5\ cm/s^2\\1 \text{ for } \|a(t)\|\geq 5\ cm/s^2\end{cases}$	Kramer and Mitchell (2006)
12	Acceleration spectrum intensity	ASI	$\int_{0.1}^{0.5}S_a(T,\xi=5\%)\ dT$	Von Thun et al. (1988)
13	Velocity spectrum intensity	VSI	$\int_{0.1}^{0.5}S_v(T,\xi=5\%)\ dT$	
14	Housner intensity	HI	$\int_{0.1}^{0.5}PSV(T,\xi=5\%)\ dT$	Housner (1952)
15	Sustained maximum acceleration	SMA	Third highest absolute value of acceleration/velocity in the time-history.	Nuttli (1979)
16	Sustained maximum velocity	SMV		
17	Effective design acceleration	EDA	PGA found after lowpass filtering the input time history with a cut-off frequency of 9 Hz.	Benjamin and Associates (1988)
18	A95 parameter	A95	$a(t_{95})$, where $(\frac{\pi}{2g}\int_0^{t_{95}}[a(t)]^2\ dt)/AI=0.95$	Sarma and Yang (1987)
19	Shaking intensity rate	SIR	$=AI_{5-75}/D_{5-75}$, where AI_{5-75} is the change in AI from 5 to 75% of its total value, and D_{5-75} is its corresponding time duration.	Dashti et al. (2010b)
20 21	Pseudo spectral acceleration at a specified period	$PSA[T_{So}]$ or $PSA[1.5T_{So}]$	Spectral acceleration at fundamental period of the site, T_{So}, or $(1.5\times T_{So})$	-
22 23		$PSA[T_{STo}]$ or $PSA[1.5T_{STo}]$	Spectral acceleration at fundamental fixed-base period of the structure, T_{STo}, or $(1.5\times T_{STo})$	-
24	Predominant period	T_p	Period at which the maximum spectral acceleration occurs in a 5%-damped acceleration response spectrum.	-
25	Mean period	T_m	$(\sum c_i^2/f_i)/\sum c_i^2)$, where c_i are the Fourier amplitudes, and f_i are the discrete Fourier transform frequencies between 0.25 and 20 Hz.	Rathje et al. (1998)
26	Uniform duration	D_u	The total time during which the acceleration is larger than a given threshold value (here, 5% of PGA)	Sarma and Casey (1990)
27	Bracketed duration	D_b	The total time elapsed between the first and the last excursions of a specified level of acceleration (here, 5% of PGA)	Bolt (1973)
28	Significant duration	D_S	The interval of time over which a proportion (percentage) of the total AI is accumulated (here, the interval between the 5 and 95% thresholds). Other percentages (e.g., 5 to 75%) can similarly be estimated.	Trifunac & Brady (1975)

Table 6. 3. Selected rock, horizontal acceleration time histories (fault-normal components for near-source motions), applied to the base of the model in the numerical parametric study.

#	Earthquake	Year	Station	M_w	Mechanism	R (km)	PGA (g)	AI (m/s)	D_{5-95} (s)	T_p (s)	SF
	Near-source motions										
1	Imperial Valley-06	1979	EMO	6.53	strike slip	0.07	0.27	0.53	10.2	0.48	1.0
2	Imperial Valley-06	1979	E07	6.53	strike slip	0.56	0.34	0.86	6.4	0.71	1.0
3	Imperial Valley-06	1979	E06	6.53	strike slip	1.35	0.30	1.20	9.3	0.31	1.0
4	Imperial Valley-06	1979	E08	6.53	strike slip	3.86	0.50	1.21	6.7	0.17	1.0
5	Imperial Valley-06	1979	E05	6.53	strike slip	3.95	0.46	1.43	6.7	0.34	1.0
6	Imperial Valley-06	1979	EDA	6.53	strike slip	5.09	0.44	1.84	6.3	0.15	1.0
7	Northridge-01	1994	SCE	6.69	reverse	5.19	0.52	2.66	7.0	0.21	1.0
8	Northridge01	1994	SYL	6.69	reverse	5.30	0.59	3.73	5.9	0.44	1.0
9	Northridge-01	1994	JEN	6.69	reverse	5.43	0.64	5.36	5.7	1.05	1.0
10	Northridge-01	1994	WPI	6.69	reverse	5.48	0.34	0.96	8.7	0.51	1.0
11	Imperial Valley-06	1979	E04	6.53	strike slip	7.05	0.47	1.23	6.2	0.22	1.0
12	Imperial Valley-06	1979	ECC	6.53	strike slip	7.31	0.21	0.83	7.9	0.63	1.0
13	Northridge-01	1994	SPV	6.69	reverse	8.44	0.70	5.73	7.8	0.23	1.0
14	Loma Prieta	1989	STG	6.93	rev. oblique	8.50	0.35	1.00	8.4	0.21	1.0
15	Imperial Valley-06	1979	E10	6.53	strike slip	8.60	0.23	0.64	11.6	0.22	1.0
16	Northridge-01	1994	ARL	6.69	reverse	8.66	0.29	1.57	13.7	0.24	1.0
17	Loma Prieta	1989	WVC	6.93	rev. oblique	9.31	0.24	0.82	12.4	0.36	1.0
18	Northridge-01	1994	RO3	6.69	reverse	10.05	0.40	1.42	15.3	0.22	1.0
19	Imperial Valley-06	1979	BRA	6.53	strike slip	10.42	0.21	0.40	13.7	0.29	1.0
20	Loma Prieta	1989	GOF	6.93	rev. oblique	10.97	0.30	0.65	9.8	0.43	1.0
21	Loma Prieta	1989	G02	6.93	rev. oblique	11.07	0.29	085	11.4	0.20	1.0
22	Imperial Valley-06	1979	E11	6.53	strike slip	12.56	0.37	1.95	8.3	0.24	1.0
23	Imperial Valley-06	1979	PTS	6.53	strike slip	12.69	0.18	0.19	17.0	0.20	1.0
24	Loma Prieta	1989	G03	6.93	rev. oblique	12.82	0.42	1.40	9.0	0.20	1.0

Table 6.3. Continued …

#	Earthquake	Year	Station	M_w	Mechanism	R (km)	PGA (g)	AI (m/s)	D_{5-95} (s)	T_p (s)	SF
25	Northridge-06	1994	SCS	5.28	reverse	14.67	0.20	0.27	2.0	0.40	1.0
26	Imperial Valley-06	1979	WSM	6.53	strike slip	15.25	0.33	1.06	18.0	0.23	1.0
	Ordinary motions										
27	Landers	1992	MVH	7.28	strike slip	17.36	0.17	0.77	29.9	0.60	1.0
28	Superstition Hills-02	1987	ICC	6.54	strike slip	18.20	0.22	0.66	20.2	0.24	1.0
29	Landers	1992	CLW	7.28	strike slip	19.74	0.34	1.28	8.55	0.44	1.0
30	Imperial Valley-06	1979	E01	6.53	strike slip	21.68	0.09	0.16	17.9	0.26	1.0
31	Whittier Narrows-01	1987	OR2	5.99	rev. oblique	24.54	0.22	0.42	9.5	0.68	1.0
32	Umbria-03 ITA	1984	PTL	5.6	normal	24.69	0.11	0.07	6.5	0.14	1.0
33	Joshua Tree	1992	IJR5294	6.1	strike slip	25.04	0.33	0.77	6.9	0.63	1.0
34	Imperial Valley-06	1951	ELC9	5.6	strike slip	25.24	0.03	0.02	27.3	0.67	1.0
35	Whittier Narrows-01	1987	ING	5.99	rev. oblique	25.86	0.22	0.29	10.4	0.19	1.0
36	Whittier Narrows-01	1987	BUE	5.99	rev. oblique	26.34	0.25	0.42	8.9	0.31	1.0
37	Sierra Madre	1991	OBR	5.61	reverse	27.4	0.20	0.23	7.5	0.28	1.0
38	Taiwan SMART1(5)	1981	O02	5.9	reverse	27.51	0.24	0.21	8.9	0.23	1.0
39	Northwest China-04	1997	JIA	5.8	norm. oblique	27.86	0.17	0.25	10.5	0.22	1.0
40	Northern Calif-05	1967	FRN	5.6	strike slip	28.73	0.20	0.09	16.7	0.18	1.0
41	Whittier Narrows-01	1987	OR2	5.99	rev. oblique	24.54	0.22	0.42	9.5	0.68	1.0
42	Imperial Valley-06	1979	PLS	6.53	strike slip	30.33	0.05	0.05	10.4	0.20	1.0
43	Imperial Valley-06	1979	PLS	6.53	strike slip	30.33	0.26	1.18	10.4	0.2	5.0
44	Loma Prieta	1989	HVR	6.93	rev. oblique	30.49	0.11	0.24	15.2	0.50	1.0
45	Loma Prieta	1989	HVR	6.93	rev. oblique	30.49	0.23	0.96	15.2	0.50	2.0
46	Morgan Hill	1984	HCH	6.19	strike slip	30.76	0.07	0.12	21.2	0.63	1.0
47	Loma Prieta	1989	PAE	6.93	rev. oblique	30.81	0.20	0.72	26.8	0.19	1.0
48	Loma Prieta	1989	PAE	6.93	rev. oblique	30.81	0.40	2.87	26.8	0.19	2.0
49	Loma Prieta	1989	SLC	6.93	rev. oblique	30.86	0.15	0.47	12.5	0.47	1.0
50	Loma Prieta	1989	SLC	6.93	rev. oblique	30.86	0.30	1.88	12.5	0.47	2.0

Table 6.3. Continued …

#	Earthquake	Year	Station	M_w	Mechanism	R (km)	PGA (g)	AI (m/s)	D_{5-95} (s)	T_p (s)	SF
51	N. Palm Springs	1956	H06	6.06	rev. oblique	30.97	0.04	0.03	24.8	0.18	1.0
52	Northridge-01	1994	PIC	6.69	reverse	31.33	0.11	0.17	18.8	0.63	1.0
53	Kobe JPN	1995	TDO	6.9	strike slip	31.69	0.23	0.84	33.1	0.19	1.0
54	Morgan Hill	1984	SJL	6.19	strike slip	31.88	0.07	0.14	18.6	0.45	1.0
55	Morgan Hill	1984	SJR	6.19	strike slip	31.88	0.06	0.08	19.0	0.29	1.0
56	Imperial Valley-06	1979	VCT	6.53	strike slip	31.92	0.15	0.21	37.4	0.18	1.0
57	Imperial Valley-06	1979	VCT	6.53	strike slip	31.92	0.31	0.85	37.4	0.18	2.0
58	Loma Prieta	1989	SJW	6.93	rev. oblique	32.78	0.08	0.17	21.3	0.22	1.0
59	Loma Prieta	1989	SJW	6.93	rev. oblique	32.78	0.17	0.69	21.3	0.22	2.0
60	Landers	1992	PSA	7.28	strike slip	36.15	0.06	0.25	39.8	0.96	1.0
61	Imperial Valley-06	1979	NIL	6.53	strike slip	36.92	0.08	0.13	26.2	0.20	1.0
62	Imperial Valley-06	1979	NIL	6.53	strike slip	36.92	0.32	2.07	26.2	0.20	4.0
63	Northridge-01	1994	LV2	6.69	reverse	37.24	0.07	0.05	12.4	0.18	1.0
64	Northridge-01	1994	LV4	6.69	reverse	37.57	0.07	0.09	15.1	0.38	1.0
65	Northridge-01	1994	LV5	6.69	reverse	37.80	0.12	0.21	14.8	0.32	1.0
66	Northridge-01	1994	LV6	6.69	reverse	38.03	0.14	0.27	11.1	0.20	1.0
67	Morgan Hill	1984	CAP	6.19	strike slip	39.08	0.11	0.21	13.4	0.18	1.0
68	San Fernando	1971	WND	6.61	reverse	39.45	0.11	0.12	18.0	0.23	1.0
69	San Fernando	1971	WND	6.61	reverse	39.45	0.33	1.06	18.0	0.23	3.0
70	Northridge-01	1994	LOA	6.69	reverse	39.91	0.10	0.15	22.9	0.32	1.0
71	Anza-02	2001	SAG	4.92	norm. oblique	41.10	0.01	0.00	11.34	0.15	1.0
72	Chi-Chi Taiwan-06	1999	TCU087	6.3	reverse	41.15	0.02	0.02	25.6	0.23	1.0
73	Whittier Narrows-01	1987	A-STC	5.99	rev. oblique	41.69	0.1	0.16	19.3	0.25	1.0
74	N. Palm Springs	1986	IND	6.06	rev. oblique	41.93	0.05	0.03	23.9	0.29	1.0
75	Whittier Narrows-01	1987	A-HNT	5.99	rev. oblique	44.58	0.04	0.02	23.1	0.17	1.0
76	Chi-Chi Taiwan-06	1999	TCU105	6.3	reverse	45.07	0.07	0.04	21.2	0.26	1.0
77	Northridge-06	1994	ANA	5.28	reverse	47.20	0.01	0.00	13.9	0.28	1.0
78	Anza-02	2001	DOR	4.92	norm. oblique	49.97	0.02	0.00	5.73	0.18	1.0

Measures of shaking duration (e.g., $D_{5\text{-}95}$, D_u, D_b) were generally amplified from the base through a liquefiable deposit. The predominant and mean periods of shaking (T_p and T_m) were also often increased (sometimes significantly) from the base to the soil surface.

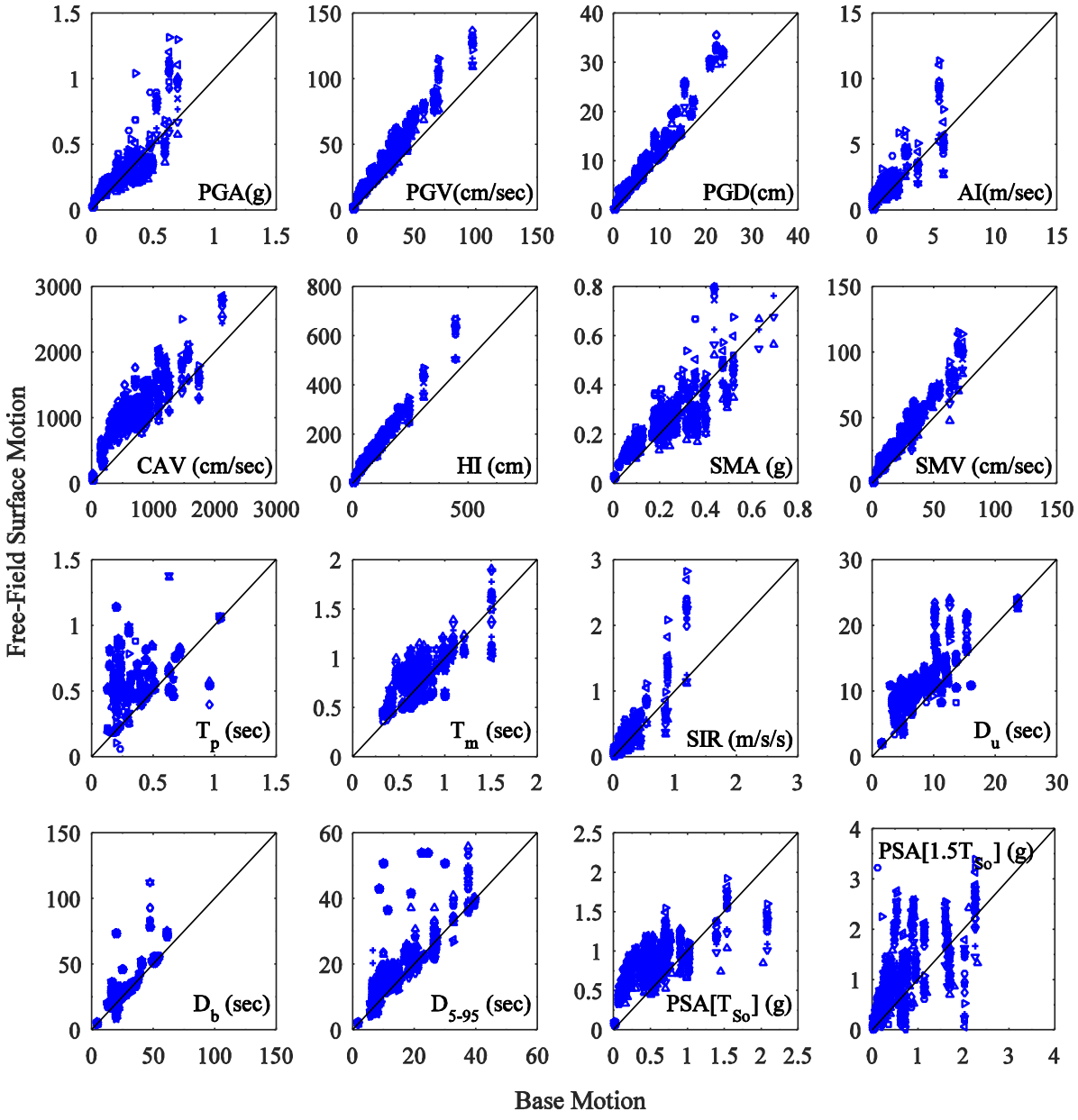

Figure 6. 4. Comparison of ground motion parameters at the base and surface of the soil in the free-field (1-D site-response) from the parametric study.

The amplification of the motion at higher periods and its de-amplification at lower periods is expected through a softened soil column, which led to the increase in T_p and T_m.

Figure 6.5 shows the change in the PGA alone through the site for a few representative soil profiles considered in the parametric study (model 1, 5 and 6). For comparison, although not applicable to liquefiable soil conditions, the relationships proposed by Seed et al. (1997) for soils ranging from deep, soft clays (site class C4, D, E) to relatively stiff, cohesionless soils (site class B, C1, C2) is also presented in this figure. A similar and consistent pattern is observed in PGA: initial amplification followed by de-amplification at stronger base PGA's due to the reduction in soil's shear modulus and increased damping. The response of model 6 (a dense layer of saturated sand) was consistent with the Seed et al. (1997) model for relatively stiff, cohesionless soils. The response of soil models 1 and 5 was generally at or below the curve predicted by Seed et al. (1997) for deep, soft clays, which was expected because of soil liquefaction and excessive softening in these profiles, particularly model 5 with a thick, loose layer of saturated sand. The results became more scattered in all cases at higher PGA values. Further, beyond a base PGA of approximately 0.3g, the surface PGA in all three models started to increase again, likely due to the dilation cycles that followed softening in a liquefied layer.

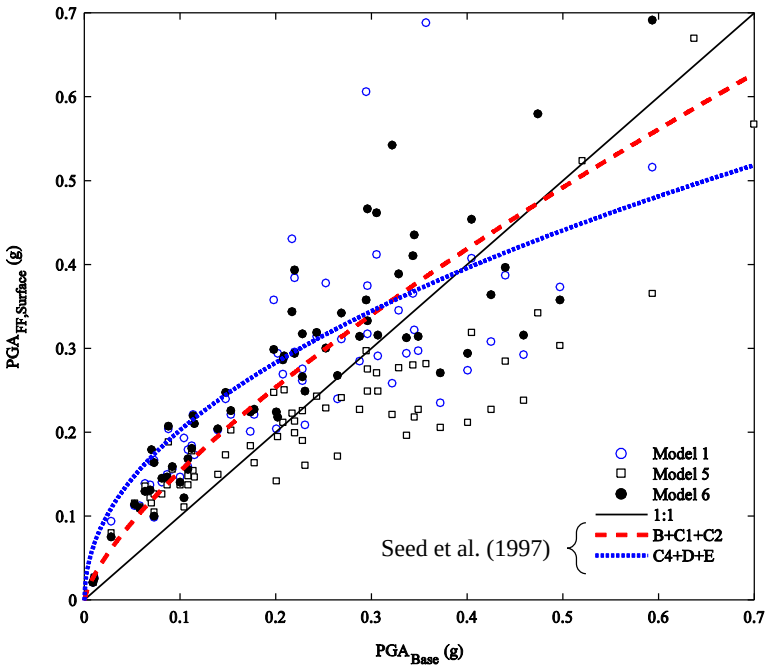

Figure 6. 5. Relationship between PGA at the surface to base in the free-field for different soil profiles considered in the parametric study.

Figure 6.6 compares the ground motion parameters on the building foundation with those at the soil surface in the free-field, to evaluate the influence of the building's inertial and kinematic interaction on foundation accelerations and the demand applied back onto the soil. Overall, no significant change was predicted in ground motion parameters due to SSI effects for the cases considered, but a small degree of de-amplification was evident in a few foundation IMs compared to free-field only at stronger levels of shaking (e.g., PGA, SMA, and PSA[T_{So}]). The predominant period (T_p) of the foundation motion was significantly altered compared to that in the free-field, likely due to the influence of the building's inertial response. However, the mean period (T_m), which is a more robust measure of the period at which most of the motion's energy is concentrated (Rathje et al. 1998), was mostly unchanged on the foundation. The spectral acceleration at the 1.5 times the initial site period, PSA[$1.5T_{So}$], de-amplified in many cases under stronger level of shaking, which can be attributed to the SSI effect between the flexible-based structure and the softened ground (e.g., rocking). These observations may not apply to significantly heavier or stiffer structures, or structures on deep foundations. Nevertheless, in this study, the properties of the base (input rock) motion were used to identify optimal IMs for evaluating the liquefaction hazard and its consequences instead of free-field surface or foundation motions, which is consistent with the approach adopted by Kramer and Mitchell (2006). This is because the uncertainties associated with the estimation of free-field surface (or foundation) motion IMs reduce the confidence level in and the accuracy of the predicted response parameters of interest.

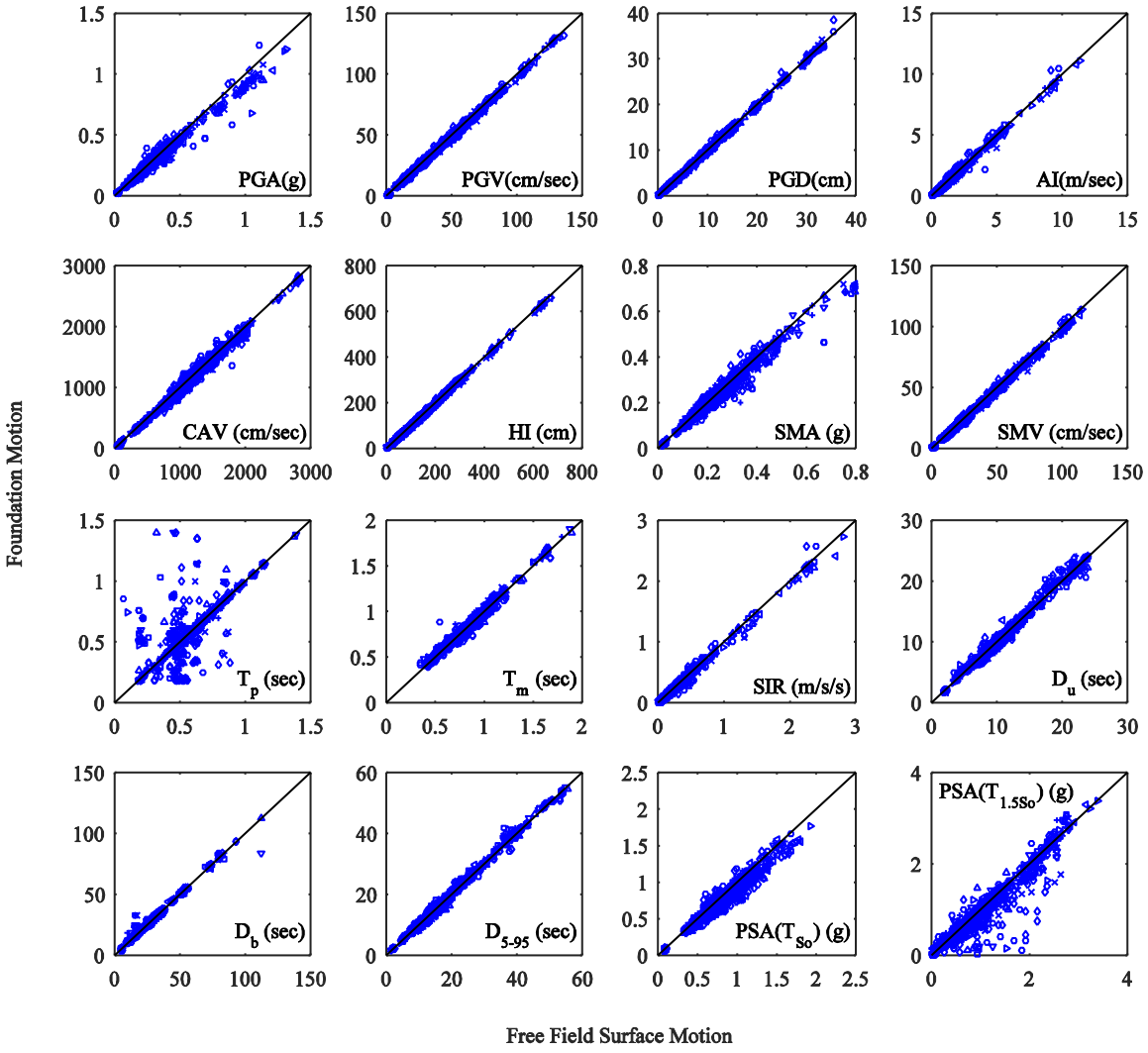

Figure 6. 6. Figure 6. 7.Comparison of ground motion parameters at the soil surface in the free-field and on the rigid foundation affected by soil-structure interaction from the parametric study.

6.2.4. Effects of Intensity Measures on Excess Pore Water Pressures

Figure 6.7 through Figure 6.9 show the influence of four representative IMs of the base motion on the peak value of excess pore pressure ratio ($r_{u,peak}$) predicted in the middle of the liquefiable layer (i.e., the EDP) in the free-field, under the center of the foundation, and under the foundation edge halfway along its length, respectively.

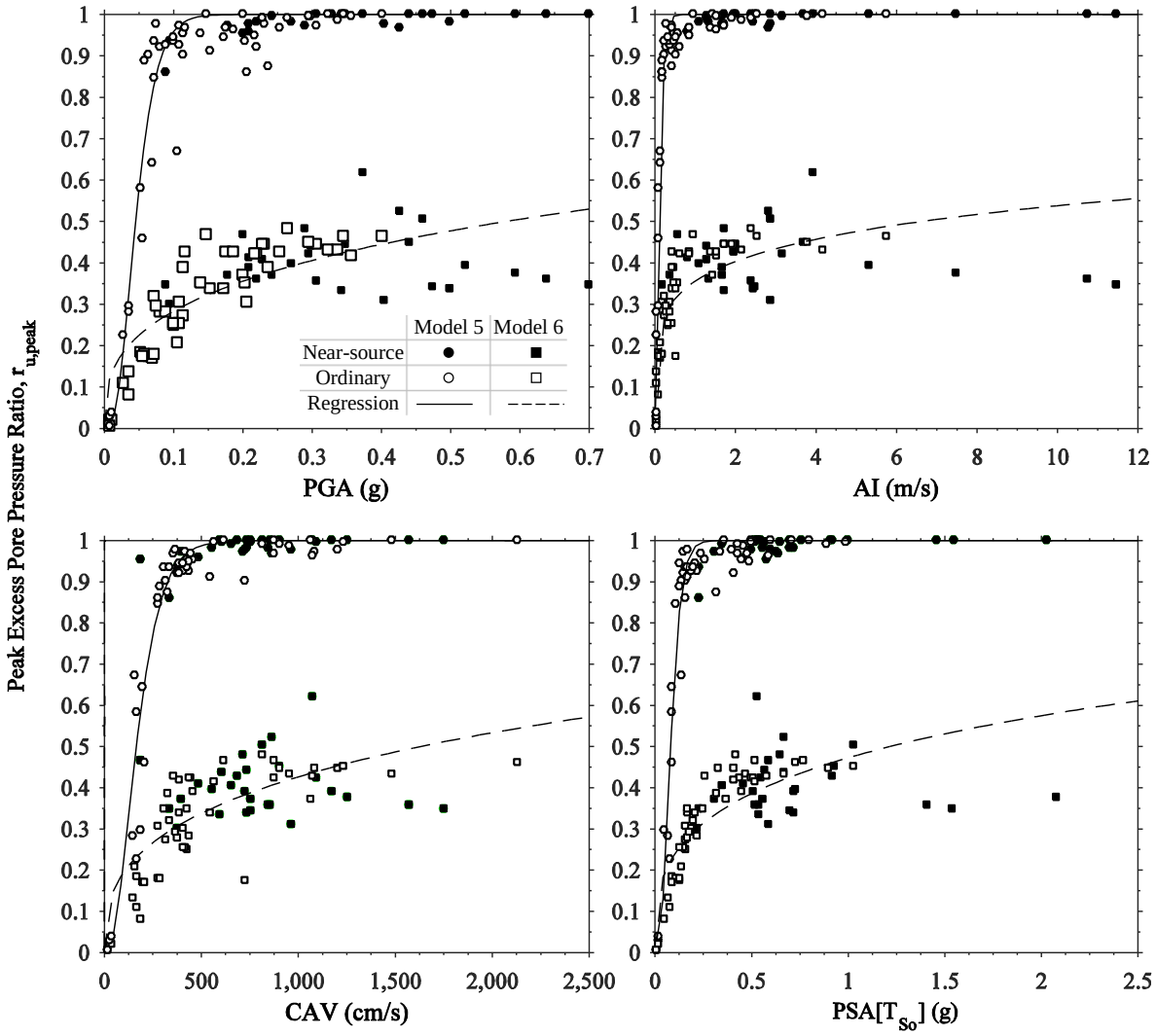

Figure 6. 8. Peak excess pore water pressure ratios ($r_{u,peak}$) in the middle of the liquefiable layer in the free-field of models 5 and 6 as a function of four representative IMs of base motion.

The EDPs of interest were computed for all the twenty one models simulated (Table 6.2), but only two (models 5 and 6) are presented at each location for clarity. The IMs were computed from the input (bedrock) motions. The variation of EDP given an IM (i.e., EDP|IM) was estimated for each of the twenty one conditions using regressions in the form of an integrated beta distribution suggested by Kramer and Mitchell (2008). Although different symbols are used for the data corresponding to near-source and ordinary motions in these figures, the regressions were developed for the combination of these data, because no

significant difference was observed in the predicted trends for the cases considered. The quality of each IM was evaluated later based on the concepts of efficiency, sufficiency, and predictability, as will be discussed in later sections.

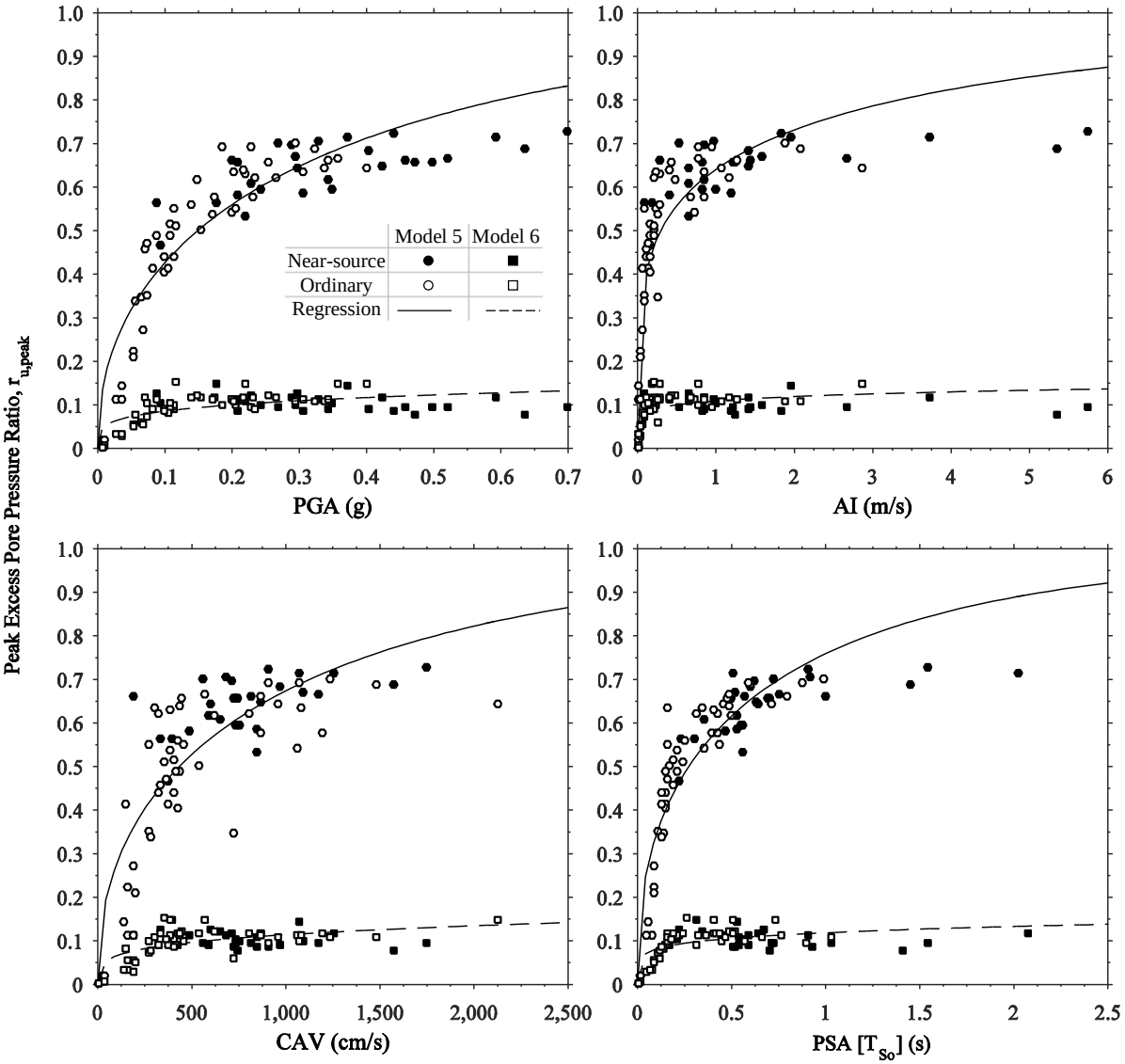

Figure 6. 9. Peak excess pore water pressure ratios ($r_{u,peak}$) under the foundation center in the middle of the liquefiable layer in models 5 and 6 as a function of four representative IMs of base motion.

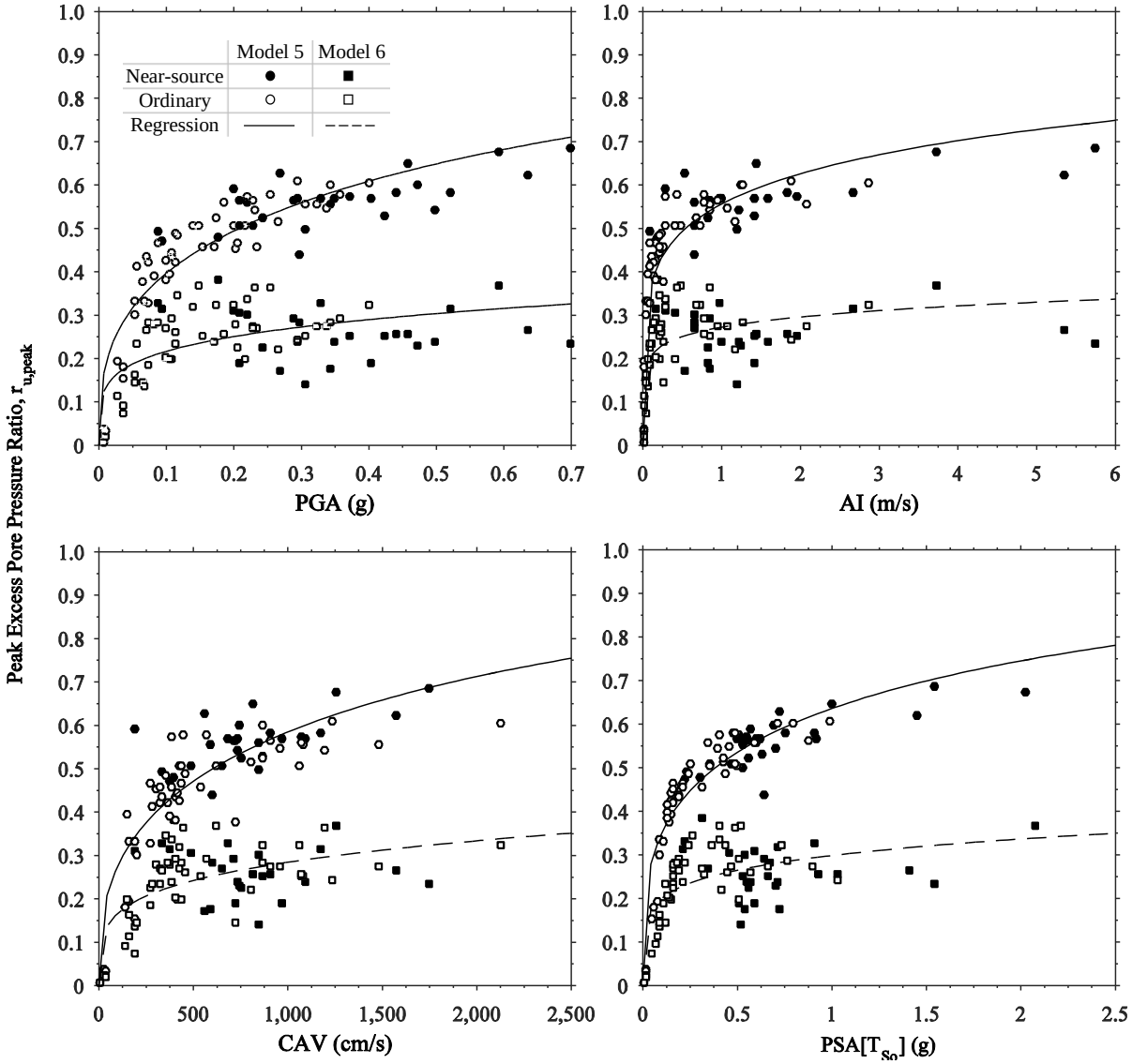

Figure 6. 10. Peak excess pore water pressure ratios ($r_{u,peak}$) under the edge of the foundation and in the middle of the liquefiable layer in models 5 and 6 as a function of four representative IMs of base motion.

Figure 6.11 shows the influence of relative density (D_r) of, thickness (H_L) of, and depth (D_L) to the liquefiable layer on the regressions developed for free-field $r_{u,peak}$ as a function of the base motion PGA, while keeping other factors constant. PGA is chosen in this figure, because of its traditional use in liquefaction triggering analyses. As expected, decreasing the soil D_r and increasing H_L amplified the predicted $r_{u,peak}$ in the middle of the liquefiable layer for a given PGA. Decreasing soil's D_r reduces its resistance to liquefaction and amplifies the extent of excess pore pressure generation for a given IM. Increasing H_L increases the volume

of soil generating large excess pore pressures, which dissipate and redistribute slower compared to a smaller H_L, increasing the net value of $r_{u,peak}$. The influence of D_L on $r_{u,peak}$ was minor for the depths considered (2 through 4m), but the effect is anticipated to increase at greater depths with a more significant variation in confining pressure and drainage path to the surface. Soil D_r was observed to have the most significant influence on $r_{u,peak}$ for the cases considered.

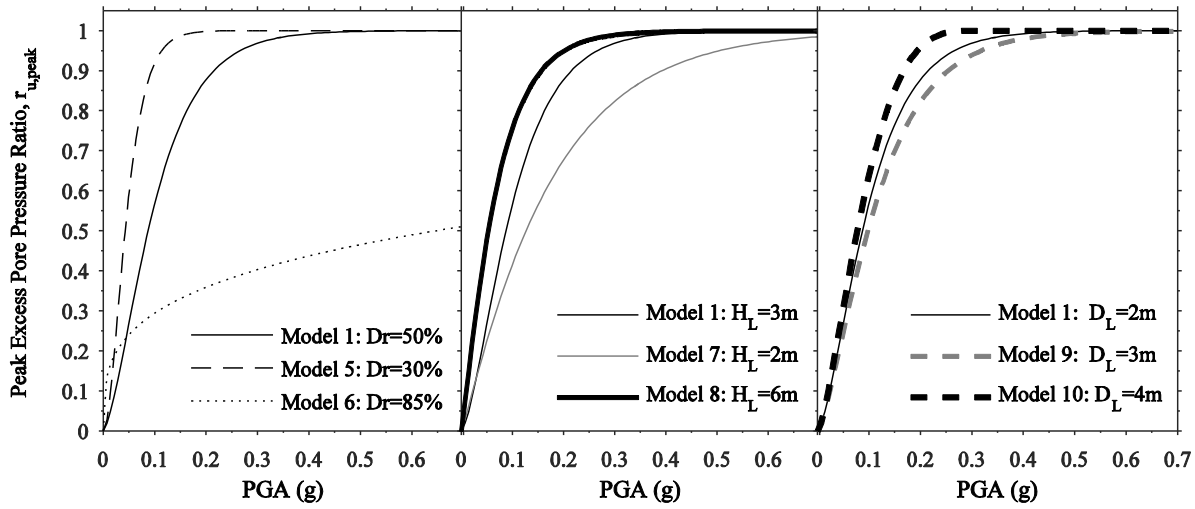

Figure 6. 11. The influence of relative density (D_r) of, thickness (H_L) of, and depth (D_L) to the liquefiable layer on the regressions developed for free-field peak excess pore water pressure ratios ($r_{u,peak}$) as a function of base motion PGA.

It is important to note that with the exception of soil model 6 (D_r = 85%), liquefaction (defined as $r_{u,peak}$ =1.0) was observed relatively rapidly in the free-field for both near-source and ordinary motions. However, $r_{u,peak}$ = 1.0 was not achieved under the center and edge of the foundation for any of the conditions investigated, even for base motions with a PGA of near 0.7g. This is attributed to the influence of the building's confining pressure and static shear stresses (near the edges), which increase the soil's resistance to liquefaction triggering. However, generally, larger net excess pore water pressures were predicted under the structure compared to the free-field at stronger levels of shaking, leading to an outward flow direction away from the foundation, similar to those measured by Dashti et al. (2010a,b) in centrifuge.

The response of a denser soil profile was more influenced by the presence of the foundation compared to looser soils (comparing $r_{u,peak}$ in model 6 in Figure 6.8 and Figure 6.9 to that in Figure 6.7). This confirms that the influence of soil relative density on its resistance to excess pore pressure generation depends on the stresses imposed by the superstructure, a pattern that was consistent with previous experimental observations.

Figure 6.12 shows the development of excess pore pressure ratio under the foundation center and edge for model 1 (with B×L) and model 21 (with 1.5×B×L). In these two models all soil and structural properties were kept constant except the foundation contact area. As shown in this figure, the extent of net excess pore pressure development was greater when the foundation contact area was increased. This was due to the longer drainage path for the generated excess pore pressure to dissipate and also greater stresses introduced by the foundation in model 21 compared to model 1, increasing the capacity of the underlying soil for generating larger excess pore pressures under stronger level of shaking.

6.2.5. Near-Source Effects

Near-source motions with the forward-directivity effect are known for their characteristic velocity pulse, higher period content, and shorter durations compared to ordinary motions (Somerville et al. 1997a). Because many (not all) of IM values were greater for near-source compared to ordinary motions, in many cases larger $r_{u,peak}$ values were predicted for near-source motions. But for the same level of IM, no significant difference was observed in $r_{u,peak}$ values predicted for ordinary and near-source motions, for the cases considered.

Spectral acceleration ratios of free-field surface (FF) to base motions and foundation (FM) to FF motions are plotted in Figure 6.13 for all twenty one models simulated and all ground motions, this time separated for ordinary and near-source motions. The peak values of FF surface to base spectral ratios are expected to occur near the effective, strain-compatible, fundamental period of the site (T'_{So}) during different motions, which were on average near 0.5s

for near-source motions and 0.8s for ordinary motions. A longer T'_{So} and a smaller peak in spectral ratios on average indicate a more softened soil state under ordinary compared to near-source motions with the forward-directivity effect. This may be caused by the shorter-duration (with fewer cycles), pulse-like nature of the near-source motions that did not soften the soil to the same degree as longer-duration, ordinary motions on average. The spectral ratios of FM/FF were on average close to 1.0, as also shown previously in Figure 6.6, both for near-source and far-field motions.

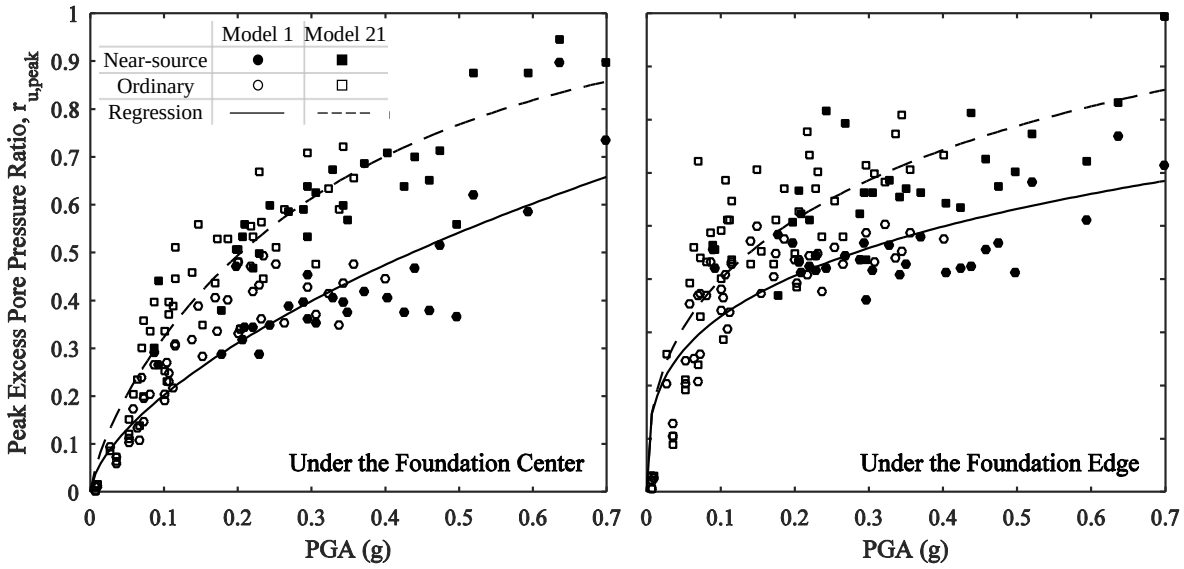

Figure 6. 12. The influence of the foundation contact area (B×L) on the regressions developed for peak excess pore pressure ratios ($r_{u,peak}$) in the middle of liquefiable layer and under the foundation center or under the foundation middle-edge as a function of base motion PGA.

6.4. Selection of Optimum Intensity Measures to Predict Liquefaction Triggering

A strong candidate IM is the one with optimum efficiency, sufficiency, and predictability, which reduces the dispersion of a given EDP and improves its accuracy in future predictions. The variability and dispersion in the predicted EDP (i.e., $r_{u,peak}$ in the middle of the liquefiable layer in the free-field and near-field), quantified with the standard deviation about the regression curve for a given IM, was used to evaluate the efficiency of that IM. The degree

of independence of the EDP from the source magnitude and distance (M_w and R) was used to assess the sufficiency of the candidate IM. And lastly, the availability of attenuation relations and the uncertainty in the estimation of a given IM was considered to evaluate its overall predictability.

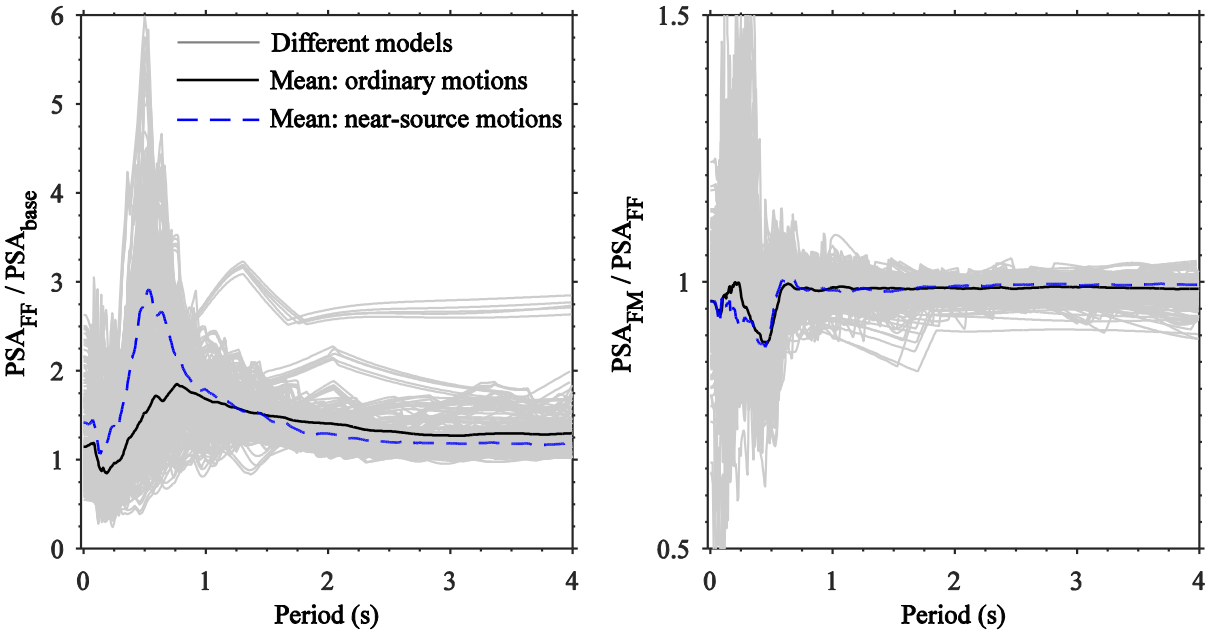

Figure 6. 13. Pseudo spectral ratios (5%-damped) of: a) free-field surface (FF) to base acceleration; b) foundation (FM) to free-field soil surface (FF) acceleration.

The candidate IMs were first ranked based on their efficiency in predicting $r_{u,peak}$ both in the free-field and near the building. The residual sum of squared errors between the regression curve and numerical results (i.e., standard deviation or $\sigma_{ru,peak|IM}$ was computed for all twenty one models and compared among different IMs. The $\sigma_{ru,peak|IM}$ for each model was calculated only for $r_{u,peak}$ values of less than 1.0, because the primary objective was to evaluate the scatter in data before the point of liquefaction. As $r_{u,peak}$ approached 1.0, the scatter in the predicted results substantially reduced in all cases, which was not considered in the comparisons. Figure 6.14 shows the individual and average values of $\sigma_{ru,peak|IM}$ obtained for each model simulated and each candidate IM. The number associated with a given IM shown in this figure was previously summarized in Table 6.2. The IMs with the smallest overall σ

were ranked the highest (e.g., PSA[T_{So}], CI, and AI in the free-field). Once the more efficient IMs were determined for each location, they needed to be evaluated in terms of their sufficiency in predicting the EDP of interest.

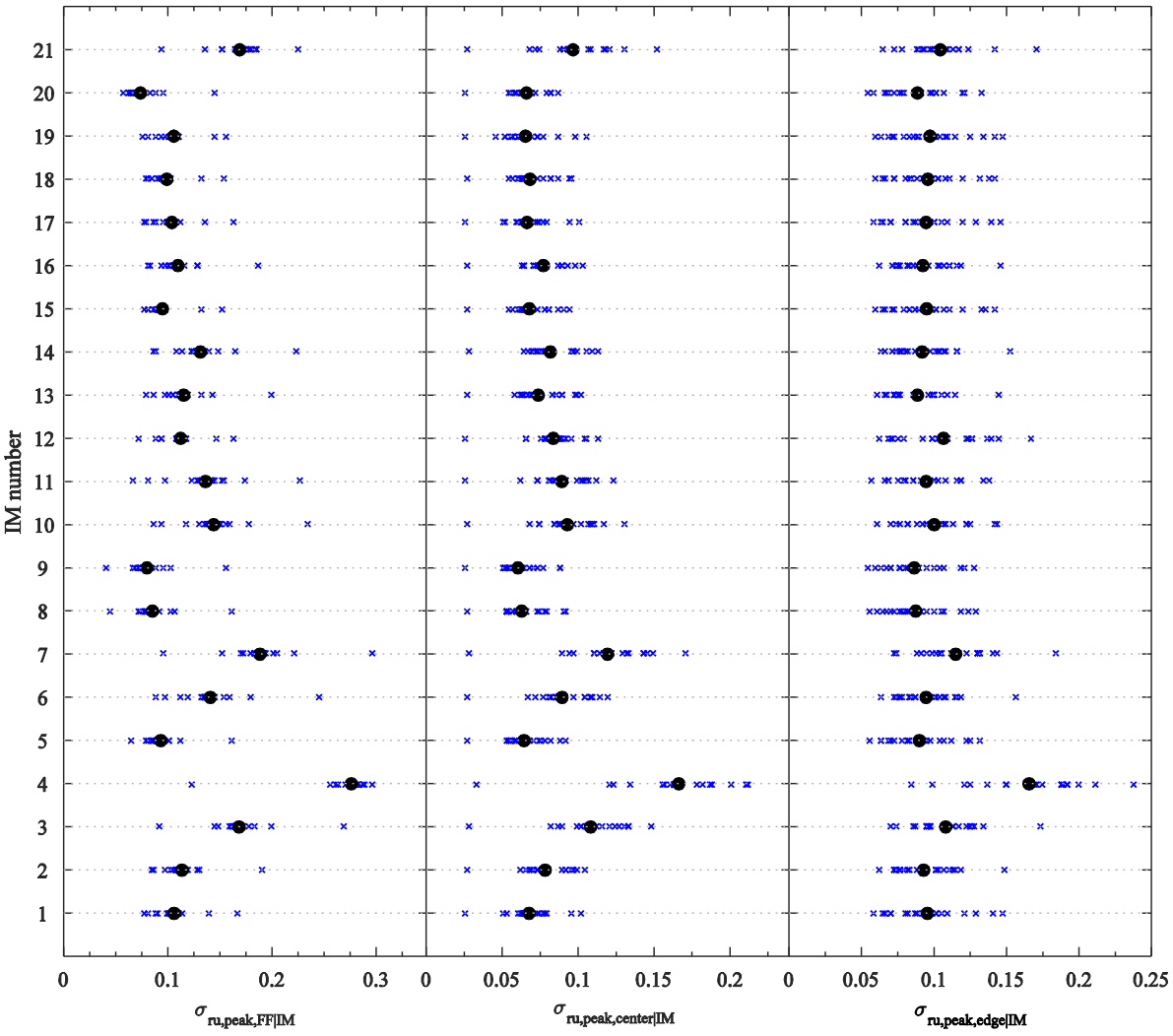

Figure 6. 14. The standard deviation (σ in $r_{u,peak}$ in the free-field as well as the center and edge of the foundation for each candidate IM. The blue crosses indicate individual □ values and the black circles show the average σ among the twenty one simulations.

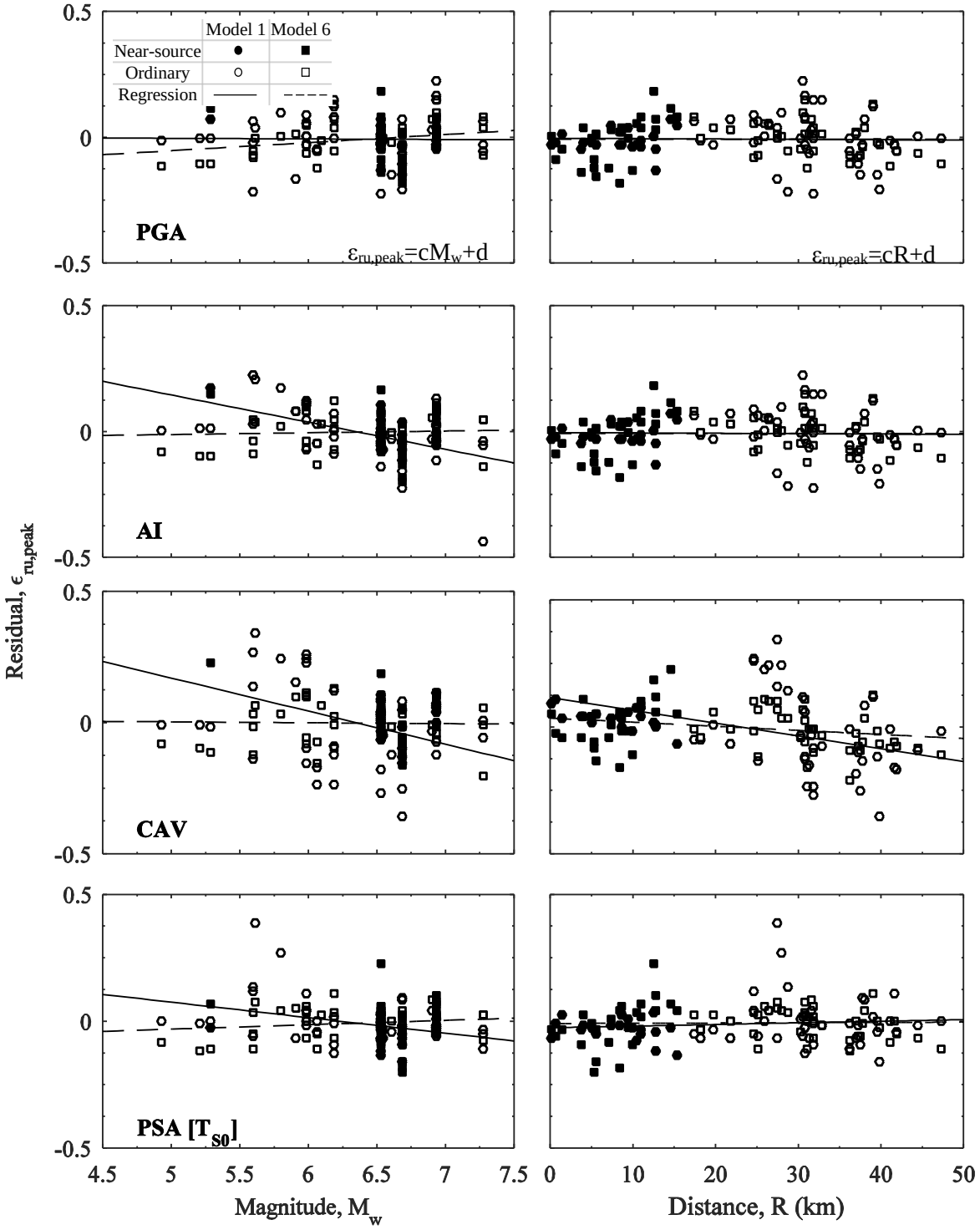

Figure 6. 15. Residuals of peak excess pore pressure ratio ($r_{u,peak}$) in the free-field for different intensity measures $\varepsilon_{ru,peak}|IM,$, as a function of source moment magnitude (M_w) and distance (R).

Figure 6.15 compares the residuals of $r_{u,peak}$ predicted in the free-field for four representative IMs (e.g., PGA, AI, CAV, PSA[T_{So}]) as a function of source M_w and R. In these

plots, the few scaled motions were removed, in order to have an accurate estimate of M_w and R for a given motion. Standard linear regressions were obtained on each set of residuals, and the slope of the regression line (c) was used to quantify and judge the dependence of the residual separately on M_w and R for each model. Similar to the efficiency evaluations, the near-source and ordinary motions were not separated in obtaining the regressions, which was important because neither group alone could capture a wide range of distances and a sufficient number of data points.

Figures 6.16 and 6.17 summarize the individual and average values of slope (c) corresponding to the linear regression of residuals for each candidate IM as a function of M_w and R, respectively. Those IMs with the smallest overall and average slopes (i.e., |c| values closest to zero) were ranked highest in sufficiency. For the set of conditions presented and the EDP's investigated in this chapter ($r_{u,peak}$ in the free-field and near-field), the best combination of efficiency and sufficiency was found in the following IMs: 1) PSA[T_{So}] and SMA in the free-field and under the edge of the foundation; and 2) SIR and EDA under the center of the foundation.

Pseudo spectral acceleration (PSA) brings in the influence of intensity and frequency content of the ground motion, but it is not affected by duration. Hence, the sufficiency of PSA[T_{So}] with respect to M_w was not ideal. However, overall, it ranked highly compared to other IMs in terms of both efficiency and sufficiency for the purpose of predicting $r_{u,peak}$. In selecting an optimum IM, it is also important to consider the availability of attenuation models and the uncertainty in the estimation of that IM. Attenuation relations are available for pseudo spectral accelerations, PSA, at any period T (e.g., Abrahamson et al. 2014; Campbell and Bozorgnia 2014).

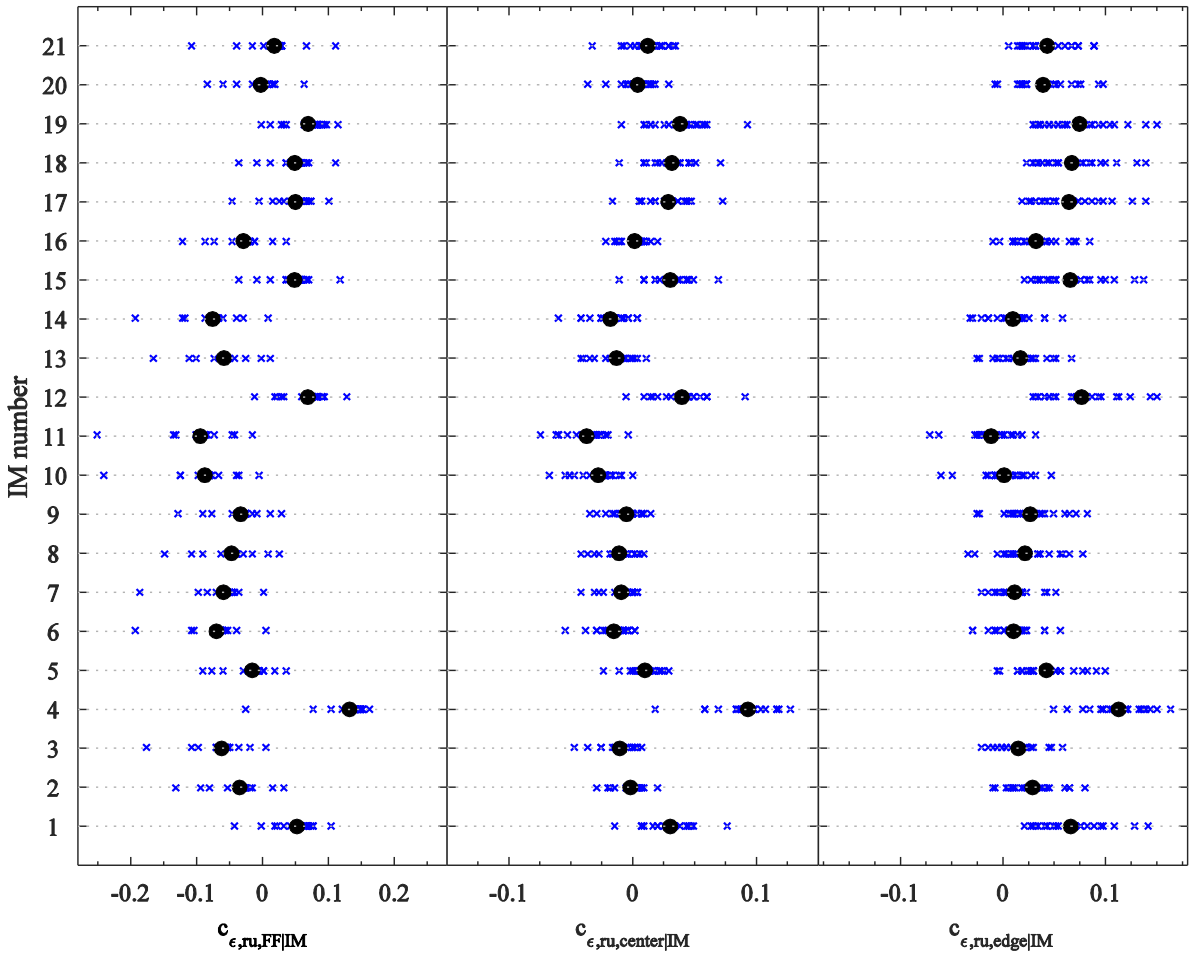

Figure 6. 16.The slope (c) values corresponding to the linear regression of residuals in $r_{u,peak}$ for a given candidate IM as a function of source M_w. The blue crosses indicate individual c values and the black circles show the average c among the twenty one simulations.

The prediction of PSA[T] for a rock site in an active crustal region is currently one with the least uncertainty among other IMs. Many of the available attenuation relations consider site response by using the average, small-strain, shear wave velocity of soil in the top 30 m ($\overline{V}_{s,30}$), but none of these relations are anticipated for use on liquefiable ground. The small-strain fundamental period of the site, T_{So}, may be estimated as $4H/\overline{V}_s$, where $\overline{V}_s$ is the average small-strain, shear wave velocity (which can be readily estimated using empirical procedures or field measurements), and H is the height of the entire soil column above bedrock (as opposed to only the top 30 m). The PSA of the input rock motion may then be estimated at T_{So} using any of the

attenuation models available for a given tectonic environment (e.g., Abrahamson et al. 2014 and Campbell and Bozorgnia 2014 developed for shallow earthquakes in active plate margins).

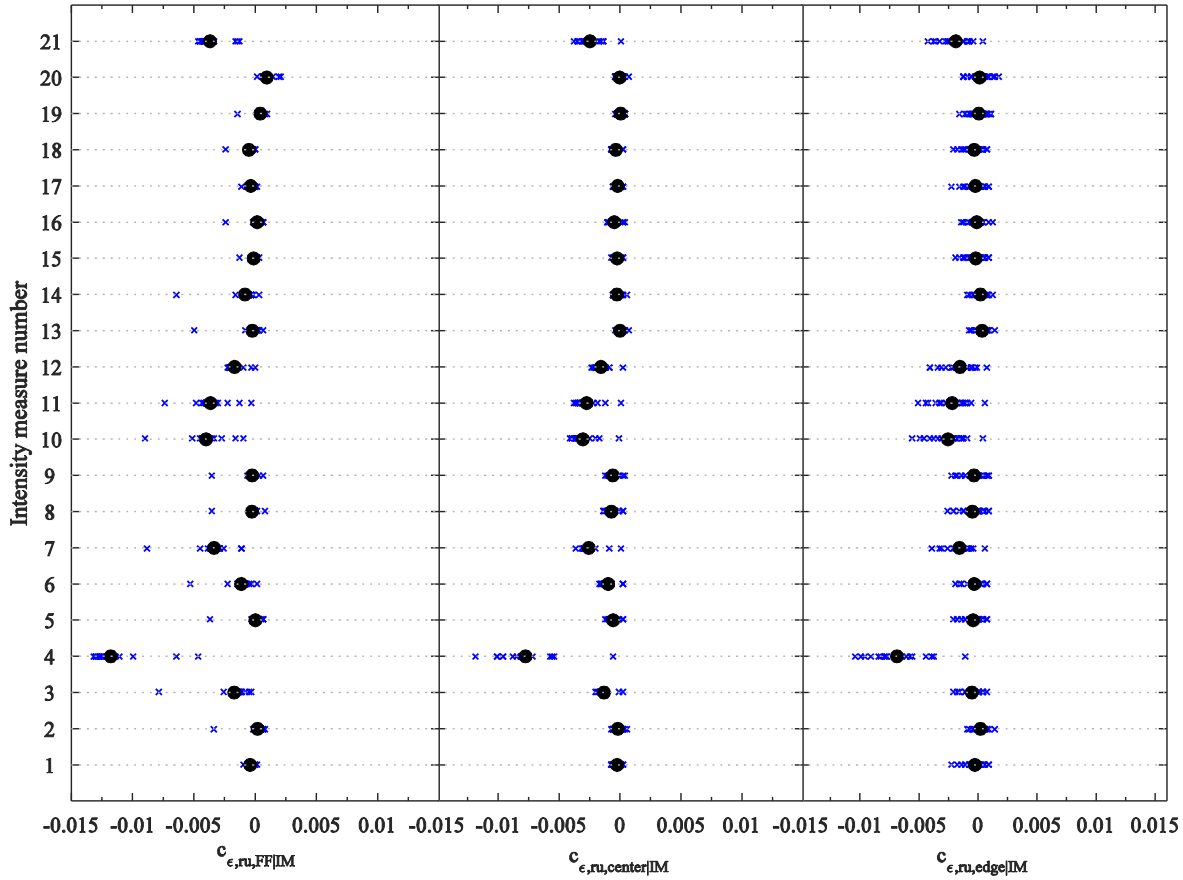

Figure 6. 17. The slope (c) values corresponding to the linear regression of residuals in $r_{u,peak}$ for a given candidate IM as a function of source R. The blue crosses indicate individual c values and the black circles show the average c among the twenty one simulations.

The Shaking Intensity Rate ($SIR=AI_{5\text{-}75}/ D_{5\text{-}75}$) was also determined as an overall efficient and sufficient IM in predicting $r_{u,peak}$ under the center of the foundation. This parameter roughly represents the rate of earthquake energy build up, and has been shown in previous experiments to correlate well with the effects of soil liquefaction on buildings (Dashti et al. 2010b). This IM is influenced by intensity, duration, and frequency content of the motion. Though with greater uncertainty compared to PSA[T], Arias Intensity (AI) may also be predicted for future scenario events using the relationships proposed by Travasarou et al.

(2003) and Significant Duration (e.g., D_s) using Abrahamson and Silva (1996) or Kempton and Stewart (2006), which are the key ingredients of SIR. At this time, the prediction of SMA and EDA at a given site lead to greater uncertainty, until appropriate attenuation models are developed for their prediction.

Based on the considerations above, to estimate $r_{u,peak}$ both in the free-field and near-field, among the candidate IMs identified, the best combination of efficiency, sufficiency, and predictability was found in the following for the input rock motion: 1) PSA(T_{So}); and 2) SIR. Typically the soil under the foundation edge and in the free-field experiences a greater risk of liquefaction ($r_{u,peak}$ approaching 1.0) compared to the center of the foundation. Hence, for the purpose of evaluating the liquefaction hazard alone ($r_{u,peak}$), free-field or foundation edge may suffice. However, when the extent of strength loss, flow tendencies, and the subsequent effects on soil and structure performance need to be evaluated, excess pore pressures under the center of the foundation also become important.

Kramer and Mitchell (2006) performed extensive site response analyses to identify the most optimum ground motion IM for prediction of liquefaction triggering in the free-field, during which CAV_5 was selected as the best candidate IM, while in this study, PSA(T_{So}) came out on top as the most efficient and sufficient IM. In this study, the author used the PDMY02 soil constitutive model in finite element numerical simulations. PDMY02 was simultaneously calibrated against cyclic element level tests (e.g., cyclic simple shear test), centrifuge experiments, and field data to capture different aspects of important soil responses. The purpose of such extensive calibration processes was to capture various evolutionary soil responses, such as acceleration and displacement time histories, in addition to the pore pressure time histories, and onset of liquefaction. More importantly, in this study, the redistribution (or dissipation) of pore pressure during and after cyclic loading that strongly affects the dynamic response of the liquefiable deposit was considered. However, Kramer and Mitchell (2006) used UWsand (Li

2000) soil constitutive model in finite difference numerical simulations. The UWsand was only calibrated against field data to capture peak excess pore pressure generation or the onset of liquefaction (CRR vs. $N_{1,60}$) in typical sand. In the site response numerical analyses performed by Kramer and Mitchell (2006), excess pore pressure redistribution was not considered (i.e., fully undrained condition was assumed). In other words, excess pore pressures were at their peak at the end of time-domain analyses. Overall, considering the effects of all mentioned parameters above, between these two numerical studies, the author believes that the influence of excess pore pressure redistribution has the most significant impact on the responses that led to the identification of different optimum IMs for prediction of liquefaction hazard.

6.5. Conclusions

This chapter presents the results of a numerical parametric study to evaluate the influence of ground motion parameters on the liquefaction hazard in the vicinity of structures. In performance-based earthquake engineering (PBEE), the triggering of liquefaction and its consequences on the performance of the site and structure need to be evaluated for a range of ground motions. The existing procedures for evaluating liquefaction triggering rely on ground motion Intensity Measures (IMs) that are not optimum in terms of their ability to reduce variability in the predicted response, independence from source characteristics, and their predictability (e.g., peak ground acceleration at the surface in the free-field, $PGA_{FF\text{-}Surface}$). Knowledge of the influence of ground motion characteristics on the predicted liquefaction hazard and use of an optimum IM in selecting and scaling input motions will reduce variability and improve the accuracy of the predicted Engineering Demand Parameter (EDP) of interest, in this case the peak value of excess pore pressure ratio ($r_{u,peak}$).

Solid-fluid, fully-coupled, 3D, nonlinear, dynamic finite element simulations of structures founded on a layered soil profile, including a liquefiable layer, were first validated using centrifuge experimental results. The validated models were then employed in a

parametric study for a range of soil and structural conditions and ground motions. Contrary to previous studies, the presented simulations directly take into account excess pore pressure redistribution and soil-structure interaction (SSI) in evaluating the liquefaction hazard and effects on structures. The results from this parametric study were used to identify improved IMs for predicting the generation of excess pore pressures, hence the liquefaction potential in saturated sandy soils not just in the free-field, but also in the vicinity of structures.

Different IMs were first compared in predicting the EDP ($r_{u,peak}$) in the free-field as well as under the center and edge of the foundation in terms of their efficiency, sufficiency, and predictability. The standard deviation of predicted results compared to the regression curves were computed for all models and compared among different IMs. The IMs with the smallest overall standard deviation ranked highest in efficiency. Then residuals of predicted EDPs given an IM ($r_{u,peak|IM}$) were computed as a function of earthquake magnitude and distance (M_w and R). Standard linear regressions were obtained on each set of residuals, and their slopes (c) were used to quantify and judge the dependence of the residuals on M_w and R. Those with the smallest slopes were ranked highest in sufficiency. Near-source and ordinary motions were combined in deriving regressions for both efficiency and sufficiency evaluations. Lastly, in selecting an optimum IM, its predictability was also considered, which was judged based on the uncertainty in the estimation of that IM with the existing attenuation models.

Overall, the best combination of efficiency, sufficiency, and predictability was found in the following IMs for predicting $r_{u,peak}$: 1) PSA[T_{So}] in the free-field and under the edge of the foundation; and 2) SIR under the center of the foundation. It must be emphasized, however, that the conclusions made in this study are limited to the soil and structural conditions evaluated numerically and may not apply to other types of structures, foundations, or soil stratigraphy (e.g., sloping ground). Further, as future attenuation relationships are developed for other more efficient and sufficient IMs with smaller residuals, these conclusions should be re-visited.

CHAPTER 7

GROUND MOTION INTENSITY MEASURES TO EVALUATE THE PERFORMANCE OF SHALLOW-FOUNDED STRUCTURES ON LIQUEFIABLE GROUND

This chapter is based on the following reference:

Karimi, Z., and Dashti, S. (forthcoming). Ground Motion Intensity Measures to Evaluate II: the Performance of Shallow-Founded Structures on Liquefiable Ground. Earthquake Spectra, EERI (under review).

7.1. Introduction

An effective mitigation of soil liquefaction requires a reliable assessment of the hazard and its consequences in terms of the performance of soil and building for a range of ground motions. The available simplified, empirical procedures (e.g., Youd et al. 2001; Seed et al. 2003; Idriss and Boulanger 2008; Tokimatsu and Seed 1987; Ishihara and Yoshimine 1992) do not take into account the influence of a building on excess pore pressure generation and settlement in soil, which is known to be important (e.g., Dashti et al. 2010a,b). More recently, Shahir and Pak (2010), Cetin et al. (2012), and Karamitros et al. (2013) recommended simplified procedures for assessing liquefaction triggering and its resulting settlements under

shallow-founded, mostly rigid structures. These procedures, developed based on numerical simulations that were validated against experimental or field data, offer significant improvements compared to previous methods by considering the important influence of structures on excess pore pressure generation and settlement in soil. Yet, these methods are based on Intensity Measures (IMs) that may not be optimum in reducing variability of the predicted response or its independence from additional parameters, such as source magnitude and distance (M_w and R). Further, even though Cetin et al. (2012) considered the influence of building's fundamental mode on liquefaction triggering, the combined influence of ground shaking, excess pore pressure generation, and permanent soil settlements on the performance and damage potential of non-rigid buildings is currently not well understood.

Fully-coupled, nonlinear, dynamic numerical simulations of the soil-structure system are increasingly used in research and practice to assess the performance of structures on softened ground, a trend that is expected to continue, particularly as more nonlinear models are validated against laboratory or field data. However, the results of these advanced analyses are sensitive to the selection and scaling of input ground motions. Knowledge of the efficiency and sufficiency of different ground motion IMs in predicting Engineering Demand Parameters (EDPs) that specifically relate to building performance (e.g., permanent settlement, tilt, and inter-story drift) is currently lacking. This understanding is required to reduce the variability and improve the confidence level in the prediction of critical EDPs, before the liquefaction hazard can be reliably mitigated.

In chapters 6 and 7 of this dissertation, the author presents the results of a solid-fluid, fully coupled, nonlinear, dynamic, 3D finite element parametric study that was previously validated using centrifuge experimental results for a range of soil, structure, and ground motion characteristics. Different IMs are evaluated and compared for each soil and structure EDP in terms of their efficiency, sufficiency, and then predictability. In the chapter 6, the focus was

primarily on excess pore pressure development and liquefaction triggering in soil (EDP = $r_{u,peak}$), both in the free-field and near-field. In this chapter, we explore the effects of different IMs on EDPs that specifically relate to building performance and damage potential (e.g., permanent settlement, tilt, and peak inter-story drift caused by rocking and flexural distortion). This understanding is a necessary step before the benefits of performance-based earthquake engineering (PBEE) can be realized in the evaluation and mitigation of the liquefaction hazard.

7.2. Approach in Modeling the Soil-Structure System

7.2.1. Numerical Simulations and Validations with Centrifuge Experiments

As discussed in more detail in previous chapters, dynamic centrifuge experiments performed by Dashti et al. (2010a,b) were used to validate the results of solid-fluid, fully-coupled, nonlinear, 3D finite element simulations of the response of single-degree-of-freedom (SDOF), elastic, shallow-founded structures on a layered soil deposit, including a liquefiable layer. Figure 7.1 presents a schematic drawing of the soil-structure model investigated both experimentally and numerically.

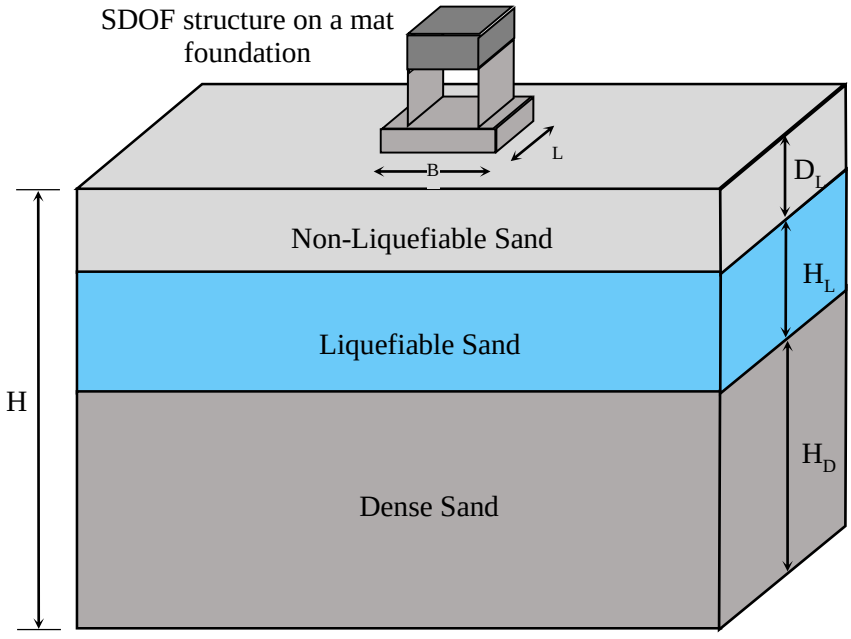

Figure 7. 1. Schematic of the soil-structure system evaluated in the centrifuge and in the numerical simulations (Dashti et al. 2010a,b, Karimi and Dashti 2015).

Although centrifuge tests do not capture all the complexities of real field conditions, they enable a systematic and fundamental evaluation of the underlying mechanisms of damage as well as a validation of numerical tools that can later be used to model more complex and realistic conditions. The dominant mechanisms of building settlement were identified through centrifuge experiments (Dashti et al. 2010a) as: (a) volumetric types due to: rapid drainage ($\varepsilon_{p\text{-}DR}$), sedimentation ($\varepsilon_{p\text{-}SED}$), and consolidation ($\varepsilon_{p\text{-}CON}$), and (b) deviatoric types due to: partial bearing capacity loss ($\varepsilon_{q\text{-}BC}$) and soil-structure-interaction (SSI) induced building ratcheting ($\varepsilon_{q\text{-}SSI}$). Accordingly, in order to capture the dominant settlement mechanisms near a shallow-founded structure, it was important to perform fully-coupled, effective-stress numerical simulations that account for soil nonlinearity, softening and re-stiffening due to liquefaction, excess pore pressure generation and redistribution during cyclic loading, and importantly 3D SSI and drainage effects near structures.

Solid-fluid, fully-coupled, 3D, finite element analyses of the centrifuge tests were performed using the pressure-dependent, multi-yield-surface, plasticity-based soil constitutive model (PDMY02) implemented in OpenSees by Elgamal et al. (2002) and Yang et al. (2003 and 2008). The properties of the structures, soil profiles, and base motions as well as the constitutive model parameters and their calibration were discussed in detail by Dashti et al. (2010a,b), Karimi and Dashti (2015b,2016).

The accuracy of numerical predictions was evaluated with respect to experimental observations by Karimi and Dashti (2015b) in terms of residuals (see Eq. 6.1).

Figure 7.2 compares the numerically predicted and experimentally measured permanent building settlements, tilts, and transient peak inter-story drift ratios. Because of the large degree of transient and permanent rocking often observed on structures founded on liquefiable ground, it is important to consider the contribution of rigid body rotation (rocking) and flexural deformation to total inter-story drift separately (Karimi and Dashti 2016). Flexural inter-story

drift is expected to serve as a proxy for building damage. Hence, it is of particular importance to structural engineers when evaluating building performance.

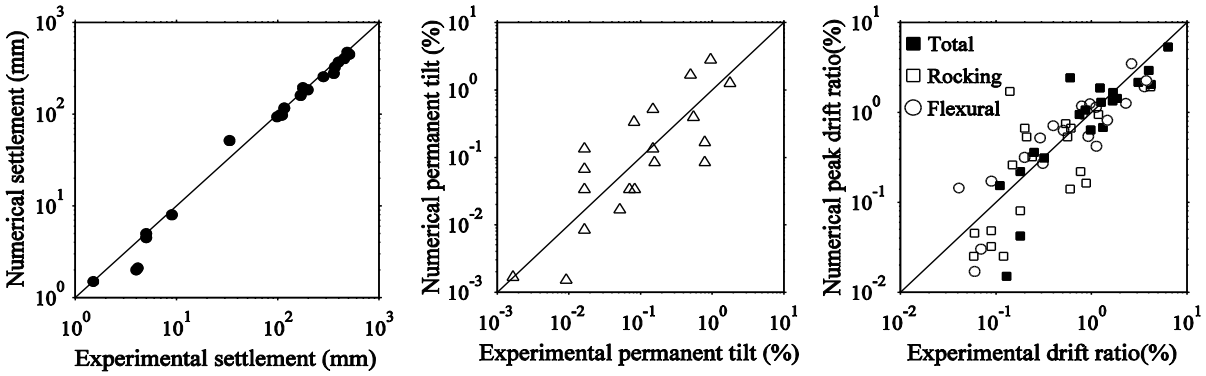

Figure 7. 2. Experimentally measured and numerically predicted values of: (a) permanent foundation settlement, (b) permanent foundation tilt, and (c) transient peak total, rocking, and flexural inter-story drift ratios.

In summary, settlements in the free-field, which are controlled by volumetric strains due to sedimentation, partial drainage, and consolidation ($\varepsilon_{p\text{-}SED}$, $\varepsilon_{p\text{-}DR}$, and $\varepsilon_{p\text{-}CON}$) were highly underestimated by the numerical simulations. This was primarily attributed to the underestimation of soil volumetric compressibility by the constitutive model and a changing hydraulic conductivity in soil during shaking, which was not taken into account numerically (Karimi and Dashti 2015b). Total settlements under the structures, on the other hand, which are dominated by shear type deformations and volumetric strains due to partial drainage ($\varepsilon_{q\text{-}BC}$, $\varepsilon_{q\text{-}SSI}$, and $\varepsilon_{p\text{-}DR}$), were captured well numerically, with residuals ranging from approximately -0.19 to 0.3. The residuals increased to approximately -1.0 to 0.98 for the predicted building permanent tilt and transient inter-story drift ratios. The residuals decreased for inter-story drift at stronger levels of shaking and larger drifts.

Predicting the accumulated foundation tilt was particularly difficult, because it is governed by complex interactions among changing soil properties, the characteristics of the ground motion and structure, and the interface condition between the soil and foundation. The

soil properties in the numerical simulations were assumed to stay constant throughout the entire earthquake loading, which is known to be an inaccurate assumption both in terms of soil stiffness and hydraulic conductivity (Karimi and Dashti 2015b; Shahir et al. 2012). Further, the foundation elements were attached to the soil elements, allowing no separation or sliding of the foundation relative to soil, which tend to alter the nature of dynamic loading and damping near the foundation edges. The complexity of tilt and these numerical simplifications were likely responsible for larger errors observed in the prediction of permanent foundation tilt. The uncertainty observed in the predicted structural EDPs and the numerical error compared to experimental (and field) observations must be considered and propagated into any future probabilistic, predictive model that is based on those numerical predictions.

7.2.2. Numerical Parametric Study

Identification of optimal IMs for evaluating the response of the structure was accomplished by performing similar 3D, solid-fluid, fully-coupled, nonlinear finite element analyses of layered liquefiable soil deposits and elastic SDOF structures on stiff mat foundations undergoing a range of ground motions with different characteristics. The high performance computing facility of Network for Earthquake Engineering Simulation, NEEShub (Hacker et al. 2013), and the parallel version of OpenSees (OpenSeesSP 2.4.3, McKenna et al. 2000; McKenna and Fenves 2008) were used to reduce the running time of each simulation. Several measures of the performance of the structure were explored from the results of these simulations and plotted as a function of each candidate IM. The primary structural EDPs selected and presented in this chapter are the permanent (accumulated) average settlement and tilt of the foundation as well as the total, rocking, and flexural peak transient inter-story drift ratios of the structure.

The previous chapter summarized the properties of the soil-structure systems evaluated in the parametric study (see Table 6.1). Twenty one cases were simulated, in which the

thickness (H_L) of, depth (D_L) to, and relative density (D_r) of the liquefiable layer as well as the building's contact pressure (q) and fix-based fundamental period (T_{STo}) were varied. It was of particular interest to evaluate the influence of T_{STo} in relation to the initial period of the site (T_{So}) and ground motion (T_p or T_m) on structural performance. When a given property was changed in structure or soil, other parameters were kept the same, in order to evaluate their effects individually. For example, when the building contact pressure (q) was varied, the structural mass and T_{so} were kept unchanged by only varying the foundation pressure. When T_{so} was varied, the mass, center of gravity, and q were kept unchanged by only varying the column stiffness. The same applied to soil properties.

A total of 52 ordinary ground motions and 26 near-source ground motions were selected. The number of motions was comparable to Luco and Cornell (2007), who used 59 ordinary and 31 near-source motions, despite the large mesh size and long running time for each coupled 3D simulation of the soil-foundation-structure system employed here. Similar to Luco and Cornell (2007), the selected motions were recorded either at rock or stiff soil sites with a range of magnitude/distance combinations and were applied to the base of all the models (summarized in Table 6.3).

The previous chapter also listed the ground motion parameters that were evaluated in this study in terms of their influence on both soil and structural EDPs (see Table 6.2). Parameters that describe either one or multiple aspects of the motion's characteristics (e.g., in terms of intensity, duration, and frequency content) were considered. In addition to spectral accelerations at the fundamental period of the site (T_{So}) or structure (T_{STo}), spectral accelerations at a lengthened period of soil or structure were also evaluated (e.g., $1.5T_{So}$ or $1.5T_{STo}$), in order to roughly account for softening in soil or period elongation in structure due to a flexible-base foundation in a simplistic manner.

7.3. Insight from Numerical Parametric Simulations

7.3.1. Effects of Intensity Measures on Foundation Settlement and Tilt

The permanent foundation settlement was computed by averaging permanent settlements on the four corners of the stiff mat foundation. Permanent tilt was calculated by taking the difference in the average settlement on the two sides of the foundation and dividing that by the foundation width. Figure 7.3 shows the influence of four representative IMs (PGA, AI, CAV, PSA[T_{So}]) of the base (input rock) motion on permanent foundation settlements for two of the models simulated (models 5 and 6). The variation of permanent foundation settlement given an IM (i.e., EDP|IM) was estimated for each of the twenty one models using regressions. The data in this case was evaluated in the log-log space, in order to allow for the use of standard linear regressions. In the log-log space, the resulting variability of EDP|IM was observed to be roughly uniform over the range of IMs considered, which is one of the assumptions of a standard linear regression analysis (i.e. linear independency). Although different symbols are used for the data corresponding to near-source and ordinary motions in these figures, the regressions combine their data, because no major difference was observed in the settlement trends for different groups of motions. The quality of each IM is evaluated later based on the concepts of efficiency, sufficiency, and predictability.

The degree of scatter in the computed EDPs (in this case structural settlement, tilt, and drift) about the regression line for a given candidate IM was used to evaluate the efficiency of that IM. The degree of independence of the EDP residuals from source M_w and R was used to evaluate the sufficiency of the IM. And lastly, the uncertainty in the estimation of a given IM was used to evaluate its predictability. A strong candidate IM is aimed to reduce the dispersion in a given EDP and hence, improve its accuracy in future simulations. Similar to the previous chapter, to reduce uncertainties associated with the estimation of ground motion parameters at the surface in the free-field or on the foundation, the input rock (base) motions were used in

the subsequent evaluations. An increase in any candidate IM increased the contribution of all settlement mechanisms active near a structure, amplifying total foundation settlements.

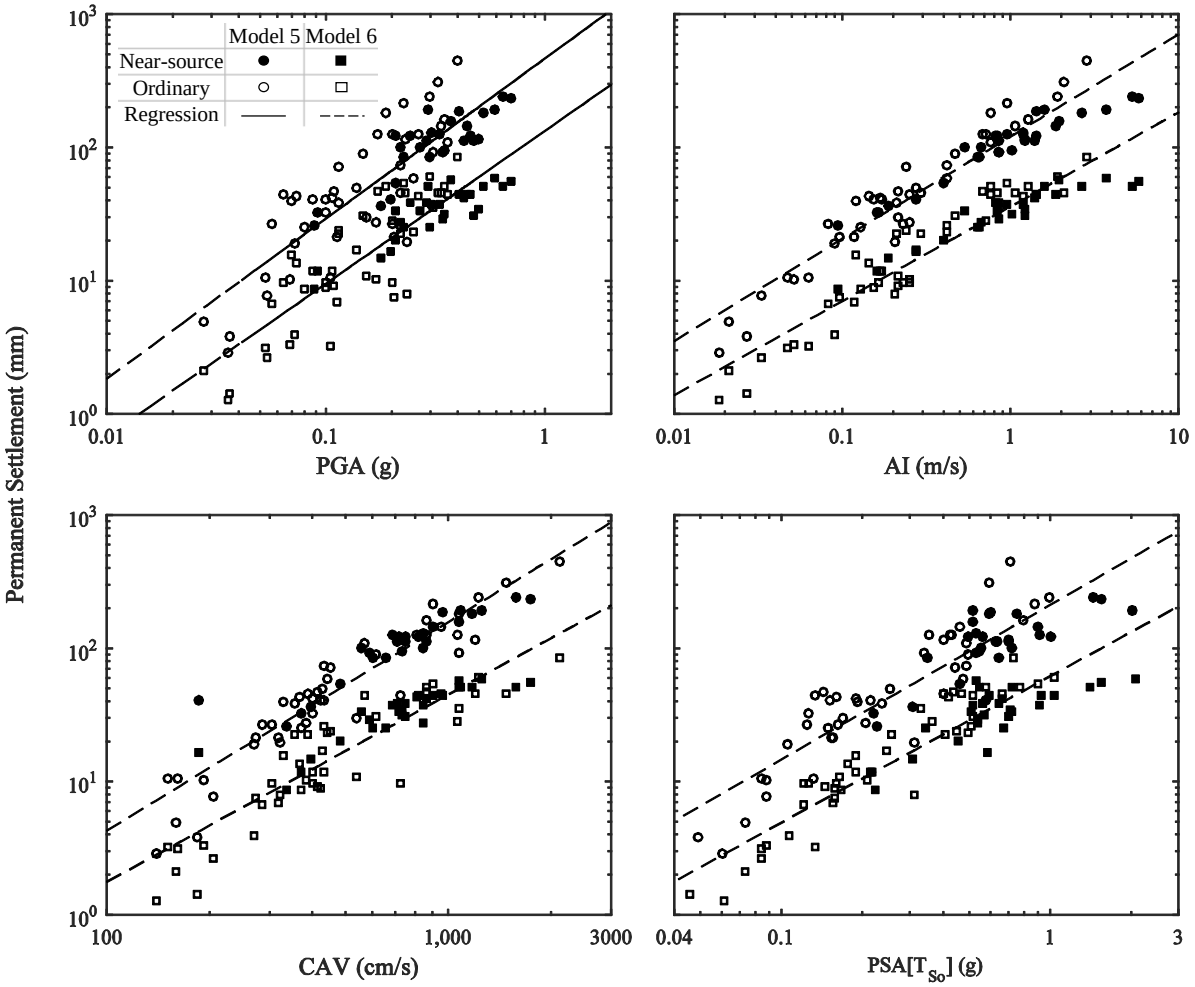

Figure 7. 3. Foundation permanent settlement versus intensity measures of base ground motions in models 5 and 6.

Figure 7.4 shows the influence of the relative density (D_r) and thickness of the liquefiable layer (H_L), as well as the building's fixed-base fundamental period (T_{STo}) on the predicted foundation settlements, keeping other factors constant, as a function of base motion PGA. PGA is used in these plots because of its traditional use in assessing the liquefaction hazard and its effects. These plots are presented in the log-linear space, in order to better visualize the influence of various parameters on permanent foundation settlement. As expected, D_r and H_L had the strongest influence on building settlements in the cases considered.

Decreasing the D_r and increasing H_L of the liquefiable soil led to a more extensive generation of excess pore pressures, softening, and strength loss in the foundation soil, which amplified deviatoric and volumetric strains (e.g., primarily $\varepsilon_{q\text{-}BC}$, $\varepsilon_{q\text{-}SSI}$, $\varepsilon_{p\text{-}DR}$) and hence, total building settlements. The changes considered in T_{STo} alone did not noticeably affect building settlement when all other building properties (including mass, contact pressure, and center of gravity) were kept constant.

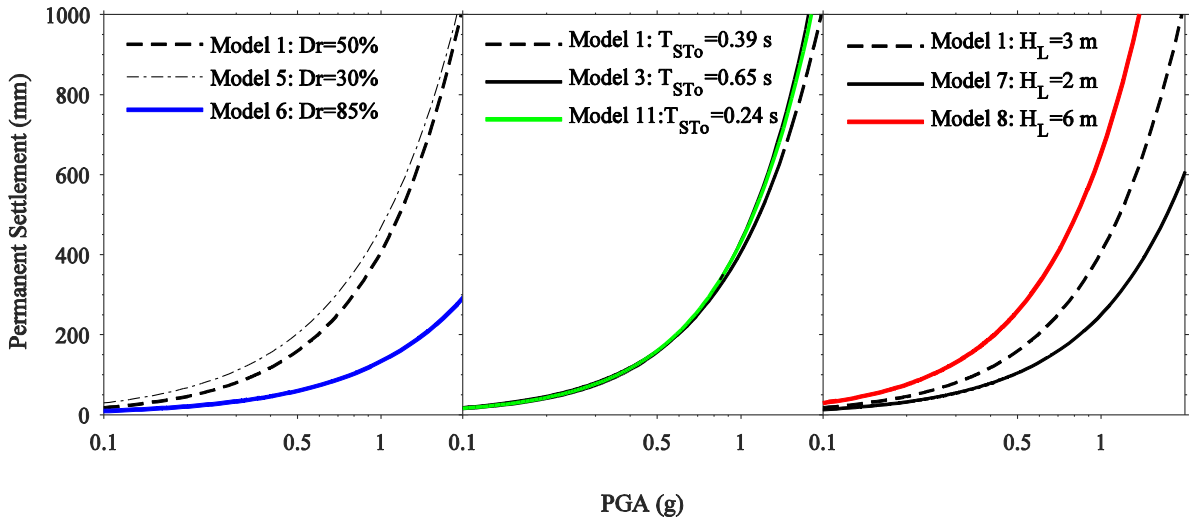

Figure 7. 4. Influence of relative density (D_r), fixed-base fundamental period of the structure (T_{STo}), and liquefiable layer thickness (H_L) on the predicted permanent foundation settlements.

The effect of foundation contact pressure (q), foundation contact area (B×L), and structure's effective height (H_{eff}) on permanent foundation settlement was also separately evaluated for several cases, as listed in Table 6.1, and the results are shown in Figure 7.5. Increasing the foundation q amplified its settlement, particularly at stronger level of shaking (e.g., greater PGA or Arias intensity). An increase in foundation area increased slightly its settlement. Net excess pore pressures generated under the center and edge of the foundation increase as the foundation area increases due to a greater capacity for excess pore pressure generation (greater induced stresses in a larger area within soil and a longer drainage path). This leads to a greater degree of softening in the underlying soil, which extends deeper into the

soil compared to a smaller foundation, with all else equal (as shown in Figure 6.12). As also shown in this figure, foundation settlement slightly increased with increasing H_{eff}, because of greater overturning moments and larger SSI-induced building ratcheting ($\varepsilon_{q\text{-}SSI}$).

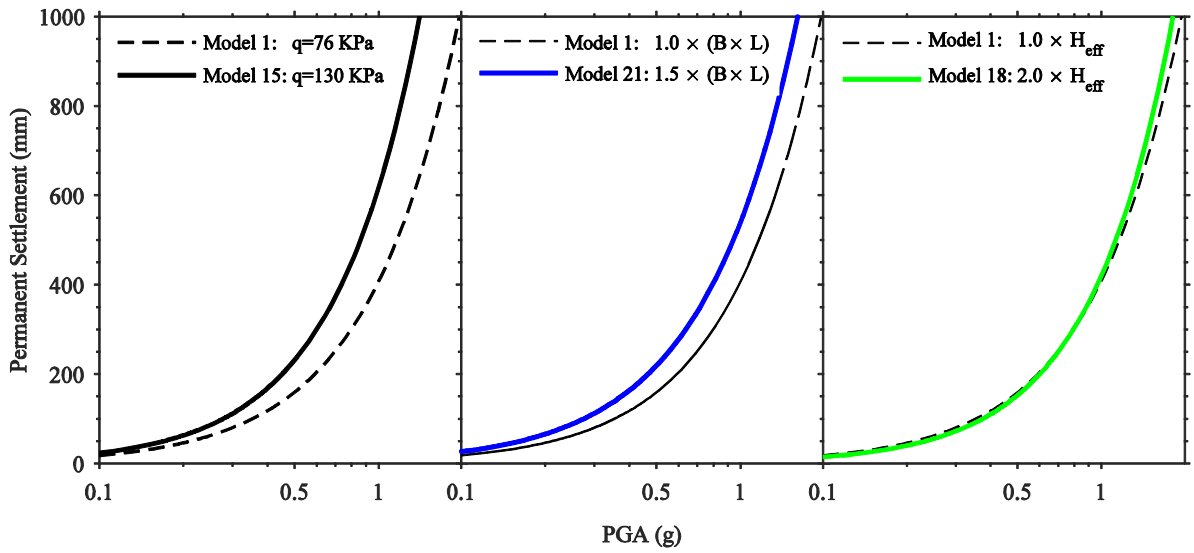

Figure 7. 5. Influence of foundation contact pressure (q), foundation contact area (B×L), and structure's effective height (H_{eff}), separately, on the predicted permanent foundation settlements.

In general, increasing the relative density and hence, stiffness of the underlying soil was observed to decrease the predicted permanent foundation tilt. However, the permanent tilt for the structures considered in this study did not appear to follow a clear pattern with change in any of the IMs considered and showed a significant amount of scatter. Figure 7.6 shows the foundation's permanent tilt predicted for two example models 5 and 6 as a function of five different IMs of input rock motions. The relationship between tilt and ground motion IMs at other locations (free-field surface or foundation) were also explored, and no major improvement was observed in their scatter or trend. Additionally, given the relatively large residuals previously observed in the prediction of permanent building tilt compared to experimental results (e.g., shown in Figure 7.2) and the large degree of uncertainty embedded

in its prediction, the influence of different IMs on this EDP were not further evaluated in this study.

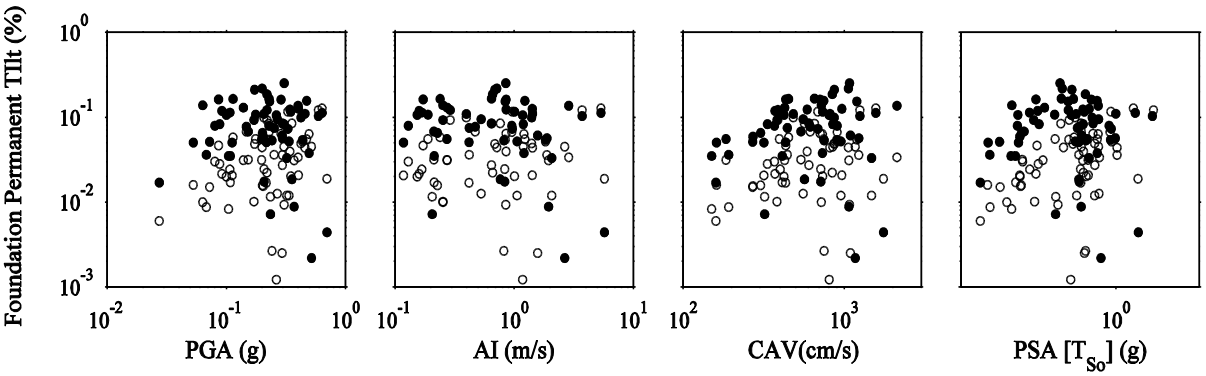

Figure 7. 6. Foundation permanent tilt as a function of five representative Intensity Measures of ground motions recorded at the base of the model.

7.3.2. Effects of Intensity Measures on Inter-Story Drift

The transient lateral displacement of the structure mass relative to its foundation is a critical EDP that influences building's performance. In this study, the total relative displacement between the mass and foundation is referred to as "total" drift (δ_T), which has two components (Gelagoti et al. 2012; Karimi and Dashti 2016): 1) flexural drift (δ_F) due to the flexural distortion of the structure, and 2) rocking drift (δ_R) due to the rigid body rotation or rocking of the whole building. Flexural drift is often used by structural engineers as a proxy for building's damage potential. Hence, the reliability of its prediction is of high importance, particularly in designing mitigation strategies that aim to improve the overall performance of the structure. Numerical predictions of drift were obtained from the lateral displacement of the mass and foundation and the vertical displacement of the two sides of foundation, as explained by Karimi and Dashti (2016).

Figure 7.7 through Figure 7.8 show the influence of four representative IMs on δ_T, δ_R, and δ_F for one model simulated out of twenty one (model 5), for clarity. The variation of these EDPs (different forms of drift) given an IM of the base motion (i.e., EDP|IM) was estimated

for each of the twenty one models analyzed using linear regressions in the log-log space. Similar to settlements, the data from near-source and ordinary motions were combined in deriving these linear regressions. No major influence was observed from near-source motions on the trends predicted in building drift, although generally, with stronger IMs, near-source motions often led to larger drifts.

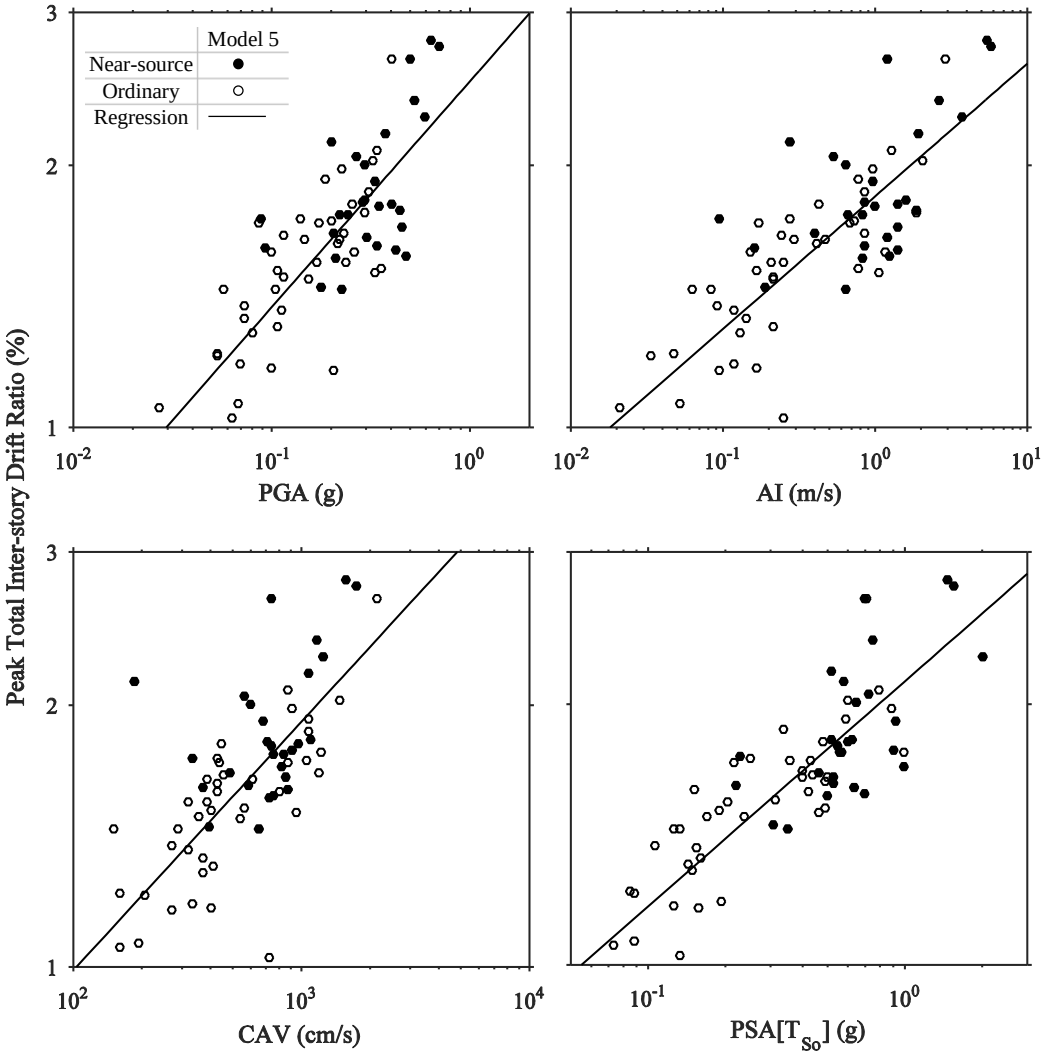

Figure 7. 7. Peak, transient, total inter-story drift ratios versus intensity measures of base ground motions in model 5.

Generally, all types of drift increased with the increase in different IMs. However, the highest degree of variability or scatter was observed in flexural drift, which contributed to the

large scatter observed in total drift. This scatter is quantified and evaluated in more detail in the next section with standard deviations about the regression line.

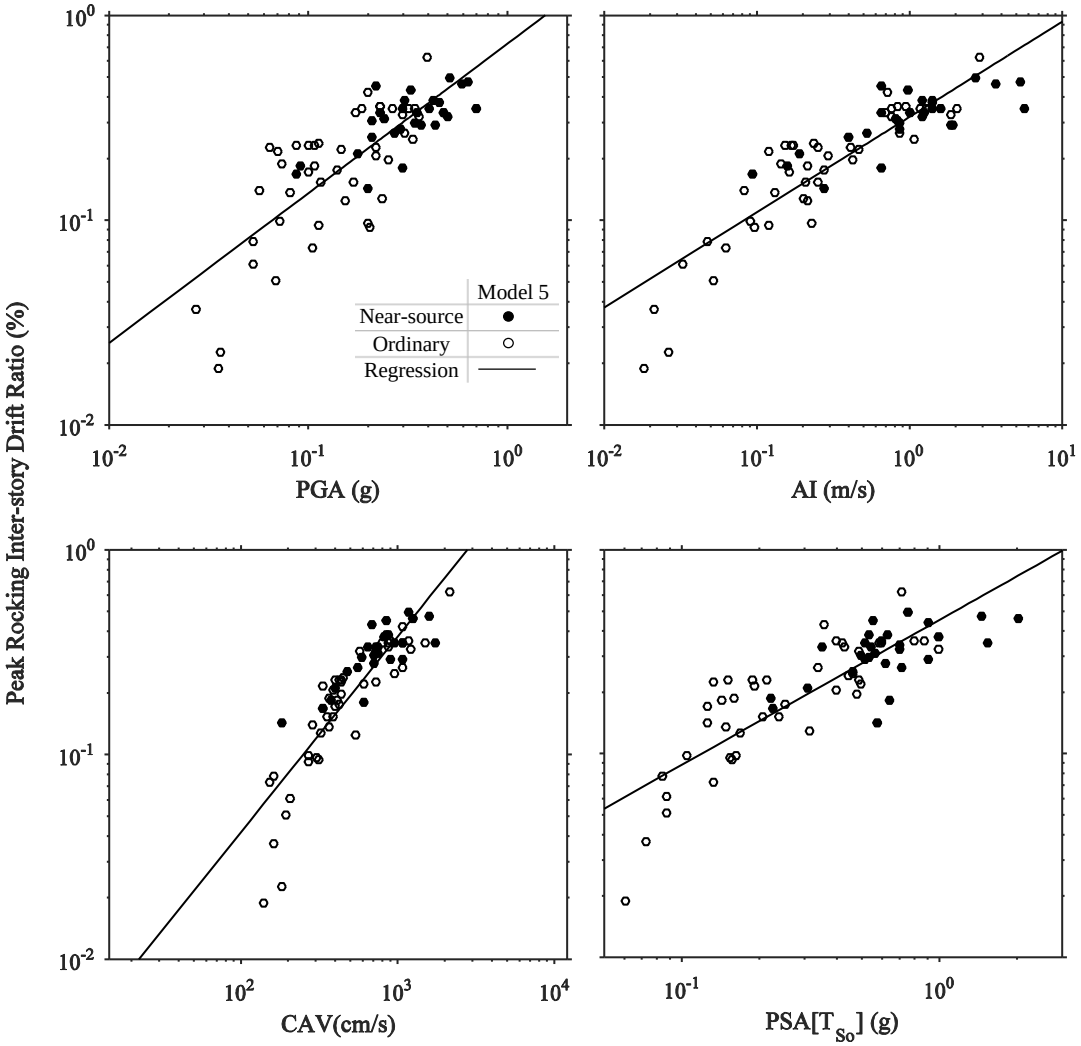

Figure 7. 8. Peak, transient, rocking inter-story drift ratios versus intensity measures of base ground motions in model 5.

7.4. Selection of Intensity Measures to Predict Structural Performance

A strong candidate IM for predicting each of the EDPs of interest (structure's permanent settlement and different components of peak transient inter-story drift ratio) is one that reduces the dispersion of the EDP (i.e., efficiency), makes the prediction of the EDP independent of source M_w and R (i.e., sufficiency), and can itself be predicted with the least uncertainty (i.e., predictability).

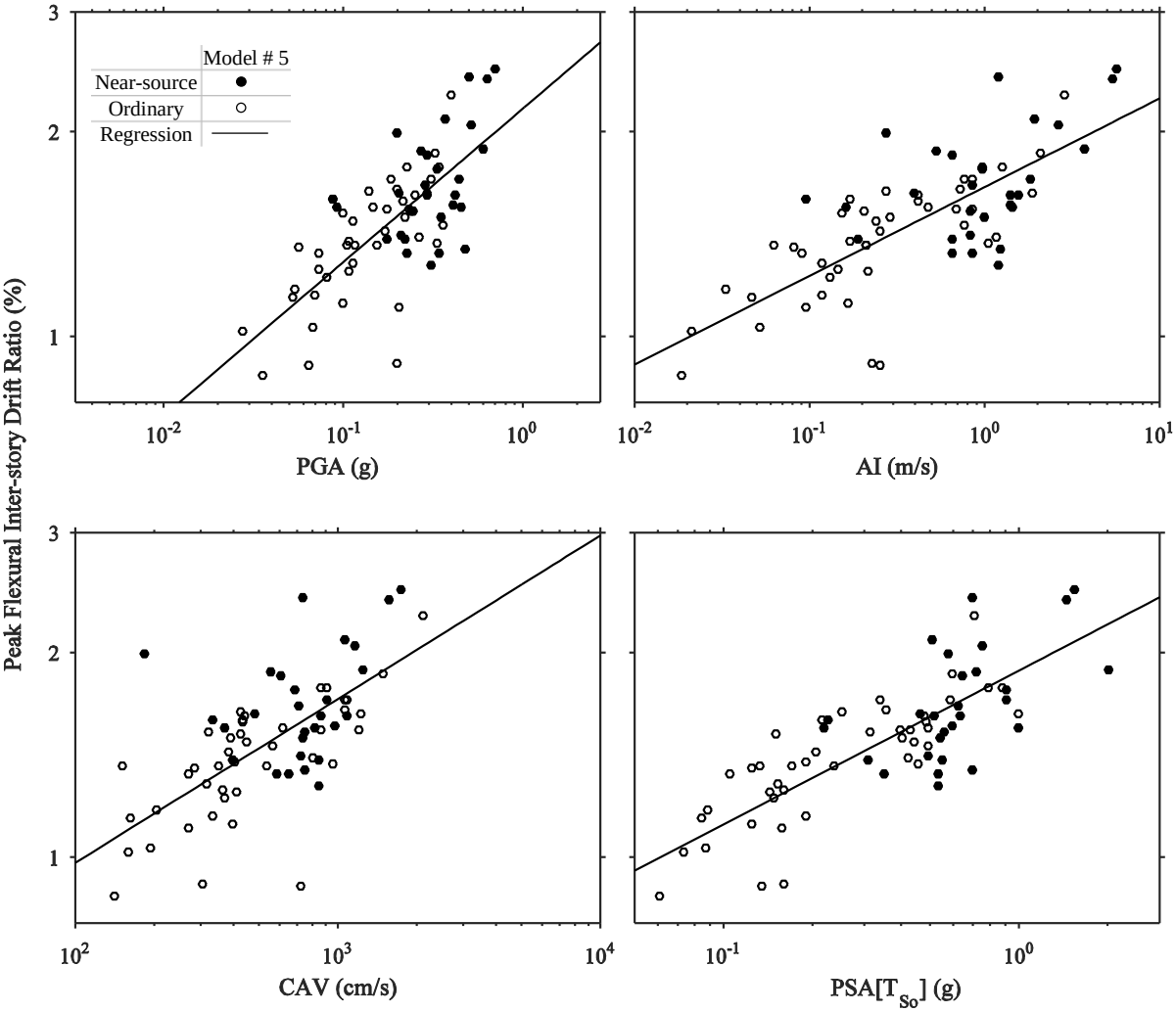

Figure 7. 9. Peak, transient, flexural inter-story drift ratios versus intensity measures of base ground motions in model 5.

The IMs were first ranked based on their efficiency in predicting a given EDP, which was quantified as the residual sum of squared errors between the regression curve and numerically predicted EDPs (i.e., standard deviation or σ). Figure 7.10 shows the individual and average values of σ in each of the four EDPs (permanent foundation settlement as well as transient total, rocking, and flexural inter-story drift ratios) for each candidate IM among the twenty one models simulated. The numbers associated with each IM in this figure were summarized in Table 6.2. The IMs with the smallest overall σ were ranked the highest (e.g., CAV and CAV_5 for settlement).

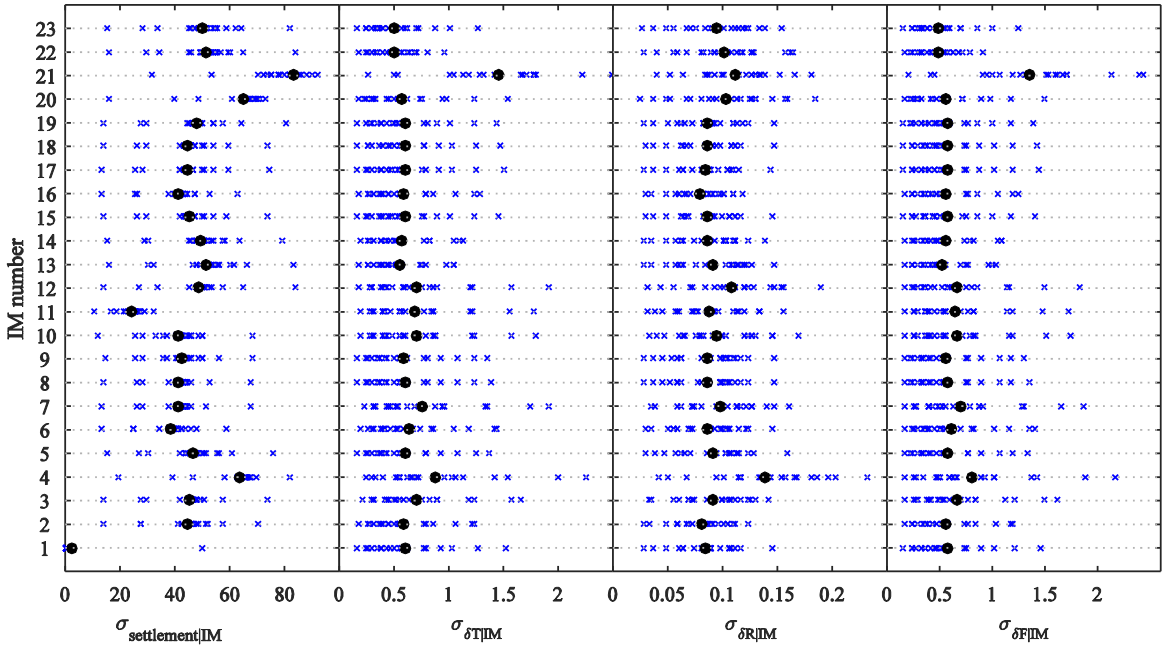

Figure 7. 10. The standard deviation (σ in building settlement as well as peak transient total, rocking, and flextural drift ratios) for each candidate IM. The blue crosses indicate individual σ values and the black circles show the average σ among the twenty one simulations.

After the more efficient IMs were identified for each EDP, they needed to be evaluated in terms of their sufficiency. Figure 7.11 and Figure 7.12 compare the residuals of total settlement and total inter-story drift ratios for four representative IMs (e.g., PGA, AI, CAV, PSA[T_{So}]) separately as a function of source M_w and R. The residuals were also estimated in a similar manner for rocking and flexural inter-story drift ratios. The plots are shown only for one model simulated (e.g., model 5), for clarity. Standard linear regressions were obtained on each set of residuals. The slope of the regression line (c) was used for each model to quantify and judge the dependence of the EDP residual on M_w and R. In all cases, near-source and ordinary motions were combined in obtaining regressions, in order to evaluate sufficiency over a range of distances.

Figure 7.13 and Figure 7.14 summarize the individual and average values of c corresponding to the linear regressions of residuals for each EDP and IM considered among different models as a function of M_w and R, respectively. The scaled motions were removed

from this evaluation. The IMs with the smallest overall c values (|c| near zero) were ranked highest in terms of sufficiency.

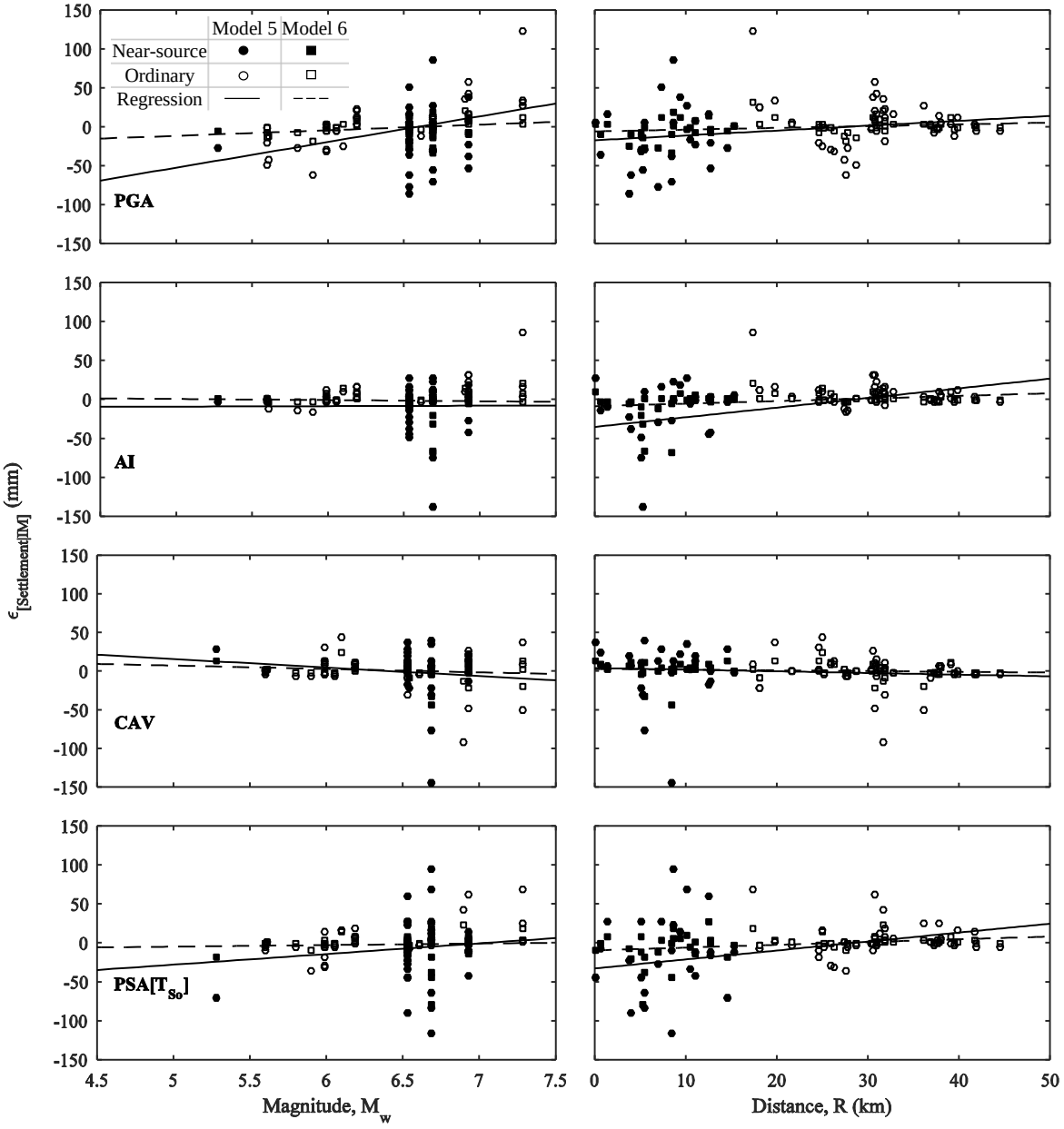

Figure 7. 11. Residuals of permanent foundation settlement for four representative intensity measures as a function of source moment magnitude (M_w) and distance (R).

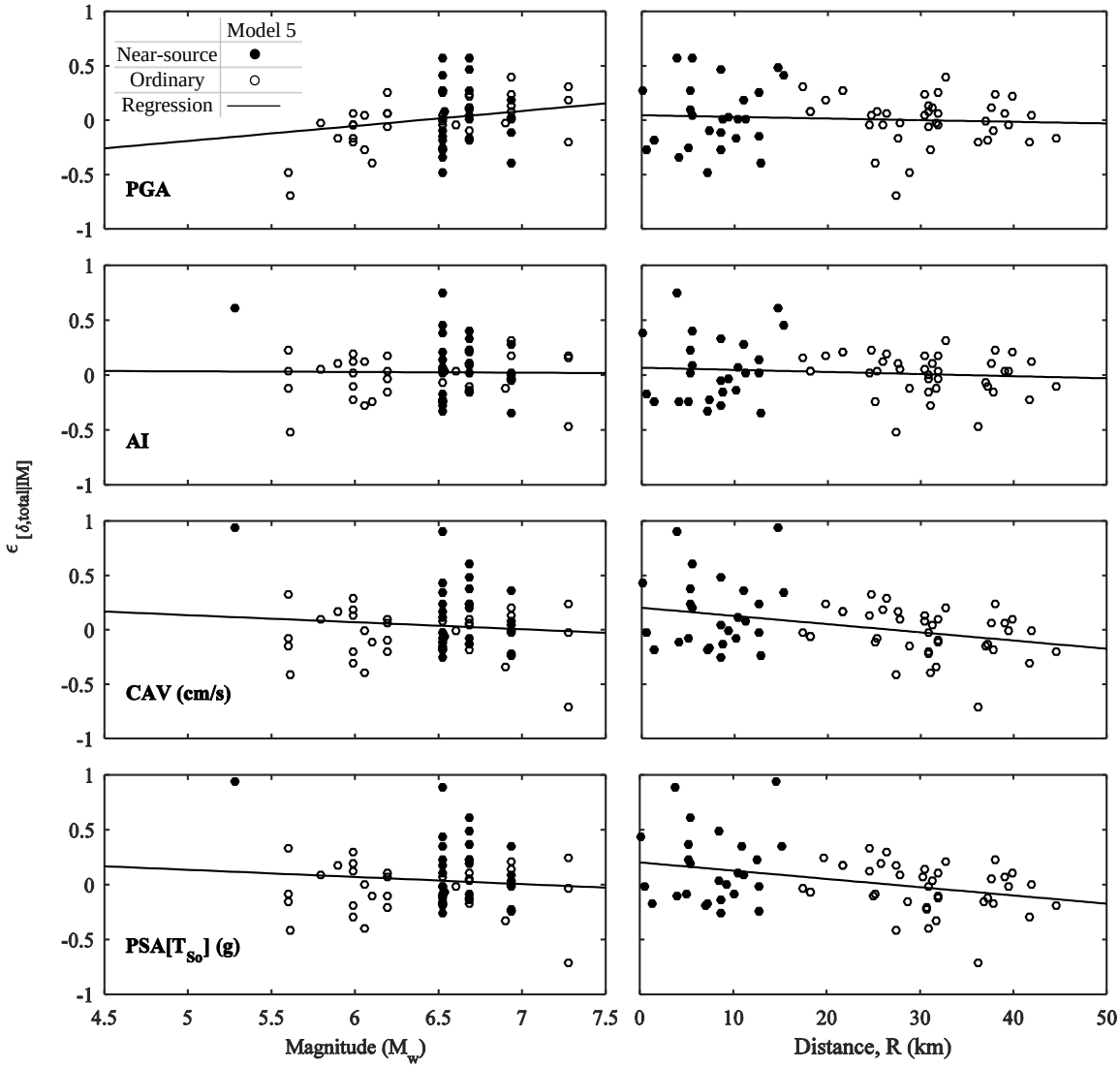

Figure 7. 12. Residuals of peak transient total inter-story drift ratio for four representative intensity measures as a function of source moment magnitude (M_w) and distance (R).

In general, the slopes of these linear regressions were considerably smaller against source R compared to M_w for all the EDPs investigated in this study. This shows that generally, the residual in the EDPs investigated were more dependent on source M_w and ground motion characteristics that are influenced by M_w (e.g. duration) compared to R. In selecting a sufficient IM, therefore, a higher priority was given to those that ranked highly with respect to M_w. While the sufficiency rank of the IM against R was considered important, it was emphasized less, as the slopes of regressions were generally small against R. For the set of conditions evaluated in

this study and the EDPs investigated, the following IMs were identified with the best combination of efficiency and sufficiency: 1) CI and AI for permanent foundation settlement; 2) CI and AI for total inter-story drift ratio; 3) v_{RMS} and AI for rocking drift ratio; and 4) CI and AI for flexural drift ratio.

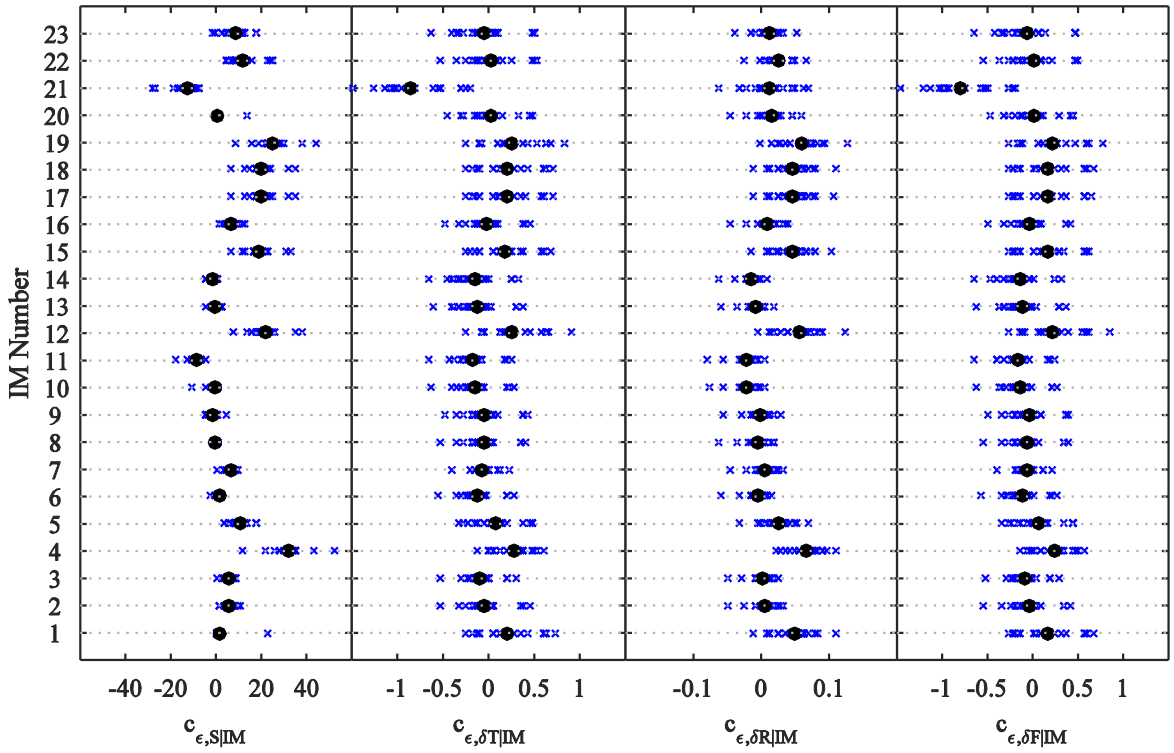

Figure 7. 13. The slope (c) values corresponding to the linear regression of residuals in structure settlement as well as peak transient total, rocking, and flexural drift ratio for a given candidate IM as a function of source M_w. The blue crosses indicate individual c values and the black circles show the average c among the twenty one simulations.

In selecting an optimum IM, it is important to consider its predictability: the accuracy with which the IM can be predicted. Among the IMs identified above, the Arias Intensity (AI) can be predicted for a future scenario event using the relationship proposed by Travasarou et al. (2003). AI is a holistic parameter that brings in the intensity, frequency content, and duration of the motion, and it was identified as a common parameter for all four EDPs considered in this study. Even though the residuals associated with its prediction are not small (particularly as related to spectral accelerations), because it was identified as a relatively efficient and

sufficient parameter in the presented analyses, it is proposed for the purpose of predicting structure's performance on softened ground. The future development of new or improved attenuation models for AI and other efficient and sufficient IMs identified here are highly recommended, in order to improve the reliability of any predictive tool in evaluating and mitigating the liquefaction hazard within a performance-based earthquake engineering (PBEE) framework.

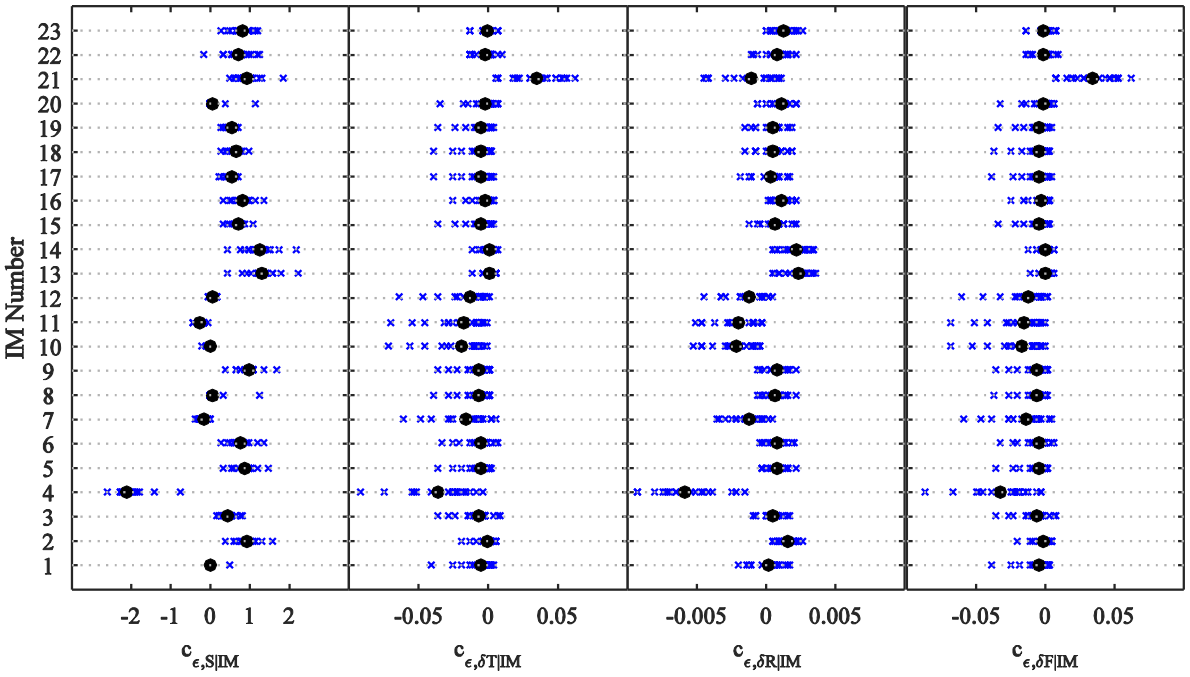

Figure 7. 14. The slope (c) values corresponding to the linear regression of residuals in structure settlement as well as peak transient total, rocking, and flexural drift ratio for a given candidate IM as a function of source R. The blue crosses indicate individual c values and the black circles show the average c among the twenty one simulations.

Use of spectral acceleration at the fixed-base period of the structure (PSA[T_{STo}]), as a proxy of structural damage (e.g., peak flexural inter-story drift ratio) and demand imposed on the structural elements is more common and widely used by structural engineers. However, in the presented study, AI was identified as the most optimum ground motion IM for prediction of different components of peak inter-story drift ratios of the structure (e.g., flexural, rocking and total drifts), in addition to the permanent foundation settlement. This is because of better

capability of AI in describing and capturing various aspects of SFSI and subsequent structural performance on the softened ground. AI is an evolutionary IM that contains most properties of the ground motion, such as intensity, duration, and frequency content. Therefore, it could better describe the evolutionary soil responses, such as excess pore pressure, acceleration, displacement time histories. Consequently, flexible-base responses of the structure (e.g., period lengthening, settlement, and drift ratios), which are controlled by the underlying soil displacement responses were better described by AI.

7.5. Conclusions

Liquefaction hazard analysis within a performance-based earthquake engineering (PBEE) framework places increasing emphasis on the optimal characterization of input ground motions used in the evaluation of the hazard and its consequences. Knowledge of the efficiency and sufficiency of ground motion Intensity Measures (IMs) in predicting the performance and damage potential of buildings founded on liquefiable ground is currently lacking. This gap prevents a reliable selection and scaling of ground motions that reduce variability and improve accuracy of the predicted building performance. This gap needs to be addressed, before the benefits of PBEE can be realized in the evaluation and mitigation of the liquefaction hazard.

In this study, the author presents the results of a fully-coupled, 3D, nonlinear, dynamic parametric numerical simulation, which was previously validated using centrifuge experimental results. The goal of this parametric study was to evaluate the influence of different ground motion parameters on the performance of site and structures on liquefiable ground. Single-degree-of-freedom (SDOF), linear-elastic structures founded on stiff, mat foundations were modeled on a layered soil profile, including a liquefiable layer. The properties of the soil, structures, and ground motions were varied numerically to evaluate their effects on building performance. A series of 52 ordinary and 26 near-source rock motions with different characteristics were used as input in all simulations and their effects evaluated.

In the previous chapter, the author evaluated the liquefaction hazard (in terms of the peak excess pore pressure ratio) in the free-field and near-field under different ground motions. The primary Engineering Demand Parameters (EDP) investigated in this chapter relate to the performance of the building: permanent foundation settlement as well as peak transient total, rocking, and flexural inter-story drift ratio.

Flexural drift ratio is of particular interest to structural engineers, as it often serves as a proxy for building damage potential. Different IMs were evaluated and compared in terms of their ability to reduce variability in the predicted EDP (efficiency), independence form source characteristics (sufficiency), and uncertainty in their prediction for future scenario events (predictability). The IM with the best combination of efficiency, sufficiency, and predictability in predicting all four structural EDPs of interest was identified as Arias Intensity (AI). Arias Intensity is an evolutionary IM that contains important properties of the ground motion, such as intensity, duration, and frequency content. Hence, it could better describe evolutionary responses of the soil (e.g., excess pore pressure, acceleration, and deformation time histories) and its consequences on the structural performance, such as different types of peak inter-story drift ratios, in addition to the foundation permanent settlement. The future development of new or improved attenuation models for predicting AI are strongly recommended, in order to reduce the uncertainty in predicting this IM and hence, improve its predictability for future simulations.

CHAPTER 8

CONCLUSIONS AND FUTURE RESEARCH RECOMMENDATIONS

8.1. Summary

The overarching objective of this research is to comprehensively evaluate and quantify the liquefaction hazard and the seismic performance of shallow-founded structures on liquefiable ground using experimental and numerical studies. Results from a series of centrifuge experiments including single-degree-of-freedom (SDOF), linear-elastic structures on liquefiable layered soil deposits are used to: 1) gain insight into the mechanisms of liquefaction-induced deformation near structures and identify the key parameters affecting the soil and structural response; 2) calibrate, validate, and identify the capabilities and weaknesses of a state-of-the-art numerical tool in capturing the integrated response of the soil-structure system by a direct comparison between experimental and numerical measurements. This validation is a necessary step before the model may be employed reliably in predicting structural response under more general conditions.

Lastly, a numerical parametric study, validated against centrifuge experiments is performed, in which the different soil, structural, and ground motion Input Parameters (IPs) are systematically varied. The parametric study serves two purposes: 1) to investigate the influence and relative importance of different IPs on soil and structural response, which is not possible

experimentally; 2) to search for and identify optimum Intensity Measures (IMs) in selecting and scaling ground motions that minimize the variability and uncertainty in estimating different Engineering Demand Parameters (EDPs) of interest.

Previous case histories and physical model studies have shown that the presence and properties of a structure can affect the static and dynamic stresses and flow patterns in the underlying soil in a three-dimensional (3D) manner, which strongly influence liquefaction triggering and the resulting accelerations and deformations. The available methods ignore the presence of the structure, its interaction with the underlying liquefiable soil, and the key displacement mechanisms that are active under a structure. Hence, they cannot reliably evaluate the consequences of liquefaction, the need for ground improvement, and the subsequent evaluation of the proposed mitigation scheme in terms of improved building performance.

Two different series of centrifuge experiments in parallel with calibrated solid-fluid, fully-coupled, nonlinear, dynamic, finite element simulations of the Soil-Foundation-Structure (SFS) systems were considered in this study to evaluate dynamic soil-foundation-structure interaction (SFSI) effects on softened ground and the underlying mechanisms of damage. The first series of experiments were performed by the author on a uniform layer of saturated, medium-dense, Nevada Sand in the free-field and in the vicinity of a linear-elastic, single-degree-of-freedom (SDOF) shallow-founded structure at the University of Colorado Boulder. The goal was to fundamentally study the seismic response of soil and structure and validate the numerical model for a range of earthquake motions with different characteristics, while keeping the soil profile uniform and relatively simple. The second series of centrifuge experiments performed by Dashti et al. (2010a,b) investigated the seismic response of different SDOF structures with stiff, mat foundations on a layered deposit, including a liquefiable layer

covering a wider range Input Parameters (IPs), such as different structures, soil relative densities and layering, and ground motion characteristics.

Class C, solid-fluid, fully-coupled, 3D, nonlinear finite element numerical simulations of the centrifuge tests were performed subsequently using the pressure-dependent, multi-yield-surface, plasticity-based soil constitutive model (PDMY02), previously implemented in OpenSees by Elgamal et al. (2002) and Yang et al. (2003 and 2008). Due to the large number of unknowns in the numerical models of the SFS systems, parallel processing on supercomputers at the NEEShub facility (Hansen) and University of Colorado Boulder (Janus) were employed. Direct comparisons between numerically computed and experimentally measured excess pore pressures, accelerations, and settlements in the free-field (FF) and near-field (NF) soil, horizontal acceleration of the foundation and structural mass, settlement and tilt of the foundation, and transient roof total, rocking, and flexural inter-story drifts were made to better understand the capabilities and limitations of this numerical tool in capturing the key EDPs.

Class-C simulations were followed by an extensive parametric study, to evaluate the influence and relative importance of different IPs on the key EDPs and to identify the most optimum ground motion Intensity Measures (IMs) for predicting liquefaction triggering and consequences on building performance.

8.2. Conclusions

Nonlinear, 1-D, site response analyses captured free-field soil behavior well in terms of excess pore pressures and accelerations during different motions, particularly during the initial cycles, while settlements were largely under-estimated. This was mainly attributed to the use of a constant hydraulic conductivity in the simulations as well as the under-estimation of soil volumetric compressibility.

Smaller net excess pore pressures were generated within the liquefiable layer under the structure with the highest contact pressure and H/B ratio for the cases considered. This may be partially explained by a higher resistance to excess pore pressure generation under higher confinement and partially by the relatively small contact area of the footing facilitating more efficient dissipation of excess pore pressures in a 3D manner. The patterns in the degree of excess pore pressure generation observed experimentally were captured well numerically.

The observed settlement patterns in experiments suggest that the contribution of post-earthquake volumetric settlements to the total building settlement was relatively minor. Volumetric strains due to partially drained cyclic loading as well as deviatoric strains under the static and dynamic shear stresses imposed by the building were responsible for the majority of building settlements, all of which primarily occurred during shaking. The numerical model could predict deviatoric displacements and hence, foundation settlements reasonably well by capturing excess pore pressures and accelerations under and near the foundation. For the cases considered in this study, numerical predictions of building permanent settlement compared fairly well with experimental results, while the predictions of permanent foundation tilt did not compare as well with the experiments. It should be pointed out that the strain gradient in the softened soil at the immediate interface of soil and foundation were relatively large that adds more nonlinearity and complexity in capturing large accumulated plastic deformations.

The numerical model generally captured kinematic and inertial interaction by reasonably capturing the change in foundation motion compared to the free-field, the reduction in building's flexible-based fundamental frequency compared to fixed-based, and the building's rocking amplitude and fundamental frequency. This study showed both experimentally and numerically that no significant de-amplification of the foundation motion may be observed at higher frequencies compared to the free-field when significantly lower excess pore pressures are generated under the foundation. Hence, in saturated sand, smaller

excess pore pressures and larger accelerations may develop under the foundation compared to free-field. In such cases, ignoring SFSI will not be conservative.

Numerical simulations captured the different components of building inter-story drift ratio (e.g., total, rocking, and flexural drifts) reasonably. Increasing the structure's contact pressure and H/B generally amplified its rocking and total drift, but not necessarily the flexural drift. Importantly, increasing the relative density of soil amplified flexural drift (an indicator of damage) by decreasing excess pore pressures in the foundation soil and building's rocking tendencies, while amplifying foundation accelerations and seismic demand.

Once validated against experimental data, covering a wide range of conditions, numerical simulations may be employed in design or in developing improved simplified procedures for evaluating building performance on softened ground. Thus, the validated models were employed in a parametric study for a range of soil and structural conditions and ground motions that could not be investigated experimentally. Contrary to the previous studies, the presented simulations directly take into account excess pore pressure redistribution and soil-structure interaction (SSI) in evaluating the liquefaction hazard and effects on structures. The primary EDPs investigated in this study are: a) liquefaction triggering or excess pore pressure generation; and b) building performance: permanent foundation settlement and tilt as well as peak transient total, rocking, and flexural inter-story drift ratios. Flexural drift ratio is of particular interest to structural engineers, as it often serves as a proxy for building damage potential. Near-source and ordinary motions were combined to evaluate the ability of their different IMs in reducing variability in the predicted EDP (efficiency), independence from source characteristics (sufficiency), and uncertainty in their prediction for future scenario events through existing attenuation relationships (predictability).

The ground motion IMs with the best combination of efficiency, sufficiency, and predictability in predicting different EDPs were identified as follow: 1) for peak excess pore

pressure ratio ($r_{u,peak}$) in the free-field and under the edge of the foundation, pseudo spectral acceleration at the initial period of the site (PSA[T_{So}]); 2) for $r_{u,peak}$ under the center of the foundation, shaking intensity rate (SIR); 3) and for all four structural EDPs of interest (i.e., foundation settlement and total, rocking, and flexural inter-story dirft ratios), Arias Intensity (AI). This was because of better capturing the evolutionary responses of the soil (e.g., pore pressure, acceleration, and deformation time histories) and consequent effects on the structure by an evolutionary IM such as AI, which contains most aspects of the ground motion properties such as intensity, duration, and frequency content. It must be emphasized, however, that the conclusions made in this study are limited to the soil and structural conditions evaluated numerically and may not apply to other types of structures, foundations, or soil stratigraphy (e.g., sloping ground). Further, as future attenuation relationships are developed for other more efficient and sufficient IMs with smaller residuals, these conclusions should be re-visited.

8.3. Future Research Directions and Recommendations

- The observations made in this dissertation are limited to the soil, structural, and loading conditions investigated in this study. Additional element level tests on granular soils under sinusoidal and irregular loading as well as different confining pressures will improve numerical models and their calibration. Moreover, further calibrations of the numerical tool against available and relatively well-documented information from case histories (e.g., Wildlife Liquefaction Array and 1987 Superstition Hill Earthquake), although they provide limited information, is recommended.
- The structures employed in centrifuge and numerical simulations were simplified, linear-elastic, SDOF structures. The response of inelastic, MDOF structures that are capable of damage needs to be investigated on liquefiable ground with and without

mitigation in future experimental and numerical studies, in order to better evaluate the effectiveness of remediation strategies in the context of building performance.

- The influence and importance of multi-dimensional cyclic loading (as opposed to 1-D shaking) on the seismic performance of structures on softened ground need to be investigated in future studies. This is anticipated to influence the overall performance of the soil-structure system.
- The integrated response of soil-foundation-structure (SFS) system will improve by more accurately modeling the force-displacement relationship (e.g., use of zero length element) between the response of soil and foundation at their immediate interface. Moreover, the effect of possible migration of fluid along the soil-foundation interface is recommended to be introduced into future numerical simulations.
- Additional numerical simulations that introduce a wider range of conditions (i.e., more IPs), validated against case history measurements with more complexities are recommended prior to the development of a reliable probabilistic performance-based procedure to predict the response of buildings on liquefiable ground.
- Most soil constitutive models for liquefaction purposes are known to be incapable of capturing volumetric strains during and after cyclic loading, mainly caused by sedimentation. They need to be improved for better predicting volumetric strains under the constant stress ratio in liquefiable soils simultaneously with accelerations and excess pore pressures.
- In most of the cases, it was observed that the rate of post-shaking excess pore water pressure dissipations estimated by PDMY02 was larger than what was observed in the centrifuge experiments. The author believes this inaccuracy is due to the fact that the model has been developed and verified based on the results of some element level tests with fully undrained conditions (e.g., cyclic simple shear test), in which the effects of

partial drainage during cyclic loading and post-shaking pore water pressure dissipation were not considered. Further, in a fully undrained condition, the value of soil permeability does not influence the rate of shear induced pore water pressure buildup. This can be improved by adjusting the rate of net excess pore pressure inside the numerical model formulations.

- A number of efficient and sufficient IMs were identified in this study for predicting different EDPs related to the seismic response of soil and structures on liquefiable ground, which are not predictable (with no widely-accepted attenuation relationships). Future development of attenuation models for predicting various IMs that are more holistic than PGA or spectral accelerations, such as characteristic intensity (CI), root mean square of acceleration, velocity, and displacement (a_{RMS}, v_{RMS}, and d_{RMS}, respectively), and cumulative absolute velocity (CAV) are recommended.
- In dense urban environments, further complications arise from the interaction of adjacent buildings, due to changes in stress distributions (overlapping stress bulbs), drainage paths, and more importantly, structure-soil-structure interaction. Future physical model and numerical studies are needed to investigate the mutual influence of adjacent structures and the effectiveness of liquefaction remediation strategies.

BIBLOGRAPHY

Abrahamson, N. A., and Silva, W. J. (1996). Empirical Ground Motion Models. *Report to Brookhaven National Laboratory.*

Abrahamson, N. A., Silva, W. J., and Kamai, R. (2014). Summary of the ASK14 ground motion relation for active crustal regions. *Earthquake Spectra*, EERI, 30 (3), 1025-1055.

Abrahamson, N. A., Somerville, P. G., and Cornell, C. A. (1990). Uncertainty in numerical strong motion predictions. *Proc. 4th U.S. Nat. Conf. on Earthquake Engrg.,* EERI, El Cerrito, Calif., 407-416.

Ambraseys, N., & Zatopek, A. (1969). The Mudurnu valley earthquake of July 22nd 1967. *Bull Seismol Soc Am,* 59(2), 521–89.

Andrianopoulos, K. I., Bouckovalas, G. D., Karamitros, D. K., and Papadimitriou, A. G. (2006). Effective Stress Analysis for the Seismic Response of Shallow Foundations on Liquefiable Sand. *Numerical Methods in Geotechnical Engineering,* F. Schweiger, ed., Taylor & Francis Group, London, 211-216.

Andrianopoulos, K. I., Papadimitriou, A. G., Bouckovalas, G. D. (2010). Bounding surface plasticity model for the seismic liquefaction analysis of geostructures. *J. of Soil Dyn. and EQ Eng.,* 30, 895-911.

Arias, A. (1970). A Measure of Earthquake Intensity in R.J. Hansen ed. *Seismic Design for Nuclear Power Plants*, MIT Press, Cambridge, Massachusetts, 438-483.

Arulmoli, K., Muraleetharan, K. K., Hossain, M. M., and Fruth, L. S. (1992). VELACS: Verification of liquefaction analyses by centrifuge studies, Laboratory Testing Program. Project No. 90–0562, *The Earth Tech. Corp., Irvine, Calif.*

Ashford, S. A., Boulanger, R. W., Donahue, J. L., & Stewart, J. P. (2011). Geotechnical Quick Report on the Kanto Plain Region during the March 11, 2011, Off Pacific Coast of Tohoku Earthquake, Japan. Geotechnical Extreme Events Reconnaissance (GEER). *GEER Association Report No. GEER-025a.*

Bardet, J. P., Certin, K. O., Lettis, W., Rathje, E., Rau, G., Seed, R. B., & Ural, D. (2000). Soil liquefaction, landslides and subsidences. *Earthquake Spectra,* 16(1), 141–62.

Bardet, J. P., Huang Q., and Chi, S. W. (1993). Numerical Prediction for model No 1. *Proc. Of the Int. Conf. on the Verification of Numerical Procedures for the Analysis of Soil Liquefaction Problems*, ed., Arulanandan, K., and Scott, R. F., Davis, CA, 17-20 Oct.

Benjamin, J. R. and Associates. (1988). A criterion for determining exceedance of the Operating Basis Earthquake. EPRI Report NP-5930, *Electric Power Research Institute,* Palo Alto, California.

Biot, M. A. (1962). The mechanics of deformation and acoustic propagation in porous media. *J. Applied Physics*, 33(4), 1482-1498.

Bird, J. F., and Bommer, J. J. (2004). Earthquake losses due to ground failure. *Engineering Geology*, 75, 147-179.

Bolt, B., (1973). Duration of strong motion. *Proceedings of the 5th World Conference on Earthquake Engineering,* Rome, Italy, Vol. 6D, Paper no. 292.

Bouckovalas, G. D., Valsamis, A. I., and Andrianopoulos, K. I. (2005). Pseudo static vs. performance based seismic bearing capacity of footings on liquefiable soil. *Proc. of the TC4 satellite conference, 16th ICSMGE*, 22–29.

Bray, J. D., Stewart, J. P., Baturay, M. B., Durgunoglu, T., Onalp, A., Sancio, R. B., Ural, D., Ansal, A., Bardet, J. B., Barka, A., Boulanger, R., Cetin, O., and Erten, D. (2000). Damage Patterns and Foundation Performance in Adapazari. *Earthquake Spectra*, 16 (S1), 163-189.

Broadhead, G. C. (1902). The New Madrid Earthquake. *The American Geologist*, 30, 76-87.

Byrne, P. M., Park, S., Beaty, M., Sharp, M., Gonzalez, L., Abdoun, T. (2004). Numerical modeling of liquefaction and comparison with centrifuge tests. *Can. Geotech. J.*, 41, 193–211.

Campbell, K. W., and Bozorgnia, Y. (2014). NGA-West2 ground motion model for the average horizontal components of PGA, PGV, and 5% damped linear acceleration response spectra, *Earthquake Spectra,* EERI, 30 (3), 1087–1115.

Cascone, E., and Bouckovalas, G. (1998). Seismic bearing capacity of footings on saturated sand with a clay cap. *Proc., 11th European Conf. on Earthquake Engineering*, Paris.

Cetin, K. O., Youd, T. L., Seed, R. B., Bray, J. D., Sancio, R., Lettis, W., Yilmaz, M., Durgunoglu, H. T. (2002). Liquefaction-induced ground deformations at Hotel Sapanca during Kocaeli (Izmit), Turkey earthquake. *Soil Dynamics and Earthquake Engineering*, 1083–1092, 1083–1092.

Cetin, K., Youd, T., Seed, R., Bray, J., Stewart, J., Durgunoglu, H., Lettis, W., and Yilmaz, M. (2004). Liquefaction-Induced Lateral Spreading at Izmit Bay During the Kocaeli

(Izmit)-Turkey Earthquake. *Geotechnical and Geoenvironmental Engineering,* 130(12), 1300-1313.

Cetin, K.O., Unutmaz, B., Jeremic, B., 2012. Assessment of seismic soil liquefaction triggering beneath building foundation systems. *Soil Dynamics and Earthquake Engineering,* 43, 160-173.

Chan, A. H. C. (1988). A Unified Finite Element Solutoin to Static and Dynamic Problems in Geomechanics. *PhD. Dissertation,* University College of Swansea, U.K.

Chen, Z., Hutchinson, T. C., and Trombetta, N. W. (2010). Seismic performance assessment in dense urban environments: evaluation of nonlinear building-foundation systems using centrifuge tests. *Proc. of 5th Intl. Conf. on Recent Advances in Geotch. Earthq. Eng. and Soil Dynamics,* San Diego, CA.

Coffman, J. L., & von Hake, C. A. (1973). Earthqake History of United States. *Department of Commerce, National Oceanic and Atmospheric Administration,* Publication 41-1, Washington, D.C., US.

Coulter, H. W., & Migliaccio, R. R. (1966). Effect of the earthquake of March 27, 1964 at Valdez, Alaska. U.S. *Geological Survey Professional Paper,* 542-C, 36 p.

Cubrinovski, M., and McCahon, I. (2012). Short Term Recovery Project 7: CBD Foundation Damage. *Natural Hazards Research Platform,* University of Canterbury, Christchurch, New Zealand.

Cubrinovski, M., Bradley, B., Wotherspoon, L., Green, R., Bray, J., Wood, C., Pender, M., Allen, J., Bradshaw, A., Rix, G., Taylor, M., Robinson, K., Henderson, D., Giorgini, S., Ma, K., Winkley, A., Zupan, J., O'Rourke, T., DePascale, G., Wells, D. (2011a).

Geotechnical Aspects Of The 22 February 2011 Christchurch Earthquake. *Bulletin Of The New Zealand Society For Earthquake Engineering*, 44(4), 205-226.

Cubrinovski, M., Bray, J. D., Taylor, M., Giorgini, S., Bradley, B., Wotherspoon, L., & Zupan, J. (2011b). Soil Liquefaction Effects in the Central Business District during the February 2011 Christchurch Earthquake. *Seismological Research Letters*, 82(6), 893-904.

Dafalias YF, Manzari MT. 2004. Simple plasticity sand model accounting for fabric change effects. *J Eng Mech*,130(6):622–34.

Dafalias YF. 1986. Bounding surface plasticity, I: mathematical foundation and hypoplasticity. *J Eng. Mech.*, 112(9):966–87.

Dashti, S., and Bray, J.D. (2013). Numerical Simulation of Building Response on Liquefiable Sand. *J. Geotech. and Geoenv. Eng*., ASCE, 139 (8), 1235-1249.

Dashti, S., Bray, J. D., Pestana, J. M., Riemer, M. R., and Wilson, D. (2010a). Centrifuge testing to evaluate and mitigate liquefaction-induced building settlement mechanisms. *J. Geotech. Geoenviron. Eng.*, 136(7), 918-929.

Dashti, S., Bray, J. D., Pestana, J. M., Riemer, M. R., and Wilson, D. (2010b). Mechanisms of seismically-induced settlement of buildings with shallow foundations on liquefiable soil. *J. Geotech. Geoenviron. Eng.*, 136(1), 151-164.

Dashti, S., and Karimi, Z. (forthcoming). Ground Motion Intensity Measures to Evaluate I: the Liquefaction Hazard in the Vicinity of Shallow-Founded Structures. *Earthquake Spectra,* EERI (under review).

Derleth, J. C. (1907). The destructive extent of the California earthquake of 1906; its effect upon structures and structural materials within the earthquake belt, California earthquake of 1906. D. S. Jordan, Ed., *Bruce Brough Press,* San Francisco.

Dobry, R., Ladd, R. S., Yokel, F. Y., Chung, R. M., Powell, D. (1982). Prediction of Pore Water Pressure Buildup and Liquefaction of Sands During Earthquakes by the Cyclic Strain Method, *NBS Building Science Series 138*, Nat. Bureau of Standards, Gaithersburg, MD, 150 pp.

Eckel, E. B. (1967). Effect of earthquake of March 27, 1964, on air and water transport, communications, and utilities system in south-central Alaska. *U. S. Geological Survey Professional Paper*, 545-B, 27 p.

Elgamal, A. (2007). Nonlinear Modeling of Large-scale Ground-Foundation-Structure Seismic Response. *ISET Journal of Earthquake Technology*, Paper No. 488, 44(2), 325-339.

Elgamal, A., Lu, J., and Yang, Z. (2005a). Liquefaction-induced settlement of shallow foundations and remediation: 3D numerical simulation. *J. Earthquake Eng.*, 9(spec01), 17–45.

Elgamal, A., Yang, Z., Lai, T., Kutter, B. L., and Wilson, D. W. (2005b). Dynamic Response of Saturated Dense Sand in Laminated Centrifuge Container. *J. Geotech. Geoenviron. Eng.*, 131(5), 598-609.

Elgamal, A., Yang, Z., and Parra, E. 2002. Computational modeling of cyclic mobility and post-liquefaction site response, *Soil Dynamics and Earthquake Engineering*, 22 (4), 259-271.

EPRI-NP-5930, 1988. A criterion for determining exceedance of the operating basis earthquake. Tech. rep., *Electrical Power Research Institute* (EPRI), Palo Alto, CA (1988).

Fenves, G.L. (2003). A Vision for Computational Simulation in Earthquake Engineering. *Community Workshop on Computational Simulation and Visualization Environment for the Network for Earthquake Engineering Simulation (NEES),* Sponsored by NSF, Roddis, K., editor, Lawrence, KS.

Gastro, G., Seed, R. B., Keller, T. O., and Seed, H. B. (1992). Steady-State Strength Analysis of the Lower San Fernando Dam Slide. *Journal of Geotechnical engineering,* 118(3), 406-427.

Gelagoti, F., Kourkoulis, R., Anastasopoulos I., and Gazetas, G. (2012). Rocking isolation of low-rise frame structures founded on isolated footings. *Earthquake Eng. and Struct.* Dyn. (41), 1177–1197.

Ghayoomi, M., and Dashti, S. (2015). Effect of Ground Motion Characteristics on Seismic Soil-Foundation-Structure Interaction. *Earthquake Spectra*. (31), No 3, 1789-1812.

Ghayoomi, M., Dashti, S., & McCartney, J. S. (2013). Performance of a transparent Flexible Shear Beam container for geotechnical centrifuge modeling of dynamic problems. *Soil Dynamics and Earthquake Engineering*, (53), 230-239.

Green, R. A., Allen, A., Wotherspoon, L., Cubrinovski, M., Bradley, B., Bradshaw, A., Cox, B., and Algie, T. (2011). Performance of levees (stopbanks) during the 4 September Mw7.1 Darfield and 22 February 2011 Mw6.2 Christchurch, New Zealand, earthquakes. *Seismological Research Letters*, 82, 939-949.

Hacker, T., Eigenmann, R., and Rathje, E. (2013). Advancing earthquake engineering research through cyber infrastructure, *J. Struct. Eng.*, 10.1061/(ASCE)ST.1943-541X.0000712, 1099–1111.

Hariri-Ardebili, M. A., and Saouma, V. E. (2016). Probabilistic seismic demand model and optimal intensity measure for concrete dams. *Structural Safety*, 59, 67-85.

Hausler, E. A. (2002). Influence of ground improvement on settlement and liquefaction: A study based on field case history evidence and dynamic geotechnical centrifuge tests. *Ph.D. dissertation,* Univ. of California at Berkeley, Berkeley, CA.

Housner, G. W. (1952). Spectrum intensities of strong-motion earthquakes, in: Symposium on Earthquakes and Blast Effects on Structures. *Earthquake Engineering Research Institute*, Los Angeles, CA.

Howell, R., Rathje, E., and Boulanger, R. (2015). Evaluation of Simulation Models of Lateral Spread Sites Treated with Prefabricated Vertical Drains. *J. Geotech. Geoenviron. Eng.*, 141(1), 04014076.

Husid, L. R. (1969). Características de terremotos, análisis general (Characteristics of earthquakes, general analysis), *Revista del IDIEM*, 8, 21-42 (in Spanish).

Idriss, I. M., and Boulanger R. W. (2008). Soil Liquefaction During Earthquakes, *Earthquake Engineering Research Institute*, USA.

Ishihara, K., and Yoshimine, M. (1992). Evaluation of Settlements in Sand Deposits Following Liquefaction during Earthquakes. *Soils and Foundations,* 32 (1), 173-188.

Iwan, W. D. (1967). On a Class of Models for the Yielding Behavior of Continuous and Composite Systems. *Journal of Applied Mechanics,* ASTM, 34, 612-617.

Kammerer, A., Wu, J., Pestana, J., Riemer, M., and Seed, R. (2000). Cyclic simple shear testing of Nevada sand for PEER Center, project 2051999. *Geo. Eng. Res. Rep.* UCB/GT/00-01, Univ. of California, Berkeley, CA.

Kammerer, A., Wu, J., Riemer, M., Pestana, J., and Seed, R. (2004). A new multi-directional simple shear testing database. *Proc., 13th World Conf. on Earthquake Engineering*, Paper 2083, Canadian Association for Earthquake Engineering, Ottawa, ON.

Karamitros, D. K., Bouckovalas, G. D., and Chaloulos, Y. K. (2013). Insight into the seismic liquefaction performance of shallow foundations. *ASCE J. Geotech. Geoenviron. Eng.*, 139, 599-607.

Karimi, Z., and Dashti, S. (2015a). Numerical Simulation of Earthquake Induced Soil Liquefaction: Validation against Centrifuge Experimental Results. *IFCEE 2015, Geo-institute,* ASCE, USA, 11-20. doi: 10.1061/9780784479087.002.

Karimi, Z., and Dashti, S. (2015b). Numerical and Centrifuge Modeling of Seismic Soil–Foundation–Structure Interaction on Liquefiable Ground. *J. Geotech. Geoenviron. Eng.*, 10.1061/(ASCE)GT.1943-5606.0001346 , 04015061.

Karimi, Z., and Dashti, S. (2016). Seismic Performance of Shallow Founded Structures on Liquefiable Ground: Validation of Numerical Simulations using Centrifuge Experiments, *J. Geotech. Geoenviron. Eng.,* 10.1061/(ASCE)GT.1943-5606.0001479.

Karimi, Z., and Dashti, S. (forthcoming). Ground Motion Intensity Measures to Evaluate II: the Performance of Shallow-Founded Structures on Liquefiable Ground. *Earthquake Spectra,* EERI (under review).

Kausel, E. (2010). Early History of Soil-Structure Interaction. *Journal of Soil Dynamics and Earthquake Eng.,* Elsevier, 30, 822-832.

Keefer, D. K., & Tannaci, N. E. (1981). Bibliography on Landslides, Soil Liquefaction, and Related Ground Failures in Selected Historic Earthquakes. Department of the Interior United States Geological Survey.

Kempton, J. J., and Stewart J. P. (2006). Prediction Equations for Significant Duration of Earthquake Ground Motions Considering Site and Near-Source Effects. *Earthquake Spectra,* EERI, 22 (4), 985-1013.

Kim, S., and Stewart, J. P. (2003). Kinematic Soil-Structure Interaction from Strong Motion Recordings. *ASCE J. Geotech. Geoenv. Eng.*, 129(1), 323-335.

Kramer, S. L., and Mitchell R. A. (2006). Ground Motion Intensity Measures for Liquefaction Hazard Evaluation. *Earthquake Spectra,* Earthquake Engineering Research Institute, 22 (2), 413–438.

Kramer, S. L., and Stewart, J.P. (2004). Ch4. Geotechnical Aspects of Seismic Hazards. In Earthq. Eng.: from Eng. Seismology to Performance-Based Eng., Bozorgnia and Bertero (Ed.), CRC Press.

Kramer, S.L., (1996). Geotechnical Earthquake Engineering, *Prentice Hall, NJ*.

Kuribayashi, E., & Tatsuoka, F. (1977). History of Earthquake-Induced Soil Liqefaction in Japan (Vol. 31). Tokyo, Japan, Bulletin of Public Works Research Institute.

Lambe, T. W. (1973). Predictions in soil engineering. *Geotechnique*, 23(2), 149-202.

Li, P. (2000). Seismic pile response and pile stiffness in liquefiable soils. *Masters Thesis*, Department of Civil Engineering, University of Washington, 175 pp.

Liu, L., and Dobry, R. (1997). Seismic response of shallow foundation on liquefiable sand. *J. Geotech. Geoenviron. Eng.*, 123(6), 557-567.

Lopez-Caballero, F., and Farahmand-Razavi A. M. (2008). Numerical simulation of liquefaction effects on seismic SSI. *Soil Dynamics and Earthquake Engineering*, 28(2), 85-98.

Lopez-Caballero, F., and Farahmand-Razavi A. M. (2013). Numerical simulation of mitigation of liquefaction seismic risk by preloading and its effects on the performance of structures. *Soil Dynamics and Earthquake Engineering*, 49, 27-38.

Lu, J., Peng, J., Elgamal, A., Yang, Z., and Law, K.H. (2004). Parallel Finite Element Modeling of Earthquake Ground Response and Liquefaction. *Earthquake Engineering and Engineering Vibration*, 3(1), 23–37.

Luco, N., and Cornell, C. A., 2007. Structure-specific scalar intensity measures for near source and ordinary earthquake ground motions. *Earthquake Spectra*, EERI, 23 (2), 357–392.

Malvick, E. J., Kutter, B. L., Boulanger, R. W., and Kulasingam, R. (2006). Shear localization due to liquefaction-induced void redistribution in a layered infinite slope. *J. Geotech. Geoenviron. Eng.,* 132(10), 1293–1303.

Martin, G., and Lam, I. P. (2000). Earthquake resistant design of foundation-retrofit of existing foundations. *Proceedings of GeoEngineering 2000 Conference*, Melbourne, Australia.

Mason, H. B. (2011). Seismic Performance Assessment in Dense Urban Environments. *Ph.D. dissertation,* Univ. of California at Berkeley, Berkeley, CA.

Mazzoni, S., McKenna, F., Scott, M., and Fenves, G. (2006). Open System for earthquake engineering simulation user command-language. Berkeley, CA: NEES.

McCaan, M. W., and Shah, H. C. (1979). Determining Strong-motion Duration of Earthquakes. *Bulletin of the Seismological Society of America*, 69 (4), 1253-1265.

McCartney, J. S., Kuhn, J. A., and Zornberg, J. G. (2005). Geosynthetic drainage layers in contact with unsaturated soils. *Proc., 16th ISSMGE Conf. on Geotechnical Engineering in Harmony with the Global Environment,* Ministry of Land, Infrastructure and Transport and the Ministry of the Environment, Tokyo, Japan.

McGann C. R. (2013). Numerical Evaluation of Forces on Piled Bridge Foundations in Laterally Spreading Soil. *Ph.D. dissertation*, Univ. of Washington.

McKenna, F., Fenves, G. L. (2008). Using the OpenSees interpreter on parallel computers. *Network for Earthquake Engrg. Simulations*, Berkeley, CA.

McKenna, F., Fenves, G. L., Scott, M. H., and Jeremic, B. (2000). Open System for Earthquake Engineering Simulation (OpenSees). *Pacific Earthquake Engineering Research Center*, University of California, Berkeley, CA.

Menq, F. -Y., Cox, B., Park, K., and Stokoe, K. H. (2010). Estimating dynamic strains in soil generated by the large mobile shakers at NEES@UTexas. *in proceedings 9th US National and 10th Canadian Conference on Earthquake Engineering*, Paper No. 1076, Toronto, Ontario.

Mroz, Z. (1967). On the description of Anisotropic Work Hardening. *Journal of the Mechanics and Physics of Solids*, 15, 163-175.

Naesgaard, E., Byrne, P. M., and Ven Huizen, G. (1998). Behaviour of light structures founded on soil 'crust' over liquefied ground. *Geotech. Earthquake Eng. Soil Dynamics*, 75(I), 422–433.

NCEER (1997). Proceedings of the NCEER Workshop on Evaluation of Liquefaction Resistance of Soils. Edited by Youd, T.L., Idriss, I.M., Technical Report No. NCEER-97-0022, December 31, 1997.

Olson, S. M., Green, R. A., Lasley, S., Martin, N., Cox, B. R., Rathje, E., Bachhuber, J., French, J. (2011). Documenting Liquefaction and Lateral Spreading Triggered by the 12 January 2010 Haiti Earthquake. *Earthquake Spectra*, EERI, 27(S1), S93–S116.

Park, Y., Alfredo, H. –S. A. AH-S., Y. Wen, Y. K. (1985). Seismic damage analysis of reinforced concrete buildings. *Journal of Structural Engineering*, 111 (4), (1985) 740–757.

Parra, E. (1996). Numerical Modeling of Liquefaction and Cyclic Mobility and Dilative Behavior in Soil Systems. *Ph.D. dissertation,* Dept. Civil Eng., Rensselaer Polytechnic Institute.

Pecker, A., and Pender, M. (2000). Earthquake resistant design of foundations: new construction. *Proceedings of GeoEngineering 2000 Conference*, Melbourne, Australia.

Pitilakis, D., Dietz, M., Wood, D. M., Clouteau, D., and Modaressi, A. (2008). Numerical Simulation of Synamic Soil-Structure Interaction in Shaking Table Testing. *Journal of Soil Dynamics and Earthq. Eng.*, Elsevier, 28, 453-467.

Popescu, R., and Prevost, J. H. (1993). Centrifuge validation of a numerical model for dynamic soil liquefaction. *Soil Dynamics and Earthquake Engineering* 12, 73-90.

Popescu, R., Prevost, J. H., Deodatis, G., and Chakrabortty, P. (2006). Dynamics of nonlinear porous media with applications to soil liquefaction. *Soil Dyn. Earthquake Eng.*, 26(6-7), 648–665.

Prevost, J. H. (1985). A Simple Plasticity Theory for Frictional Cohesionless Soils. *Soil Dynamics and Earthquake Engineering*, 4(1), 9-17.

R.W. Boulanger and K. Ziotopoulou. (2013). Formulation of a sand plasticity plane-strain model for earthquake engineering applications. *Soil Dynamics and Earthquake Engineering*, 53, 254–267.

Rathje, E. M., Abrahamson, N. A., Bray, J. D. (1998). Simplified frequency content estimates of earthquake ground motions, *Journal of Geotechnical and Geoenvironmental Engineering*, 124 (2), 150-159.

Rathje, E. M., Bachhuber, J., Dulberg, R., Cox, B. R., Kottke, A., Wood, C., Green, R. A., Olson, S., Wells, D., Rix, G. (2011). Damage Patterns in Port-au-Prince during the 2010 Haiti Earthquake. *Earthquake Spectra*, 27(S1), S117–S136.

Sancio, R., Bray, J. D., Durgunoglu, T., and Onalp, A. (2004). Performance of buildings over liquefiable ground in Adapazari, Turkey. *Proc., 13th World Conf. on Earthquake Engineering*, St. Louis, Mo., Canadian Association for Earthquake Engineering, Vancouver, Canada, Paper No. 935.

Sarma, S. K., and Casey, B. J. (1990). Duration of strong motion in earthquakes. *Proceedings of the 9th European Conference on Earthquake Engineering*, Moscow, USSR, 10A, 174–183.

Sarma, S. K., and Yang, K. S. (1987). An evaluation of strong motion records and a new parameter A95. *Earthquake Engineering and Structural Dynamics*, 15 (1), 119-132.

Scawthorn, C., and Johnson, G. S. (2000). Preliminary report Kocaeli (Izmit) earthquake of 17 August 1999. *Engineering Structures* (NEED REVISE), 22, 727-745.

Schofield AN, Wroth CP. (1986). Critical state soil mechanics. New York: McGraw-Hill.

Schofield, A. N. (1981). Dynamic and Earthquake Geotechnical Centrifuge Modelling. *Proc. Int. Conf. on Recent Advances in Geotech. Earthquake Engrg. and Soil Dynamics*, Univ. of Missouri, Rolla, Mo, USA, 3,1081-1100.

Seed, H. B., & Idriss, I. M. (1967). Analysis of Soil Liquefaction: Niigata Erthquake. *Soil Mech. and Fdn. Div.*, 93(3), 83-108.

Seed, H. B., and Idriss, I. M. (1970). Soil moduli and damping factors for dynamic response analyses. *Report No. EERC 70-10, Earthquake Engineering Research Center*, Univ. of Cali., Berkeley, CA, 40p.

Seed, H. B., Idriss, I. M., Lee, K. L., & Makadisi, F. I. (1975b). Dynamic Analysis of the Slide in the Lower San Fernando Dam during the Earthquake of February 9, 1971. *Geotechnical Engineering Devision,* 101(9), 889-911.

Seed, H. B., Makdisi, F. I., Idriss, I. M., Lee, K. L., & Lee, K. L. (1975a). The Slides in the San Fernando Dams During the Earthquake of February 9, 1971. *Geotechnical Engineering Division,* 101(7), 651-688.

Seed, R. B., Chang, S. W., Dickenson, S. E., and Bray, J. D. (1997). Site-Dependent Seismic Response Including Recent Strong Motion Data. *Proc., Special Session on Earthquake Geotechnical Engineering, XIV International Conf. On Soil Mechanics and Foundtion Engineering, Hamburg, Germany,* A. A. Balkema Publ., 125-134.

Seed, R.B., Cetin, K. O., Moss, R. E. S., Kammerer, A. M., Wu, J., Pestana, J. M., Riemer, M. F., Sancio, R. B., Bray, J. D., Kayen, R. E., and Faris, A. (2003). Recent Advances in Soil Liquefaction Engineering: A Unified and Consistent Framework. *26th Annual ASCE Los Angeles Geotechnical Spring Seminar,* ASCE, USA.

Shahir, H., and Pak, A. (2010). Estimating liquefaction-induced settlement of shallow foundations by numerical approach. *Computers and Geotechnics*, 37, 267-279.

Shahir, H., Pak, A., Taiebat, M., and Jeremic, B. (2012). Evaluation of variation of permeability in liquefiable soil under earthquake loading. *Computers and Geotechnics*, 40, 74–88.

Somerville, P. G., Smith, N. F., Graves, R. W., and Abrahamson, N. A., (1997a). Modification of empirical strong ground motion attenuation relations to include the amplitude and duration effect of rupture directivity. *Seismol. Res. Lett.* 68, 199–222.

Stewart, D. P., Chen, Y. R., and Kutter, B. L. (1998). Experience with the Use of Methylcellulose as a Viscous Pore Fluid in Centrifuge Models. *Geotechnical Testing Journal*, GTJODJ, 21(4): 365-369.

Stewart, J. P., Fenves, G. L., and Seed, R. B. (1999a). Seismic Soil-Structure Interaction in Buildings. I: Analytical Methods. *ASCE Journal of Geotech. and Geoenv. Eng.*, 125(1), 26-37.

Stewart, J. P., Seed, R. B., and Fenves, G. L. (1999b). Seismic Soil-Structure Interaction in Buildings. II: Experimental Findings. *ASCE Journal of Geotech. and Geoenv. Eng.*, 125(1), 38-48.

Taiebat, M. and Dafalias, Y. F. (2008). SANISAND: simple anisotropic sand plasticity model. *International J. for Numerical and Analytical Methods in Geomechanics*, 32(8), 915-948.

Taylor, C. E., Seligson, H. A., Fowler, D., & Tillman, C. W. (1994). Preliminary Statistics on Losses Associated with Ground Deformation. The Loma Prieta, California, Earthquake of October 17, 1989-Loss Estimation and Procedures, Prof. Paper 1553-A, 63-77.

Tokimatsu, K., and Seed, H. B. (1987). Evaluation of settlements in sands due to earthquake shaking. *J. Geotech. Engrg.*, 113(8), 861-878.

Tokimatsu, K., Kojima, J., Kuwayama, A. A., and Midorikawa, S. (1994). Liquefaction-induced damage to buildings I 1990 Luzon Earthquake. *J. Geotech. Engrg.*, 120(2), 290-307.

Travasarou, T., Bray, J. D., and Abrahamson N. A. (2003). Empirical attenuation relationship for Arias Intensity, Earthquake *Engng Struct. Dyn.,* 32, 1133–1155.

Travasarou, T., Bray, J. D., Sancio, R. B. (2006). Soil-Structure Interaction Analyses of Building Responses During the 1999 Kocaeli Earthquake. *In: Proceedings, 8th US Nat. Conf. EQ Engrg., 100th Anniv. EQ Conf. Comm. the 1906 San Francisco Earthquake*, EERI, USA, Paper no. 1877.

Trifunac, M. D., and Brady, A.G., 1975. A study on the duration of earthquake strong motion. *Bulletin of the Seismological Society of America,* 65, 581–626.

Von Thun, J. L., Rochim, L. H., Scott, G. A., Wilson, J. A. (1988). Earthquake ground motions for design and analysis of dams. *Earthquake Engineering and Soil Dynamics II* - Recent Advances in Ground-Motion Evaluation, Geotechnical Special Publication, 20, 463-481.

Wakamatsu, K. (1992). Liquefaction history 416-1990, in Japan. *Proc. of the 4th U. S.-Japan Workshop on Earthquake Res. of Lifeline Facilities and Countermeasures Against Soil Liquefaction.* NCEER-92-0019, pp. 97-114. Honolulu, Hawaii: NCEER, Buffalo, NY.

Wijewickreme, D. (2010). Cyclic shear response of low plastic Fraser River Silt."\ *Proc., 9th U.S. National and 10th Canadian Conf. on Earthquake Engineering,* Earthquake Engineering Research Institute, Oakland, CA.

Wison, S. D. (1967). Landslides in the city of Anchorage. The Prince William Sound, Alaska, Earthquake of 1964 and Aftershoks, pp. 253-297.

Yang, Z. (2000). Numerical modeling of earthquake site response including dilation and liquefaction. *Ph.D. Thesis*, Dept. of Civil Engineering and Engineering Mechanics, Columbia University, New York, NY.

Yang, Z., Elgamal, A., and Parra, E. (2003). Computational model for cyclic mobility and associated shear deformation. *J. Geotech. Geoenviron. Eng*, 129(12), 1119-1127.

Yang, Z., Lu, J., and Elgamal, A. (2008). OpenSees Soil Models and Solid-Fluid Fully Coupled Elements: User's Manual. Department of Structural Engineering, University of California, San Diego.

Yoshimi, Y., and Tokimatsu, K. (1977). Settlement of buildings on saturated sand during earthquakes. *Soils Found.*, 17(1), 23-38.

Youd, T., Idriss, I., Andrus, R., Arango, I., Castro, G., Christian, J., Dobry, R., Finn, W., Harder, L., Jr., Hynes, M., Ishihara, K., Koester, J., Liao, S., Marcuson, W., III, Martin, G., Mitchell, J., Moriwaki, Y., Power, M., Robertson, P., Seed, R., and Stokoe, K., II. (2001). Liquefaction Resistance of Soils: Summary Report from the 1996 NCEER and 1998 NCEER/NSF Workshops on Evaluation of Liquefaction Resistance of Soils, *J. Geotech. Geoenviron. Eng.*, 127 (10), 817–833.

Zienkiewicz. O. C., Chan, A. H. C., Pastor, M., Paul, D. K., and Shiomi, T. (1990). Static and Dynamic Behaviour of Soils: A Rational Approach to Quantitative Solutions: I. Fully Saturated Problems. *Proc. Royal. Society of London, Series A, Mathematical and Physical Sciences*, Royal Society Publishing, London, U.K., 429, No. 1877, 285-309.